EXPLORING ANTIBIOTIC CONJUGATION TO CATIONIC AMPHIPHILIC POLYPROLINE HELICES

by

Samantha M. Zeiders

A Dissertation

Submitted to the Faculty of Purdue University

In Partial Fulfillment of the Requirements for the degree of

Doctor of Philosophy

Department of Chemistry

West Lafayette, Indiana

May 2021

THE PURDUE UNIVERSITY GRADUATE SCHOOL

STATEMENT OF COMMITTEE APPROVAL

Dr. Jean Chmielewski, Chair

Department of Chemistry

Dr. Angeline Lyon

Department of Chemistry

Dr. Herman Sintim

Department of Chemistry

Dr. Betsy Parkinson

Department of Chemistry

Approved by:

Dr. Christine Hrycyna

Dedicated to my family.

A secondary dedication to STEM PhD students struggling with mental illness, of whom 40% reported symptoms consistent with generalized anxiety disorder and 37% with major depressive disorder in 2020. (Science Magazine, 2020)

ACKNOWLEDGMENTS

Albert Einstein had said “failure is success in progress”, and that thinking truly resonates the healthy mindset we must accept in our work. As this trying part in my education comes to an end, I am nothing but thankful for those who have had a hand in keeping me sane, developing my skills, and pushing me to succeed despite the many obstacles that graduate school has a habit of affording. I want to highlight the great number of people have positively impacted my personal and professional progress these last few years, contributing immensely to my wellbeing and scientific growth.

First, I would like to acknowledge my thesis advisor, Jean, for being a reliable mentor and scientific role model. She certainly lit the fire that pushed me toward my potential in setting and achieving my goals. Not only has she been a mentor professionally, but she has also influenced my confidence in science and myself through her example as a distinguished scientist and woman in STEM. Among the faculty and staff at Purdue, I also need to thank Ann Cripe and Rob Reason for lending a listening ear to my many complaints and offering advice; in addition to Trisha Herrera for listening to my financial complaints and her help with many paycheck fiascos.

I certainly can not forget to thank my former and current work acquaintances, many whom have become lifelong friends. To start, I want to thank Manish Nepal and Neha Agrawal who introduced me to the lab and settled me into the hectic schedule of graduate school. Monessha Nambiar was such a great friend and mentor in both the lab and life with the best personal advice and great example of work ethic. The stories of Jenny Rowe will live in infamy through her effortless humor and genuine comical actions. Reena Blade and Moises Morales became some of the best friends I’ve ever had. I know it took a while for Reena to warm up to me, but I’m so thankful she did. Moises is one of the hardest people to read, but I came to be one of the few to understand his sense of humor. I am so grateful for their company all those long days and nights in the lab. These two truly had my back through thick and thin and helped me through so many personal obstacles. Professionally, I also must thank them for their research efforts that I have built on and continued through my dissertation.

I could go on forever about the rest of the lab but must keep this short and sweet. Vallabh Suresh was a go-to lab mate to shoot off some wild ideas whenever I got stuck. Ryan Curtis is one of the kindest people I have met, and I couldn’t have picked a better lab buddy to join the lab at

the same time. Glad we could share many mutual friends and kick back outside of lab with the homies. Corey Johnson and Tad Dietsche are some weirdos, but you kept the lab light and fun with your silly behavior and jokes. That aside, I must thank Corey and Tad for their company and regular entertainment of being the target of many jokes. I need to thank Vinny Menon for becoming a great friend and coffee/lunch buddy, as well as an outlet for venting. A thank you goes to Michael Jorgensen for his baking skills, always positive attitude, and rigorous work ethic. Although COVID-19 impacted most of the beginning of Ambar and Nosa's time in lab, I can already see their perseverance shining through in these difficult times from the little time I've spent around you two. I'd also like to thank Paulo Pitasse, who was a year-long visiting scholar, for his insane example of work ethic and motivation, as well as the research he conducted with our group that I have continued.

Undoubtedly, the most important people I cannot thank enough are my husband and children. They came into my life during my graduate career and I can't imagine where I would be without their motivation and encouragement. My family has certainly reminded me what is important in life, health and happiness, especially in these times of isolation and social distancing. I have never depended so much on my familial support, and they have not once faltered in providing me with the love and stability I needed to finish this degree. I hope my dedication to this has also provided them with inspiration to set goals and achieve them, no matter what life hands them or what pandemic strikes next.

The research conducted throughout this dissertation was made possible through the funding opportunities awarded by the National Science Foundation with grant CHE-1807407 and funding provided as an NSF GRFP awardee with grant DGE-1333468.

TABLE OF CONTENTS

LIST OF TABLES

LIST OF FIGURES

LIST OF SCHEMES

LIST OF ABBREVIATIONS

AcOH	Acetic Acid
ACN	Acetonitrile
AFU	Arbitrary Fluorescence Units
AMP	Antimicrobial Peptide
Ar	Argon
Boc	t-butyl carbonate
CAPH	Cationic Amphiphilic Polyproline Helices
CBP	Chlorobiphenyl
Cbz	Carboxybenzyl
CPP	Cell-penetrating Peptide
DCM	Dichloromethane
DIEA	N, N'-diisopropylethylamine
DiSC3(5)	3,3'-Dipropylthiadicarbocyanine Iodide
DMEM	Dulbecco's Modified Eagle Medium
DMF	N,N-dimethylformamide
DMSO	Dimethylsulfoxide
DIW	Deionized Water
ESI	Electrospray Ionization
EtOAc	Ethyl Acetate
FACS	Fluorescence Activated Cell Sorting
FBS	Fetal Bovine Serum
FDA	Food and Drug Administration
Fl	Fluorescein
Fmoc	Fluorenylmethyloxycarbonyl
Fmoc-OSu	N-(fluorenylmethyloxycarbonyloxy) succinamide
HATU	Hexafluorophosphate Azabenzotriazole Tetramethyl Uronium
HFIP	Hexafluoroisopropanol
hRBC	Human Red Blood Cells

HPLC	High Performance Liquid Chromatography
IPTG	Isopropyl β-D-1-thiogalactopyranoside
KHMDS	Potassium Hexamethyldisilazide, Potassium bis(trimethylsilyl)amide
MALDI-TOF	Matrix Assisted Laser Desorption Ionization-Time of Flight
MgSO4	Magnesium Sulfate
MBC	Minimum Bactericidal Concentration
MeOH	Methanol
MIC	Minimum Inhibitory Concentration
Mtt	4-methyltrityl
MRSA	Methicillin-resistant Staphylococcus aureus
N2	Nitrogen
NaH	Sodium Hydride
NHS-Fl	N-hydroxy-succinimidyl-ester-fluorescein
NPN	N-Phenylnaphthalen-1-amine
ONPG	ortho-Nitrophenyl-β-galactoside
prAMP	Proline-rich Antimicrobial Peptides
PBS	Phosphate Buffered Saline
PPII	Type II Polyproline Helix
Rh	Rhodamine
RP-HPLC	Reverse Phase High Performance Chromatography
RT	room temperature
Tat	transactivator of transcription
Tb	Tuberculosis
TB	Trypan Blue
TFA	Trifluoroacetic Acid
THF	Tetrahydrofuran
TIPS	Triisopropylsilane
VRE	Vancomycin-resistant Enterococci
WHO	World Health Organization
Z-Hyp-OH	N-carboxybenzyl-hydroxy-L-proline

ABSTRACT

Pathogenic bacteria present a critical threat to modern medicine. Therapeutic strategies to target and eliminate resilient bacteria are not advancing at the same rate as the emergence of bacterial resistance. An associated urgent concern regarding antibiotic resistance is the existence and proliferation of intracellular bacteria, which find refuge from bactericidal mechanisms by hiding within mammalian cells. Therefore, many once-successful antibiotics become ineffective through the development of resistance, or through failure to reach intracellular locations in therapeutic concentration. To overcome these challenges, the covalent combination of a conventional antibiotic with an antibiotic, cell-penetrating peptide was explored to develop dual-action antibiotic conjugates.

Herein, we utilized a strategy in conjugating the antibiotics by a cleavable linkage to cationic amphiphilic polyproline helices (CAPHs) to improve vancomycin and linezolid antibiotics. This approach enables the conjugate to penetrate cells and deliver two potent monomeric antimicrobial drugs. The vancomycin-CAPH conjugate, **VanP14S**, showed enhanced mammalian cell uptake compared to vancomycin, a poor mammalian cell-penetrating agent; and **VanP14S** was capable of cleaving and releasing two antibiotics under mimicked physiological conditions. Enhanced antibacterial activity was observed against a spectrum of Gram-positive and Gram-negative pathogens, including drug-resistant strains. Further investigation revealed that this conjugate's bactericidal activity was not entirely the result of significant membrane perturbation such as a lytic mode of action. Mammalian cell toxicity and red blood cell lysis were insignificant at relevant bactericidal concentrations below 20 μM. The current results suggest an enhanced binding to the peptidoglycan of bacteria, the target of vancomycin, although more work is needed to justify this claim. Preliminary results on **VanP14GAPS**, a conjugate with a more rigid CAPH, convey similar activity to **VanP14S;** however, moderate increases in red blood cell lysis and cytotoxicity were observed.

Regarding the **LnzP14** conjugate, preliminary data reveal that the conjugate has Gram-negative activity against *Escherichia coli*, whereas linezolid is ineffective in killing Gram-negative bacteria. This conjugate showed significant enhancement in cellular uptake compared to the CAPH, and the release of linezolid and CAPH in physiological conditions was confirmed. Overall, arming a conventional antibiotic with an antimicrobial, cell-penetrating peptide appears to be a powerful strategy in providing novel antibiotic conjugates with the propensity to overcome the limitations in treating challenging pathogens.

CHAPTER 1. STRATEGIES IN DEVELOPING POTENT ANTIBIOTICS THROUGH PEPTIDE CONJUGATION

1.1 The Imminent Threat of Pathogens

Antibiotics have transformed medicine across the globe since the first antibiotic was discovered nearly a century ago. However, almost as quickly as each antibiotic became available for widespread usage, resistance has eclipsed the clinical usefulness of many of these antimicrobial drugs (**Table 1.1**).[1-2] The isolation of pathogens resistant to most, if not all, available antibiotics is occurring routinely, such as drug-resistant *N. gonorrhoeae, A. baumannii* and *C. auris* infections, each listed as an urgent threat by the US Centers for Disease Control.[3] Over time the development of new antibiotics has slowed. Pharmaceutical companies traditionally dominated antibiotic research and development, but many withdrew their efforts due to the lack of long-term success and low financial return of bringing new drugs to market.[4] There is currently an urgent need to address resistance and only two of the eight antibiotics approved since 2017 represent a new chemical scaffold.[5] As of December 2019, approximately a quarter of the 41 drugs in development represented a novel drug class or mechanism of action, however none have targeted activity against Gram-negative ESKAPE pathogens or critical threat pathogens identified by the World Health Organization. [6]

In addition to small molecule antibiotics, antimicrobial peptides (AMPs) have been extensively examined and are a promising class of antibiotics. Their antimicrobial activities target a range of Gram-negative and Gram-positive bacteria, fungi, parasites, and viruses through a variety of mechanisms including membrane disruption, cellular penetration, and immunomodulation.[7-8] Currently there are ten peptide-based antibacterials, including glycopeptides, approved for use with just over 40 more in the clinical pipeline.[9] Undesired characteristics and barriers to AMP clinical treatment have driven a push toward synthetic peptides and peptide mimics that offer greater flexibility in structure. These synthetic peptides may overcome toxicity and stability disadvantages and improve antimicrobial efficacy and selectivity.[10-11]

Table 1.1. Onset of bacterial resistance after antibiotic release[3]

Antibiotic	Year Released	Resistance Identified	Year Identified
Penicillin	**1941**	Penicillin-resistant *Staphylococcus aureus* Penicillin-resistant *Streptococcus pneumoniae* Penicillinase-producing *Neisseria gonorrhoeae*	**1942** **1967** **1976**
Vancomycin	**1958**	Plasmid-mediated vancomycin-resistant *Enterococcus faecium* Vancomycin-resistant *Staphylococcus aureus*	**1988** **2002**
Amphotericin B	**1959**	Amphotericin B-resistant *Candida auris*	**2016**
Methicillin	**1960**	Methicillin-resistant *Staphylococcus aureus*	**1960**
Cephalosporins	**1980**	Extended-spectrum beta-lactamase- producing *Escherichia coli*	**1983**
Azithromycin	**1980**	Azithromycin-resistant *Neisseria gonorrhoeae*	**2011**
Imipenem	**1985**	Klebsiella pneumoniae carbapenemase (KPC)-producing *Klebsiella pneumoniae*	**1996**
Ciprofloxacin	**1987**	Ciprofloxacin-resistant *Neisseria gonorrhoeae*	**2007**
Fluconazole	**1990**	Fluconazole-resistant *Candida*	**1988**
Caspofungin	**2001**	Caspofungin-resistant *Candida*	**2004**
Daptomycin	**2003**	Daptomycin-resistant methicillin-resistant *Staphylococcus aureus*	**2004**
Ceftazidime-avibactam	**2015**	Ceftazidime-avibactam-resistant KPC-producing *Klebsiella pneumoniae*	**2015**

Not only is the development of resistance an impediment in treating bacterial infections, but mammalian membrane penetration is also an obstacle for antibiotics to reach their full therapeutic potential. For instance, options in treating intracellular *Staphylococcus* infections are limited due to the poor mammalian membrane permeability of many hydrophilic antibiotics, including aminoglycosides and glycopeptides.[12-16] Therefore, even if an antibiotic is effective against extracellular bacteria, it may be ineffective in clearing intracellular pathogens that may proliferate and trigger a reinfection. A route to contest both antimicrobial resistance (AMR) and therapeutically restricted infections that focuses on modifying existing antibiotics is promising.[17] Peptides may provide such a tool for use in tandem with antibiotics to combat challenging bacterial infections. Whereas some peptide classes may improve the potency of antibiotics and their delivery to target intracellular locations.

1.2 Cell-Penetrating Peptides

Accessing intracellular target sites is a major challenge for many therapeutic agents. The use of cell-penetrating peptides (CPPs; protein transduction domains, PDTs) over the past few decades has proved to be a powerful tool in overcoming this obstacle. CPPs enable the delivery of

cargo such as proteins, nucleic acids, and small molecule drugs at therapeutic concentrations to cellular and intracellular target sites.[18-20] Unlike other delivery methods, CPPs provide advantages such as versatility, efficiency, and low toxicity. These short peptides are typically cationic with multiple arginine or lysine residues, or amphiphilic. Classic examples of CPPs include the Tat peptide derived from the HIV-1 Tat protein, penetratin derived from the third helix of the *Antennapedia* homeodomain protein, and oligomers of arginine or lysine (**Table 1.2**). Over a thousand CPPs have been isolated or synthetically designed, and a CPP delivery database is available that may meet a therapeutic need.[21]

Table 1.2. Examples of common cell-penetrating peptides

Peptide	**Sequence**
Tat	GRKKRRQRRRPQ
Penetratin	RQIKIWFQNRRMKWKK
Transportan	GWTLNSAGYLLGKINLKALAALAKKIL
Poly-arginine	$(Arg)_R$ R=6-12

1.2.1 Antibacterial CPPs

AMPs and cell-penetrating peptides share similar physiochemical properties such as short peptide length, cationic character, and at times amphiphilicity.[22] This structural redundancy leads to some peptides behaving as both AMPs and CPPs, leading to a more effective therapy. The ability of these dual-function peptides to penetrate and disrupt bacterial membranes, yet nondestructively translocate across mammalian phospholipid bilayers has been reasoned to be a result of electric potential differentiation among bacterial and mammalian membranes.[23-24] Therefore, membrane-interacting peptides may exhibit a dual functionality as some AMPs can cross mammalian cell membranes, and a few CPPs display antimicrobial activity.[25]

Recently, the CPP Tat has also demonstrated modest broad-spectrum antimicrobial activity. In dimerizing Tat, the authors found an increase in antibacterial activity through bacterial membrane disruption, but a decrease in mammalian cell membrane translocation.[26] In this instance, there seems to be a tradeoff in AMP and CPP capability for the Tat peptide. Similarly, the well-known penetratin CPP has also been examined for antimicrobial activity. Penetratin displays broad-spectrum antibacterial activity through bacterial membrane disruption. Moreover,

dimerization of penetratin increases cytotoxicity, and an amino acid shuffling modification decreases CPP mammalian cell penetration.[25, 27]

The cationic AMP LL-37 exhibits antimicrobial and anti-biofilm activity against Gram-positive and Gram-negative pathogens through pore formation on bacterial membranes.[28-30] LL-37 discriminates against bacterial membranes while leaving mammalian membranes intact in its CPP capacity. Through non-covalent linkage, LL-37, has guided the delivery of DNA into mammalian cells, thereby demonstrating CPP activity.[29-30]

Within the past decade, cyclic cell-penetrating peptides (cCPPs) have been comprehensively studied as an improved method of reaching intracellular targets.[31-32] Oh and coworkers showed that a library of amphiphilic cCPPs, rich in tryptophan and arginine residues, displayed moderate broad-spectrum antibacterial activity. These peptides also showed synergistic effects with tetracycline in time-kill experiments against multidrug-resistant pathogens.[33]

Bacterial membrane permeation and disruption with AMPs is a conventional mode of action in bactericidal activity;[34] however, in some cases CPPs display antimicrobial activity without bacterial membrane disruption. In the case of synthetic cationic amphiphilic polyproline helices (CAPHs), cell penetration has been observed with subcellular localization, and broad-spectrum antibacterial activity was seen against bacteria in liquid culture and against intracellular infections with minimal cytotoxicity or membrane lysis.[35-45] Modifications to these CAPHs has modulated both CPP and AMP activities. Increasing cationic character with extended scaffolds increased mammalian cellular accumulation and antibacterial activity without increased bacterial membrane disruption.[41, 43, 45] These examples demonstrate that merging antibacterial components and cell-penetrating components can expand therapies in treating difficult intracellular infections.

1.2.2 Coadministration of antibiotics and CPPs

The effectiveness of antibiotics and ancillary drug combinations of has been verified at the clinical level and is gaining support in designing new strategies to overcome microbial resistance. For instance, it is common to see the use of β-lactam antibiotics with β-lactamase inhibitors to suppress the emergence of resistance;[46] as well as the well-known combination therapy of isoniazid (INH), rifampin (RIF), ethambutol (EMB), and/or pyrazinamide (PZA) in treating tuberculosis.[47-48] There is evidence beginning to surface that antibiotic efficacy may be improved through co-administration with cell-penetrating peptides (CPPs).

Randhawa and coworkers have shown that two arginine-rich cationic CPPs, labeled P3 and P8, with little antibiotic activity alone, synergistically improved the efficacy and delivery of conventional antibiotics against MRSA.[49] Oxacillin, norfloxacin, and vancomycin MICs with sensitive and resistant *S. aureus* were significantly lowered by the combination with P3 and P8 CPPs, thus decreasing the antibiotic cytotoxicity observed with higher dosing. Recently, a non-conjugated curcumin and octa-arginine R8 combination showed enhanced antibacterial activity against Gram-negative and positive bacterial isolates and faster killing kinetics. This complex showed enhanced mammalian cellular accumulation compared to curcumin alone; and the complex displayed bacterial membrane damage to *E. coli* and *S. aureus* as a proposed mode of bactericidal action (**Figure 1.1**).[50]

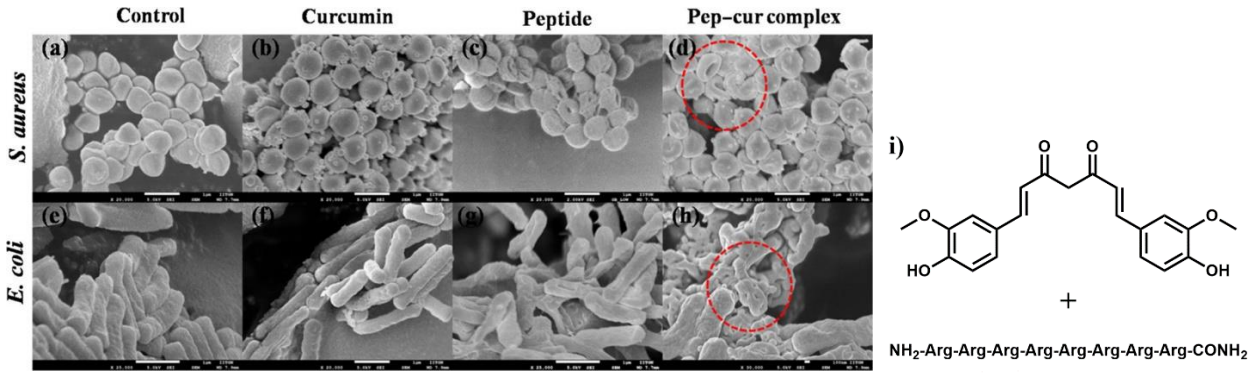

Figure 1.1. SEM micrographs of bacteria, the top panel shows images of *S. aureus* while the bottom one shows images of *E. coli*. (a,e) Control and (b,f) treated with 17 nmol raw curcumin; (c,g) treated with 7.9 nmol peptide; (d,h) treated with MIC90 concentration of the peptide–curcumin complex (1:5). (i) Structure of curcumin and R8. Reprinted (adapted).[50] Copyright (2020), American Chemical Society.

There is great interest in using antibiotic-CPP conjugates. Enhanced activity against resistant bacterial strains and reduced side-effects or toxicity is the objective in the administration of antibiotics with CPPs.[51] This review will highlight and further investigate the recent progress on antibiotic-CPP covalent conjugates to effectively target and treat drug-resistant bacterial infections, while minimizing mammalian cell toxicity, and efforts to treat intracellular pathogenic bacteria.

1.3 Cell Penetrating Peptide Conjugates with Antibiotics

1.3.1 Glycopeptide-CPP conjugates

Vancomycin is a glycopeptide antibacterial used to treat several Gram-positive infections, typically those unresponsive to other antibiotics, thus deeming it the "antibiotic of last resort". Many strategies to overcome vancomycin-resistance and improve mammalian cellular penetration have been presented. Recent examples include combining positively charged groups and lipophilic components. The Haldar group has explored the conjugation of vancomycin to cationic lipids [52-56] and bacterial cell wall pyrophosphate binding moieties.[57-58] The incorporation of sulfonium-based cationic lipophilic components to vancomycin led to enhanced interaction with the negatively charged bacterial cell membrane and increased bactericidal activity through membrane disruption.[59] Boger and coworkers have built upon the chlorobiphenyl (CBP) modification used in ortavancin to incorporate a quaternary ammonium ion for membrane activity resulting in better bactericidal activity.[60-61] Other lipophilic and cell surface-interacting vancomycin derivatives have shown increased activity in treating vancomycin resistance.[62-67]

The simple addition of an arginine to the C-terminus of vancomycin by amide linkage showed that the narrow spectrum Gram-positive antibiotic was capable of inhibiting resistant Gram-negative bacterial infections through enhanced membrane permeability and cell wall synthesis disruption.[68] An elongated version with an octaarginine transporter on the C-terminus, V-r8, showed great activity against antibiotic-insensitive bacteria due to enhanced cell-wall interaction (**Figure 1.2**). This conjugate also was able to eradicate pre-formed MRSA biofilms at 80 μM concentration and persister cells at 10 μM *in vitro*. In an *in vivo* skin wound biofilm model, a 0.05% solution of V-r8 significantly reduced bacterial load with no toxicity.[69]

Blaskovich and coworkers designed selective membrane active vancomycin conjugates. Their design involved a threefold coupling of vancomycin to a lysine-rich electrostatic effector peptide sequence (EEPS) coupled to a lipid membrane insertive element. This EEPS mediates membrane binding in bacteria and mammalian cells. These cationic lipoglycopeptides showed enhanced activity against MRSA and other Gram-positive bacteria with some vancaptins showing a 100-fold improvement in MIC. Although they did not report intracellular activity, they focused on the mode of action these conjugates displayed in antibacterial activity. Membrane interaction of their vancaptins, rather than enhanced ligand binding or dimerization accounted for the excellent activity.[70]

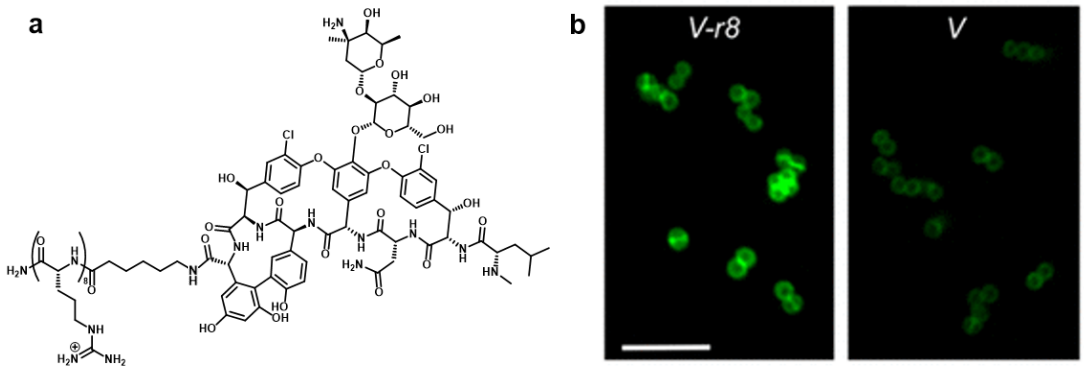

Figure 1.2. (a) structure of vancomycin-r8 (V-r8). (b) MRSA USA400 MW2 bacteria treated with Fl-V–r8 exhibits greater cell-associated and protoplast-associated fluorescence than Fl-V. Confocal microscopy of bacteria treated with 5 μM Fl-V–r8 and Fl-V for 5 min. Reprinted (adapted) with permission.[69] Copyright (2018), American Chemical Society.

The penetrating activity of PP-G, a flexible guanidinium-rich polypeptide, was previously shown to be greater than that of Tat and oligo-arginine CPPs.[71] The PP-G polypeptide was conjugated to vancomycin (**Figure 1.3 a**) using click chemistry and found to display exceptional intracellular and *in vivo* antibacterial activity against resistant *S. aureus.* This activity was through a dual mechanism of action; vancomycin targeting bacterial cell wall synthesis and the polypeptide targeting bacterial cell membrane disruption. This conjugate showed efficient mammalian cell internalization (**Figure 1.3 b**) to effectively eradicate extracellular and intracellular MRSA with an MIC of 3 μM and an IMBC of 9 μM, respectively. Additionally, this VPP-G conjugate eradicated extracellular and intracellular VRE with an MIC of 12 μM and an IMBC of 48 μM, respectively. In a mouse intravenous MRSA infection model, this VPP-G conjugate outperformed vancomycin and effectively eradicated MRSA at 72 mg/kg.

Other locations on vancomycin were explored as options in conjugation. The C-terminus and vancosamine locations of vancomycin were modified with PEG tethers of varying lengths to covalently conjugate vancomycin and the CPP transportan (TP10). Locations of conjugation on TP10 were also used. All conjugates showed increased antibacterial activity against resistant *S. aureus* and most showed activity against *E. faecium*. Notably, the conjugates displayed intracellular antibacterial activity against MRSA in HEK293 cells, and accumulation across the blood brain barrier.[72]

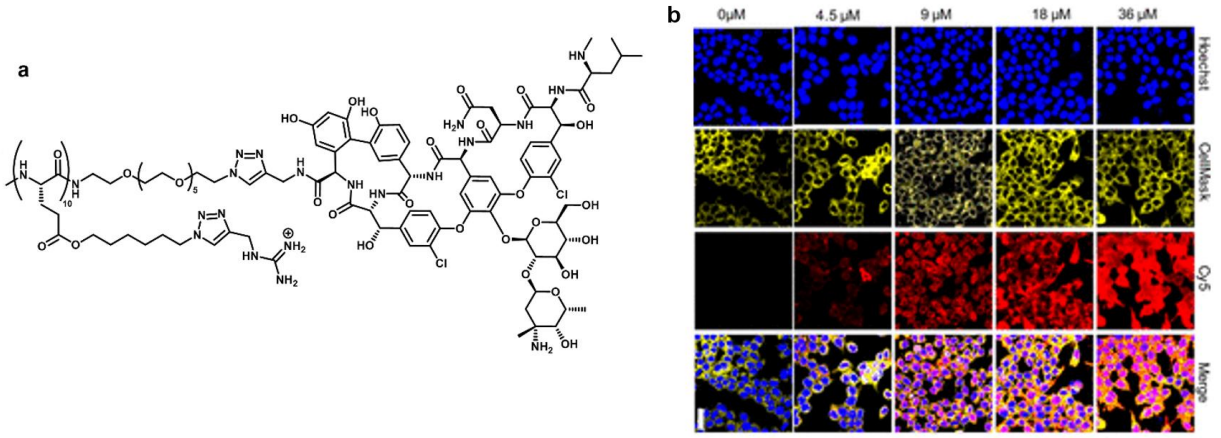

Figure 1.3. (a) Structure of VPP-G. (b) Cellular internalization and membrane penetration of VPP-G. Confocal images of RAW264.7 macrophages treated with Cy5-VPP-G of various concentrations. Blue: Hoechst; yellow: CellMask; red: Cy5-VPP-G. Scale bar: 20 μm. Reprinted (adapted).[71] Copyright (2020), American Chemical Society.

Modifying different positions of vancomycin linkage to poly-arginine CPPs through a maleimide was investigated by the Uhl group.[73-74] In one example, Muhlberg and coworkers explored conjugating triarginine and a fatty acid to different locations on vancomycin.[74] The most potent vancaptin conjugate was that which the peptide and lipid were conjugated from the vancosamine handle of vancomycin. This conjugate showed exemplary activity against VanA, VanB, and VanC resistant *enterococci*. The Uhl group also used the same maleimide linker strategy to conjugate a 6-mer polyarginine CPP on various positions of vancomycin.[73] In their lead conjugate, FU002, the hexaarginine was conjugated from the secondary amine handle of vancomycin and displayed activity against all three types of vancomycin-resistant enterococci with MICs less than 1 x 10^{-6} mmol/mL. Both examples of vancomycin conjugates showed negligible cytotoxicity at relevant concentrations, but the authors did not explore intracellular efficacy in mammalian cells.

1.3.2 Aminoglycoside-CPP conjugates

Aminoglycosides are a class of antibiotics traditionally used to treat Gram-negative infections, with inhibiting essential bacterial protein syntheses. Common antibiotics in this class include streptomycin, kanamycin, tobramycin, gentamicin, and neomycin. For instance, gentamicin is an antibiotic with potent antibacterial activity against extracellular bacteria, but fails

to accumulate intracellularly to treat internalized bacteria within mammalian cells. Gomarasca and colleagues presented the conjugation of gentamicin to CPPs including Tat, α1H and, α2H (isolated from *Y. enterocolitica*) through a maleimide linker strategy.[75] These conjugates did not alter the *in vitro* bactericidal activity of gentamicin, however, the CPPs successfully delivered gentamicin to intracellular locations of HBMEC and HeLa cells and reduced the intracellular bacterial loads of Gram-negative pathogenic *E. coli*, *Shigella*, and *Salmonella*. Interestingly, the addition of non-conjugated CPPs and gentamicin also reduced the bacterial load compared to free gentamicin in *E. coli*-infected HBMEC by at least 5-fold, suggesting a synergy between the compounds.

The broad-spectrum aminoglycoside, kanamycin, is used to treat a range of bacterial infections and tuberculosis, but primarily used to treat Gram-negative bacteria. This antibiotic was conjugated to a synthetic cationic amphiphilic polyproline helix (CAPH), P14LRR using a reversible disulfide linkage.[76-77] The disulfide moiety in the linker of the conjugate was shown to successfully reduce and release both free kanamycin and P14LRR-SH under physiological conditions (**Figure 1.4 A**). The reduction of disulfide and intramolecular rearrangement was modeled after a luciferin-r8 conjugate.[78-79] Further, this conjugate showed impressive antimicrobial activity against a spectrum of Gram-negative pathogens including intracellular *Salmonella, Brucella,* and *Shigella* infections at 10 μM concentration (**Figure 1.4 B**). Not only did this conjugate display excellent antimicrobial activity against a broad-spectrum range of susceptible and drug-resistant strains, but it was also able to efficiently accumulate within mammalian macrophage cells to effectively eradicate intracellular *Mycobacteria* at 5 and 10 μM concentrations (**Figure 1.4 C**) and significantly reduce *Salmonella* in a *C. elegans in vivo* model. This conjugate also was found to disrupt 30%, 50%, 70%, and 80% of mature Gram-positive *S. epidermidis* biofilm mass at 8, 16, 32 and 64 μM, respectively; and clear Gram-negative *P. aeruginosa* and *A. baumannii* at 32 μM.[76-77]

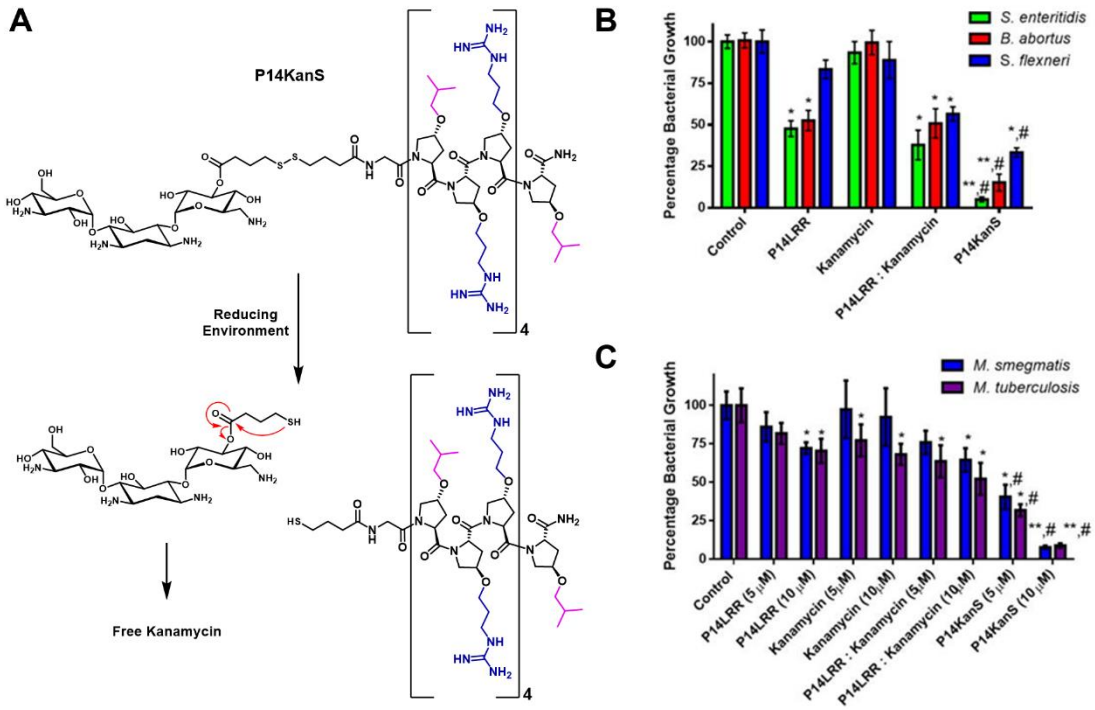

Figure 1.4 (A) Kanamycin-CAPH releases both antibiotics under reducing conditions. (B, C) Intracellular clearance of selected pathogens with P14LRR, kanamycin, and P14KanS. Reprinted (adapted).[76] Copyright (2016), American Chemical Society.

Membrane-active antibiotic-peptide conjugates (MAAPCs) composed of a short sequence from the CPP penetratin and the broad-spectrum aminoglycoside tobramycin, traditionally used for Gram-negative bacteria, were designed and investigated by Deshayes and coworkers. These conjugates had selective bactericidal membrane permeation and displayed broad-spectrum antibacterial activity including persister cells of pathogenic *E. coli* and *S. aureus.* Although the authors reported selective bacterial membrane disruption over mammalian membranes, intracellular activity against bacteria within mammalian cells was not noted.[80]

Paromomycin (PMM) is another poorly absorbed broad-spectrum aminoglycoside antibiotic used to treat infections caused by bacteria and parasites. This antibiotic was conjugated to Tat peptide through a flexible PEG spacer and amide linkage. This conjugate successfully accumulated intracellularly in *Leishmania* parasites and penetrated within *Leishmania* ulcers better than the poorly penetrating paromomycin (**Figure 1.5**). Although intracellular accumulation into the cytoplasm of parasites was observed, killing assays and mammalian cellular accumulation were not investigated.[81]

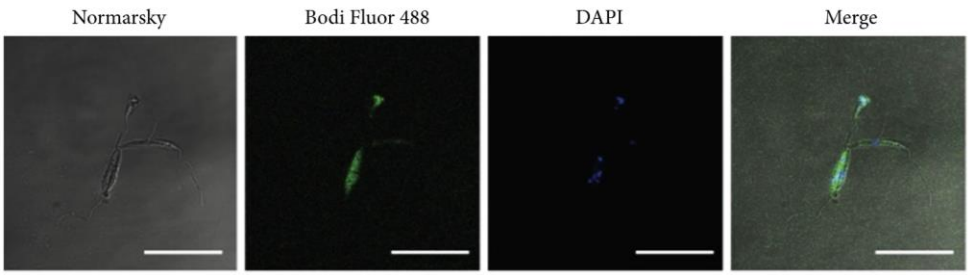

Figure 1.5. Fluorescence of *Leishmania donovani* promastigotes incubated with Bodi Fluor 488-labeled PMM-Tat conjugate (9 μM, 4 h, 26°C) and stained with DAPI (5 μg/mL) immediately before observation, unfixed. Settings: conjugate (green, = 488 nm/ = 520 nm); DAPI (blue, = 350 nm/ = 460 nm). Bar = 20 μm. Experiment is representative of two other ones performed independently. Reprinted (adapted) with permission.[81] Copyright (2017), Hindawi.

1.3.3 Other small molecule antibiotic-CPP conjugates

Levofloxacin and a truncated levofloxacin-Q, broad-spectrum fluoroquinolone antibiotics, were conjugated to the cyclic CPP R4W4 and its linear equivalent through the carboxylic acid group and the terminal lysine on the CPP.[82] It was shown that the levofloxacin-Q-[R4W4] conjugate and non-conjugated mixture of levofloxacin-Q and CPP had increased antibacterial activity against MRSA and *Klebsiella* with MICs of 8 and 32 μM compared to inactive levofloxacin-Q alone. Interestingly, the levofloxacin-cCPP conjugate did not show an improvement in antibacterial activity compared to levofloxacin alone. The conjugates incorporating the linear equivalent of the CPP were less potent than those with cCPP. Ghaffar and coworkers also investigated amide-linked and ester-linked levofloxacin-CPP conjugates.[83] Unfortunately, neither of their levofloxacin-Tat conjugates or the non-conjugated mixture of levofloxacin and Tat cleared bacterial infections more efficiently than antibiotic alone. Another levofloxacin (LVX)-CPP was designed with an acid-reducible thioester linkage.[84] Upon endocytosis-mediated internalization of conjugate in mammalian cells, the acidic internal endosomal conditions were proposed to cleave the thioester linkage between antibiotic and the CPP, CGAFPHR. The authors showed successful cleavage and release of CPP and free LVX in a 4.5 pH environment. However, in regard to bactericidal activity, only a modest improvement in antibacterial activity was seen for the conjugate against *S. aureus* and *E. coli* cultures.

The treatment of intracellular *Listeria monocytogenes* using methotrexate (Mtx) and a synthetic cyclohexyl- and guanidinium-rich CPP was explored by the Kelley group.[85] This Mtx-peptide exhibited enhanced bactericidal activity compared to Mtx with MICs of 3.7 and 13.1 μM

against extracellular and intracellular *L. monocytogenes*, respectively. The authors tailored the CPP and demonstrated that charge and hydrophobicity play a role in mammalian cellular uptake and intracellular location in promoting the most efficacious clearance of intracellular *Listeria*. Another fascinating pro-drug delivery strategy explored by the Kelley group was designed and investigated using methotrexate (Mtx) to treat intracellular phagosolic mycobacterial infections.[86] Their intricate three-fold drug design included a cyclohexyl and guanidinium-rich CPP conjugated to Mtx with a cleavable negatively charged shielding peptide to promote endosomal uptake (**Figure 1.6**). Once inside the cell and in the vicinity of intracellular mycobacteria that secrete β-lactamases when active, they showed that the cephalosporin linkage between the shielding peptide and Mtx-CPP was cleaved. The internalized Mtx-CPP successfully accumulated in mammalian cells and eradicated localized intracellular mycobacteria in RAW264.7 cells with minimal observed cellular toxicity.

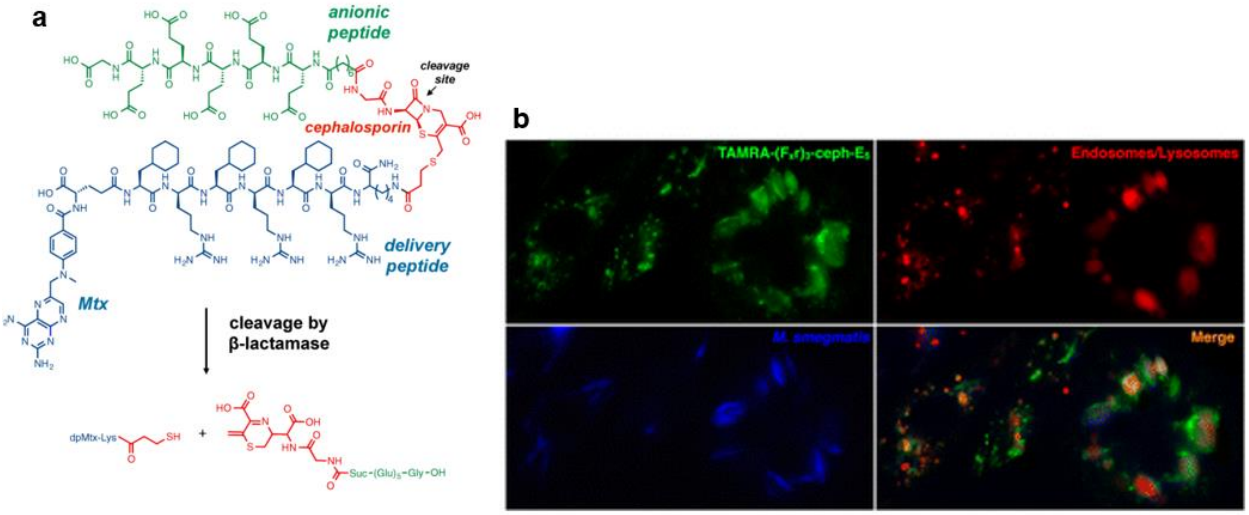

Figure 1.6. (a) Drug design of $(F_xr)_3$-Ceph-E_5 conjugate. (b) Wide-field fluorescence microscopy of TAMRA-$(F_xr)_3$-Ceph-E_5 (6 μM) with endosomes/lysosomes (dextran, Alexa Fluor 647; 10 kDa MW) and M. smegmatis (labeled with Marina Blue-NHS) after 24 h of incubation in RAW264.7 macrophages. Reprinted (adapted) with permission.[86] Copyright (2015), American Chemical Society."

More recently, the Kelley group facilely conjugated the same cyclohexyl and guanidinium-rich CPP to nalidixic acid, a quinoline-based Gram-negative antibiotic with poor pharmacokinetics.[87] In doing so, their conjugates exhibited increased bacterial uptake in *S. aureus* and enhanced

antibacterial activity against sensitive and drug-resistant *S. aureus.* The authors determined that the CPP conjugation allowed nalidixic acid to overcome the intrinsic resistance of *S. aureus* and inhibit bacterial DNA gyrase as the mode of action.

Fosmidomycin, an antibiotic used to treat Gram-negative bacterial and parasitic infections, was improved through amide conjugation to the CPP octa-arginine. Not only was this covalent conjugate and non-covalently bound complex effective against parasitic *Plasmodium* and *Toxoplasma*, the conjugate was effective in accumulation within the parasite or bacteria, and displayed activity against *Mycobacterium*, for which fosmidomycin is ineffective (**Figure 1.7**).[88] Another antiparasitic drug, miltefosine (MT), was conjugated to the CPP Tat via a cleavable disulfide or non-cleavable thioether linkage. Both conjugates enter and kill both promastigote and intracellular amastigote forms of *Leishmania*. Additionally, the Tat peptide mediated the accumulation of MT in both *Leishmania*, macrophages, and intracellular *Leishmania*, demonstrating an effective strategy in treating intracellular infections.[89-90]

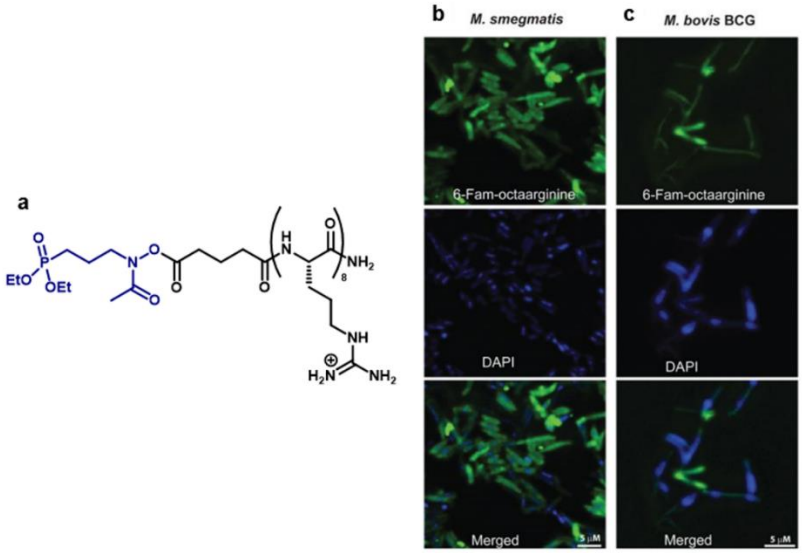

Figure 1.7. (a) Structure of fosmidomycin-R8 (FAM-octaarginine). (b and c) Fluorescent micrographs of *Mycobacterium smegmatis* (b) and *Mycobacteria bovis* BCG (c) showing incorporation of FAM-octaarginine (green). DAPI (blue) is shown as a reference for bacterial DNA. Reprinted with permission.[88] Copyright 2013, The American Society of Microbiology.

Antimicrobial photodynamic therapy (PDT) has shown promise in treating infections, due to the mechanism of generating singlet oxygen and radical species to kill bacteria. Bourré and coauthors developed a maleimide linked Tat-porphyrin conjugate.[91] Interestingly, Bourré's Tat-

porphyrin conjugate was effective in killing both Gram-negative and Gram-positive bacteria where PDT is typically less effective in Gram-negative bacteria. It was concluded that the activity of this Tat conjugate was the result of the combined effects of membrane destabilization from Tat and induction of toxic reactive oxygen species from the porphyrin photosensitizer.

1.3.4 AMP-CPP conjugates

Antimicrobial peptides and cell penetrating peptides can be combined to afford a therapy with the shared advantages of each. For instance, Wang and coworkers constructed a cell-penetrating peptide and antimicrobial peptide (CPP-AMP) conjugate.[92] They used N2, an AMP with excellent antimicrobial activity against Gram-negative infections such as *E. coli* and S. *typhimurium*, and conjugated it via an amide linkage to the CPPs, Tat or bLFcin$_6$. Intracellular uptake was visualized, and both conjugates were localized primarily in endosomes of RAW264.7 macrophage cells (**Figure 1.8**). The N2 peptide alone did not display strong fluorescence, justifying that the CPP-conjugate improved intracellular delivery. Both conjugates also displayed enhanced *in vitro* bactericidal activity against *Salmonella* as compared to N2 alone, and both eradicated over 90% of intracellular *Salmonella* after 3 hours at 10 μM concentration in macrophage cells. These authors also designed a CPP-AMP conjugate using a cathepsin-cleavable linker conjugating Tat to a similar cyclic AMP, N6.[93] They showed enhanced cellular uptake in macrophage cells compared to N6, and over 65% enhanced antimicrobial activity against intracellular *S. typhimurium* in RAW264.7 macrophage cells with almost no hemolysis or cytotoxicity. The survival of *S. typhimurium*-infected mice also improved by over 65% compared to N6.

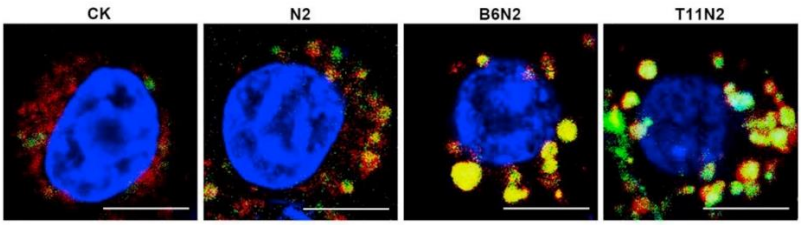

Figure 1.8. FITC-labeled CPPs-N2 uptake in RAW264.7 cells. Partially enlarged details of figures analyzed by confocal microscopy. Scale bar = 7.5 μm. CK: Control of free FITC. Cells were incubated with 5 μM FITC-labeled CPPs-N2 conjugates (green); the nucleus and cell membrane were counterstained with Hoechst 33342 nucleus stain (blue) and FM 4–64 endosomal membrane stain (red), respectively. Reprinted with permission.[92] Copyright 2018, from Elsevier.

AMPs magainin and M15 were conjugated to polyarginine, R9, through simple amide linkage and peptide elongation.[94] Both AMP-CPP conjugates displayed broad-spectrum antimicrobial activity with a modest increases against Gram-positive activity and a 4- to 16-fold increase against Gram-negative bacteria compared to AMPs alone. The conjugates also showed an increase in bacterial internalization in *E. coli* and DNA affinity. Thus, this suggests additional antimicrobial functions like internal targeting of the AMP-CPP conjugates, adding to the AMP membrane disruption as the primary mode of action.

Using a similarly straightforward peptide synthesis and elongation strategy, a hydrophobic peptide pheromone (DILIIVGG) of *Streptococcus agalactiae* and a CPP (KERKKRRR) were conjugated and investigated by the Lyu and Shan groups.[95] A series of conjugates with truncated and rearranged amino acids were synthesized to explore the best conjugate with targeted intracellular antibacterial activity. The authors reasoned that adding the hydrophobic pheromone to the cationic CPP, would not only increase the specificity of the conjugate but also increase the amphiphilicity to impart antibacterial character to the conjugate, as amphiphilicity is a common characteristic of AMPs. Thus, they proposed a specific, antimicrobial, and cell penetrating therapy. Multiple conjugates displayed good broad-spectrum antibacterial activity against *S. aureus, S. epidermidis, S. agalactiae, E. coli, P. aueruginosa,* and *S. typhimurium*. These peptides also reduced S. agalactiae load by over 95% in RAW264.7 macrophage cells and reduced the bacterial load in a mouse *in vivo* model.

Peptide nucleic acids (PNAs) are conjugates that offer a delivery method for antimicrobial gene silencing nucleic acids in order to reach their intracellular targets within mammalian and/or bacterial cells. Through the conjugation of oligonucleotides to CPPs to generate a PNA, enhanced

intracellular and gene-specific killing of bacteria can be accomplished. A phosphorodiamidate morpholino oligonucleotide was amide coupled to a CPP derived from a protein found in human T cells, YARVRRRGPRGYARVRRRGPRRC, via an amide linkage. This conjugate was used to target a highly conserved *Gyrase A* gene of *E. coli* and change gene expression to ultimately kill bacteria.[96-97] Furthermore, this conjugate was effective in accumulating within bacteria due to its CPP component and successful in inactivating a broad-spectrum of bacteria with the conserved gene sequences. The Seleem group has used a similar strategy and also used PNAs that silence essential genes within bacteria.[98] The nucleic acid sequence targeted the *rpoA* gene, which encodes a subunit of RNA polymerase that is essential for *L. monocytogenes* viability. Through conjugation of CPPs (Tat, $(RXR)_4XB$, and $(RFR)_4XB$) to the nucleic acid sequence, the authors demonstrated that an *L. monocytogenes* infection could be cleared in *in vitro* culture within 20 minutes at 8 μM and in infected J774A.1 macrophage cells after 4 hours at 8 μM. These PNAs also displayed nearly 100% reduction in *L. monocytogenes* in a *C. elegans* model at 16 and 32 μM.

1.4 Conclusions and Perspective

Nearly a century has passed since the discovery of the first antibiotic. In this "golden era", optimism for treating diseases reached its peak, and quickly faded as antibiotic resistance overshadowed the practicality of permanently curing transmissible diseases. The modification of existing antibiotic scaffolds by conjugation with cell-penetrating peptides to provide drug-peptide conjugates shows potential in reviving ineffective treatments. Accessing internalized targets, improving pharmacokinetics, and managing resistance are all advantages in employing CPPs.

In this review, we highlighted many examples of antibiotic-CPP conjugates with improved antibacterial activity compared to the unaccompanied antibiotic. Many conjugates displayed activity against a range of drug-resistant bacteria and bacteria within mammalian cells. Traditional antibiotics such as aminoglycosides and glycopeptides were demonstrated to reach intracellular locations with little to no toxicity to mammalian cells. The CPPs not only play a role in accessing previously inaccessible locations, but also may interact with bacterial membranes in a synergistic fashion to improve the bactericidal action.

Increasing the arsenal of antimicrobial drugs from those previously dismissed due to poor internalization or disposition to resistance can be achieved. Additional optimization and translation to clinical trials for these conjugates is highly anticipated for the future. The outlook is bright for

antibiotic-CPP conjugates, and these therapies provide a potential avenue to address challenging bacterial infections.

CHAPTER 2. DESIGN, SYNTHESIS, AND INVESTIGATION OF BROAD-SPECTRUM, DUAL-THERAPEUTIC VANCOMYCIN-CAPH CONJUGATES

2.1 Introduction

Vancomycin is a glycopeptide antibiotic widely used to treat Gram-positive bacterial infections. Since its introduction more than 50 years ago, vancomycin has been regarded as critically important for human health by the World Health Organization.[99] In addition, it is deemed the "antibiotic of last resort" to treat life-threatening methicillin-resistant *S. aureus* infections. Vancomycin showed great promise for 30 years until a range of vancomycin-resistant strains of bacteria surfaced.[100] Vancomycin-resistant enterococci and methicillin-resistant *S. aureus* are listed as "serious threats" by the CDC due to the limited options in treating these infections.

In drug-sensitive bacteria, vancomycin forms five hydrogen bonds with a pentapeptide on Lipid II in the peptidoglycan layer of a Gram-positive cell wall. Specifically, vancomycin binds the terminal D-Ala-D-Ala sequence **(Figure 2.1 A**). Through this interaction, vancomycin blocks the bacterial transpeptidase enzyme from cross-linking the components of the peptidoglycan to form a fully intact cell wall. The resulting internal pressure bursts the cell wall, thus killing the bacteria. For vancomycin-resistant strains (VanA, VanB, and VanC) of bacteria, the target of vancomycin binding is altered to prevent the tight binding necessary for activity.[100-101] A lactic acid (VanA, VanB) or serine (VanC) residue is substituted in place of the terminal alanine residue in the pentapeptide chain. In the altering an amide bond to an ester (VanA, VanB), the loss of a single hydrogen bond and the destabilizing lone pair/lone pair electrostatic interaction introduced with the ester oxygen results in a 1000-fold decrease in binding affinity (**Figure 2.1 B**).[102-103] VanC resistance has been documented only in a few clinical isolates. The hydroxymethyl sidechain of D-serine is thought to sterically disrupt the optimal geometry for vancomycin binding, resulting in about a sixfold decrease in affinity for vancomycin.[104-105] The decrease in binding affinity allows the transpeptidase enzyme to displace vancomycin and crosslink the peptidoglycan strands, leading to an intact cell wall. There is an urgent need to produce modified vancomycin antibiotics that can restore or enhance binding affinity to the peptidoglycan or create an alternative route to combat resistance.

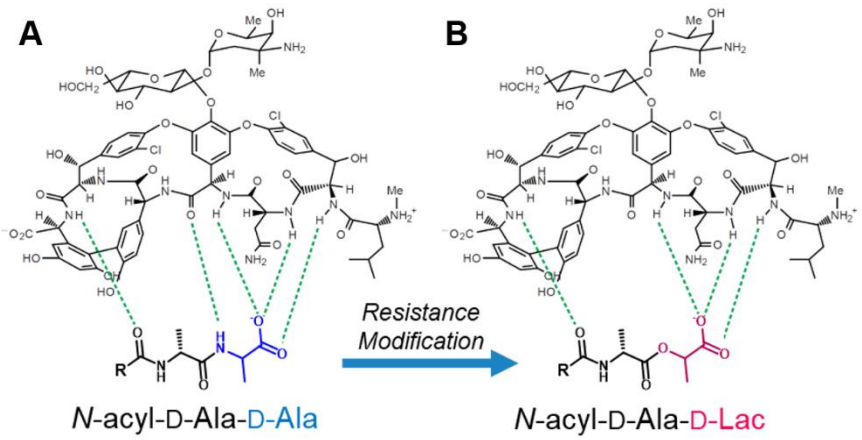

Figure 2.1 The binding affinity of vancomycin to the peptidoglycan pentapeptide (A) decreases due to the loss of a hydrogen bond in resistant bacteria (B).[104]

Vancomycin's inability to traverse bacterial membranes accounts for its narrow spectrum of activity against Gram-positive infections. Gram-positive bacteria possess only the cytoplasmic membrane; therefore, vancomycin can target the peptidoglycan layer without crossing a bacterial membrane (**Figure 2.2 A**).[106] Vancomycin is ineffective in treating Gram-negative infections due to the presence of an outer membrane; therefore vancomycin cannot localize with the peptidoglycan target (**Figure 2.2 B**).

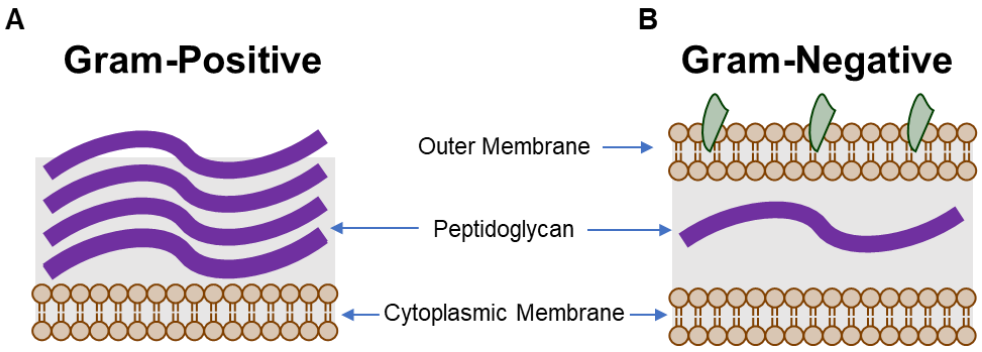

Figure 2.2. The differences in bacterial walls between (A) Gram-positive and (B) Gram-negative bacteria.

Not only is resistance an impediment in treating infections with vancomycin, but mammalian membrane penetration is also an obstacle in vancomycin reaching its full therapeutic potential. Many pathogens causing acute infections are cleared through the host immune system

or by conventional antibiotics. However, a subcategory of intracellular pathogens can establish persistent and chronic infections by residing and proliferating inside host immune cells, primarily macrophages.[107-108] *Staphylococcus aureus* is a well-known Gram-positive pathogen that possesses diverse survival strategies among strains and host cell types, including intracellular survival. Once internalized by phagocytosis, *S. aureus* can replicate in the phagosome or freely in the cytoplasm of its host cells. It induces cell death mechanisms upon escape from the phagosome to the cytoplasm of phagocytes.[109-110] Options in treating intracellular *Staphylococcus* infections within mammalian cells are limited due to the poor mammalian membrane permeability of many hydrophilic antibiotics, including vancomycin and other glycopeptides.[12-15] Some modifications, such as the lipophilic encapsulation of these hydrophilic antibiotics like vancomycin and gentamicin, has been used to bypass the mammalian membrane and deliver drugs to the mammalian intracellular environment.[111-113] Such modifications can improve delivery, but do not alter bacterial resistance to vancomycin.

Vancomycin exhibits poor efficacy against intracellular methicillin-susceptible, methicillin-resistant, vancomycin-intermediate and vancomycin-resistant *S. aureus*.[114-115] Therefore, even if an antibiotic is effective against extracellular bacteria, it may be ineffective in clearing intracellular pathogens that may become infectious in time. In order to effectively treat intracellular bacteria, and open the possibility of broad-spectrum activity, increasing the hydrophobicity of vancomycin to permeate mammalian membranes is necessary for improved vancomycin activity. Utility of cell-penetrating agents with vancomycin has also been explored to improve mammalian cell penetration and activity, yet improvements can be made.

2.1.1 Vancomycin modifications and derivatives

Since the discovery of vancomycin resistance in the late-1980s, many approaches have been used to increase the potency of vancomycin toward drug-resistant and/or intracellular Gram-positive bacteria, in addition to increase the spectrum of activity against Gram-negative bacteria.[116-117] Bringing new drugs to the clinic as resistance develops is a constant battle, but continual progress is ongoing. Over the years, novel glycopeptides such as teicoplanin and the more recent telavancin, dalbavancin, and ortavancin have gained approval and have had longevity in clinic due to their relatively slow development of resistance.[118] This progress has been made through the careful study of vancomycin's pharmacokinetic properties and mode of action.

A number of core and peripheral modifications have been made to vancomycin to improve binding to the target pentapeptide and the resistant lactic acid adaptation. Core modifications to the amino acid residues required significant synthetic manipulations but afforded an increase in affinity for terminal D-Ala-D-Lac, thus improving strategies in treating resistant bacteria.[60, 103, 119-122] Peripheral modifications provide synthetic ease, and the use of the carboxylic acid terminus as a handle for manipulation has provided the opportunity to form an additional direct hydrogen bond with the pentapeptide ligand.[123] The Haldar group has made use of the C- terminal modification of vancomycin, in addition to using membrane and cell wall interacting components through the addition of lipophilic sugars,[124] cationic lipids,[52-56] and pyrophosphate binding moieties.[57-58] Furthermore, the incorporation of sulfonium-based cationic lipophilic components to the periphery of vancomycin led to enhanced interaction with the negatively charged bacterial cell membrane and increased bactericidal activity through membrane disruption.[59] Boger and coworkers have built upon the chlorobiphenyl (CBP) modification used in ortavancin to incorporate a quaternary ammonium ion for membrane activity resulting in better bactericidal activity.[60-61] Other lipophilic and cell surface-interacting vancomycin derivatives have shown increased activity in treating vancomycin resistance as described in Chapter 1.[62-67] Clearly, modifying vancomycin to treat resistant and broad-spectrum bacteria is continuing to broaden our future arsenal of antibiotic treatments.

2.1.2 Cationic amphiphilic polyproline helices (CAPHs)

A novel class of peptides with both antimicrobial and cell-penetrating characteristics have been developed and engineered in the Chmielewski lab to serve as dual therapeutic agents. These cationic amphiphilic polyproline helices (CAPHs) are composed of both cationic and amphiphilic components appended to a polyproline backbone. The polyproline backbone allows for the peptide to adopt a stable, yet flexible, polyproline type II (PPII) secondary structure (**Figure 2.3 A**).[125] Proline-rich antimicrobial peptides (PrAMPs) present an advantage over traditional AMPs in that many are not membrane lytic.[39] PrAMPs can also be translocated within both bacterial and mammalian cells, and they have multiple intracellular targets within bacteria that can slow the emergence of resistence.[126-127] Although CAPHs are designed with unnatural proline derivatives, they share some characteristics such as secondary structure, antibacterial properties, and non-lytic membrane proclivity.

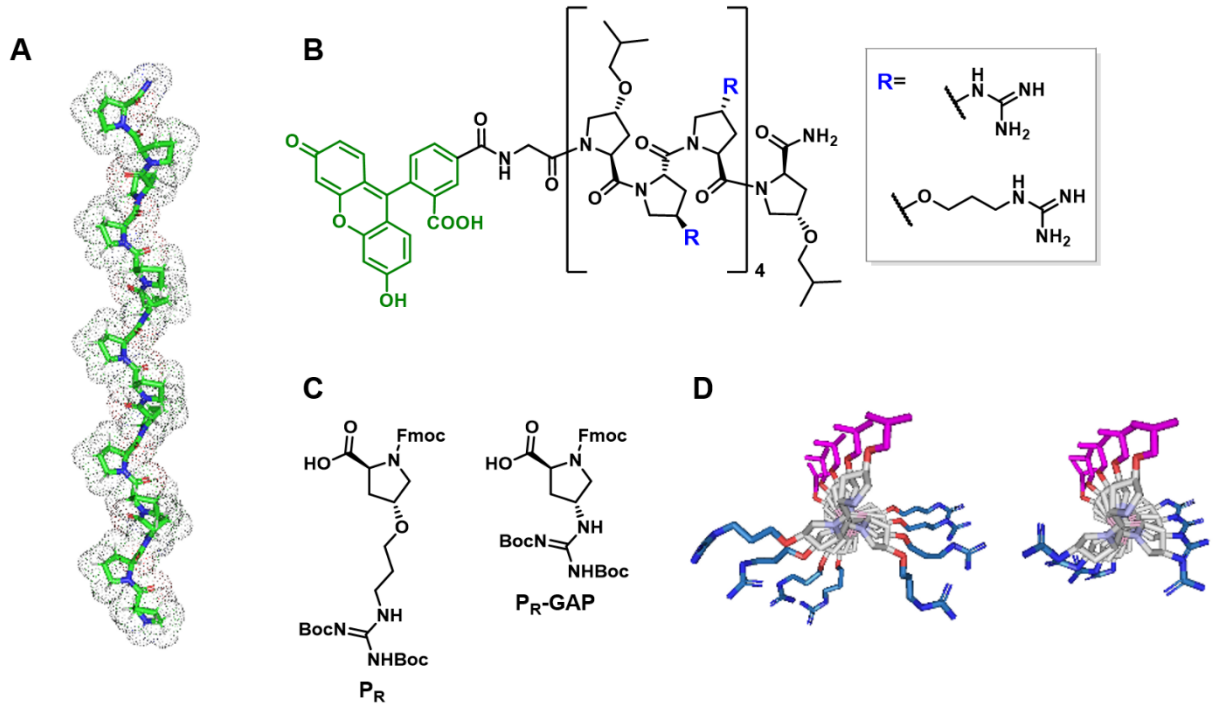

Figure 2.3. (A) Side view of a polyproline helix, PPII secondary structure. (B) Structure of CAPHs with P_R or P_R-GAP cationic amino acids. (C) Cationic amino acids Fmoc-P_R and Fmoc-P_R-GAP. (D) Top view of CAPHs, P14LRR and P14GAP.

Amphiphilicity with cationic and hydrophobic residues on the faces of the CAPH PPII prove to be vital in the specificity and intracellular location of mammalian cellular accumulation. Previous work has revealed that variations in the hydrophobic residues of a CAPH can result in changes to cell selectivity[36] and changes in mammalian subcellular location.[35, 40-42] Changes in the cationic residues generally resulted in changes in mammalian cellular uptake. For instance, the CAPHs with an arginine-like guanidinium modification accumulated in mammalian cells two times greater than the lysine-like primary amine modification.[37] By substituting the P_R-GAP amino acid for P_R, consequently shortening the length of the guanidinium group from the proline backbone, a more rigid scaffold was designed (**Figure 2.3 B, C, D**). This **P14GAP** peptide had better cell accumulation than **P14LRR** (up to 7-fold), and this peptide displayed significantly increased antibacterial activity against a range of pathogens. **P14GAP** was also able to completely eradicate two major pathogenic bacteria, *A. baumannii* and *Shigella*, from macrophage cells, as well as drastically decreased the amount of *Listeria, MRSA, and S. epidermidis in cyto* experiments.[42] The

dramatic increase in cell uptake and intracellular clearance support the potential of this peptide for antimicrobial therapy.

The length of the CAPHs also play a role in activity. Because CAPHs are composed of a repeating triad, peptide length increases corresponded to the addition of one repeating triad unit where the net charge of the peptide increased by two. Conventionally, the increase in charge of a peptide has resulted in increased mammalian cell uptake while also increasing bacterial membrane disruption and minimum inhibitory concentration (MIC).[128-129] The increase in charge for CAPHs ranging from P8LRR-P17LRR yielded consistent corresponding increases in mammalian cell uptake and MICs.[35, 37, 43, 45] This class of peptides has shown its potential in offering tunable antibiotic activity.

2.1.3 Vancomycin-Cationic Amphiphilic Polyproline Helix (CAPH) Strategy

Conjugating lipophilic and cationic components to vancomcyin has recently appeared as a promising strategy in treating difficult bacterial infections by combining different mechanisms of action to overcome resistance. Vancomycin homodimers were some of the first conjugates to address vancomycin resistance. The strategy behind dimerizing vancomycin lies in the back-to-back hydrogen bond-based dimerization that vancomycin adopts in binding its target.[130] Therefore, multiple adaptations of linker strategies to covalently dimerize vancomycin have shown an increase in binding affinity and resulting increases in potency.[131-137]

The conjugation of vancomycin to other antibiotics has also been explored. For instance, nisin, an antimicrobial peptide that binds pyrophosphate of lipid II, was conjugated to vancomycin with successful increase in potency against resistant bacteria.[138] Conjugates between vancomycin and β-lactam antibiotics have been investigated to improve potency against sensitive and resistant bacterial strains.[139-141] Conjugation of vancomycin to cathelicidin-related antimicrobial peptides (CRAMPs) provided vancomycin with an additional mode of action against bacteria, disruption of cytoplasmic membrane. A variety of linkers between the vancomycin and CRAMPs was used and many of the compounds showed broad-spectrum activity in addition to antibiofilm formation.[142]

Although vancomycin shows poor mammalian membrane penetration, ortavancin and telavancin glycopeptides show an improvement in clearing intracellular infections.[114-115] Strategies of conjugating cell-penetrating peptides to vancomycin have been reported (described in Chapter 1). Herein, we wish to describe further strategies in targeting bacteria residing within mammalian

cells. The Chmielewski group has described a reversible kanamycin-P14LRR conjugate that that potently clears intracellular pathogens (described in Chapter 1). Given the success of this kanamycin-CAPH conjugate design, we were poised to investigate new antibiotic-CAPH conjugates with vancomycin replacing kanamycin. This approach would allow, under similar physiological conditions, the delivery of a poorly penetrable antibiotic and antimicrobial peptide to cellular locations without compromising mammalian cell integrity (**Figure 2.4 B**). We hypothesize that the conjugate will be capable of a dual method of killing bacteria. As a conjugate in the extracellular environment, we anticipate bactericidal activity; and, once delivered inside a mammalian cell, we anticipate the reduction of the disulfide linkage to release both antibiotics for dual killing of bacteria.

Herein, we designed a reducible disulfide-linked conjugate, **VanP14S**, and a non-reducible conjugate, **VanMalP14** (**Figure 2.4 A**). The use of two different conjugation approaches will allow us to determine whether intracellular release of vancomycin and **P14LRR-SH** is necessary for the most potent activity in mammalian cells. The **VanMalP14** conjugate linkage was chosen to undergo a facile thiol-maleimide click reaction with **P14LRR-SH**. Moreover, a fluorescent analog, **FlVanP14S**, was synthesized to monitor vancomycin-CAPH activity in fluorescence-based assays. These vancomycin-peptide design modifications had the potential to yield interesting antibiotic activity against a range of pathogens through the combination of a Gram-positive antibiotic, vancomycin, and broad-spectrum antibiotic, **P14LRR**.

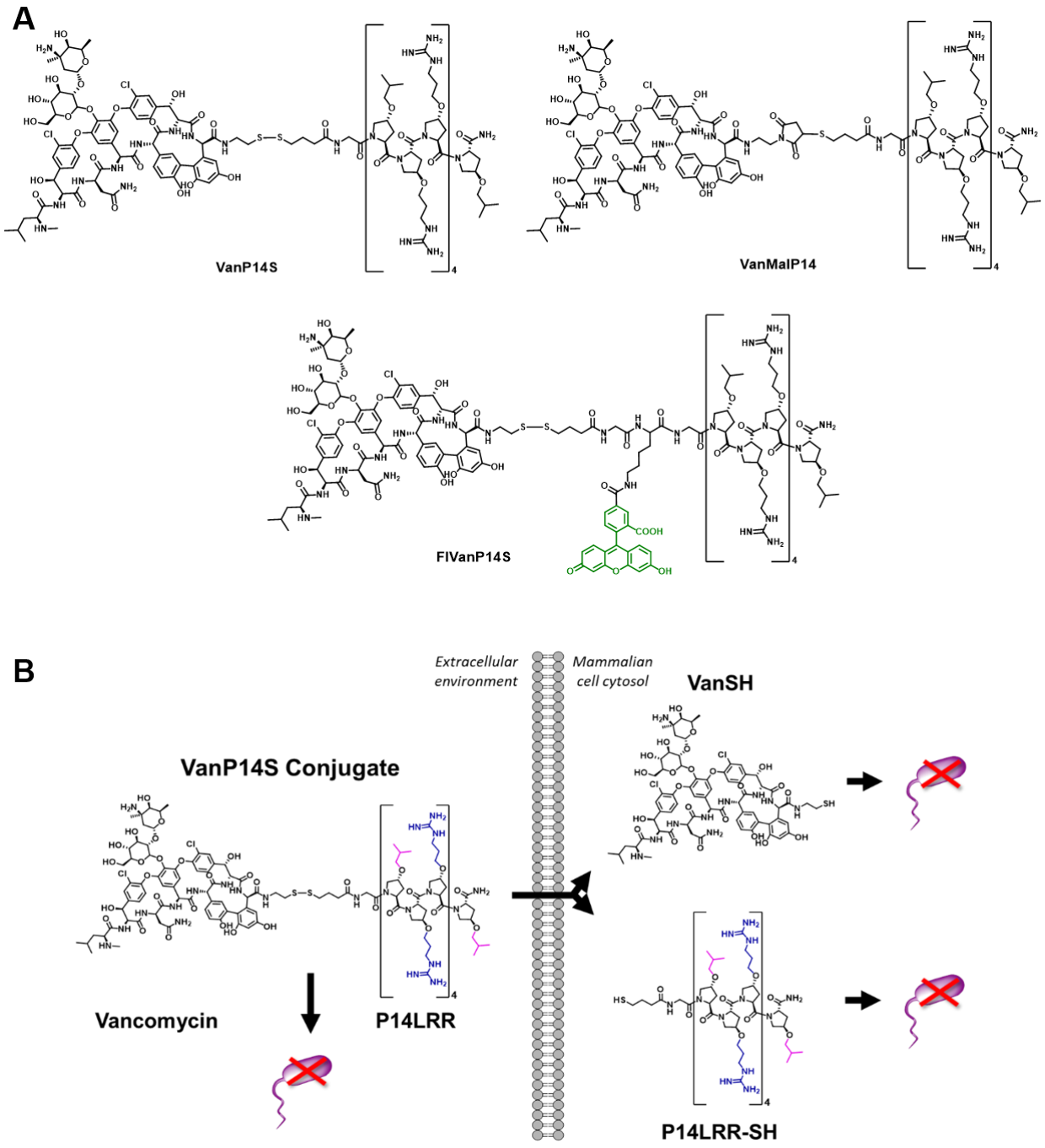

Figure 2.4. (A) Structures of vancomycin-CAPH conjugates. (B) Vancomycin-CAPH strategy in clearing drug-resistant and intracellular bacteria residing in mammalian cells. Once within a reducing environment, the disulfide linker releases vancomycin and CAPH antibiotics.

2.2 Results and Discussion

2.2.1 Synthesis of CAPH amino acids and CAPHs

To begin the synthesis of the conjugates described above, we needed the amino acids for the synthesis of the CAPH, **P14LRR-SH**. Two unnatural amino acids have been used previously, Fmoc-P_L and Fmoc-P_R. The synthesis of Fmoc-P_R has been a challenging step in the synthesis of CAPHs since their development.[37] Over the years, minor adjustments in protocol have been made to increase the yield of the final amino acid from the original published yield of 19% to 25% using a similar five step reaction scheme (**Scheme 2.1 A**). Recently, I developed a new strategy has improved the synthesis of P_R through fewer steps and an improved yield of 50% overall (**Scheme 2.1 B**).

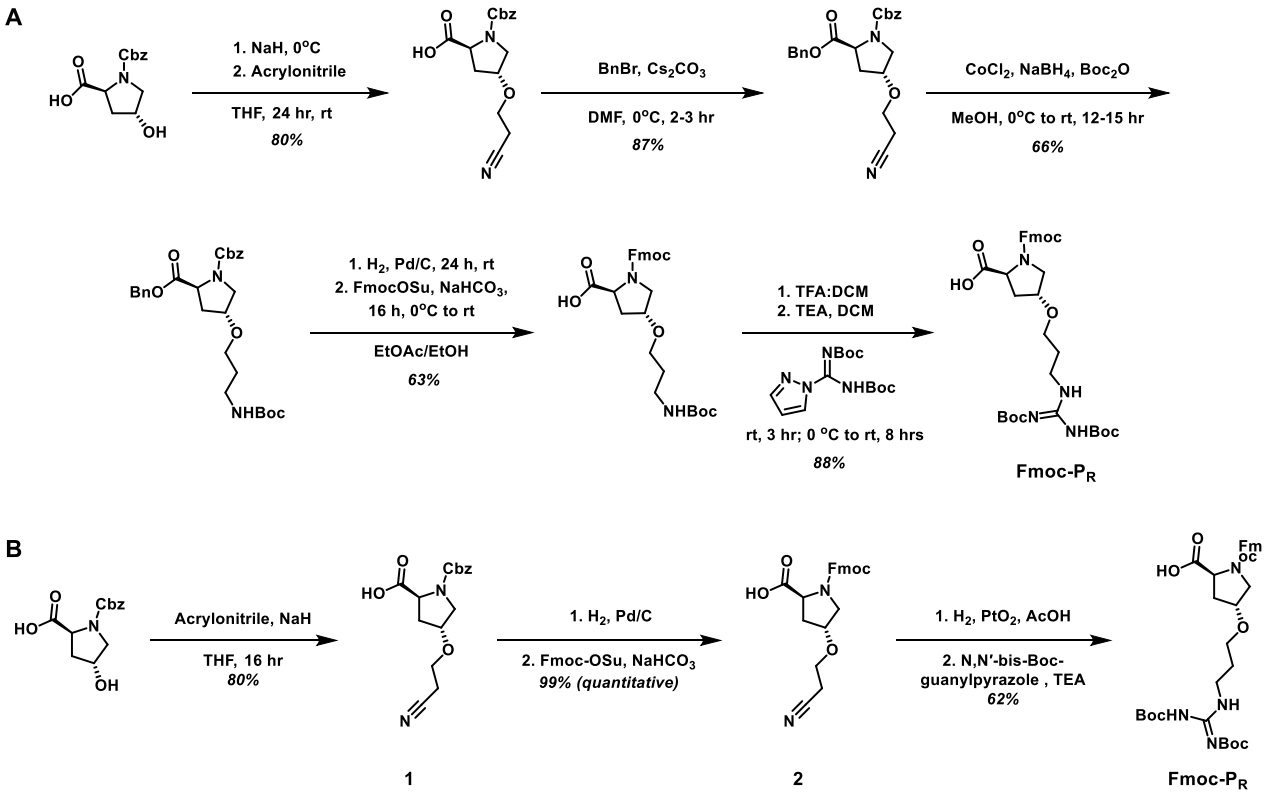

Scheme 2.1 (A) Previous five-step synthesis of Fmoc-P_R (B) Improved three-step synthesis of Fmoc-P_R

The synthesis of Fmoc-P_R begins with the O-alkylation of commercially available Z-L-hydroxyproline with acrylonitrile to form ether intermediate **1**. Hydrogenation with palladium on

carbon removed the Cbz protecting group of **1**. The resulting amine was Fmoc protected to afford intermediate **2** in quantitative yield (99% for two steps). Reduction of the nitrile of **2** was achieved using hydrogen and platinum oxide, followed by the addition of N, N'-bis-Boc-1-guanylpyrazole to yield the final product, **Fmoc-P_R**. The synthesis of hydrophobic CAPH amino acid, **Fmoc-P_L**, proceeded by the two-step literature procedure[37].

Once both unnatural amino acids were synthesized, Fmoc-based solid phase peptide synthesis (SPPS) was performed to provide the CAPH component of the conjugates. Briefly, **P14LRR-SH** and **FlP14LRR-SH** peptides were synthesized from the C- to N-terminus using a high loading (0.48 mmol/mg) ChemMatrix H-Rink Amide resin. Each amino acid was activated with HATU, coupled to the peptide-bound resin, and the semi-permanent Fmoc group was deprotected with 30% piperidine in DMF. This iterative process was continued until all amino acids were coupled (**Scheme 2.2**).

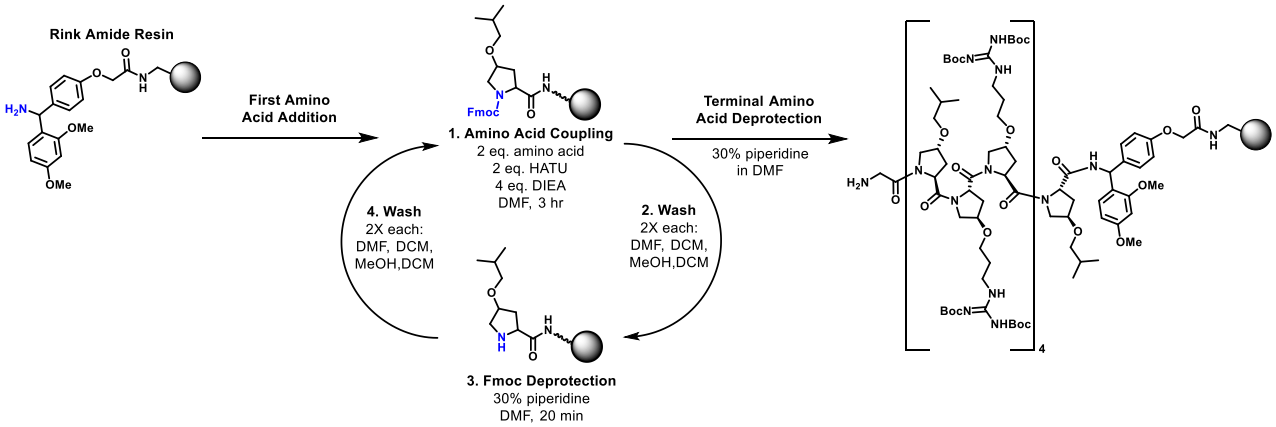

Scheme 2.2. Fmoc-based solid phase peptide synthesis of CAPHs on the Rink amide resin.

After the **P14LRR** peptide was synthesized on resin, the terminal Fmoc was removed and HATU-activated trityl-4-thiobutyric acid was added. Global deprotection and cleavage from the resin was performed using a cocktail of trifluoroacetic acid, ethanedithiol, triisopropylsilane, and water to yield crude peptide (**Scheme 2.3**). **P14LRR-SH** was purified using reverse phase HPLC (RP-HPLC) and the desired product mass was confirmed using matrix-assisted laser desorption ionization – time of flight (MALDI-ToF) mass spectrometry. A fluorescent variant, **FlP14LRR-SH,** was synthesized in order to perform experiments that require fluorescent visualization. Additional steps were taken to add fluorescein once the **P14LRR** peptide was synthesized

(**Scheme 2.4**). Two additional amino acids, Fmoc-Lys(Mtt)-OH and Fmoc-Gly-OH, were coupled. Then, the Mtt group was selectively deprotected using 30% hexafluoroisopropanol (HFIP) in DCM, followed by the coupling of fluorescein-NHS ester. Addition of trityl-4-thiobutyric acid, followed by global deprotection/cleavage, and purification of peptide by RP-HPLC proceeded similarly to **P14LRR-SH**.

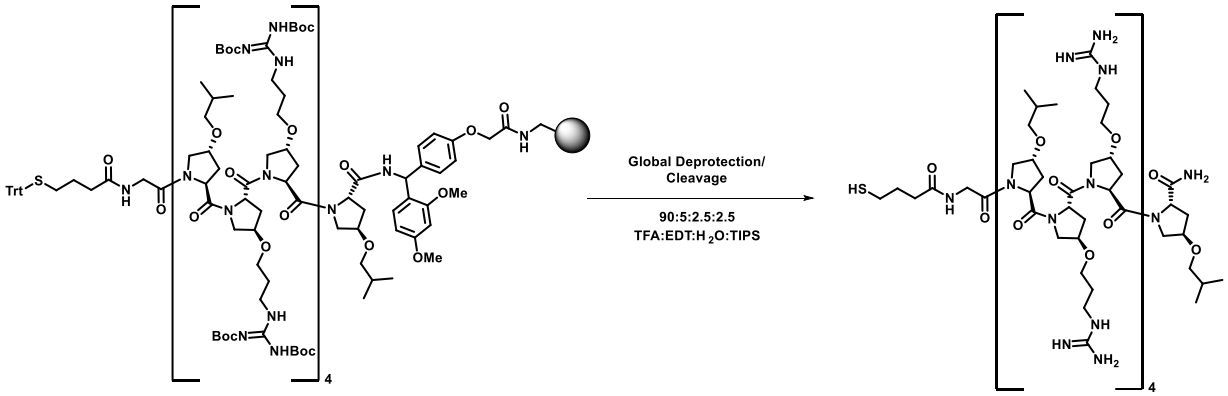

Scheme 2.3. Global deprotection and cleavage from resin with conditions for **P14LRR-SH**.

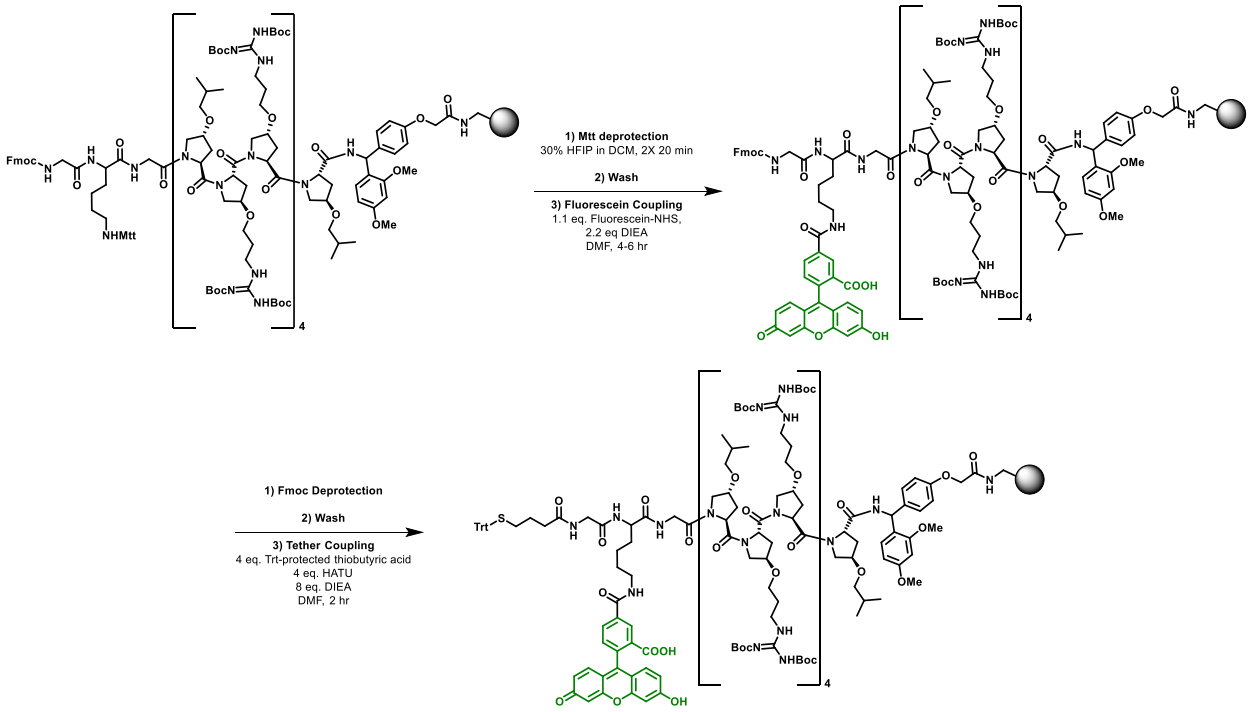

Scheme 2.4. Addition of fluorescein and thiol tether for synthesis of **FlP14LRR-SH**.

2.2.2 Activating vancomycin and conjugating vancomycin-CAPHs

Vancomycin contains a single carboxylic acid that can be modified without interrupting binding activity to the pentapeptide in the peptidoglycan of Gram-positive bacteria.[123] This position was used to covalently link the antibiotic to a CAPH. Two different moieties were chosen to determine whether cleavable or non-cleavable attachment of CAPHs is necessary for more potent activity of the conjugate. A maleimide and an activated disulfide were chosen to link the **P14LRR-SH** peptide to vancomycin to produce the non-cleavable and cleavable conjugates, respectively. Vancomycin hydrochloride was activated for coupling with CAPHs through PyBOP-mediated coupling with amine tethers to generate **VanMalP14** and **VanP14S**, respectively (**Scheme 2.5**, **Figure 2.4 A**). A fluorescent conjugate, **FlVanP14S** (**Figure 2.4 A**), was produced by disulfide exchange in the same manner as **VanP14S,** substituting the CAPH peptide, **FlP14LRR-SH** for **P14LRR-SH**.

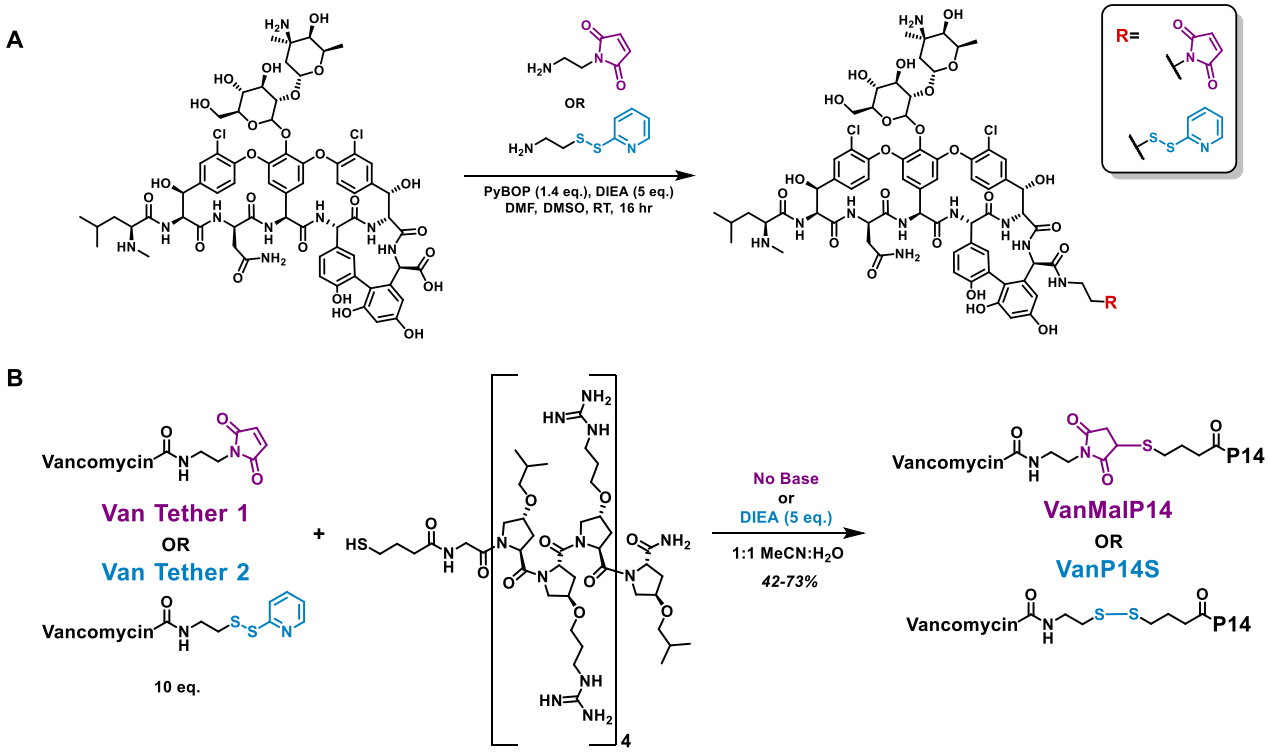

Scheme 2.5. (A) Coupling of functionalized amines to vancomycin for the synthesis of Van Tethers. (B) Conjugation of thiol-reactive vancomycin derivatives to **P14LRR-SH**

2.2.3 Synthesis of fluorescent controls

Later on, we will discuss experiments to visualize and explore mammalian cellular uptake and bacterial uptake of the fluorescent conjugate and controls. **FlP14LRR** has been widely used as a control peptide in the Chmielewski group and was synthesized by the same route as previously reported.[37, 41-42, 44-45] Fluorescent vancomycin controls were synthesized by literature procedure using fluorescein isothiocyanate (FITC) and rhodamine isothiocyanate (RhITC/RITC) (**Figure 2.5**).[69] Upon completion of the reactions, the desired products were isolated by RP-HPLC. The location of the fluorophore on the secondary amine was determined by MALDI-ToF mass spectrometry by the analysis of the fragmentation pattern (**Figure A 27** and **Figure A 28**). We confirmed by mass spectrometry that the fluorophore did not react with the glucosamine sugar of the glycopeptide.

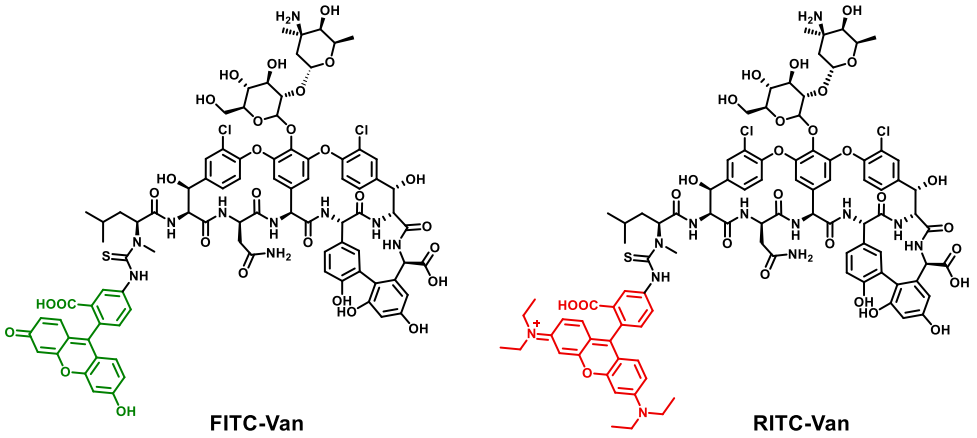

Figure 2.5. Fluorescent vancomycin controls, **FITC-Van** and **RITC-Van**.

2.2.4 Minimum inhibitory concentration against bacterial isolates

First, we wished to determine if these conjugates exhibited superior antibacterial activity compared to controls using a microbroth dilution assay (**Table 2.1**). The tested bacteria included ESKAPE pathogens, Gram-negative and Gram-positive bacteria that are the leading cause of nosocomial and multidrug-resistant infections.[143] Additionally, a range of susceptible and drug-resistant *S. aureus* were tested. Both conjugates, **VanP14S** and **VanMalP14**, displayed moderate activity against the Gram-negative *E. coli*, *A. baumannii* and *K. pneumonia.* With the same bacteria, Vancomycin, **P14LRR**, and the one-to-one mixture of vancomycin and **P14LRR**, were

not as effective against the same bacteria. This suggests that the conjugation of the two antibiotics appears necessary for bactericidal activity. Both **VanP14S** and **VanMalP14** exhibited similar activity, with a slight improvement of **VanMalP14** over **VanP14S** with *A. baumannii* 19606 and *Klebsiella*.

Table 2.1. Minimum inhibitory concentrations (MICs) of vancomycin conjugates against pathogenic bacteria isolates using the microbroth dilution assay after 20 h of treatment. Values reported in μM.

Bacteria strains (-/+)[a]	**Vancomycin**	**P14LRR**	**VanP14S**	**VanMalP14**	**Van+P14 (1:1)**
***E. coli* ATCC 25922 (-)**	>16	16	**8**	**8**	16
***A. baumannii* ATCC 19299 (-)**	>16	>16	**8**	**8**	>16
***A. baumannii* ATCC 19606 (-)**	>16	16	**4**	**2**	16
***K. pneumonia* ATCC 1706 (-)**	>16	>16	**4**	**2**	>16
***P. aeruginosa* ATCC 15442 (-)**	>16	>16	16	16	>16
***E. cloacae* ATCC 1143 (-)**	>16	>16	>16	>16	>16
***L. monocytogenes* ATCC 19111 (+)**	0.25	>16	0.5	0.5	0.25
***S. aureus* ATCC 10537 (+)**	0.5	> 16	2	2	1
MRSA USA300 (+)	0.25	>16	1	0.5	0.25
VRSA 10 (+)	>16	>16	**1**	**0.5**	>16
VRSA 7 (+)	>16	>16	**0.5**	**0.5**	>16
VRSA 5 (+)	>16	>16	**1**	**0.5**	>16
VRSA 3A (+)	>16	>16	**1**	**0.5**	16
VRSA 1 (+)	>16	>16	**0.5**	**0.5**	>16
***E. faecium* ATCC 700221 (+)**	>16	16	**0.5**	**1**	8

[a] (-/+) denotes Gram-negative or Gram-positive pathogens

Both **VanP14S** and **VanMalP14** exhibit excellent bactericidal activity against Gram-positive bacteria. For *L. monocytogenes*, susceptible *S. aureus* 10537 and *MRSA* USA300, the conjugates display good activity, however, they display an equivalent potency as vancomycin or a 1 to 1 mixture of vancomycin and **P14LRR**. Astonishingly, **VanP14S** and **VanMalP14** display exceptional activity against a range of vancomycin-resistant *S. aureus* and *Enterococcus* (MIC values of 0.5 to 1 μM), whereas vancomycin and **P14LRR,** or their 1:1 mixture, are not as effective (8, 16, or >16 μM). The activity of conjugates to each other is comparable, with **VanMalP14**

showing slightly better activity in some instances. These data show that both conjugates can overcome resistance that vancomycin typically displays. These data indicate a broad-spectrum activity previously unobserved for vancomycin, and notably improved activity for the broad-spectrum CPP, **P14LRR**.

2.2.5 Time to kill experiments with *S. aureus*

We next investigated the time-to-kill curves of the conjugates against *S. aureus* (**Figure 2.6**). By observing the time to kill bacteria, we can verify whether drugs are bacteriostatic or bactericidal.[144] Rapid killing of bacteria has often been reported for cationic AMPs that disrupt bacterial membrane integrity and function, resulting in bacterial death.[145] Both conjugates, **VanP14S** and **VanMalP14**, exhibited rapid bactericidal killing at 4-6 hours and 2-4 hours as compared to vancomycin at 2X and 5X their MIC values, respectively. At 2X MIC, **VanP14S** kills somewhat faster than **VanMalP14**, while the opposite is observed at 5X MIC. Although slightly different times to eradicate bacteria *in vitro* were observed, the comparable times of the two conjugates may indicate that the reversible and irreversible linkages between vancomycin and CAPH do not play a differing role in antimicrobial action. This increased speed of killing for the conjugates compared to vancomycin may indicate enhanced bacterial membrane disruption, common to AMPs.

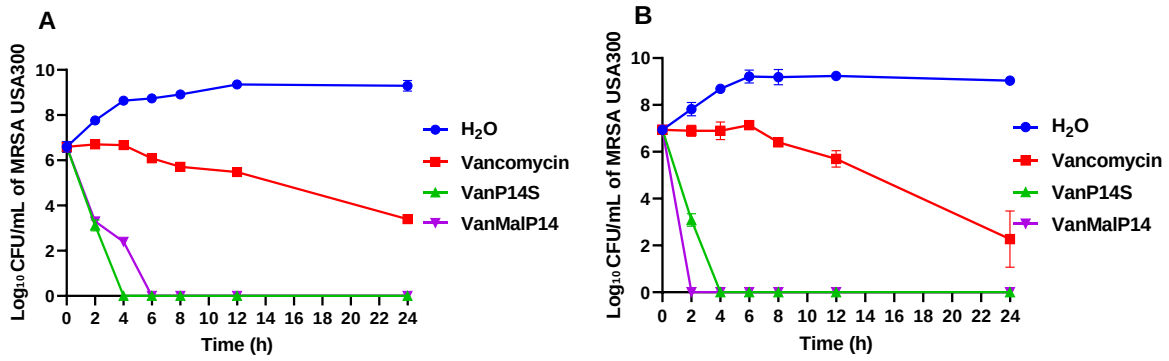

Figure 2.6. Killing kinetics of vancomycin-P14LRR conjugates in comparison to vancomycin at (A) 2X and (B) 5X their MIC values against methicillin-resistant *Staphylococcus aureus* NRS 384 (MRSA USA 300) over a 24-hour incubation period. Water served as a negative control and vancomycin served as a control drug. Error bars represent standard deviation values obtained from triplicate samples used for each test agent.

2.2.6 Cell toxicity studies

Having established excellent antibacterial activity, we next wanted to probe toxicity toward human red blood cells (hRBC) and mammalian macrophage cells (J774A.1). Although the CPP **P14LRR** peptide has reported antimicrobial activity, it does not demonstrate a lytic mechanism of action like many antimicrobial peptides, such as melittin.[146] In this experiment, conjugates were incubated for one hour with hRBCs. If the RBCs were lysed by the compounds, heme would be released and detected in the supernatant by UV-Vis spectroscopy. After one hour of incubation with hRBCs, we confirmed that neither conjugate displayed red blood cell hemolysis at concentrations up to 40 µM, consistent with the individual non-lytic behaviors of vancomycin and **P14LRR** (**Figure 2.7 A**).

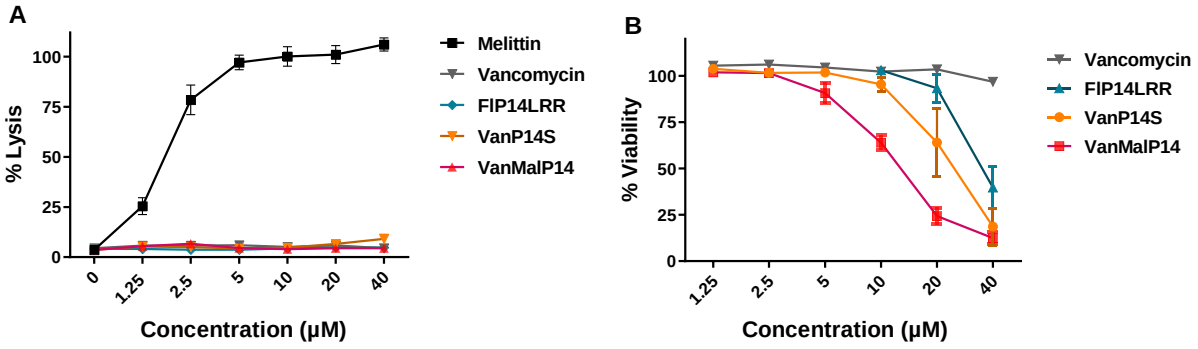

Figure 2.7. (A) Hemolysis assay measuring the release of hemoglobin from hRBC. Melittin was used as a positive control, and values normalized against 0.1% triton X-100. (B) Cytotoxicity measuring J774A.1 cell viability using an MTT assay after 9-hour incubation with compounds.

Because macrophage cells are capable of harboring bacteria in a refuge from external antibiotics, we wish to carry out internalization experiments with a J774A.1 macrophage cell line. Therefore, we evaluated the viability of mammalian cells in the presence of vancomycin-P14LRR conjugates at concentrations ranging from 1.25 µM to 40 µM for 9 hours (**Figure 2.7 B**).[147] The results show increased cytotoxicity of both conjugates compared to vancomycin and P14LRR, but the decreased viability starts at 10 µM and 20 µM for **VanMalP14** and **VanP14S**, respectively. Although there is a decrease in viability at 10 µM and 20 µM, these concentrations are greater than most Gram-negative bacterial MICs and about 10-fold higher than the selected *S. aureus* and

Enterococcus MICs. Because the cytotoxic concentrations of conjugates remain higher than MICs, toxicity should not be an obstacle in the implementation of these conjugates.

2.2.7 Confocal microscopy to visualize cellular internalization of FlVanP14S conjugate

Although mostly understood as an extracellular pathogen, *Staphylococcus aureus* is a pathogen that has long been known to evade antibiotics through internalization within macrophages and neutrophils.[148-151] Once engulfed, professional phagocytes like macrophages can harbor intracellular *S. aureus* within intracellular compartments such as phagosomes and phagolysosomes, where bacteria can replicate, kill host cells, and infect other cells in a continuous infection cycle. Residence and consequential persistence within host cells enables long-term survival. Thus, relapses in illness due to chronic infection result from the clinical failure in eradicating these intracellular reservoirs.[109] In order to effectively clear these intracellular infections, it is ideal for antibiotics to localize within the same intracellular compartments to successfully kill bacteria.

Based on the previous results that **FlP14LRR** was found to penetrate macrophage cells, we wished to study the cellular uptake of the vancomycin-CAPH conjugates. Therefore, the fluorescent vancomycin-P14LRR conjugate, **FlVanP14S**, was incubated at a concentration of 5 μM with J774A.1 macrophage cells for 1 hour. Following incubation, we further labeled cells with an endosomal marker (Lysotracker red, 300 nM) or a mitochondrial marker (Mitotracker red, 100 nM). Faint green fluorescence is observed in the cytosol; however, most of the green fluorescence appears strong and punctate. When incubated with the endosomal marker, strong overlap of the green **FlVanP14S** and red marker appears as a yellow-orange color (**Figure 2.8 A**). Whereas incubation with the red mitochondrial marker, no overlap is seen and both green and red fluorescence is partitioned (**Figure 2.8 B**). After 1 hour incubation with 10 μM **FlVanP14S**, the same results are observed; there is strong colocalization with the endosomes, and no colocalization with the mitochondria (data not shown). It can be concluded that **FlVanP14S** primarily colocalizes with endosomal vacuoles at this concentration and incubation time with some cytosolic localization. The results of this study provide evidence that this vancomycin-CPP conjugate can appropriately localize within similar vacuoles as observed for *S. aureus.*

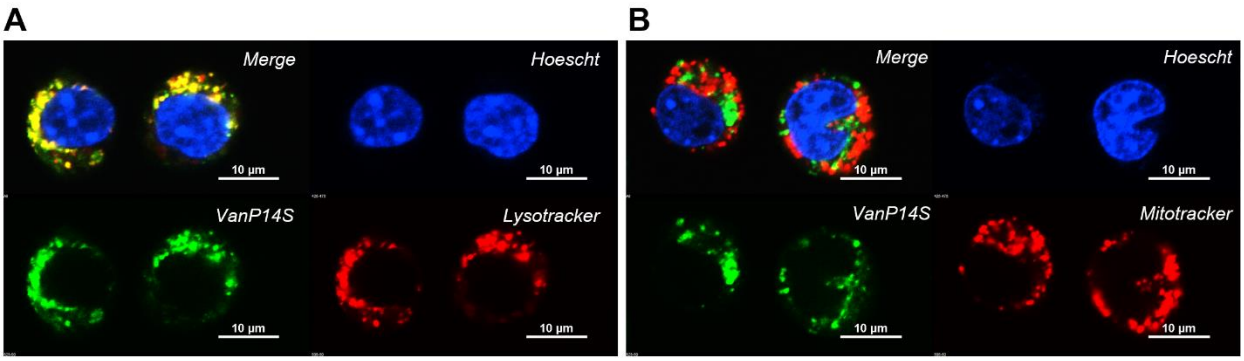

Figure 2.8. Confocal microscopy images of J774A.1 macrophage cells incubated with 5 µM FlVanP14S for 1 hr. (A) Merge (top left) and separate laser channels with Hoescht 33342 nuclear stain (blue), conjugate (green), and lysotracker lysosomal stain (red). (B) Merge (top left) and separate laser channels with Hoescht 33342 stain (blue), conjugate (green), and mitotracker mitochondrial (red). A yellow-orange color indicates colocalization of conjugate and selected red stain.

2.2.8 Flow cytometry to quantify mammalian cellular accumulation of FlVanP14S

With qualitative knowledge of conjugate location within macrophage cells, we next wanted to quantify the amount of conjugate entering mammalian cells in comparison to the poorly internalized vancomycin control, **FITC-Van**. Insufficient accumulation of therapeutic concentrations of drugs is one of the major obstacles in treating intracellular pathogens. A potential therapy for intracellular bacterial infection must efficiently enter cells and maintain an effective concentration to kill intracellular pathogens. Therefore, we monitored the cell accumulation of **FlVanP14S** in J774A.1 macrophage cells using flow cytometry. Cells were treated with a range of compound concentrations for both 1-hour and 3-hour incubation times. **FlP14LRR**, a previously reported CAPH with better cell penetration than the well-known Tat-peptide, was used as a control.[41] In this experiment, all compounds entered cells, even **FITC-Van** (**Figure 2.9**). **FlP14LRR** showed at least three-fold higher accumulation than **FITC-Van** at all concentrations at both incubation times. Encouragingly at 1-hour incubation, **FlVanP14S** showed about a 6- to10-fold increase as compared to **FITC-Van** uptake at all concentrations; whereas at a 3-hour incubation, **FlVanP14S** showed about 16- to 19-fold increases in fluorescence as compared to **FITC-Van**. These results demonstrated that **FlVanP14S** had about a 1- to 2-fold increase in uptake from **FlP14LRR** after 1-hour incubation and about a 4-fold increase at 3-hour incubation. Although unexpected, the conjugation of vancomycin to the CAPH CPP led to the increased uptake of **FlVanP14S** compared to **FlP14LRR**. Thomas Dietsche and Chmielewski coworkers have

shown N-terminal modification to the **P14LRR** peptide results in a change of cellular uptake of peptides; [44] therefore, the addition of vancomycin to the N-terminus of **P14LRR** could explain this change in cellular accumulation. Moreover, the additional cationic groups on vancomycin may also lead to an increase in cellular uptake of the conjugate compared to **P14LRR**. For instance, the extension CAPHs from **P14LRR** to **P17LRR** resulted in an increase in cellular uptake presumed to be the result of the increase in cationic character.[35, 43]

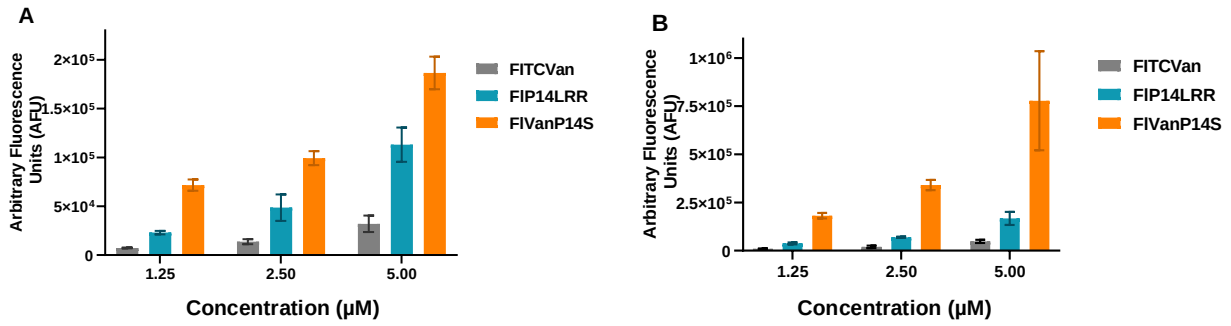

Figure 2.9. Screening the fluorescence of J774A.1 cells incubated with compounds at (A) 1-hour and (B) 3-hour incubation times.

To determine if the conjugates were fully internalized within the cells, or bound to the membrane, we used trypan blue to quench the fluorescence of surface-bound conjugates.[152-153] The amount of surface-bound **FlVanP14S** versus internalized **FlVanP14S** was measured by comparing the arbitrary fluorescence units (AFU) of cellular fluorescence quenched by trypan blue to the AFU of cells not quenched with trypan blue after 1- and 3-hour incubations using flow cytometry. After 1-hour incubation with **FlVanP14S**, surface binding accounted for 17% of the total fluorescence at 2.5 μM concentration and less than 3% of the total fluorescence at 5 μM concentration (**Figure 2. 10 A, Figure 2. 10 B**). After 3 hours of incubation with **FlVanP14S**, increased surface binding was seen, yet the majority of **FlVanP14S** was internalized. A 34% and 38% decrease in fluorescence was seen at 2.5 and 5 μM concentration, respectively (**Figure 2.10 C, Figure 2.10 D**). In all situations, **FlVanP14S** shows less than 40% surface binding as 60% of the conjugate is internalized. Accordingly, **FlVanP14S** translocation into the cell is time-dependent as the fluorescence with trypan blue more than doubles from 1 to 3 hours. More peptide accumulating into the cells, rather than remaining surface-bound, is beneficial for reaching and achieving intracellular

pathogen clearance. Confocal microscopy images confirm similar cell internalization and minimal surface-bound conjugate at 1 hour (**Figure 2.8**).

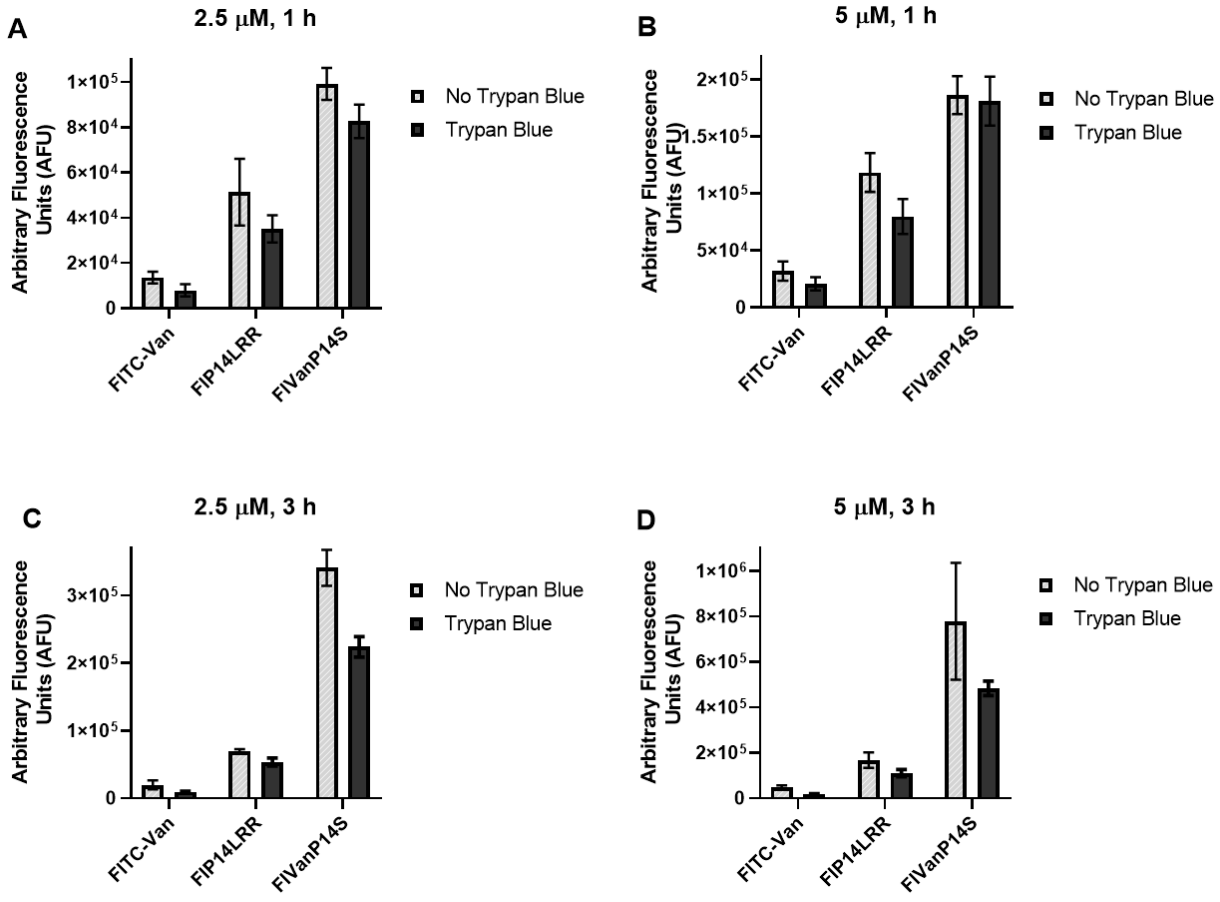

Figure 2.10. Cellular uptake studies of **FlVanP14S**, **FlP14LRR**, and **FITC-Van** at (A, B) 1 h and (C, D) 3 h in J774A.1 cells after incubation at (A, C) 2.5 μM and (B, D) 5 μM with trypan blue treatment (black bar) and without trypan blue treatment (gray bar).

2.2.9 Release kinetics of reduced Vancomycin-SH from VanP14S conjugate

VanP14S was designed with a reducible disulfide linkage to release thiol-modified vancomycin and **P14LRR-SH**, two individual antibiotics (**Figure 2.11 A**). Because vancomycin was modified from the C-terminal carboxylic acid, the reduced **Van-SH** is expected to retain equivalent activity as vancomycin. The carboxylic acid on vancomycin does not directly interact with the peptidoglycan target, therefore, the small modification should not detrimentally impact binding.[123, 154] To evaluate the half-life of the conjugate, **VanP14S** was treated with 10 mM

dithiothreitol (DTT) in PBS (pH 7.4) (**Figure 2.11 B**). **Van-SH** release was monitored using UPLC-MS and the half-life of release ($t_{1/2}$) was calculated to be about 1 minute for a single trial. This rapid reduction prompted us to move to more appropriate physiological conditions. Therefore, **VanP14S** was treated with 10 mM glutathione (GSH) in PBS (pH 7.4) (**Figure 2.11 C**).[70] **Van-SH** release was monitored using UPLC/MS and the half-life of release ($t_{1/2}$) was calculated to be 150 minutes (2.5 hours) for the experiment performed in duplicate. These studies indicate **VanP14S** is responsive to reducing environments similar to those *in cyto*.

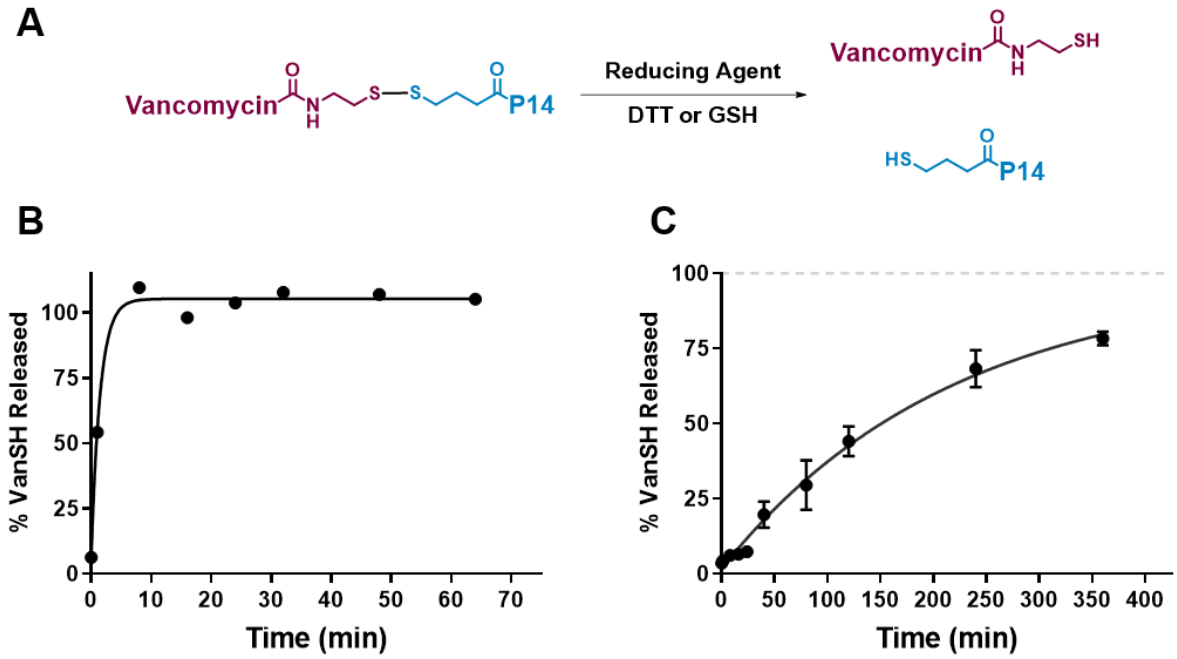

Figure 2.11. (A) Scheme of disulfide reduction and release of vancomycin-SH from VanP14S. (B) Reduction and release of vancomycin-SH using 10 mM DTT in PBS. (C) Reduction and release of vancomycin-SH using 10 mM GSH in PBS.

2.2.10 Mechanism of action studies

Both conjugates, **VanP14S** and **VanMalP14**, displayed similarly potent antibacterial activity. Therefore, we next wanted to probe their mode(s) of action. The mechanism of action common to glycopeptides is the inhibition of bacterial cell-wall synthesis through binding peptidoglycan precursors and hindering the crosslinking of the cell wall to result in cell death. Approved glycopeptides dalbavancin, ortavancin, and telavancin also possess additional interactions to disrupt membrane potential and membrane permeability.[118] We first want to explore

potential membrane interactions that these new conjugates may use in their mechanism to kill broad-spectrum and resistant pathogens.

Gram-negative membrane leakage

We first explored whether the inner membrane of Gram-negative bacteria was permeabilized by either **VanP14S** or **VanMalP14** conjugate through a β-galactosidase leakage experiment. Solutions of conjugates at concentrations 2X and 4X their MIC values were used for incubation with *E. coli* ATCC 25922. Melittin, a known membrane-lytic AMP, was used as a positive control. Bacteria were induced using isopropyl-β-D thiogalactopyranoside (IPTG), then incubated with conjugates at various concentrations for 1 hour. Next, a β-galactosidase substrate, 2-nitrophenyl-β-D-galactopyranoside (ONPG), was added. The β-galactosidase enzyme, which is released into the supernatant at concentrations relative to the amount of membrane permeability, cleaves ONPG and releases the colormetric indicator, O-nitrophenol. The concentration of the indicator can be measured by UV-Vis spectroscopy and is proportional to the amount of membrane permeability (**Figure 2.12**). The absorbance of the indicator was measured over a period of 1 hour. At both concentrations, no significant absorbance was measured for either conjugate compared to negative control. These results indicate that no significant inner membrane leakage was the result of either conjugate at the tested concentrations.

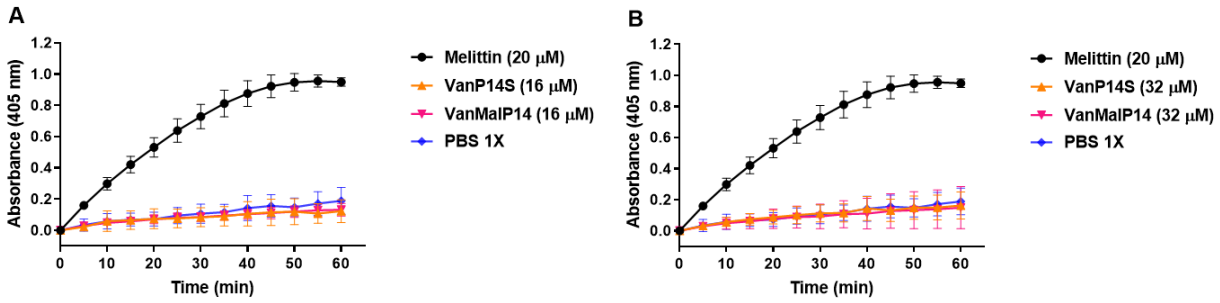

Figure 2.12. Monitoring the release of β- galactosidase over 1 hour from *E. coli* ATCC 25922 after 1 hour incubation with conjugates. Positive control Melittin (20 μM) and conjugates at (A) 2X and (B) 4X MIC.

Gram-negative outer membrane permeability

Looking into the outer membrane of Gram-negative bacteria, a membrane disruption assay using the fluorescent dye, N-phenylnaphthylamine (NPN) was employed.[155] In the presence of membrane disruption, NPN binds within the lipophilic environment of the membrane and produces a fluorescent signal relative to the amount of membrane disruption. Both **VanP14S** and **VanMalP14** conjugates and **P14LRR** were studied, along with a bactenecin control, a known cyclic AMP with known outer membrane permeation as a positive control (**Figure 2.13**).[156-157] All values were normalized with 1% Triton X-100, which was assumed to cause total disruption to the membrane. Both conjugates showed equivalent outer membrane disruption in a concentration-dependent manner when incubated at values within MIC range. **P14LRR** also displayed analogous concentration-dependent outer membrane disruption to the conjugates, whereas membrane permeation attributable to vancomycin was minimal. Given that **P14LRR**, **VanP14S**, and **VanMalP14** do not cause inner membrane leakage as discussed previously, the bactericidal activity may not be solely the result of the outer membrane permeation displayed by these compounds. These results may indicate that the conjugates and **P14LRR** cause membrane permeation for access and entry to the peptidoglycan of Gram-negative bacteria.[158-159]

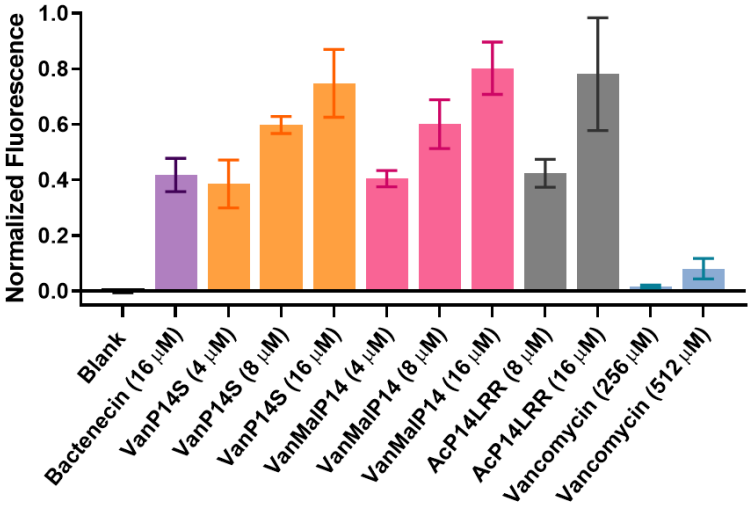

Figure 2.13. Outer membrane permeability assay using NPN as fluorescent probe to monitor the disruption of the outer membrane of Gram-negative bacteria, *E. coli* ATCC 25922.

Gram-positive membrane leakage

Next, we wanted to investigate the effects that the conjugates had on the membrane of Gram-positive bacteria such as *S. aureus*. **VanP14S** and **VanMalP14** were incubated with MRSA USA300 for 30 minutes (**Figure 2.14**). Water and vancomycin were used as negative controls; and lysostaphin was used as a positive control because of its known induction of membrane permeability through the degradation of the bacterial cell wall.[160] After the incubation period, a UV-Vis NanoDrop spectrometer was used to quantify the concentration of released DNA (ng/µL) by analysis of the 260 and 280 nm absorbing components of nucleic acids.[161] The concentration of released DNA is proportional to the extent of membrane damage. Both conjugates equally display 20% membrane leakage compared to the lysostaphin control, with the negative control value subtracted. Although the conjugate concentrations used were at 5X their MIC values, both conjugates show analogous results that correspond to a small, yet significant, amount of membrane damage. Like other membrane-insertive lipidated-glycopeptide analogs, it may be that the amphiphilic CAPH component of the conjugates is interacting with the membrane and causing disruption at high concentrations. This could be a secondary interaction in addition to the known peptidoglycan binding of vancomycin, leading to enhanced bacteria death.

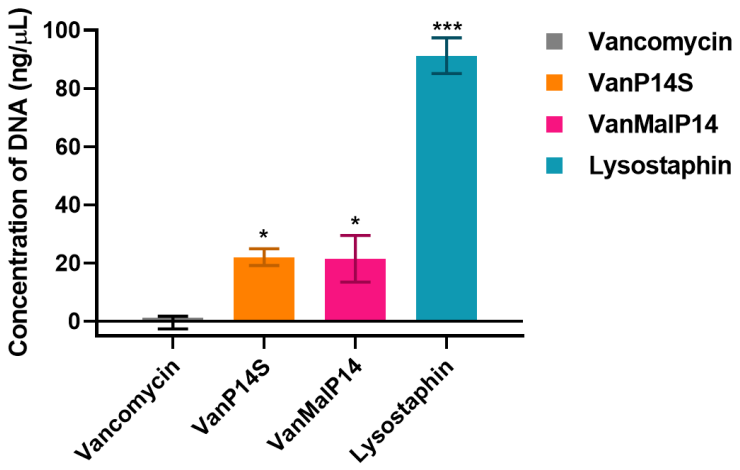

Figure 2.14. Leakage of nucleic acids resulting from vancomycin-P14 conjugate (5X MIC) incubation with MRSA USA300. Data were analyzed by one-way ANOVA. H_2O was negative control and Lysostaphin (20 µg/mL) was positive control. Asterisks (*/**/***) correspond to adjusted P-values ($\alpha = 0.05$) of $< 0.033/< 0.002/< 0.001$.

Membrane depolarization

The membrane potential of the cytoplasmic membrane is crucial to bacterial survival. Dissipation of the transmembrane potential resulting from pore formation would lead to an electrical failure of a bacterium's primary defense. Dissipation could also result from other methods of increasing ion permeability.[162] To examine whether **VanP14S** or **VanMalP14** can disrupt the bacterial membrane potential of the cytoplasmic membrane, we used the fluorescent voltage-sensitive probe 3,3'-dipropylthiadicarbocyanine iodide ($diSC_3$-5). This dye is self-quenching upon intercalating within the bacterial membrane. Upon dissipation of the membrane potential, the dye is released and produces a fluorescent signal proportional to the amount of membrane potential dissipation. In this experiment, bacteria were incubated with $diSC_3$-5 for 1 hour. Then, concentrations of **VanP14S**, **VanMalP14**, **P14LRR**, and vancomycin were added to the bacteria and the fluorescence of the $diSC_3$-5 release was obtained on a spectrometer. Triton X-100 (1%) served as a positive control as it digests bacterial membranes (**Figure 2.15**).

Among the tested compounds, **VanMalP14**, **P14LRR** and vancomycin, did not produce significant fluorescence signals from depolarization of the cytoplasmic membrane in the Gram-negative *E. coli* (**Figure 2.15 A**). However, a low level of dissipation of the membrane potential was observed for **VanP14S,** with about 5% dissipation compared to the Triton X positive control at all three concentrations. For Gram-positive *S. aureus*, both conjugates, **VanP14S** and **VanMalP14**, exhibited a concentration-dependent dissipation of the membrane potential (**Figure 2.15 B**). **VanP14S** showed 9%, 17%, and 18% dissipation at 4, 8, and 16 µM, respectively. VanMalP14 showed 12%, 18%, and 20% dissipation at 4, 8, and 16 µM, respectively. Upon analysis of these results, the conjugates show minimal dissipation of membrane potential in the Gram-negative *E. coli* at concentrations near the MIC values. Moreover, **VanP14S** and **VanMalP14** both show low, but significant levels of membrane dissipation potential at concentrations near reported MIC values in the Gram-positive *S. aureus.* These data validate that disrupting membrane potential, especially in Gram-positive bacteria, may be an aspect in the mode of killing from these conjugates.

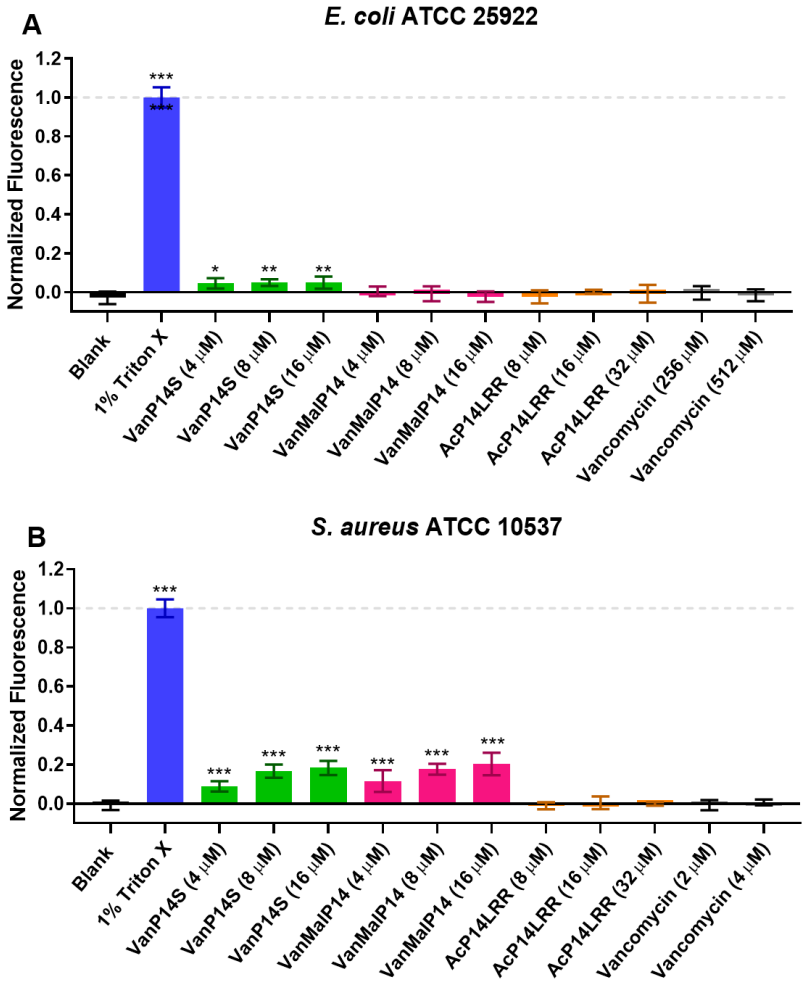

Figure 2.15. Cytoplasmic membrane potential disruption assay using $disc_3$-5 as fluorescent probe to monitor the quantity of potential dissipation in (A) Gram-negative *E. coli* and (B) Gram-positive *S. aureus* bacteria. Data were analyzed by one-way ANOVA. Asterisks (*/**/***) correspond to adjusted P-values ($\alpha = 0.05$) of < 0.033/< 0.002/< 0.001.

2.2.11 Confocal microscopy to visualize bacterial internalization of compounds

In order to evaluate the bacterial localization of the **FlVanP14S** conjugate and controls, **FITC-Van** and **FlP14LRR**, we utilized confocal imaging. Previously, fluorescent vancomycin has been shown to localize in the cell wall of non-replicating Gram-positive bacteria, and in the septa during cell division, owing to vancomycin binding to lipid II of the peptidoglycan layer of the cell wall.[69, 163]

First, we investigated the fluorescent uptake in Gram-negative *E. coli* ATCC 25922 after 10 minute and 1 hour incubation times with 20 μM **FITC-Van**, **FlP14LRR**, and **FlVanP14S**.

Only minimal fluorescence was observed for **FITC-Van** with *E. coli* even up to 20 µM, consistent with vancomycin's inability to penetrate through the outer membrane (data not shown). However, incubation of *E. coli* with 20 µM **FlP14LRR** showed rapid internalization to cytoplasm as previously described (**Figure 2.16 A, B**).[45] At the same concentration and times, **FlVanP14** shows much less consistent results. After 10 minutes of incubation, some bacteria show minimal uptake and spotty uptake around the cell wall (**Figure 2.16 C**). After 1 hour of incubation, more internalization is visible yet most bacteria with fluorescence exhibit inconsistent and spotty uptake (**Figure 2.16 D**). These results are reasonable, with respect to the mechanism of action studies whereby **VanP14S** showed outer membrane permeability without displaying inner membrane perturbation. Perhaps the conjugate both binds peptidoglycan and also slowly translocates to the bacterial cytoplasm through both membranes due to sufficient permeability of the CAPH.

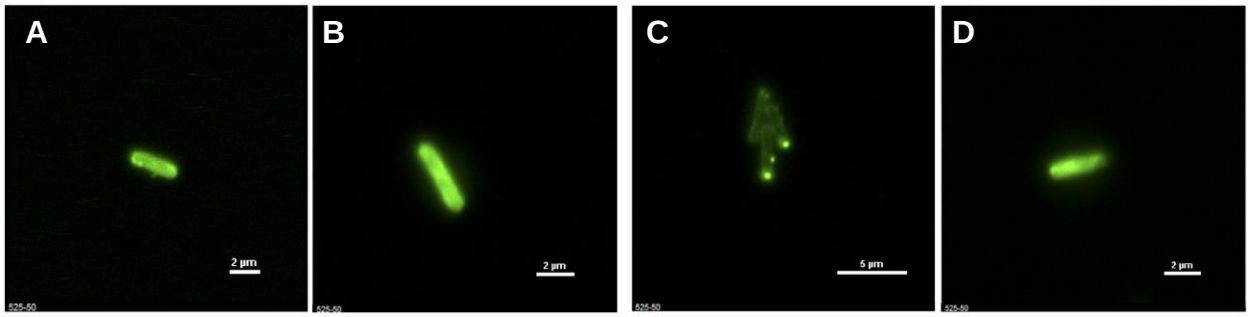

Figure 2.16. Confocal microscopy imaging of *E. coli* ATCC 25922 with 20 µM concentration of (A, B) **FlP14LRR** after (A) 10 minutes and (B) 1 hour incubation, and (C, D) **FlVanP14S** after (C) 10 minutes and (D) 1 hour incubation.

We next investigated the fluorescent uptake in Gram-positive *S. aureus* ATCC 10537 after 10 minute and 1 hour incubation times with 5 µM **FITC-Van**, **FlP14LRR**, and **FlVanP14S** (data not shown). All three compounds displayed strong cell wall fluorescence and minimal internal fluorescence after both incubation times. Interestingly, the **FlP14LRR** cell-penetrating peptide does not visually internalize within *S. aureus* to the same extent as within *E. coli*. **FITC-Van** was consistent with the literature, where vancomycin targets and localizes in the cell wall in Gram-positive bacteria.[163] Next, we wanted to investigate any visual differences in bacterial uptake location between the compounds. Therefore, we incubated a red fluorescent vancomycin, **RITC-Van**, with either green fluorescent **FlP14LRR** or **FlVanP14S** for 10 minutes. After incubation of 5 µM **RITC-Van** with **FlP14LRR**, we observe both compounds localize around the cell wall of

S. aureus ATCC 10537 after 10 minutes (**Figure 2.17**). The colocalization of the green **FlP14LRR** and red **RITC-Van** is expressed by a yellow-orange color in the merge of both channels (**Figure 2.17 A**). Performing the same experiment with 5 µM **RITC-Van** and 5 µM **FlVanP14S**, yielded analogous results (**Figure 2.18**). We observe both compounds localize around the cell wall of *S. aureus* ATCC 10537 after 10 minutes. The colocalization of the green **FlVanP14S** and red **RITC-Van** is expressed by a yellow-orange color in the merge of both channels (**Figure 2.18 A**). **FlVanP14S,** analogous to vancomycin, was observed to localize within the cell wall and the septa of replicating cells. These data provide insight that the **FlVanP14S** conjugate may target the peptidoglycan and/or cell membrane in its mode of action in killing Gram-positive bacteria.

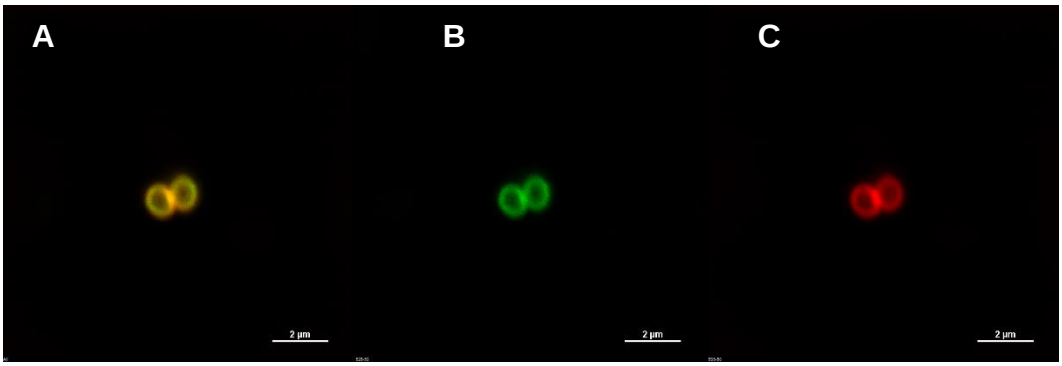

Figure 2.17. Confocal microscopy imaging of *S. aureus* ATCC 10537 with 5 µM **RITC-Van** and 5 µM **FlP14LRR** after 10 minutes of incubation. (A) Overlay of green and red channels, yellow-orange color represents colocalization. (B) Green channel representing **FlP14LRR** fluorescence. (C) Red channel representing RITC-Van fluorescence.

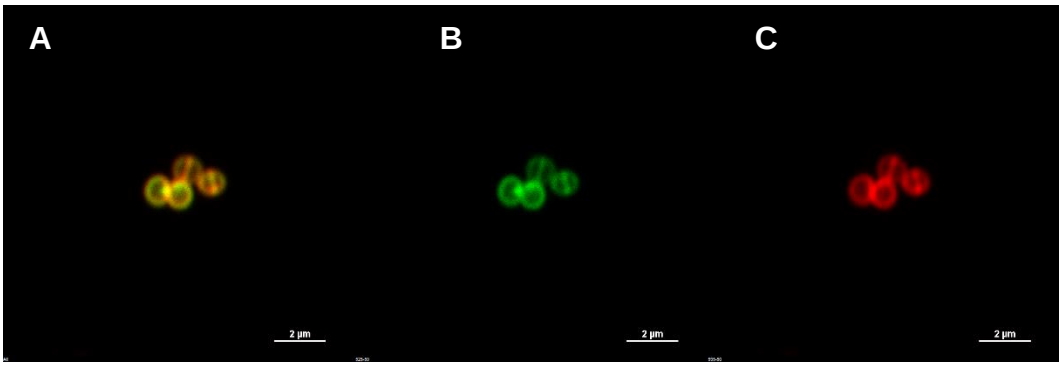

Figure 2.18. Confocal microscopy imaging of *S. aureus* ATCC 10537 with 5 µM **RITC-Van** and 5 µM **FlVanP14S** after 10 minutes of incubation. (A) Overlay of green and red channels, yellow-orange color represents colocalization. (B) Green channel representing **FlVanP14S** fluorescence. (C) Red channel representing **RITC-Van** fluorescence.

2.2.12 Flow cytometry to quantify bacterial accumulation of compounds

To thoroughly examine the spatial localization of **FlVanP14S** with both *E. coli* and *S. aureus*, we used flow cytometry with and without trypan blue (TB) to quench the surface-bound fluorophores.[69, 163-165] If bacterial membranes remain intact, the membrane impermeable TB will quench only surface-bound fluorescence from **FITC-Van**, **FlP14LRR** or **FlVanP14S**. Therefore, we can determine the extent of internalized fluorescence. The amount of surface-bound **FlVanP14S** versus internalized **FlVanP14S** was measured by comparing the arbitrary fluorescence units (AFU) of cellular fluorescence quenched by trypan blue to the AFU of cells not quenched with trypan blue after 10 minute and 1-hour incubations using flow cytometry (**Figure 2.19**). In *E. coli*, 88% and 94% of the external fluorescence was quenched by TB for **FlVanP14S** at 10 minute and 1-hour times, respectively. The fluorescence intensities for **FlP14LRR** and **FlVanP14S** were comparable to each other, and much stronger than **FITC-Van** for both incubation times; consistent with **FITC-Van** confocal imaging and poor penetration into *E. coli*. Longer incubation time increased intensity of fluorescence for **FlP14LRR** and **FlVanP14S,** demonstrating a time-dependent uptake in *E. coli*.

In *S. aureus*, we observed a 95% and 97% decrease in fluorescence quenching by TB for 10 minute and 1 hour incubation times with **FlVanP14S**, respectively. **FlP14LRR** also exhibited an 86% and 92% decrease in fluorescence with TB quenching after 10 minutes and 1-hour incubations. This is consistent with confocal imaging showing strong fluorescence in the cell wall for both **FlP14LRR** and **FlVanP14S**. Additionally, **FlVanP14S** showed 4-fold higher increase in uptake than **FlP14LRR** at both 10 minute and 1-hour incubation times without trypan blue. **FlP14LRR** showed 12- and 8-fold higher increases in uptake than **FITC-Van** at 10 minute and 1-hour incubation times without trypan blue. These results are consistent with a proposed mechanism of enhanced association of the **FlVanP14S** conjugate with the lipid II of the peptidoglycan and/or membrane.

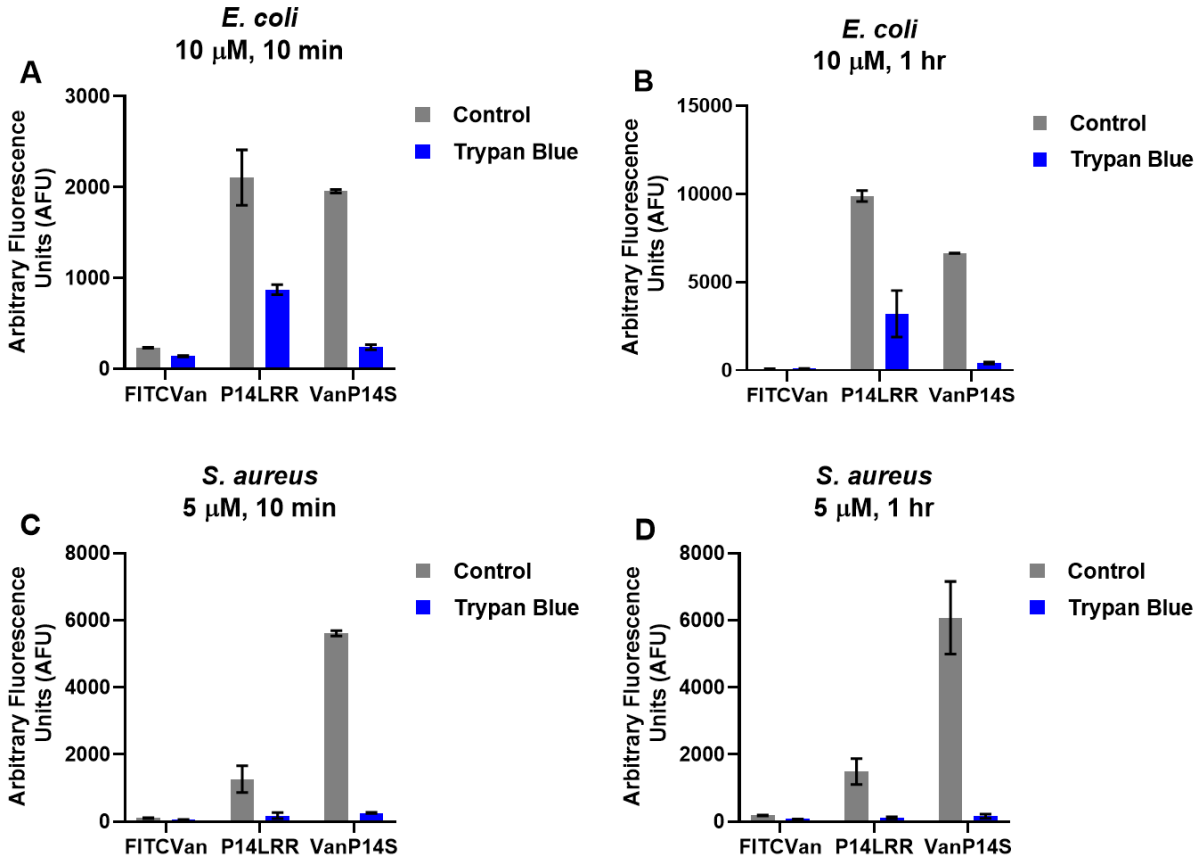

Figure 2.19. Bacterial uptake studies of **FlVanP14S**, **FlP14LRR**, and **FITC-Van** in (A, B) 10 μM concentrations with *E. coli* and (C, D) 5 μM concentrations with *S. aureus* after (A, C) 10 minute and (B, D) 1 hour incubation periods. 2 mg/mL trypan blue treatment (blue bar) and without trypan blue treatment (gray bar).

2.2.13 Vancomycin-P14GAP conjugates

From previous research in the Chmielewski group, a modified CAPH had shown improved antibacterial activity and cellular uptake in comparison to the **P14LRR** peptide. This cell-penetrating peptide, **P14GAP**, consists of the same polyproline backbone with modification to the cationic amino acid.[42] The cationic guanidinium moiety on the modified amino acid, Fmoc-P_{GAP}, is directly connected to the proline, allowing the charged groups to be held closer to the backbone, than with the Fmoc-P_R of **P14LRR**. We sought to exploit the increased antibacterial activity of **P14GAP** and generate a vancomycin-P14GAP conjugate with improved features compared to the vancomycin-P14LRR conjugate. We used an identical strategy to synthesize **VanP14GAPS** and **FlVanP14GAPS** as that for **VanP14S** and **FlVanP14S** (**Figure 2.20**).

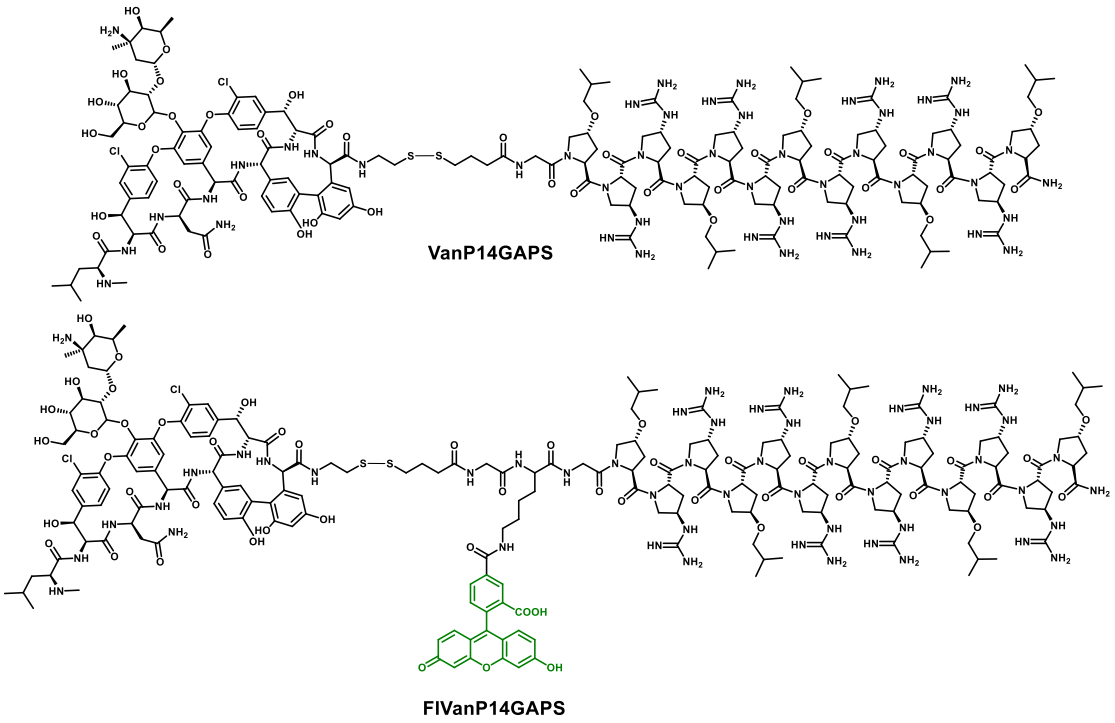

Figure 2.20. Structures of **VanP14GAPS** (top) and **FlVanP14GAPS** (bottom)

Minimum inhibitory concentrations against pathogenic isolates

First, antibacterial activity was determined against a broad selection of pathogenic bacteria (**Table 2.2**). **VanP14GAPS**, **P14GAP**, vancomycin and gentamicin were incubated with bacteria in logarithmic growth phase for 24 hours, and minimum inhibitory concentrations were visible determined by assessing the growth. The **VanP14GAPS** conjugate exhibits good to moderate activity against almost all pathogens tested, including most of the notable ESKAPE pathogens.[166] Similar to **VanP14S (Table 2.1)**, **VanP14GAPS** also displays excellent activity against *S. aureus* strains and moderate activity against a selection of Gram-negative pathogens. **VanP14GAPS** exhibits similar MICs to **VanP14S** in *E. faecium* 700221, *S. aureus* NRS 384 (USA300), *A. baumannii, L. monocytogenes* 19111, VRSA 5, and VRSA 10. **VanP14GAPS** showed an enhanced MIC for ESKAPE pathogen *E. cloacae* 1143 at 8 µM, while **VanP14S** was >16 µM. A decrease in potency was observed for *P. aeruginosa* 1706 with **VanP14S** and **VanP14GAPS** displaying MICs of 4 µM and >16 µM, respectively. When comparing to **P14GAP** from an independent experiment, **VanP14GAPS** provides comparable bactericidal activity in *S. aureus*

and *E. faecium* (0.5 – 2 μM MICs). **P14GAP**, however, was significantly more potent then **VanP14GAPS** for all Gram-negative strains tested.

Table 2.2. Minimum inhibitory concentrations (MICs) of vancomycin conjugates against pathogenic bacteria isolates using the microbroth dilution assay after 20 h of treatment. Values of **VanP14GAPS** and **P14GAP** reported in μM; and values of vancomycin and gentamicin controls reported in μg/mL.

Bacteria strain	VanP14GAPS	P14GAP[a]	Vancomycin	Gentamycin
ESKAPE Pathogens				
***E. faecium* 700221**	1	1	>32	>32
S. aureus NRS 384	0.5	2	1	≤ 0.25
***K. pneumoniae* 1706**	>16	8	>32	1
***A. baumannii* 1605**	8	0.5	>32	>32
***P. aeruginosa* 50573**	16	2	>32	1
***E. cloacae* 1134**	8	2	>32	≤ 0.25
Selected Staphylococcus and Gram-positive strains				
***S. aureus* NRS 383**	0.5	2	0.5	>32
***S. aureus* NRS 382**	1	2	2	0.5
***S. aureus* NRS 4220**	1	2	1	≤ 0.25
***S. aureus* ATCC 6538**	1	1	1	≤ 0.25
***S. epidermidis* NRS101**	1	1	2	16
VRSA 5	1	2	>32	≤ 0.25
VRSA 10	1	2	>32	≤ 0.25
***L. monocytogenes* 19111**	0.5	2	0.5	0.5
Selected Gram-negative strains				
***P. aeruginosa* 48982**	8	4	>32	>32
***P. aeruginosa* 31040**	16	2	>32	32
***P. aeruginosa* 31041**	8	2	>32	>32
***A.baumannii* 1747**	2	0.5	>32	≤ 0.25
***A.baumannii* 19606**	4	1	>32	16
***S. flexneri* 1a**	2	1	>32	≤ 0.25
S. enteritidis	4	1	>32	≤ 0.25
***E. coli* 25922**	8	1	>32	≤ 0.25
***S. trphimurium* LT2**	4	1	>32	≤ 0.25

[a] values were taken from an independent analysis[42]

Cell toxicity studies

When compared to the known lytic AMP, melittin, and established non-lytic AMP/CPP, **P14LRR**, **VanP14GAPS** displays significantly more lysis in hRBCs than the individual components, **P14GAP** and vancomycin (**Figure 2.21 A**). Although the lysis does not occur to the same extent as positive control melittin, we begin to see an increase of lytic behavior at 2.5 µM with 8% lysis, increasing to 15% lysis at 5 µM, and upwards at increasing concentrations. No lysis was seen for **VanP14S** at any of the tested concentrations (**Figure 2.7 A**). While **VanP14GAPS** displays unfortunate hRBC lytic characteristics, the conjugate shows similar low toxicity toward macrophage (J774A.1) cells at 5 µM as compared to **VanP14S** (**Figure 2.21 B**), and most of the population of cells are viable at concentrations up to 10 µM after a 9-hour incubation. These results show the cell viability is comparable to the **VanP14S** conjugate with a significant drop in viability at 20 µM, a concentration well above MIC values.

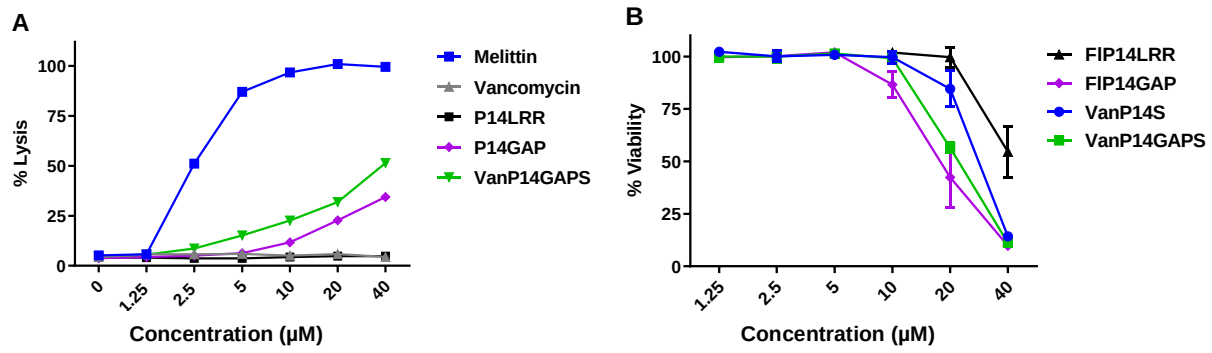

Figure 2.21. (A) Hemolysis assay measuring the release of hemoglobin from hRBC. Melittin was used as a positive control, and values were normalized against 0.1% triton X-100. (B) Cytotoxicity measuring the cell viability using an MTT assay after 9-hour incubation with compounds.

Confocal microscopy to visualize cellular internalization of FlVanGAPS conjugate

FlP14GAP showed increased membrane binding compared to **FlP14LRR**.[42] To visualize internalization of **FlVanP14GAPS**, and determine localization within mammalian cells, confocal microscopy was applied. Therefore, the fluorescent vancomycin-P14GAP conjugate, **FlVanP14GAPS**, was incubated at a concentration of 5 µM with J774A.1 macrophage cells for 1 hour. Following incubation, we further labeled cells with an endosomal marker (Lysotracker red,

300 nM) or a mitochondrial marker (Mitotracker red, 100 nM). **FlVanP14GAPS** appears to show localization within the endosomes of macrophages cells after 1-hour incubation of 5 µM concentration (**Figure 2.22 A**). No mitochondrial association is visible (**Figure 2.22 B**). Both **FlP14GAP** and **FlVanP14S** were also localized within endosomes at 5 µM concentration and timepoint previously determined. After 1 hour incubation with 10 µM **FlVanP14GAPS**, the same results are observed; there is strong colocalization with the endosomes, and no colocalization with the mitochondria (data not shown). Interestingly, **FlVanP14GAPS** also shows in increase in membrane association from **FlVanP14S**, based on the faintly visible green outline in the cell images. In conjugating vancomycin with the **P14GAP** peptide that showed strong membrane association, the vancomycin-P14GAP conjugate displays a mixture of membrane binding and internal endosomal localization, owing to the predicted mode of endosomal cellular entry.

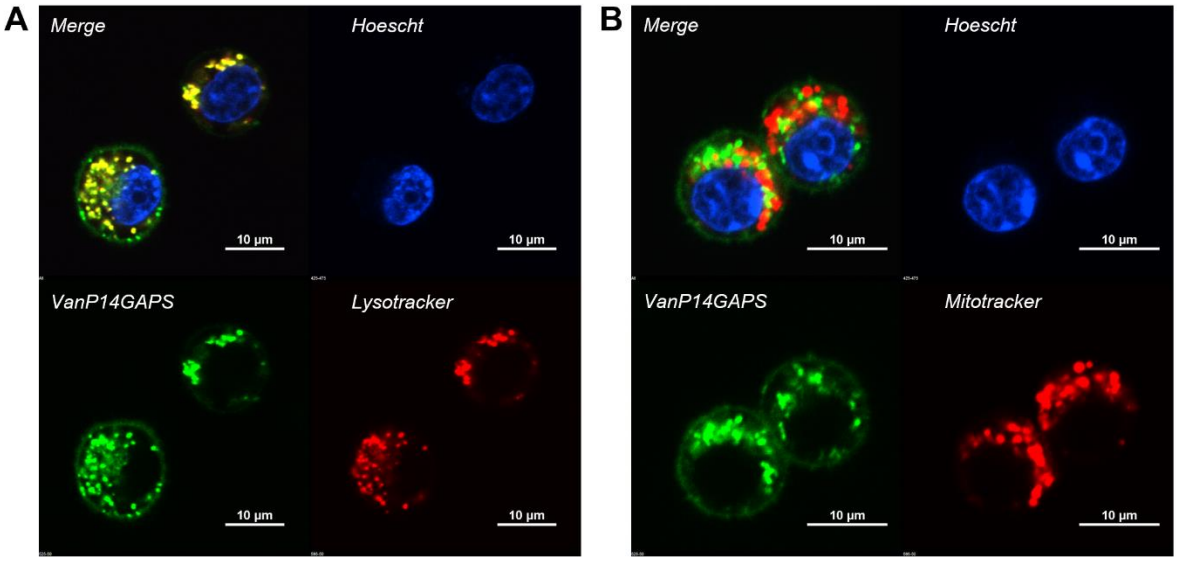

Figure 2.22. Confocal microscopy images of J774A.1 macrophage cells incubated with 5 µM FlVanP14GAPS for 1 hr. (A) Merge (top left) and separate laser channels with Hoescht 33342 stain (blue), conjugate (green), and lysotracker lysosomal stain (red). (B) Merge (top left) and separate laser channels with Hoescht 33342 nuclear stain (blue), conjugate (green), and mitotracker mitochondrial (red). A yellow-orange color indicates colocalization of conjugate and selected red stain.

Flow cytometry to quantify cellular accumulation of FlVanGAPS

To quantify the internalization of **FlVanP14GAPS** compared to that of **FlVanP14S** and the individual components of the conjugate (vancomycin and **P14GAP**), we measured cellular

fluorescence by flow cytometry. **FlVanP14GAPS**, **FlVanP14S**, **FlP14GAP**, **FlP14LRR**, and **FITC-Van** were incubated with macrophage J774A.1 for 1-hour and 3-hour incubation times; followed by flow cytometry to read cell fluorescence (**Figure 2.23**). Both conjugates, **FlVanP14GAPS** and **FlVanP14S** showed an increase in fluorescence at longer incubation times, exhibiting time-dependent uptake. Both conjugates also exhibited significantly lower (about 3-fold) cell fluorescence than **FlP14GAP** at 5 µM concentrations, but significantly higher (60-80%) fluorescence than the reference **FlP14LRR** cell-penetrating peptide at both incubation times. **FlVanP14GAPS** showed about a 30% increase in fluorescence after 1 hour compared to **FlVanP14S** at all concentrations, but these conjugates displayed analogous fluorescence after 3-hour incubation. This indicates that **VanP14GAPS** may be initially faster at associating with or internalizing into the cell.

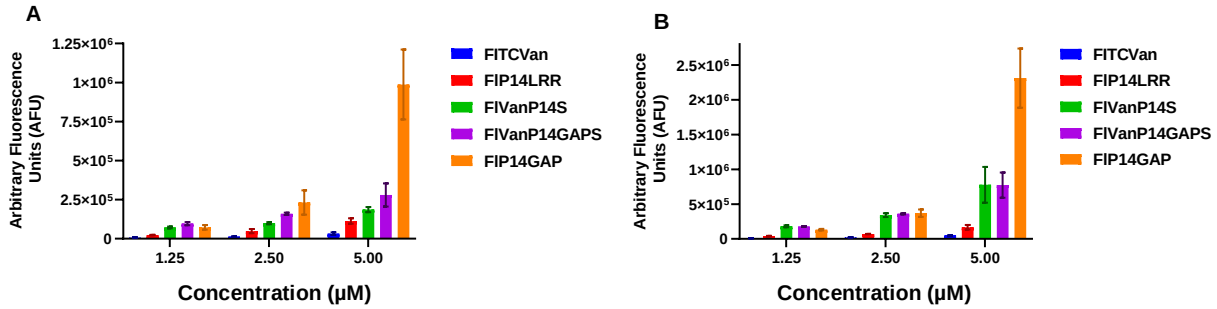

Figure 2.23. Screening of arbitrary fluorescence in J774A.1 cells incubated with compounds at (A) 1-hour and (B) 3-hour incubation times.

To quantify the amount of conjugate that associates and binds to the mammalian cellular membrane, trypan blue was used to quench external fluorescence of the surface-bound conjugates (**Figure 2.24**). **FlP14GAP** was reported to have increased membrane association with mammalian cells compared to **FlP14LRR**, so we wished to investigate whether the conjugate would show a similar association.[42] Fairly comparable fluorescence was observed in all cases with and without trypan blue. At both 2.5 and 5 µM concentrations and both time points, over 75% of the **FlVanP14GAPS** conjugate is internalized. Although the confocal images appear as though there may be more significant membrane binding of **FlVanP14GAPS** than **FlVanP14S**, the flow cytometry data show comparable decreases in fluorescence with the addition of trypan blue. These

data indicate that cellular uptake of both vancomycin conjugates is comparable, with only moderate increases in uptake for **FlVanP14GAPS** over **FlVanP14S**.

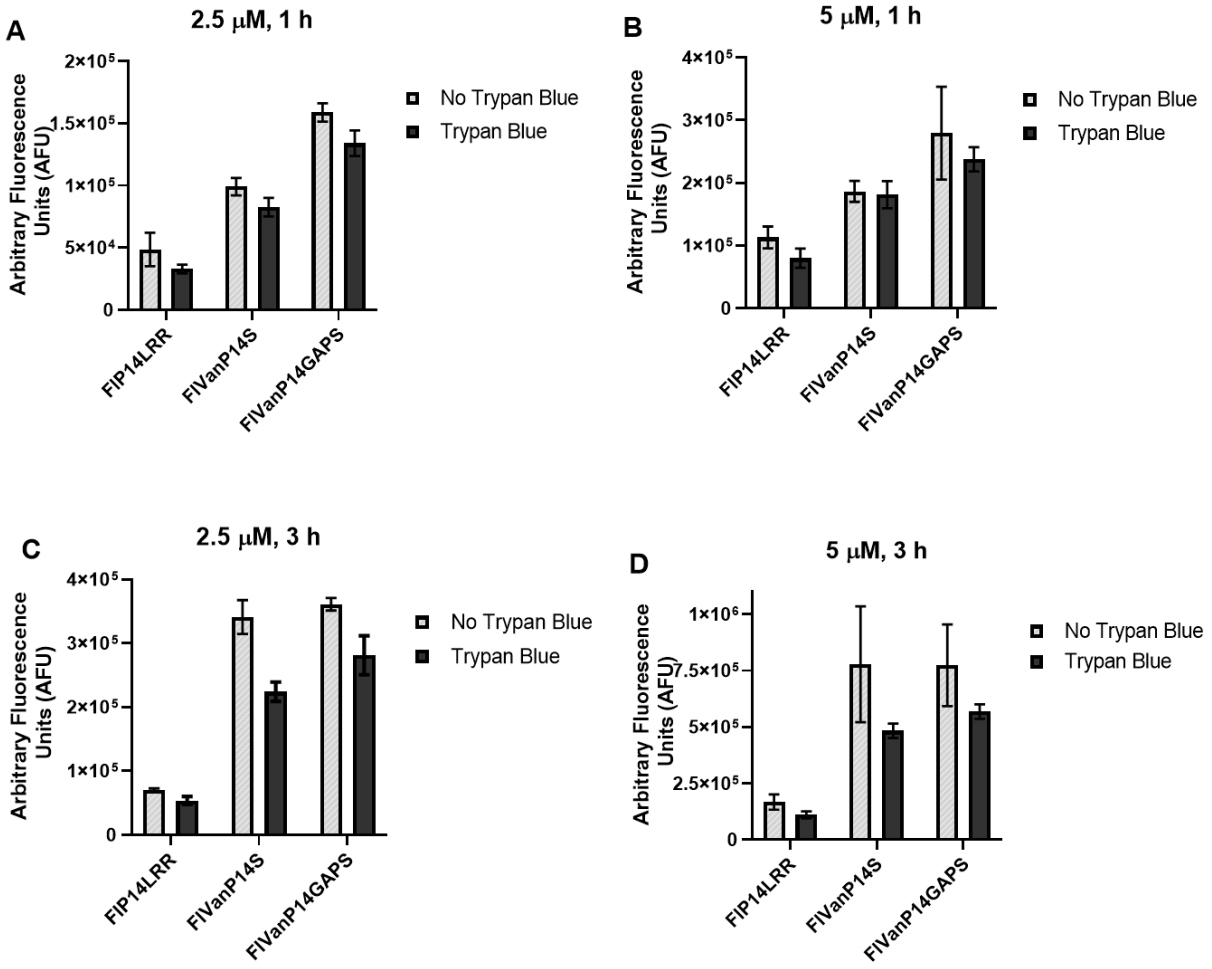

Figure 2.24. Cellular uptake studies of **FlP14LRR**, **FlVanP14S,** and **FlVanP14GAPS** at (A, B) 1 h and (C, D) 3 h in J774A.1 cells after incubation at (A, C) 2.5 μM and (B, D) 5 μM with trypan blue treatment (black bar) and without trypan blue treatment (gray bar).

2.3 Conclusions

We have demonstrated that vancomycin-CAPHs conjugates have excellent antimicrobial activity against sensitive and drug-resistant Gram-positive bacteria, in addition to moderate activity against certain Gram-negative. Although outer membrane disruption was determined in Gram-negative bacteria, no inner membrane leakage or membrane depolarization was observed.

Feasibly, the conjugate may act on Gram-negative bacteria by disturbing the outer membrane to access the peptidoglycan or by non-lytic penetration of the cell wall to access internal targets.

Both **VanMalP14** and **VanP14S** show faster killing kinetics than vancomycin with *S. aureus*. In addition, the conjugates exhibit some membrane disruption as identified through membrane leakage and membrane potential experiments. The fluorescent **VanP14S** is shown to localize within the cell wall of *S. aureus*, analogous to vancomycin and **P14LRR** individually; however, much stronger association was observed with 5-fold increases in bacterial fluorescence as compared to **FlP14LRR** alone. Although we have not addressed pentapeptide binding affinity directly, we can propose with the fluorescence data that the addition of a cationic cell-penetrating peptide, vancomycin may show increased antibacterial activity by tighter binding to lipid II in the peptidoglycan. The positive charges in **P14LRR** may enhance vancomycin's cell wall affinity through interactions negatively charged teichoic acid components dispersed in the cell wall and with the negatively charged phospholipid head groups in the membrane as described in literature.[69] The **P14LRR** cell-penetrating peptide could insert within the membrane and establish an anchoring effect as described in a similar literature example (**Figure 2.26**).[70] One or more of these interactions could promote **P14LRR** interacting with the cytoplasmic membrane and acting as an anchor for vancomycin to bind its pentapeptide target more efficiently.

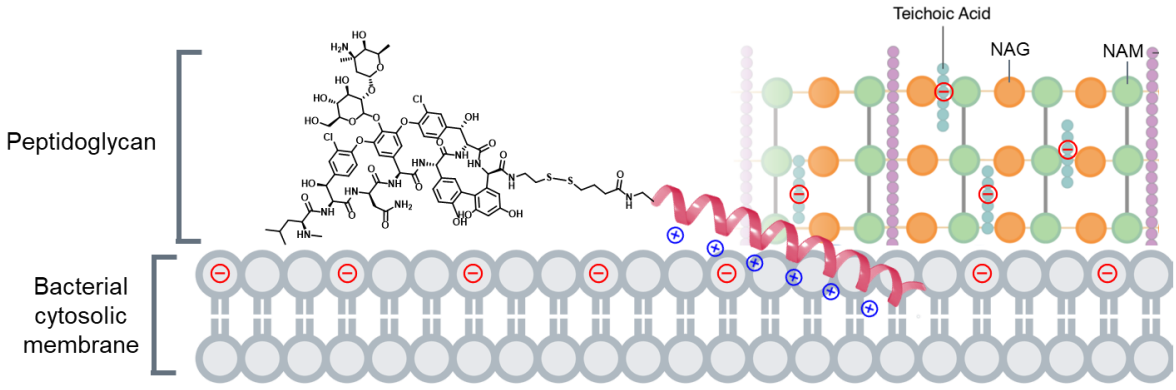

Figure 2.25. Proposed model of vancomycin-CAPHs acting on a bacterial membrane.

We also provided evidence to support that **VanP14S** should be effective as an antibiotic against intracellular pathogens, a subset of infections previously inaccessible for vancomycin. The conjugates, **VanMalP14** and **VanP14S**, showed minimal cytotoxicity and hemotoxicity at

concentrations relevant to the observed MIC values, with enhanced cellular uptake as compared to **P14LRR,** and with intracellular endosomal localization. Additionally, it was shown that **VanP14S** is capable of cleaving in a reducible environment, supporting the assertion that a CAPH could deliver vancomycin intracellularly, allowing both vancomycin and the peptide to synergistically act as independent antibiotics.

An additional conjugate was synthesized, **VanP14GAPS**, to determine if the exchange of a more potent antibiotic CPP, **P14GAP**, would result in a further improved vancomycin conjugate. Although **P14GAP** showed more potency as an antibiotic peptide compared to **P14LRR**, the vancomycin conjugate displayed comparable potency against the same *S. aureus* and enterococcus strains. Although there was some increase in mammalian cellular uptake, red blood cell hemolysis was significantly greater for **VanP14GAPS** than **VanP14S**. Based on these preliminary results, there appears to be no significant advantage in pursuing **VanP14GAPS** over the more promising **VanP14S** or **VanMalP14** conjugates.

2.4 Future Directions

Progress has been achieved with our vancomycin-CAPH conjugates, yet additional experiments are needed. Specifically, we must determine if the conjugates can clear intracellular pathogens. Up to this point, we have shown that the conjugates are excellent antimicrobials and able to accumulate within mammalian cells, but must unequivocally determine that they can accomplish both concurrently. Answering the question of whether the reducibility of the conjugate is essential is also a goal. Additionally, it would be prudent to elucidate the mode of action of these conjugates beyond that of which we have already determined, such as using lipid II binding assays. Undisputedly concluding that these conjugates show tighter binding to the peptidoglycan of bacteria than vancomycin would confirm the mode of action, with the CAPH peptide functioning as an anchor within the cell wall or as a membrane-interacting component.

2.5 Materials and Methods

2.5.1 Materials

Starting material for unnatural amino acids, Fmoc-protected natural amino acids, and coupling reagents were purchased from Chem Impex (Wood Dale, IL) or Ana Spec, Inc. (Fremont,

CA). H-Rink Amide ChemMatrix resin for peptide synthesis was purchased from PCAS Biomatrix Inc. (Quebec, Canada). Vancomycin hydrochloride was purchased from Millipore Sigma (Burlington, MA). Sterile DMEM supplemented with L-glutamine and Penicillin-Streptomycin were purchased from VWR (Batavia, IL). Buffers (1X PBS) and 10% fetal bovine serum (FBS) used in cell culture were purchased from Corning Inc. (Corning, NY) and Atlanta Biologicals, Inc. (Research and Diagnostic Systems, Inc., Minneapolis, MN), respectively. All bacteria and cell lines for culture were purchased form ATCC (Manassas, VA). All other chemicals and reagents were purchased commercially and were used without further purification unless mentioned from Sigma Aldrich (St. Louis, MO), Alfa Aesar (Haverhill, MA) or Thermo Fischer (Waltham, MA).

Peptides and conjugates were purified using a Waters Delta Prep 4000 HPLC equipped with a Phenomenex C18 semi-preparative column. CAPHs characterization was performed using matrix associated laser desorption ionization-time of flight (MALDI-TOF) mass spectrometry using an Applied Biosystem Voyager-DE TM BioSpectrometry workstation and analytical RP-HPLC using Waters Delta Prep 4000 HPLC equipped with a C18 reverse phase analytical column (5 μm, 4.6 mm x 250 mm; Phenomenex Luna). Cell uptake was measured using BD sciences Acurri and analyzed using BD software. Bacterial fluorescence uptake was measured on BD Fortessa LSR flow cytometry cell analyzer and analyzed using BD software. Absorbance readings were obtained using microplate reader TECAN SpectraFluor Plus or TECAN Infinite F PLEX. Confocal images were obtained using Nikon A1R-MP inverted confocal fluorescence microscope equipped with 60X (mammalian cell culture) or 100X (bacterial culture) oil objective. NIS Elements software was used to process images.

2.5.2 Synthesis of Z-trans-(2-cyanoethyl)hydroxyproline (1)

To a solution of NaH (1.58 g, 65.9 mmol) in THF (150 mL) with 4Å mol sieves at 0 °C and under an atmosphere of nitrogen was added an ice-cooled solution of Cbz-hydroxyproline (5.0 g, 18.8 mmol) in THF (50 mL). The mixture was stirred at 0 °C for 1 h. To this mixture was added acrylonitrile (5.0 mL, 93.4 mmol), and the reaction was allowed to warm to room temperature and stirred for 24 h. The reaction mixture was cooled to 0 °C, and water (100 mL) was added to quench the excess NaH. The THF was removed in vacuo, and 10% HCl was added to bring the solution to a pH of 1. The mixture was vacuum filtered and the resulting solution was extracted with EtOAc, the organic layer was dried over anhydrous $MgSO_4$, and the solvent was removed *in vacuo*. The

desired product was purified by silica gel column chromatography (95% CH_2Cl_2, 4% MeOH, 1% AcOH) to provide **1** as a colorless oil in 80% yield.

MS (ESI): 319 m/z ($M + H^+$).

^{1}H NMR (300 MHz, $CDCl_3$): δ 7.34 (m, 5H), 5.15 (m, 2H), 4.54 (m,1H), 3.65 (m, 3H), 2.59 (t, J = 5.6 Hz, 2H), 2.40 (m, 1H), 2.15 (m, 2H), 2.39 (m, 2H).

2.5.3 Synthesis of Z-trans-(2-cyanoethyl)hydroxyproline (2)

To a solution of **1** (600 mg, 1.9 mmol) in 20 mL ethanol was added Pd/C (60 mg, 10% wt/wt). The solution was stirred under 1 atmosphere of hydrogen for 3 h. The solution was gravity filtered through filter paper, the solvent was removed *in vacuo*, and the residue was used in the next step without further purification. The resulting material was solubilized in 10 mL DI water and was cooled to 0 °C, followed by the addition of sodium bicarbonate (475 mg, 5.7 mmol). To this cooled mixture, was added a solution of Fmoc-OSu (699 mg, 2.1 mmol) in 10 mL acetone dropwise, and the resulting slurry was allowed to warm to room temperature and stirred for 20 hours. The reaction was treated with 10% HCl to a pH of 1 and extracted with EtOAc. The organic layers were dried over anhydrous Na_2SO_4, and the solvent was removed *in vacuo*. The desired product was purified by silica gel column chromatography (96% CH_2Cl_2, 3% MeOH, 1% AcOH) to provide **2** as a colorless oil in 99%/quantitative yield.

HRMS (APCI) calculated for $C_{23}H_{22}N_2O_5$ [$M+H^+$] 407.1601 m/z, found 407.1598

^{1}H NMR (400 MHz, $CDCl_3$): δ 10.14 (br s, 1H), 7.73 (dd, J= 24 Hz, 8 Hz, 2H), 7.55 (m, 2H), 7.34 (m, 4H), 4.40-4.51 (m, 3H), 4.24-4.36 (m, 1H), 4.13 (m, 1H), 3.51-3.75 (m, 4H), 2.55 (q, J= 8 Hz, 2H), 2.33-2.48 (m, 1H), 2.11-2.26 (m, 1H).

^{13}C NMR (100 MHz, $CDCl_3$): δ177.2*, 175.6, 155.7, 154.5*, 143.6, 141.2, 129.0, 127.7, 127.0, 124.9, 119.9, 117.4, 67.9, 63.7, 57.9, 57.2*, 51.4, 47.0, 36.6*, 34.7, 19.0 (*indicates minor rotamer)

2.5.4 Synthesis of Fmoc-P_R(Boc)$_2$

To a solution of **2** (700 mg, 1.7 mmol) in 20 mL methanol was added 1 mL AcOH, then PtO_2 (70 mg, 10% wt/wt). The solution was stirred under 1 atmosphere of hydrogen overnight. The solution was filtered through celite, and the solvent was removed *in vacuo*, and the residue was washed with toluene to remove excess AcOH. The residue was used in the next step without

further purification. The resulting material was solubilized in 15 mL CH_2Cl_2 and was cooled to 0 °C. To this cooled mixture, a solution of triethylamine (0.720 mL, 5.2 mmol) in 5 mL CH_2Cl_2 was added dropwise, then N, N'-Bis-Boc-1-guanylpyrazole (695 mg, 2.2 mmol). The resulting slurry was allowed to warm to room temperature and stirred 20 hours. The reaction was washed with saturated sodium bicarbonate, the organic layer was dried over anhydrous Na_2SO_4, and the solvent was removed *in vacuo*. The desired product was purified by silica gel column chromatography (96% CH_2Cl_2, 3% MeOH, 1% AcOH) to provide Fmoc-$P_R(Boc)_2$ as a white solid in 62% yield. $[\alpha]_D^{22}$ = -30.6 (*c* 1.0 $CHCl_3$).

HRMS calcd for $C_{34}H_{44}N_2O_7$ [M + H^+] 653.3187, found 653.3185

^{1}H NMR (300 MHz, $CDCl_3$): δ 7.79 (t, J = 7.5 Hz, 2H), 7.62 (t, J = 7.5 Hz, 2H), 7.37 (m, 5H), 4.48 (m, 3H), 4.13 (m, 2H), 3.57 (m, 3H), 3.25 (m, 2H), 2.46-2.20 (m, 2H), 1.78 (m, 2H), 1.50 (s, 18H).

^{13}C NMR (75 MHz, $CDCl_3$): δ 177.2*, 175.9, 163.0, 156.0, 155.8*, 154.75, 153.1, 144.0, 143.8*, 143.7, 141.3, 141.2*, 128.3, 127.8, 127.7*, 127.2, 127.1, 125,1, 120.0, 119.9*, 83.4, 79.8, 68.2, 68.1*, 68.0, 58.2, 57.6*, 51.6*, 51.3, 47.1, 39.8, 36.8, 35.1, 28.8, 28.3, 28.1* (*indicates minor rotamer).

2.5.5 Fmoc-GAP(Boc)$_2$ synthesis[42]

To Fmoc-L-Pro(4-NHBoc)-OH(2S,4R) (200 mg, 0.44 mmol) in a 25 mL round bottom flask with a stir bar was added a trifluoroacetic acid (TFA) and dichloromethane (DCM) solution (1:1, 2 mL). The reaction was stirred for 3 h at room temperature. The TFA/DCM solution was removed *in vacuo* and dried under high vacuum for 12 h. The residue was solubilized in DCM (2 mL) with sonication and N,N'-di-tert-butoxycarbonyl-1H-pyrazole-1 (150.9 mg, 0.49 mmol) was added to the reaction flask followed by triethylamine (TEA) (249 μL, 1.77 mmol). The resulting solution was stirred for 12 h at room temperature. The organic solvent was removed *in vacuo* and the crude material was purified by flash chromatography on silica gel with an eluent composed of 93% DCM and 7% methanol (MeOH). The desired fractions were collected and the solvent was removed *in vacuo* to yield a white solid, Fmoc-GAP(Boc)2 in 50% yield.

HRMS [ESI] $C_{31}H_{39}N_4O_8$ 595.2762, observed: 595.2756

^{1}H NMR (400 MHz, CD_3CN): δ 11.48 (br s, 1H), 8.28 (br s, 1H), 7.81 (d, J = 8 Hz, 2H), 7.62 (m, 2H), 7.40 (m, 2H), 7.33 (m, 2H), 4.51 (dd, J = 4 Hz, 8 Hz, 1H), 4.18-4.43 (m, 4H), 3.72 (m, 1H), 3.31 (m, 1H), 2.25-2.38 (m, 2H), 1.42 (q, J= 8 Hz, 18H).
^{13}C NMR (100 MHz, CD_3CN): δ 163.34, 155.81, 154.03, 152.79, 143.87, 141.05, 127.62, 127.08*, 125.00, 119.88, 83.34, 78.82, 67.19, 51.23, 49.28, 48.39*, 46.92, 35.74, 34.49, 27.38, 27.06* (*indicates minor rotamer).

2.5.6 Synthesis of trityl-4-thiobutyric acid

4-butyrothiolactone (1 g, 9.6 mmol) was added to a solution of NaOH (1.96 g, 49 mmol) in 7.5 mL DI water. The mixture was heated to reflux and stirred for 15 minutes. Upon cooling to room temperature, the reaction mixture was poured directly into a separatory funnel with 7 mL of concentrated HCl. The mixture was extracted with diethylether (3X), dried over $MgSO_4$, and solvent removed *in vacuo*. In a second round bottom flask, trityl chloride (2.45 g, 1.5 eq.) was added to a round bottom flask and dissolved in 6 mL DMF. The intermediate product (0.7 g) was dissolved in 1 mL DMF and transferred to the solution of trityl-chloride. The flask was rinsed two additional times with 1 mL DMF to ensure complete transfer of intermediate. The final reaction volume was 9 mL. The reaction was left to stir at room temperature for 48 hours. The resulting mixture was poured into a beaker of 75 mL of 10% sodium acetate and the product precipitated. The solid product was isolated by vacuum filtration, dissolved in acetone, and dried overnight to yield 1.5 g of pure, white solid in 42% yield. No additional purification steps followed.
^{1}H NMR (400 MHz, $CDCl_3$): δ 7.18-7.42 (m, 15H), 2.32 (t, J = 8 Hz, 2H), 2.23 (t, J = 8 Hz, 2H), 1.68 (quintet, J = 8 Hz, 2H)

2.5.7 Solid Phase Peptide Synthesis of P14LRR CAPHs

A 10 mL peptide synthesis flask was charged with 100 mg H-rink amide resin (0.48 mmol/g loading) for the synthesis of **P14LRR-SH** and **FlP14LRR-SH**. The resin was manually crushed and washed with 5 mL of DMF (2X), DCM (2X), MeOH (2X), DCM (2X), DMF (2X). The resin was swelled in 5 mL DMF with agitation for 30 mins. The first amino acid (2 eq.) was activated by sonication with HATU (2 eq.) and DIEA (4 eq.) in 4 mL DMF, then added to the resin in the peptide flask. Reaction was agitated for 3 hr then washed with 5 mL of DMF (2X), DCM

(2X), MeOH (2X), DCM (2X), DMF (2X). The Fmoc protecting group was deprotected by adding 4 mL of 30% piperidine in DMF, and mixing for 20 minutes. The solution was drained, and resin washed with 5 mL of DMF (2X), DCM (2X), MeOH (2X), DCM (2X), DMF (2X). This cycle of coupling and deprotecting continued until all amino acids were coupled. The process was monitored by Kaiser[167] and chloranil[168] tests, and verified using test cleavages and MALDI-ToF mass spectrometry.

Synthesis of P14LRR-SH

Upon synthesis of the 100 mg resin scale of **P14LRR** peptide, the resin was split and half (about 50 mg) resin was used. The trityl-4-mercaptobutyric acid (26.1 mg, 3 mmol) was activated with HATU (27.4 mg, 3 mmol) and diisopropylethylamine (25 μL, 6 mmol) in 4 mL DMF. This mixture was added to the peptide-bound resin and agitated at room temperature for 3 hours. The reaction solution was drained and the resin and washed with 5 mL of DMF (2X), DCM (2X), MeOH (2X), DCM (2X), DMF (2X). **P14LRR-SH** was then globally deprotected and cleaved from the resin using 5 mL cleavage cocktail of 90: 5: 2.5: 2.5, TFA: EDT: TIPS: H_2O. The cleavage cocktail with the peptide-bound resin was agitated for 3 hours. The crude mixture was collected into a preweighed plastic falcon tube. The resin was washed with 5 mL DCM and collected into the preweighed plastic falcon tube. A second 5 mL aliquot of cleavage cocktail was added to the flask and agitated for an additional 30 minutes and drained into the collecting tube. The resin was washed with 5 mL DCM and collected. The crude mixture was concentrated *in vacuo*. Cold diethyl ether (15 mL) was added to the crude mixture, which led to a precipitate. After centrifugation, the supernatant was decanted and the precipitate was dried under vacuum overnight. The crude **P14LRR-SH** was resuspended in deionized water (approximately 10 mg/mL) and was purified on RP-HPLC, using a C18 column (Phenomenex, USA) with a gradient of 25-65% acetonitrile (0.1% TFA) in water (0.1% TFA) with a flow rate of 12 mL/min over 60 minutes and was visualized by UV at 214 nm. Final product mass was 21.5 mg (33% yield). The mass was confirmed using MALDI-TOF (Expected Mass: 2718 Da, Observed Mass: 2718 Da). Analytical HPLC trace shown in **Figure A 1**.

Synthesis of FlP14LRR-SH

Peptide synthesis proceeded as described previously with the following changes. Synthesis of **FlP14LRR-SH** on a 50 mg scale of H-rink amide resin was performed. After the final Fmoc-P_L, the addition of a glycine (28.5 mg, 4 mmol), an MTT-protected lysine (60.0 mg, 4 mmol), and a second glycine (28.5 mg, 4 mmol) were activated with HATU (36.5 mg, 4 mmol) and DIEA (33.4 µL, 8 mmol); and coupled for 2 hours each. The MTT group was deprotected with the addition of 4 mL 30% HFIP in DCM for 20 minutes (2X). A solution of fluorescein-NHS (12.5 mg, 1.1 mmol eq) and diisopropylethylamine (8.6 µL, 2.2 mmol) in 4 mL DMF was coupled for 4 hours and washed with 5 mL of DMF (2X), DCM (2X), MeOH (2X), DCM (2X), DMF (2X). The terminal glycine was deprotected by adding 4 mL of 30% piperidine in DMF, mixed for 20 minutes, and washed with 5 mL of DMF (2X), DCM (2X), MeOH (2X), DCM (2X), DMF (2X). Trityl-4-mercaptobutyric acid (34.8 mg, 4 mmol), activated with HATU (36.5 mg, 4 mmol) and DIEA (33.4 µL, 8 mmol) in 4 mL DMF, was added to peptide-bound resin and mixed for 3 hours. The reaction solution was drained and the resin and washed with 5 mL of DMF (2X), DCM (2X), MeOH (2X), DCM (2X), DMF (2X). **FlP14LRR-SH** was then globally deprotected and cleaved from the resin using 5 mL cleavage cocktail of 90: 5: 2.5: 2.5, TFA: EDT: TIPS: H_2O. The cleavage cocktail with the peptide-bound resin was agitated for 3 hours. The crude mixture was collected into a preweighed plastic falcon tube. The resin was washed with 5 mL DCM and collected into the preweighed plastic falcon tube. A second 5 mL aliquot of cleavage cocktail was added to the flask and agitated for an additional 30 minutes and drained into the collecting tube. The resin was washed with 5 mL DCM and collected. The crude mixture was concentrated *in vacuo*. Cold diethyl ether (15 mL) was added to the crude mixture, which led to a precipitate. After centrifugation, the supernatant was decanted and the precipitate was dried under vacuum overnight. The crude **FlP14LRR-SH** was resuspended in deionized water (approximately 10 mg/mL) and was purified on RP-HPLC, using a C18 column (Phenomenex, USA) with a gradient of 30-60% acetonitrile (0.1% TFA) in water (0.1% TFA) with a flow rate of 12 mL/min over 60 minutes and was visualized by UV at 214 nm. Final product mass was 10.5 mg (13.4% yield). The mass was confirmed using MALDI-TOF mass spectrometry (Expected Mass: 3261 Da, Observed Mass: 3261.5 Da). Analytical HPLC trace shown in **Figure A 2**.

2.5.8 Solid Phase Peptide Synthesis of P14GAP CAPHs

A 15 mL peptide synthesis flask was charged with 200 mg H-rink amide resin (0.45 mmol/g loading) for the synthesis of **P14GAP-SH** and **FlP14GAP-SH**. The resin was manually crushed and washed with 7 mL of DMF (2X), DCM (2X), MeOH (2X), DCM (2X), DMF (2X). The resin was swelled in 7 mL DMF with agitation for 30 mins. The first amino acid (2.5 eq.) was activated by sonication with HATU (2.5 eq.) and DIEA (5 eq.) in 7 mL DMF, then added to the resin in the peptide flask. Reaction was agitated for 3 hr then washed with 7 mL of DMF (2X), DCM (2X), MeOH (2X), DCM (2X), DMF (2X). The Fmoc protecting group was deprotected by adding 7 mL of 30% piperidine in DMF, and mixing for 20 minutes. The solution was drained, and resin washed with 5 mL of DMF (2X), DCM (2X), MeOH (2X), DCM (2X), DMF (2X). This cycle of coupling and deprotecting continued until all amino acids were coupled. After the final Fmoc-P_L, the addition of a glycine (107 mg, 4 mmol) was activated with HATU (136.9 mg, 4 mmol) and DIIEA (125 µL, 8 eq); and coupled for 2 hours each. The process was monitored by Kaiser[167] and chloranil[168] tests, and verified using test cleavages and MALDI-ToF mass spectrometry.

Synthesis of P14GAPSH

Upon synthesis of the 200 mg resin scale of **P14GAP** peptide, the resin was split and half (about 100 mg) resin was used. The trityl-4-mercaptobutyric acid (65.25 mg, 4 mmol) was activated with HATU (68.4 mg, 4 mmol) and diisopropylethylamine (64.2 µL, 8 mmol) in 4 mL DMF. This mixture was added to the peptide-bound resin and agitated at room temperature for 2 hours. The reaction solution was drained and the resin and washed with 5 mL of DMF (2X), DCM (2X), MeOH (2X), DCM (2X), DMF (2X). **P14GAP-SH** was then globally deprotected and cleaved from the resin using 5 mL cleavage cocktail of 90: 5: 2.5: 2.5, TFA: EDT: TIPS: H_2O. The cleavage cocktail with the peptide-bound resin was agitated for 3 hours. The crude mixture was collected into a preweighed plastic falcon tube. The resin was washed with 5 mL DCM and collected into the preweighed plastic falcon tube. A second 5 mL aliquot of cleavage cocktail was added to the flask and agitated for an additional 30 minutes and drained into the collecting tube. The resin was washed with 5 mL DCM and collected. The crude mixture was concentrated *in vacuo.* Cold diethyl ether (15 mL) was added to the crude mixture, which led to a precipitate. After

centrifugation, the supernatant was decanted and the precipitate was dried under vacuum overnight. The crude **P14GAP-SH** was resuspended in deionized water (approximately 10 mg/mL) and was purified on RP-HPLC, using a C18 column (Phenomenex, USA) with a gradient of 20-75% acetonitrile (0.1% TFA) in water (0.1% TFA) with a flow rate of 12 mL/min over 60 minutes and was visualized by UV at 214 nm. Final product mass was 25.1 mg (25% yield). The mass was confirmed using MALDI-TOF (Expected Mass: 2255 Da, Observed Mass: 2255 Da). Analytical HPLC trace shown in **Figure A 9**.

Synthesis of FlP14GAPSH

Peptide synthesis proceeded as described previously with the following changes. Synthesis of **FlP14GAP-SH** on a 50 mg scale of H-rink amide resin was performed. After the final addition of Fmoc-glycine, an MTT-protected lysine (56.2 mg, 4 mmol), and a second glycine (26.7 mg, 4 mmol) were activated with HATU (34.2 mg, 4 mmol) and DIEA (31.2 µL, 8 mmol); and coupled for 2 hours each. The MTT group was deprotected with the addition of 4 mL 30% HFIP in DCM for 20 minutes (2X). A solution of fluorescein-NHS (11.7 mg, 1.2 mmol eq) and diisopropylethylamine (8.6 µL, 2.4 mmol) in 4 mL DMF was coupled for 5 hours and washed with 5 mL of DMF (2X), DCM (2X), MeOH (2X), DCM (2X), DMF (2X). The terminal glycine was deprotected by adding 4 mL of 30% piperidine in DMF, mixed for 20 minutes, and washed with 5 mL of DMF (2X), DCM (2X), MeOH (2X), DCM (2X), DMF (2X). Trityl-4-mercaptobutyric acid (32.6 mg, 4 mmol), activated with HATU (34.2 mg, 4 mmol) and DIEA (31.2 µL, 8 mmol) in 4 mL DMF, was added to peptide-bound resin and mixed for 2 hours. The reaction solution was drained and the resin and washed with 5 mL of DMF (2X), DCM (2X), MeOH (2X), DCM (2X), DMF (2X). **FlP14GAP-SH** was then globally deprotected and cleaved from the resin using 5 mL cleavage cocktail of 90: 5: 2.5: 2.5, TFA: EDT: TIPS: H_2O. The cleavage cocktail with the peptide-bound resin was agitated for 3 hours. The crude mixture was collected into a preweighed plastic falcon tube. The resin was washed with 5 mL DCM and collected into the preweighed plastic falcon tube. A second 5 mL aliquot of cleavage cocktail was added to the flask and agitated for an additional 30 minutes and drained into the collecting tube. The resin was washed with 5 mL DCM and collected. The crude mixture was concentrated *in vacuo*. Cold diethyl ether (15 mL) was added to the crude mixture, which led to a precipitate. After centrifugation, the supernatant was decanted and the precipitate was dried under vacuum overnight. The crude **FlP14GAP-SH** was resuspended

in deionized water (approximately 10 mg/mL) and was purified on RP-HPLC, using a C18 column (Phenomenex, USA) with a gradient of 20-75% acetonitrile (0.1% TFA) in water (0.1% TFA) with a flow rate of 12 mL/min over 60 minutes and was visualized by UV at 214 nm. Final product mass was 6.1 mg (9.7% yield). The mass was confirmed using MALDI-TOF mass spectrometry (Expected Mass: 2798 Da, Observed Mass: 2798 Da). Analytical HPLC trace shown in **Figure A 10**.

2.5.9 Synthesis of Vancomycin tethers

Synthesis was adapted from literature procedure.[70] Vancomycin (100 mg, 69 mmol) was dissolved in 1 mL DMSO. A solution of N-(2-aminoethyl)maleimide (Cayman Chemical, 10.2 mg, 58 mmol) or 2-(pyridyldithio)ethylamine (Biosynth Carbosynth, 12.8 mg, 57 mmol) in 1 mL DMF was added dropwise to the vancomycin solution. PyBOP (benzotriazol-1-yl-oxytripyrrolidinophosphonium hexafluorophosphate, (41.9 mg, 81 mmol) was dissolved in 100 μL DMF and added to the vancomycin solution. The solution stirred at room temperature for 20 hours. A sample of the reaction was analyzed on a Waters Acquity UPLC with a SQD2 mass spectrometer to visualize the disappearance of vancomycin and appearance of the desired product, N-(2-aminoethyl)maleimido-vancomycin (Van Tether 1) or 2-(2-pyridinyl)dithioethylamino-vancomycin (Van Tether 2). Upon consumption of starting material, the product was precipitated with 5 mL diethylether and supernatant decanted. A second aliquot of 5 mL diethylether was added and decanted to wash the precipitate. The crude product was carried on to next steps without further purification.

2.5.10 Synthesis and purification of Vancomycin-P14 conjugates

VanP14S

Activated 2-(2-pyridinyl)dithioethylamino-vancomycin (Van Tether 2) (59.4 mg, 100% conversion, 37 mmol) was dissolved in 2 mL 1:1 water: acetonitrile. P14LRR-SH (10 mg, 4 mmol) was dissolved in 1 mL water and added to the vancomycin reaction flask. Diisopropylethylamine (3.2 μL, 18.4 mmol) was added and reaction stirred overnight. The crude mixture was purified by RP-HPLC using a C18 column (Phenomenex, USA) with a gradient of 5-60% acetonitrile (0.1% TFA) in water (0.1% TFA) with a flow rate of 12 mL/min over 60 minutes and was visualized by

UV at 214 nm. Final product mass was 10.3 mg (51% yield). The mass was confirmed using MALDI-TOF mass spectrometry (Expected Mass: 4223 Da, Observed Mass: 4224 Da). Analytical HPLC trace shown in **Figure A 3**.

FlVanP14S

Activated 2-(2-pyridinyl)dithioethylamino-vancomycin (Van Tether 2) (52 mg, 100% conversion, 32 mmol) was dissolved in 2 mL 1:1 water: acetonitrile. **FlP14LRR-SH** (10.5 mg, 3.2 mmol) was dissolved in 1 mL water and added to the vancomycin reaction flask. Diisopropylethylamine (2.8 μL, 16.1 mmol) was added and reaction stirred overnight. The crude was purified using C18 column (Phenomenex, USA) with a gradient of 10-80% acetonitrile (0.1% TFA) in water (0.1% TFA) with a flow rate of 12 mL/min over 60 minutes and was visualized by UV at 214 nm. Final product mass was 11.2 mg (73% yield). The mass was confirmed using MALDI-TOF mass spectrometry (Expected Mass: 4766 Da, Observed Mass: 4768 Da). Quantification of concentration was determined by UV-vis spectrometry and Beer's Law at 495 nm wavelength and 70,000 molar extinction coefficient. Analytical HPLC trace shown in **Figure A 5**.

VanMalP14

Activated N-(2-aminoethyl)maleimido-vancomycin (Van Tether 1) (54 mg, 100% conversion, 34 mmol) was dissolved in 500 μL DMSO and added to 1.5 mL acetonitrile. **P14LRR-SH** (8 mg, 3 mmol) was dissolved in 1 mL water and added to the vancomycin reaction flask and reaction stirred overnight. The crude was purified using C18 column (Phenomenex, USA) with a gradient of 5-70% acetonitrile (0.1% TFA) in water (0.1% TFA) with a flow rate of 12 mL/min over 60 minutes and was visualized by UV at 214 nm. Final product mass was 5.3 mg (42% yield). The mass was confirmed using MALDI-TOF mass spectrometry (Expected Mass: 4286 Da, Observed Mass: 4289 Da). Analytical HPLC trace shown in **Figure A 4**.

VanP14GAPS

Activated 2-(2-pyridinyl)dithioethylamino-vancomycin (Van Tether 2) (52 mg, 100% conversion, 32 mmol) was dissolved in 2 mL 1:1 water: acetonitrile. Approximately 10.0 mg of

P14GAP-SH (4.4 mmol) in 1 mL DI water was added to the vancomycin reaction flask (2254). Diisopropylethylamine (3.9 μL, 22.4 mmol) was added and reaction stirred for 48 hours. The crude was purified using C18 column (Phenomenex, USA) with a gradient of 5-70% acetonitrile (0.1% TFA) in water (0.1% TFA) with a flow rate of 12 mL/min over 60 minutes and was visualized by UV at 214 nm. Final product mass was 9.2 mg (55% yield). The mass was confirmed using MALDI-TOF mass spectrometry (Expected Mass: 3758 Da, Observed Mass: 3762 Da). Analytical HPLC trace shown in **Figure A 11**.

FlVanP14GAPS

Activated 2-(2-pyridinyl)dithioethylamino-vancomycin (Van Tether 2) (52 mg, 100% conversion, 32 mmol) was dissolved in 2 mL 1:1 water: acetonitrile. **FlP14GAP-SH** (6.1 mg, 2.2 mmol) was dissolved in 1 mL water and added to the vancomycin reaction flask. Diisopropylethylamine (1.9 μL, 10.9 mmol) was added and reaction stirred for 48 hours. The crude was purified using C18 column (Phenomenex, USA) with a gradient of 5-60% acetonitrile (0.1% TFA) in water (0.1% TFA) with a flow rate of 12 mL/min over 60 minutes and was visualized by UV at 214 nm. Final product mass was 5.6 mg (58% yield). The mass was confirmed using MALDI-TOF mass spectrometry (Expected Mass: 4301 Da, Observed Mass: 4308 Da). Quantification of concentration was determined by UV-vis spectrometry and Beer's Law at 495 nm wavelength and 70,000 molar extinction coefficient. Analytical HPLC trace shown in **Figure A 12**.

2.5.11 Synthesis of Vancomycin-SH

Vancomycin-SH was used to calibrate a standard curve for the disulfide reduction of **VanP14S**. To a 1-dram glass vial, 940 μL of crude Van Tether 2 in DI water (approximately 50 mg, 30.9 mmol) was added. Following the addition of 1 mL of acetonitrile, the solution was degassed for 30 minutes with N_2. Dithiothreitol (47.7 mg, 309 mmol) was added and the solution was stirred at room temperature for 20 hours. Completion of the reaction was confirmed by ESI-MS. The reaction mixture was filtered and purified by RP-HPLC (C18 column), 10-70% acetonitrile in water with 0.1% TFA over 60 min. The appropriate fractions were isolated and

lyophilized to afford 33.7 mg of white powder in 72% yield. Analytical HPLC trace shown in **Figure A 8**.

2.5.12 Synthesis of fluorescent vancomycin compounds

FITC-Vancomycin

The procedure was adapted from literature procedure.[69] Vancomycin (16.1 mg, 0.011 mmol) was dissolved in 2.5 mL of carbonate/bicarbonate buffer (pH 10) in a 1-dram vial charged with a stir bar. Fluorescein isothiocyanate (FITC) (25 mg, 0.064 mmol, 6.0 molar equiv) was dissolved in 100 µL DMSO and added to the reaction vial. The solution was stirred at 4 °C overnight. The reaction mixture was filtered and purified by RP-HPLC (C18 column), 20-85% acetonitrile in water with 0.1% TFA over 60 min. The appropriate fractions were isolated and lyophilized to afford an orange powder (6.2 mg, 26% yield). Two peaks were isolated by HPLC, accounting for the mixed isomers of FITC starting material. The mass was confirmed using MALDI-ToF. Expected Mass: $[M+H]^+$1839 Da; Observed Mass: $[M+Na]^+$ 1861 Da. Regiochemistry confirmed by loss of vancosamine sugar(s) 1696, 1533 Da. Analytical HPLC trace shown in **Figure A 6**.

RITC-Vancomycin

Procedure was adapted from literature protocol.[69] Vancomycin (11.2 mg, 0.008 mmol) was dissolved in 2.5 mL of carbonate/bicarbonate buffer (pH 10) in a 1-dram vial charged with a stir bar. Rhodamine isothiocyanate (RhITC) (25 mg, 0.047 mmol, 6.0 molar equiv) was dissolved in 100 µL DMSO and added to the reaction vial. The solution was stirred at 4 °C overnight. The reaction mixture was filtered and purified by RP-HPLC (C18 column), 15-85% acetonitrile in water with 0.1% TFA over 60 min. The appropriate fractions were isolated and lyophilized to afford a red powder (5.8 mg, 29% yield). Two peaks were isolated by HPLC, accounting for the mixed isomers of RhITC starting material. The mass was confirmed using MALDI-ToF. Expected Mass: $[M+H]^+$ 1950 Da; Observed Mass: $[M+H]^+$ 1950 Da. Regiochemistry confirmed by loss of vancosamine sugar(s) 1787, 1645 Da. Analytical HPLC trace shown in **Figure A 7**.

2.5.13 VanP14S disulfide reduction in the presence of DTT

VanP14S (25 μM) was incubated at 37 °C with 10 mM DTT in degassed phosphate buffered saline (PBS 1X, pH 7.4) containing 50 μM 6-quinolinecarboxylic acid as the internal standard in 1.0 mL total volume. When monitoring VanSH release, an aliquot of the reaction mixture was taken at different time points and directly analyzed by UPLC-MS. The time points were analyzed using RP-UPLC with a C18 column consisting of 2-50% acetonitrile in water with 0.1% formic acid (0.5 ml/min, column temperature of 40 ^{o}C). The peaks corresponding to the m/z for quinolinecarboxylic acid (+1: 174), VanSH (+1: 2113), and P14LRR-SH (+5: 545) were detected and extracted using MassLynx software. This experiment was run a single time, and the percentage of release vs time was fitted using Graph Pad Prism 7 to generate half-life.

2.5.14 VanP14S disulfide reduction in the presence glutathione

VanP14S (25 μM) was incubated at 37 °C with 10 mM glutathione (GSH) in degassed phosphate buffered saline (PBS 1X, pH 7.4) containing 50 μM 6-quinolinecarboxylic acid as the internal standard in 1.0 mL total volume. When monitoring VanSH release, an aliquot of the reaction mixture was taken at different time points and directly analyzed by UPLC-MS. The time points were analyzed using RP-UPLC with a C18 column consisting of 2-50% acetonitrile in water with 0.1% formic acid (0.5 ml/min, column temperature of 40 ^{o}C). The peaks corresponding to the m/z for quinolinecarboxylic acid (+1: 174), VanSH (+1: 2113), and P14LRR-SH (+5: 545) were detected and extracted using MassLynx software. This experiment was run in duplicate, and the percentage of release vs time was fitted using Graph Pad Prism 7 to generate half-life.

2.5.15 Minimum Inhibitory Concentration (MIC)

The minimum inhibitory concentrations (MICs) of the conjugates and control drugs were determined using the broth microdilution method, according to guidelines outlined by the Clinical and Laboratory Standards Institute (CLSI)[169] against clinically-relevant bacterial strains. Bacterial strains were grown aerobically overnight on tryptone soy agar plates at 37^{o}C. Afterwards, a bacterial solution equivalent to 0.5 McFarland standard was prepared and diluted in cation-adjusted Mueller-Hinton broth (CAMHB) (except *E. faecium* and *L. monocytogenes*) to achieve a bacterial concentration of about 5×10^5 CFU/mL. *E. faecium* and *L. monocytogenes* were diluted

in tryptone soy broth (TSB) to achieve a bacterial concentration of about 5×10^5 CFU/mL. conjugates and control drugs were added in the first row of the 96-well plates, and serially diluted with the corresponding media containing bacteria. Plates were then, incubated aerobically at 37 °C for 18-20 hours before recording the MIC results. MICs reported are the minimum concentrations of the compounds and control drugs that could completely inhibit the visual growth of bacteria.

2.5.16 Time-kill kinetics assay of vancomycin-P14 conjugates

In order to evaluate the mode of killing of vancomycin-P14 conjugates, a standard time kill assay was performed against MRSA USA 300 as described previously.[170-171] MRSA USA300 cells in logarithmic growth phase (OD600 ~1.00) were diluted to ~106 colony-forming units (CFU/mL) and exposed to concentrations equivalent to either 2X or 5X MIC (in triplicate) of VanP14S, VanMalP14 and vancomycin in tryptic soy broth. Water (the solvent of conjugates) was used as a negative control. Aliquots (100 µL) were collected from each treatment after 0, 2, 4, 6, 8, 12, and 24 hours of incubation at 37 ^{o}C and subsequently serially diluted in PBS. Bacteria were then, transferred to tryptic soy agar plates and incubated at 37 ^{o}C for 18-20 hours before viable CFU/mL was determined.

2.5.17 *E. coli* membrane disruption assessment by β-galactosidase leakage

Peptide solutions were prepared in deionized water (DIW) to make concentrations at 2X and 4X the determined MIC values for peptides and conjugates against *E. coli* ATCC 25922. Five stationary colonies of *E. coli* ATCC 25922 were inoculated in 50 mL Mueller Hinton Broth (MHB) and grown at 37 ^{o}C to for about 2 hours until the OD_{595} reached 0.1. Following, 5 mL of isopropyl-β-D thiogalactopyranoside (IPTG) (24 mg/10 mL PBS) was added to bacteria culture for final concentration of 1 mM. The bacteria was induced until an OD_{595} between 0.3 and 0.5 was reached. A 10 mL aliquot of the bacteria in the IPTG/MHB media was removed and centrifuged at 3500 rpm for 5 min and spent media was decanted. The pelleted bacteria was then washed twice with 10 mL of fresh MHB and resuspended in 10 mL of MHB. The bacteria were plated in a 96-well plate at 90 µL per well, followed by the addition of 10 µL of the peptide solution. The bacteria were incubated with the peptide treatment for 1 hour. The 96-well plate was centrifuged for 5 min at 3500 rpm, and 80 µL of the supernatant was transferred to a new 96-well plate. Then, 20 µL of

a freshly prepared 2-nitrophenyl-β-D-galactopyranoside (ONPG) (40 mg/10 mL of PBS) solution was added to each well for a final concentration of 0.8 mg/mL. The 405 nm absorbance values were read every 5 min over the course of 1 h using a TECAN microplate reader to monitor the levels of o-nitrophenol from the β-galactosidase release from *E. coli*. The leakage was calculated based on the absorbance value obtained for treated samples with a time zero absorbance value subtracted from each time point. For all experiments melittin was used as a positive control, PBS 1X was used as a negative control, and Fl-P14LRR was included as a reference. Data was obtained in duplicates from at least two independent experiments.

2.5.18 *E. coli* outer membrane disruption assay

The effect of peptides on the bacterial outer membrane permeability was characterized by measuring the uptake of N-phenyl-1-naphthylamine (NPN) adapted from a previous study.[172] Stationary colonies of *E. coli* ATCC 25922 were inoculated in Mueller Hinton Broth (MHB) and grown at 37 ^{o}C to mid-exponential phase with optical density at 595 nm between 0.5 and 0.6. An aliquot was centrifuged at 3500 rpm for 5 minutes and the supernatant was removed. Bacteria were washed with 5 mM HEPES, 5 mM glucose buffer, pH 7 and centrifuged at 3500 rpm for 5 minutes, the supernatant was removed, and the bacteria were resuspended in buffer. Bacteria were plated in a black-walled 96-well plate (Greiner Bio One, Catalog No.07-000-088) to a final OD_{595} of 0.5 and NPN was added to a final concentration of 10 μM. Fluorescence was measured with excitation of 360 nm and emission at 415 nm on a TECAN Infinite F PLEX plate reader with readings every 2 minutes. A baseline was established by reading the wells for 4 minutes. Sample concentrations of 10 μL peptides, 1% Triton X-100 (positive control), and DIW (negative control) were added and fluorescence measured for a total experiment time of 30 minutes. Data were normalized by using Triton X as 100% permeation of the outer membrane, and by taking the raw values at 16 minutes where the fluorescence stabilized. $(F_{obs} - F_o) / (T_{100} - T_o)$ where F_{obs} is the fluorescence at 16 minutes, F_o is fluorescence at time zero, T_{100} is fluorescence of Triton X-100 at 16 minutes, and T_o is fluorescence of Triton X at time zero. An ordinary one-way ANOVA for multiple comparisons was used to test statistical significance ($P < 0.05$) between results for each treatment and the untreated samples. Data were obtained in duplicates from at least two independent experiments.

2.5.19 MRSA cell membrane disruption assessment

Release of 260 and 280 nm absorbing components of nucleic acids was utilized in order to investigate the effect of the vancomycin-P14 conjugates on the integrity of the MRSA cell membrane, as previously described.[173-174] A logarithmic phase culture of MRSA USA300 was incubated with 5X MIC concentrations of **VanP14S** or **VanMalP14** (in triplicate) at 37°C for 30 minutes. Untreated MRSA cells (H_2O) and vancomycin-treated cells (in triplicates) served as negative controls. Lysostaphin (20 µg/mL, in 50 mM Tris-HCl, pH 8.00) was used as a positive control due to its ability to disrupt the staphylococcal cell membrane.[175-176] The concentration of released DNA (ng/µL) was determined using the standard nucleic acid quantification function of a NanoDrop spectrophotometer (ThermoScientific). Data are presented as the concentration of released DNA (ng/µL) for each test agent compared to that for the positive control (lysostaphin). A one-way ANOVA with post-hoc Dunnett's test for multiple comparisons was used to test statistical significance ($P < 0.05$) between results for each treatment and the untreated samples (H_2O).

2.5.20 Membrane depolarization assay

The cytoplasmic membrane depolarization activity of the peptides were characterized with the membrane potential-sensitive dye 3,3'-dipropylthiadicarbocyanine iodide ($diSC_3$-5) adapted from a previous study.[172] Stationary colonies of *E. coli* ATCC 25922 or *S. aureus* ATCC 10537 were inoculated in Mueller Hinton Broth (MHB) and grown at 37 ^oC to mid-exponential phase with an optical density at 595 nm between 0.5 and 0.6. An aliquot was centrifuged at 3500 rpm for 5 minutes and supernatant removed. Bacteria were washed with 5 mM HEPES, 20 mM glucose, 0.1 M KCl buffer, pH 7 and centrifuged at 3500 rpm for 5 minutes. The supernatant was removed and the bacteria were resuspended in buffer. Bacteria were plated in a black-walled 96-well plate (Greiner Bio One, Catalog No.07-000-088) to a final OD_{595} of 0.1 and $diSC_3$-5 was added to a final concentration of 1 µM. The bacteria were incubated at 37 ^oC for 1 hour. Fluorescence was measured with an excitation wavelength of 620 nm and emission at 670 nm on a TECAN Infinite F PLEX plate reader with readings every 30 seconds. A baseline was established by reading the wells for 1 minute. Sample concentrations of 10 µL peptides, 1% Triton X-100 (positive control), and DIW (negative control) were added and fluorescence measured for a total experiment time of

5 minutes. Data were normalized using the raw data at 4 minutes where the fluorescence stabilized. $(F_{obs} - F_o) / (T_{100} - T_o)$ where F_{obs} is the fluorescence at 4 minutes, F_o is fluorescence at time zero, T_{100} is fluorescence of Triton X at 4 minutes, and T_o is fluorescence of Triton X at time zero. An ordinary one-way ANOVA for multiple comparisons was used to test statistical significance ($P < 0.05$) between results for each treatment and the untreated samples. Data were obtained in duplicates from at least two independent experiments.

2.5.21 Flow cytometry of bacterial uptake

The procedure was adapted from literature procedure.[69] Stationary colonies of *E. coli* ATCC 25922 or *S. aureus* ATCC 10537 were inoculated in Mueller Hinton Broth (MHB) and grown at 37 °C to mid-exponential phase with an optical density at 595 nm near 0.5. A 15 mL aliquot was removed and centrifuged at 3500 rpm for 5 minutes. The supernatant was removed, and the pellet was resuspended in 15 mL fresh MHB. The bacterial culture was separated into 500 µL aliquots in Eppendorf tubes. Bacteria were centrifuged at 6000 rpm for 5 minutes, the media was removed, and the bacteria were resuspended in 300 µL of conjugate concentrations in PBS 1X. Bacteria were incubated for 10 minutes or 1 hour at 37 °C, then centrifuged at 6000 rpm for 5 minutes and washed with PBS 1X twice. Bacterial pellets were finally resuspended in 1 mL PBS 1X or 1 mL PBS with 2 mg/mL trypan blue. The fluorescence of the bacteria cells was measured using a BD Fortessa LSR flow cytometry cell analyzer (BD Biosciences). All samples were run in duplicate. The mean arbitrary florescence values of gated cells were measured and recorded upon excitation of the fluorophore, fluorescein, using the 488 nm laser. For each experiment, a negative control of cells that were not incubated with fluorescent compound (PBS only) was also analyzed.

2.5.22 Confocal microscopy of live bacteria

Stationary colonies of *E. coli* ATCC 25922 or *S. aureus* ATCC 10537 were inoculated in Mueller Hinton Broth (MHB) and grown at 37 °C to mid-exponential phase with optical density at 595 nm between 0.5 and 0.6. An aliquot was centrifuged at 3500 rpm for 5 minutes and the supernatant was removed. Bacteria were resuspended in fresh MHB and washed a second time. After resuspending with fresh MHB, 90 µL bacteria were plated and 10 µL peptide concentrations were added to a 96-well plate. The plate was incubated for 10 min or 1 hr at 37 °C. Aliquots of

bacteria were centrifuged at 12,000 rpm for 2 minutes and washed 2X with PBS 1X buffer. Bacteria were fixed with 4% paraformaldehyde in PBS for 30 minutes at room temperature. Bacterial samples were loaded on a #1.5 poly-lysine coverslip (Neuvitro) and imaged using Nikon A1R Multiphoton inverted confocal microscope using a 100X oil objective with 488 nm laser line employed.

2.5.23 Hemotoxicity of conjugates on human red blood cells

Fresh human red blood cells (hRBCs) (Innovative Research, cat # IWB3CPDA1) were collected by centrifugation at 2000 rpm for 5 min followed by washing three times with 5 mL PBS 1X, pH 7.4. The supernatant of the final wash was aspirated and 200 µL of the cell pellet was added to 4.8 mL of PBS to make a 4% suspension (v/v), with a total volume of 5 mL. To a 96-well plate, 50 µL of the hRBC solution was added, followed by 50 µL of peptide treatment prepared in PBS to achieve a 2-fold dilution of peptide and a final suspension of 2% (v/v) of hRBCs. The plate was incubated at 37 °C under 5% CO_2 for 1 h. The plate was subsequently centrifuged at 1200 rpm for 5 min at 4 °C. Next 75 µL aliquots of the supernatants in each well were carefully transferred to a new 96-well plate. The release of hemoglobin was monitored by measuring the absorbance at OD_{405} every 5 minutes for 1 hour with a TECAN micro-plate reader. As controls, hRBCs were treated with PBS 1X as a negative control, 0.1% Triton X-100 as a positive control, and melittin (Sigma M2272) as a positive control. The percent of hemolysis was calculated based on the 100% release with 0.1% Triton X-100. Data were obtained in duplicates from two independent experiments.

2.5.24 Cell culture

J774A.1 macrophage cell line was cultured in DMEM supplemented with 10% Fetal Bovine Serum, 1% L-glutamine, 1% penicillin-streptomycin. The cells were grown at 37 ^{o}C under a controlled humidified atmosphere with 5% carbon dioxide. Cells were sub-cultured biweekly.

2.5.25 *In vitro* cell viability

Analysis of the cytotoxicity of compounds against J77A.1 macrophage cells was carried out using methylthiazolyldiphenyl-tetrazolium bromide (MTT, Sigma M2128).[147] Macrophage

cells were seeded into a 96-well plate at 100 µL and density of 20,000 or 25,000 cells/well in complete DMEM media. Cells were incubated overnight (60-80% confluency) at 37 ^{o}C under a 5% CO_2 atmosphere. The spent media was aspirated, and the cells were washed with 100 µL PBS. Then, 100 µL of peptide treatment made in DMEM growth media was added to the cells at concentrations ranging from 1.25- 40 µM. After 9 hours of incubation under 5% CO_2 atmosphere at 37 °C, the treatment media was aspirated and the cells were washed with 100 µL of PBS. Then, 100 µL of fresh complete DMEM media was added, followed by the addition of 10 µL of MTT solution (5 mg /mL MTT in PBS) to each well. The cells were incubated for an additional 2 hours. The MTT solution was aspirated and 100 µL of DMSO was added to each well and agitated for 5 minutes to dissolve the formed formazan crystals. Samples were run in duplicates and each experiment was repeated at least twice. The mean absorbance for each sample was measured and recorded at 590 nm on a TECAN micro-plate reader. Percent viability was determined by taking ratio of treated cells to untreated cells.

2.5.26 Mammalian cell flow cytometry

Macrophage J774A.1 cells were plated in 500 µL of complete DMEM media at 150,000 cells/well in round bottom tubes (BD Biosciences) and incubated overnight at 37°C under 5% CO_2 atmosphere. The cells were centrifuged at 1200 rpm for 7 minutes at 4 ^{o}C, and the spent media was aspirated using a Pasteur pipet and vacuum filter. The cells were then treated with 300 µL of peptide at concentrations ranging from 2.5- 10 µM prepared in complete DMEM media and were incubated for the desired incubation time at 37°C. Upon completion of the incubation period, the cells were centrifuged, and the spent media was aspirated. The cells were then resuspended in 300 µL of cold PBS 1X and the fluorescence of the cells was measured using an Accuri flow cytometer (BD Biosciences). All samples were run in duplicate, and each experiment was repeated at least twice. The mean arbitrary fluorescence values of gated cells were measured and recorded upon excitation of the fluorophore, fluorescein, using the 488 nm laser. For each experiment, a negative control of cells that were not incubated with fluorescent compound (DMEM only) was also analyzed.

Flow cytometry with Trypan Blue

After incubation with compounds, cells were centrifuged, and media aspirated as described in protocol above. The cells were then resuspended in 300 µL of 1 mg/mL trypan blue in PBS 1X without additional washing. Fluorescence was measured and analyzed as described.

2.5.27 Confocal microscopy in live cells

High resolution imaging of mammalian cells and subcellular localization of the peptides was performed in the J774A.1 macrophage cell line using a Nikon A1R Multiphoton inverted confocal microscope with a 60X oil objective with 405 nm (blue), 488 nm (green), and 572 nm (red) 488 nm laser lines employed. J774A.1 cells were seeded into a 4-well Ibidi µ-slide 4-well culture chamber (Cat. No. 80426) at a density of 125,000 cells/well in 500 µL of complete DMEM media. The cells were grown overnight (60% confluency) in a humidified 5% CO_2 atmosphere at 37°C. Cells were washed with 500 µL PBS, then, 400 µL of peptide treatment prepared in growth media was added to the wells at desired concentrations. The cells were incubated for 1 hour or 3 hours in the presence of the peptide treatment. Following incubation, the cells were washed with 500 µL of PBS. Then, 400 µL of either 100 nM Mitotracker, 1 µM Hoescht 33342 solution prepared in growth media or 300 nM Lysotracker, 1 µM Hoescht 33342 prepared in growth media were added to the wells and the cells were incubated for 30 minutes. After incubation, the cells were washed with 500 µL of PBS. Next, 500 µL of complete DMEM media was added to each well prior to imaging. Live cells were then imaged as above.

CHAPTER 3. CONTINUING THE PURSUIT OF AN IMPROVED DUAL-ANTIBIOTIC WITH A LINEZOLID-CAPH CONJUGATE

3.1 Introduction

Linezolid is a synthetic antibiotic grouped into the newer class of oxazolidinone antibiotics. It has been approved by the U.S. Food and Drug Administration (FDA) for use against resistant Gram-positive cocci, such as vancomycin-resistant *Enterococcus*, methicillin-resistant *S. aureus*, and penicillin-resistant *Pneumococci*. Linezolid disrupts bacterial growth by targeting protein synthesis machinery and inhibiting the initiation process. The target site of inhibition occurs earlier in the initiation process than other protein synthesis inhibitors, such as chloramphenicol, clindamycin, aminoglycosides, and macrolides.[177-178] Given linezolid has remarkable pharmacokinetic properties with almost 100% oral bioavailability, it is an ideal therapy against numerous Gram-positive infections located throughout the body.[179] Additionally, linezolid is equally active against methicillin-susceptible and -resistant staphylococci, against vancomycin-susceptible and VanA, VanB or VanC resistant enterococci, and against susceptible pneumococci or penicillin- and/or macrolide- resistant strains.[180-182] Advantageously, linezolid has equivalent mammalian intracellular activity as extracellular activity, although inferior *in cyto* killing to vancomycin derivatives, telavancin and ortavancin.[183] Given the disadvantages of vancomycin therapy detailed previously (chapter 2), linezolid is one of the best alternative therapies in treating Gram-positive infections.[184-185]

An estimated 10 million people fell ill with tuberculosis (TB) in 2019, with close to 1.5 million associated deaths.[186] Recently, linezolid has been included in the standard regimen of treatment for TB, multidrug-resistant tuberculosis (MDR TB), and extensively drug-resistant tuberculosis (XDR TB).[187-188] Although linezolid is an effective second-line treatment for TB, the long-term usage in the TB treatment regimen carries considerable risk of toxicity and adverse effects.[187, 189-190]

The promising outlook of combination therapy, observed in recent TB treatment, has inspired the treatment of other difficult infections through combination of linezolid and a secondary drug.[191] In combination with rifampicin, linezolid has shown an additive activity for susceptible *S. aureus* strains and inhibited rifampicin-resistant variants; and this combination appeared to be an attractive therapy against methicillin-resistant *S. aureus* strains.[192] Although

there are increases in bactericidal activity and reduction in the emergence of drug-resistant mutants of linezolid in combination with rifampicin, some observations of have noted synergism, indifference, or slight antagonism between the two drugs.[192-195] Antagonism among combinatorial drugs is not ideal drug as it typically results in the reduction in the effectiveness of one or more of the drugs; however, information gained from antagonistic drugs may aid in developing strategies to hinder the onset of resistance.[196]

Resistance to linezolid has remained infrequent since its approval and clinical use.[197] Because linezolid inhibits protein synthesis by binding to the peptidyl transferase center on the ribosome, almost all known resistance mechanisms involve mutations to the linezolid binding site.[198-199] Although linezolid is currently the only drug approved to treat vancomycin-resistant enterococci, the threat of linezolid- and vancomycin-resistant *Enterococcus faecium* (LR-VRE) represents a major challenge for infection control.[200-201] Antibiotic resistance among *Staphylococcus epidermidis* is also an emerging problem with linezolid-resistant *S. epidermidis* (LRSE) strains being detected in Europe since 2014.[202] Such isolates have limited or no therapeutic option.

In order to mitigate these disadvantages in linezolid therapy, we utilized our antibiotic-CAPH conjugate design to yield **LnzP14** and its fluorescent equivalent, **FlLnzP14** (**Figure 3.1 A**). We have developed an alternate mean of attaching the tether to linezolid, which only has an amide group available for conjugation. An acyl-amide strategy was undertaken, with a disulfide within the tether. In a reducing environment, the resulting linezolid thiol should rearrange to regenerate linezolid (**Figure 3.1 B**). Through this strategy using a reducible disulfide linker, we expect to deliver a combination therapy with superior activity against susceptible, resistant, and intracellular bacteria, including enterococcus, staphylococcus, and mycobacteria species. In arming this conjugate with two effective antibiotics, there is an additional potential to lower the dosage of linezolid and reduce toxicity accompanied by long-term usage. Lastly, this dual-antibiotic strategy may broaden the activity of linezolid to Gram-negative bacteria, that have intrinsic resistance to linezolid by efflux pumps.[203-204] Through conjugation with a cell-penetrating peptide, this conjugate may possibly evade efflux pump mechanisms and effectively accumulate within bacterial cells to therapeutic concentrations.

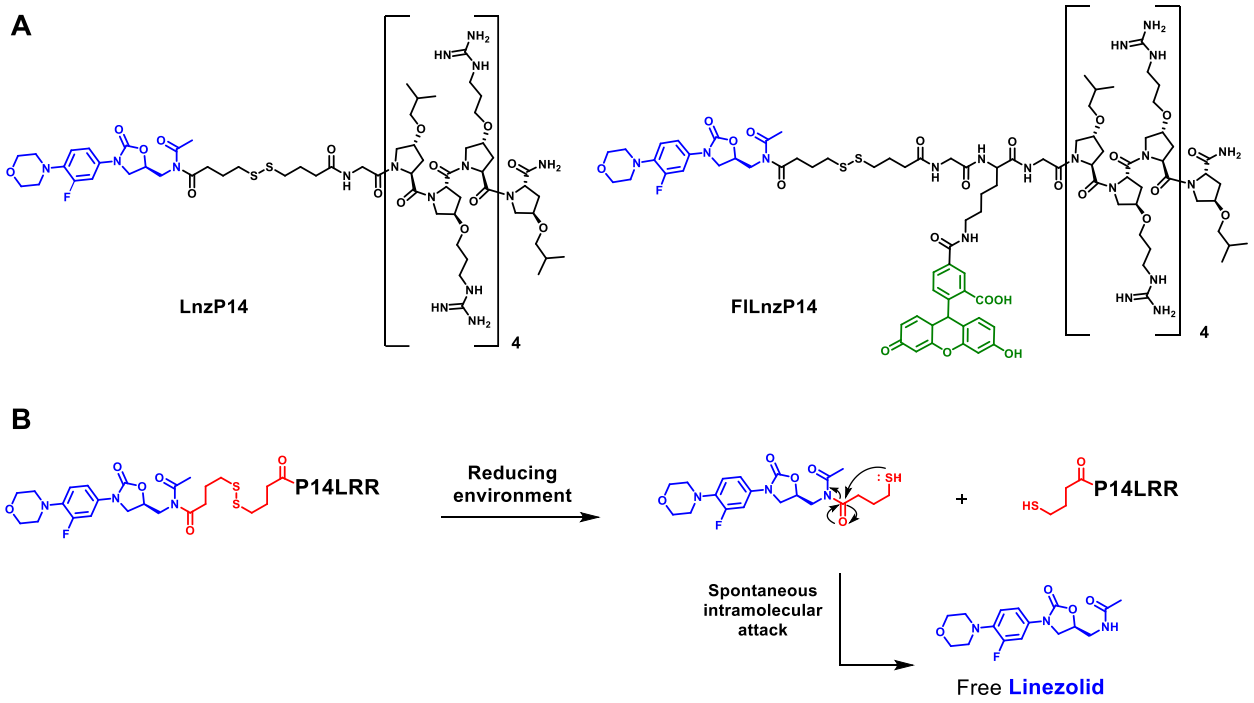

Figure 3.1. (A) Structures of linezolid-CAPHs conjugates. (B) Reduction of the **LnzP14** conjugate and regeneration of free linezolid.

3.2 Results and Discussion

3.2.1 Synthesis of thioamide linezolid (T-Lnz) and dithiobutyric acid linezolid (Lnz-DTBA)

The synthesis of the acylated linezolid derivative was carried out in the Chmielewski group by the visiting scholar, Paulo Pitasse Santos. In order to begin synthesis of the linezolid-CAPH conjugates, linezolid was first activated according to literature procedure.[205] Using Lawesson's reagent, the amide moiety in linezolid was transformed to a thioamide, **T-Lnz**, in an excellent 91% yield (**Scheme 3.1**). Next, **Lnz-DTBA** was synthesized by an Ag^{I}-promoted coupling reaction of thioamides and carboxylic acids. The **T-Lnz** intermediate and 4,4´-bis-dithiodibutyric acid (DTBA) were refluxed in the presence of silver (I) carbonate to afford the linezolid imide, **Lnz-DTBA**, in good yield, 69% (**Scheme 3.1**).

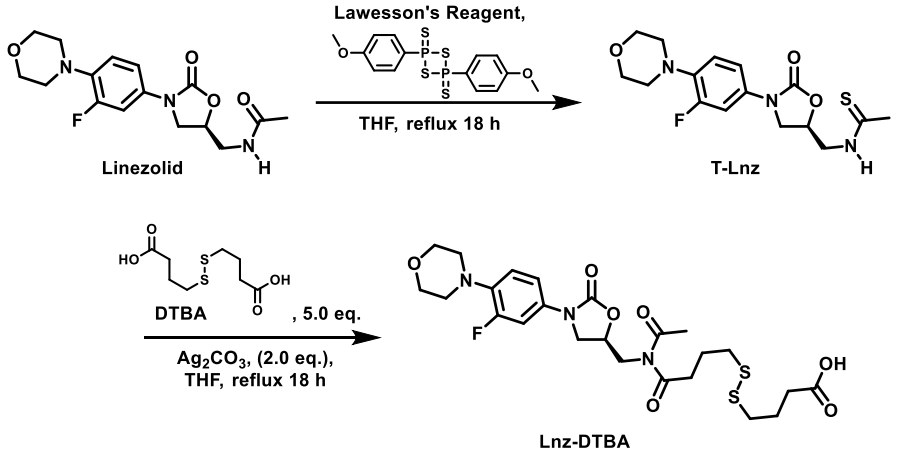

Scheme 3.1. Synthesis of tether-activated **Lnz-DTBA** as carried out by Paulo Pitasse Santos.

3.2.2 Synthesis of resin-bound conjugates LnzP14 and FlLnzP14

Peptide synthesis was carried out by Paulo Pitasse Santos and proceeded as previously described (Chapter 2, **Scheme 2.2**). Briefly, solid phase peptide synthesis (SPPS) afforded resin-bound **P14LRR** from Rink amide ChemMatrix resin (0.045 mmol/g). Amino acids were activated with HATU and DIEA in DMF and coupled to resin-bound peptide. Fmoc was deprotected with 30% piperidine in DMF. Once P14LRR was synthesized, the terminal Fmoc was removed and HATU-activated **Lnz-DTBA** was coupled to afford **LnzP14** on resin. Global deprotection and cleavage from the resin was performed using a cocktail of 96:3:1 HFIP:TIPS:$HCl_{conc.}$(final HCl concentration of 0.12 N) to yield crude conjugate (**Scheme 3.2**). These conditions were utilized to avoid hydrolysis of the imide moiety between linezolid and tether. **LnzP14** was purified using RP-HPLC and the desire product was confirmed using MALDI-ToF mass spectrometry.

The fluorescent variant, **FlLnzP14**, was synthesized similarly with minor modifications by Paulo. Fmoc-Lys(Mtt)-OH and Fmoc-Gly-OH were coupled to the **P14LRR** on resin, the Mtt group was selectively deprotected using 30% hexafluoroisopropanol (HFIP) in DCM, followed by the coupling of fluorescein-NHS ester to the free primary amine. The Fmoc on the terminal glycine was removed and HATU-activated **Lnz-DTBA** was coupled to afford **FlLnzP14** on resin. Global deprotection and cleavage from the resin was performed as described above. **FlLnzP14** was purified using RP-HPLC and the desire product was confirmed using MALDI-ToF mass spectrometry.

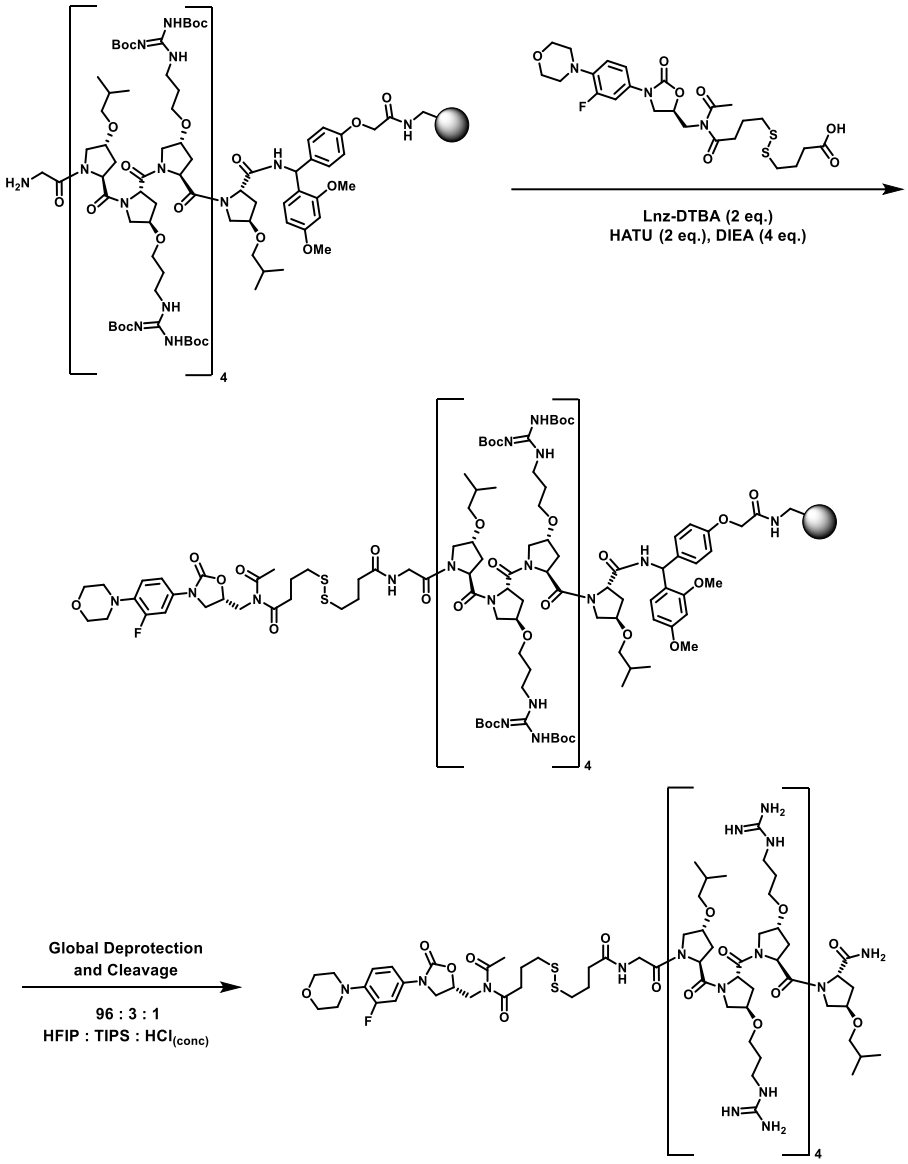

Scheme 3.2. Synthesis of **LnzP14** as carried out by Paulo Pitasse Santos.

3.2.3 Minimum inhibitory concentrations against *E. coli*

To begin our investigation into the activity of the **LnzP14** conjugates, we determined the minimum inhibitory concentrations using a microbroth dilution assay. Gram-negative *E. coli* ATCC 25922 bacteria were grown and incubated at a range of concentrations from 0.125- 16 μM with the melittin control, [206] conjugate, and 1:1 mixture of peptide and linezolid for 20 hours. The minimum inhibitory concentration (MIC) was determined using a microplate reader as the lowest concentration of drug at which no growth was observed (**Table 3.1**). Both conjugates, **LnzP14** and **FlLnzP14**, exhibited the same moderate antibacterial activity with MIC values of 4 μM. This is

an excellent increase in bactericidal activity as linezolid shows poor activity against *E. coli* ATCC 25922 with MIC greater than 256 µg/mL and other strains of *E. coli* greater than 128 µg/mL. [207-208] Additionally, the 1:1 mixture of CAPH and linezolid provided the same 4 µM MIC as the conjugates, with a slight improvement in activity compared to the CAPH alone. These data support the conjugation of CAPH to linezolid can broaden the scope of activity for linezolid, a Gram-positive antibiotic, to Gram-negative bacteria like *E. coli*.

Table 3.1. Minimum inhibitory concentrations (MICs) of linezolid conjugates against pathogenic bacteria isolates using the microbroth dilution assay after 20 h of treatment. Values reported in µM.

	MIC (µM)[a]
Melittin	2
LnzP14	4
FlLnzP14	4
FlP14LRR	8
1:1 FlP14LRR: Lnz	4

[a] conducted by Paulo Pitasse Santos

3.2.4 Bacterial lysis study using β-galactosidase assay

There are different mechanisms that antimicrobial peptides use to achieve antimicrobial activity, including targeting vital bacterial proteins or through lysing the bacterial membrane.[209-210] The P14LRR CAPH does not lyse bacteria and linezolid targets intracellular machinery as previously described. However, we wish to determine whether **LnzP14** targets the bacterial membrane in a lytic mechanism. Once the MICs were determined, we proceeded with the previously described β-galactosidase (β-Gal) assay to determine if **LnzP14** demonstrated lytic behavior in *E. coli*. At 2-times and 4-times the MIC value, **LnzP14** did not show significant lysis compared to the lytic melittin control (**Figure 3.2**). We can conclude that even at concentrations well above MIC values, **LnzP14** does not show bacterial membrane lysis as its bactericidal mechanism of action.

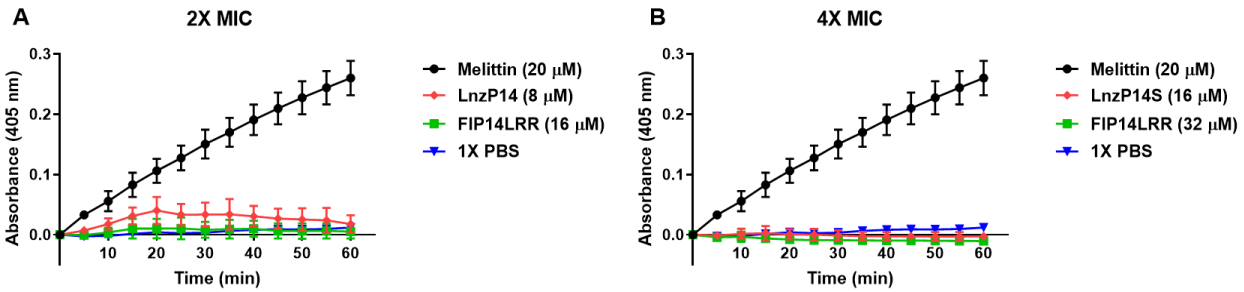

Figure 3.2. Monitoring the release of β-galactosidase over 1 hour from *E. coli* ATCC 25922 after 1 hour incubation with compounds. Positive control Melittin (20 μM) and conjugate at (A) 2X and (B) 4X MIC

3.2.5 Cell toxicity studies

With the **LnzP14** and **FlLnzP14** conjugates displaying bactericidal activity, we next needed to probe toxicity of the conjugates toward human red blood cells (hRBCs) and mammalian macrophage cells (J774A.1). We used melittin, a control AMP that demonstrates a lytic mechanism of action, and **P14LRR** as a standard for non-lytic behavior. The compounds and conjugate were incubated the with red blood cells for 1 hour. If the compounds lysed the red blood cells, heme would be released, and a signal would be observed on the spectrophotometer proportionally to the amount of lysis. Our results confirm that the **LnzP14** conjugate does not show significant lysis of red blood cells, analogous to linezolid or **P14LRR,** even at concentrations up to 40 μM (**Figure 3.3 A**). Therefore, it can be concluded that the **LnzP14** conjugate may not use a lytic mode of action that many AMPs display.

We chose to explore the mammalian cell toxicity of our conjugates with J774A.1 macrophage cells because phagocytes can engulf and harbor bacteria, and we wish to carry out conjugate internalization and *in cyto* bacterial clearance experiments on the same cell lines. Therefore, **LnzP14** and **FlLnzP14**, and **FlP14LRR** CAPH were incubated with mammalian cells for 9 and 24 hours at concentrations ranging from 0.5 to 32 μM, as carried out by Paulo Pitasse Santos. Through the addition of 3-(4,5-dimethylthiazol-2-yl)-2,5-diphenyltetrazolium bromide (MTT), we could monitor the metabolic activity of the cells in converting MTT to formazan, a colormetric indicator of cell viability that can be quantified on a spectrophotometer. After 9 hours, **LnzP14** did not show any visible cytotoxicity at concentrations up to 32 μM (data not shown). Our 24 hour results indicate that **LnzP14** and fluorescent variant, **FlLnzP14**, show similar toxicity with greater than 75% viability at 2 μM concentration (**Figure 3.3 B**). **FlP14LRR** shows less

toxicity with the viability decreasing at concentrations 8 µM and greater. Unfortunately, these results indicate that the cell viability of macrophage cells begins to decrease at the corresponding minimum inhibitory concentrations (MICs) of the conjugates. However, the MICs must be determined for a range of bacteria, including *in cyto* MICs, as only *in vitro E. coli* data has been presented.

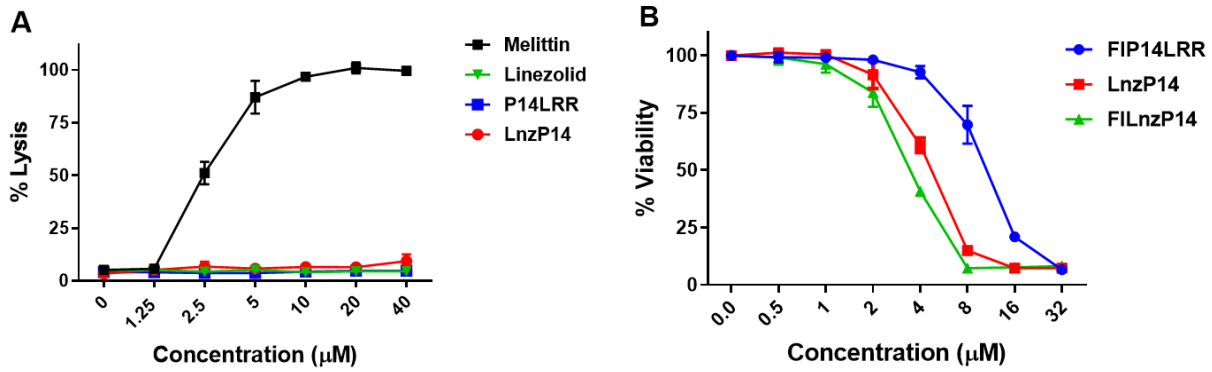

Figure 3.3. (A) Hemolysis assay measuring the release of hemoglobin from hRBC. Melittin was used as a positive control and values were normalized against 0.1% triton X-100. (B) Cell toxicity measuring the cell viability using an MTT assay after 24 h treatment of compounds, carried out by Paulo Pitasse Santos.

3.2.6 Release kinetics of linezolid from the LnzP14 conjugate

The inclusion of the disulfide linker between linezolid and **P14LRR** is a notable characteristic in the conjugate design. In the internal environment of the cell, the reductant glutathione is present in concentrations ranging from 1- 10 mM.[211] Once penetrating into the mammalian cell intracellular environment, the disulfide linkage of **LnzP14** can reduce to release **P14LRR-SH** and linezolid-SH (**Scheme 3.3**). After the disulfide is reduced, the free thiol on linezolid can intramolecularly attack the imide and release free linezolid. To evaluate the half-life ($t_{1/2}$) of the conjugate, we incubated **LnzP14** with two different reducing agents, dithiothreitol (DTT, 10 mM) and glutathione (GSH, 5 mM). Linezolid release from the conjugate was monitored using UPLC-MS for up to 90 minutes in DTT (carried out by Paulo Pitasse Santos) or 18 hours in GSH (**Figure 3.4**).

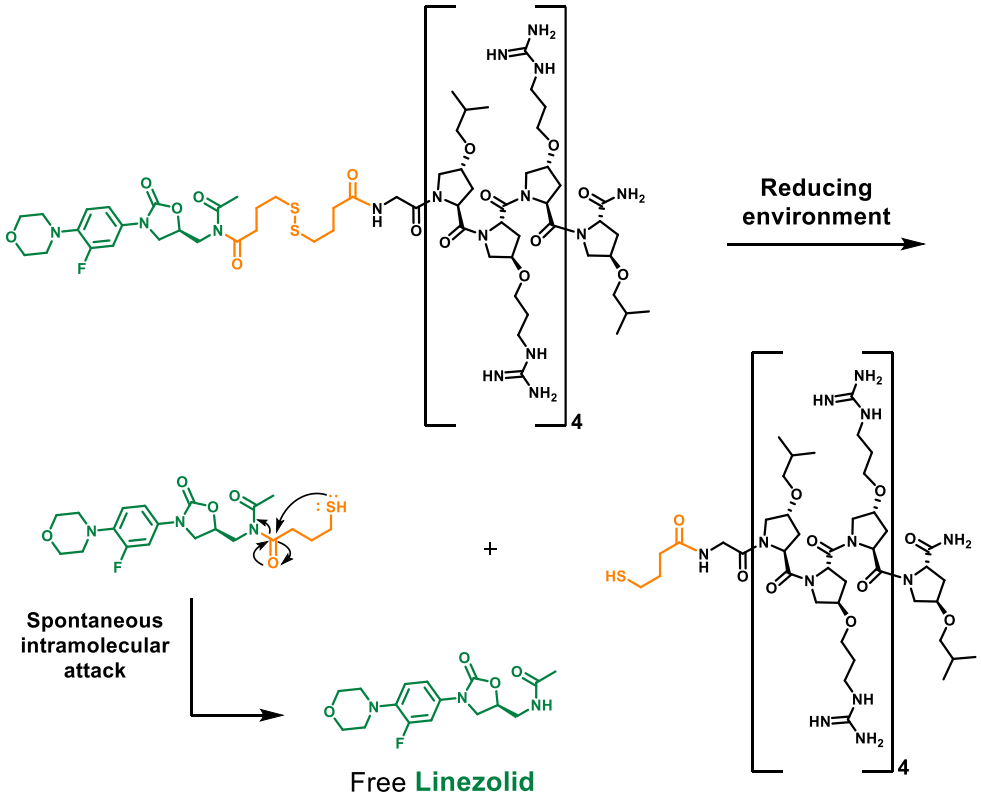

Scheme 3.3. Reduction of **LnzP14** and release of linezolid and **P14LRR-SH**.

For the DTT reduction of **LnzP14** and release of free linezolid, the half-life of the conjugate was determined to be 2.5 minutes (**Figure 3.4 A**). Ultimately, 82% of linezolid was released from the initial concentration of **LnzP14**. To examine this release under more physiological conditions, we changed reducing agents to GSH and lowered its concentration to reflect the typical intracellular environment more closely. Using 5 mM GSH, the half-life of the conjugate was calculated to be 2.5 hours and about 60% of linezolid was released from the initial concentration of **LnzP14** (**Figure 3.4 B**). The incomplete release of linezolid could be explained mechanistically. Once the conjugate is reduced to produce **P14LRR-SH** and Lnz-SH, the free thiol on linezolid may intramolecularly attack the acetyl position of the imide. Although unfavored, this rearrangement would not result in the release of free linezolid. Although 100% release of linezolid was not observed, these studies indicate that **LnzP14** is responsive to reducing environments comparable to *in cyto*.

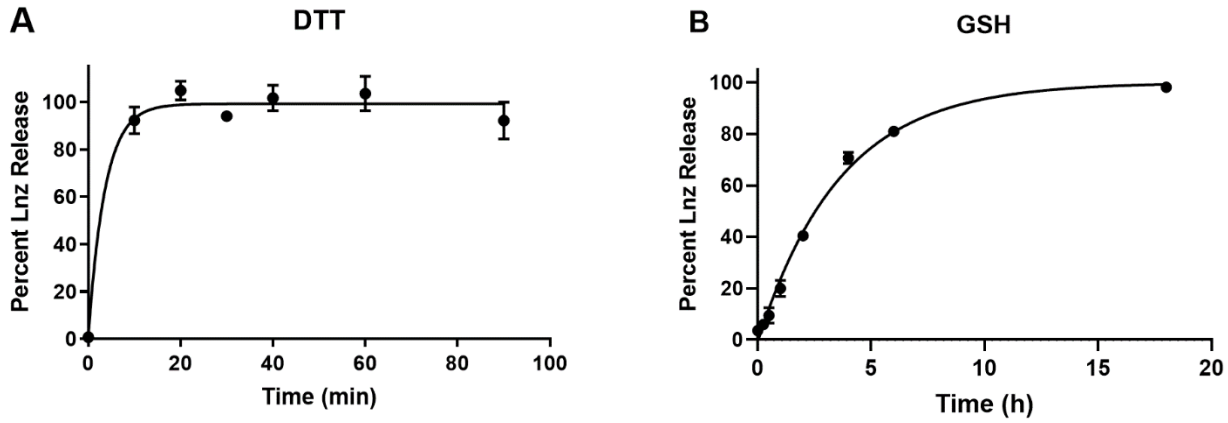

Figure 3.4. (A) Adjusted reduction and release of linezolid from **LnzP14** with 10 mM DTT in PBS buffer, as carried out by Paulo Pitasse Santos. (B) Adjusted reduction and release of linezolid from **LnzP14** with 5 mM GSH in PBS buffer.

3.2.7 Flow cytometry to quantify cellular internalization of FlLnzP14

After concluding that the **LnzP14** conjugate can reduce within the intracellular environment, we sought to quantify intracellular accumulation of the conjugate in macrophage cells. Using J774A.1 macrophage cells, 1.25 and 2.5 µM concentrations of **FlLnzP14** and **FlP14LRR** were incubated with cells for a period of 1 hour and 3 hours. These concentrations were chosen because cell viability was near 100%. After incubation, the cells were sorted by flow cytometry and cellular fluorescence was quantified. Trypan blue was used to quench surface-bound fluorescence, and quantify internal fluorescence related to the internalization of fluorescent peptide and conjugate.

First, the accumulation of both **FlP14LRR** and **FlLnzP14** is concentration and time dependent, as more fluorescence is observed after longer incubation times and higher concentrations **(Figure 3.5**). Next, **FlLnzP14** has significantly higher accumulation than **FlP14LRR** at both concentrations and time points (**Table 3.2**). At 1.25 µM, **FlLnzP14** has 3-4 times more fluorescence than **FlP14LRR**; and at 2.5 µM, **FlLnzP14** has 6-10 times more fluorescence than **FlP14LRR**. Additionally, 1 hour incubation times showed that there is a minimal level of the peptides associated with the membrane as visualized by trypan blue fluorescence quenching. About 83% and 100% of fluorescence for 1.25 and 2.5 µM **FlLnzP14** correspond to internal fluorescence after 1 hour, while about 60% of the fluorescence for

FlP14LRR is internal at both concentrations after 1 hour. Both these results conclude **FlLnzP14** is better at accumulating intracellularly than CAPH alone.

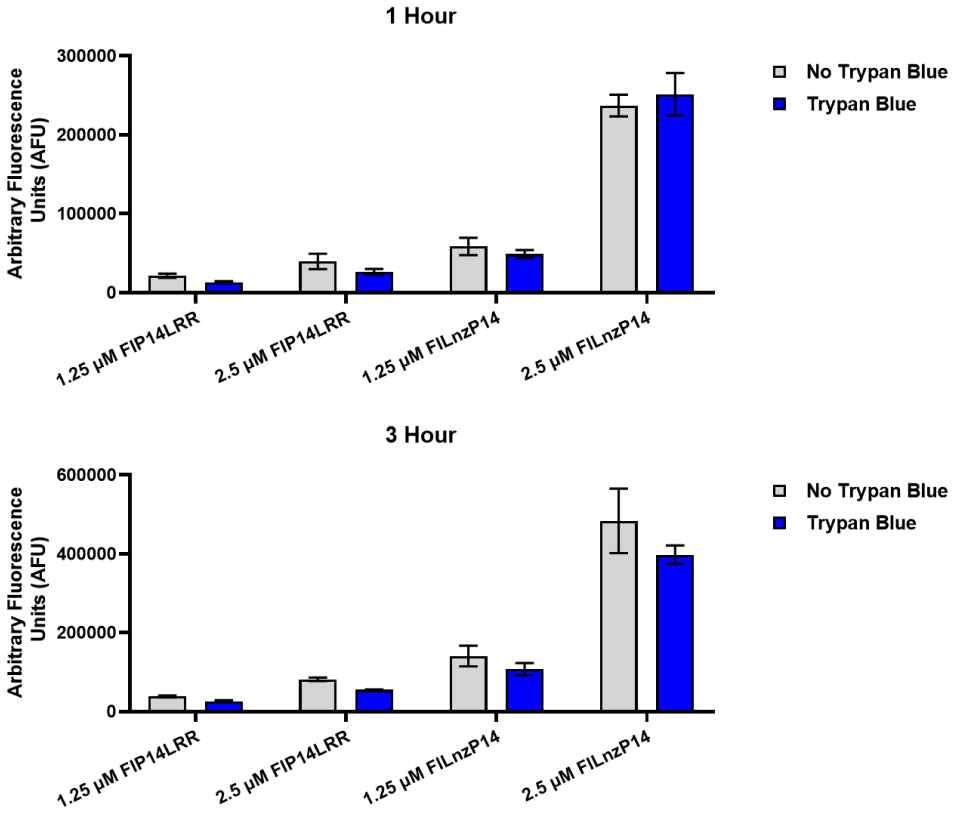

Figure 3.5. Cellular fluorescence of J774A.1 macrophage cells after 1- and 3-hour incubations. Trypan blue was used to quench surface bound fluorescence and selectively quantify internal fluorescence.

After 3 hours of incubation with CAPH and conjugate, we observe somewhat more surface-bound conjugate (**Figure 3.5**). About 80% of fluorescence for both 1.25 and 2.5 µM **FlLnzP14** corresponds to internal fluorescence after 3 hours, while about 70% of the fluorescence for **FlP14LRR** is internal at both concentrations after 3 hours. In all cases, the **FlLnzP14** conjugate showed enhanced cellular uptake and enhanced internalization of conjugate compared to **FlP14LRR.** These results indicate that surface binding is not an obstacle for **FlLnzP14**. Dietsche and Chmielewski coworkers have shown that adding hydrophobic moieties to the N-terminus of the **P14LRR** peptide results in enhanced uptake.[44] Our results reinforce that conclusion, translating to **FlLnzP14** showing enhanced penetration over the CAPH, **FlP14LRR**.

Table 3.2. Comparison of cellular uptake of **FlLnzP14** to **FlP14LRR** by flow cytometry fluorescence results.

Fluorescence Ratio of FlLnzP14 to FlP14LRR				
Concentration (μM)	**1 hr no TB**	**1 hr TB**	**3 hr no TB**	**3 hr TB**
1.25	3	4	4	4
2.5	6	10	6	7

3.2.8 Confocal microscopy to visualize cellular internalization of FlLnzP14

Not only do therapies need to penetrate and accumulate within cells, but they also need to accumulate and localize in intracellular compartments where their target bacteria may reside. For instance, engulfed *S. aureus* can reside inside phagosomes and phagolysosomes where it can replicate and survive innate immune responses and drug therapies.[109] Based on previous results in which P14LRR was found to penetrate macrophage cells, we wished to study the cellular uptake and internal localization of the linezolid-CAPH conjugate. Therefore, **FlLnzP14** was incubated with J774A.1 cells for 1- and 3-hours at a non-cytotoxic concentration, 2.5 μM (**Figure 3.6, Figure 3.7**). Following incubation, we further labeled cells with an endosomal marker (Lysotracker red, 300 nM) or a mitochondrial marker (Mitotracker red, 100 nM). In this way, if there is colocalization of **LnzP14** with either red stain, a yellow-orange color is visualized in the merge of the red and green confocal laser channels.

After the 1-hour incubation, we observe the green **FlLnzP14** fluorescence overlapping with red lysotracker stain. Therefore, the conjugate appears to primarily colocalize within endosomal compartments of the cell, and no visible localization with the mitochondria as was found with **FlP14LRR** (**Figure 3.6**).[41-42, 45] After the 3-hour incubation, we observe similar green **FlLnzP14** fluorescence overlapping with red lysotracker stain; however, we observe some faint overlapping with red mitotracker stain. The conjugate appears to primarily colocalize within endosomal compartments of the cell at 3 hours with some mitochondrial association (**Figure 3.7**). These results indicate that within the 1-3 hour time, **FlLnzP14** remains within endosomal compartments of the cell, with minimal observable association with mitochondria and release into

the cytoplasm. This suggests that **LnzP14** may be most suitable to target bacteria that remain trapped in endosomal and lysosomal compartments of mammalian cells.

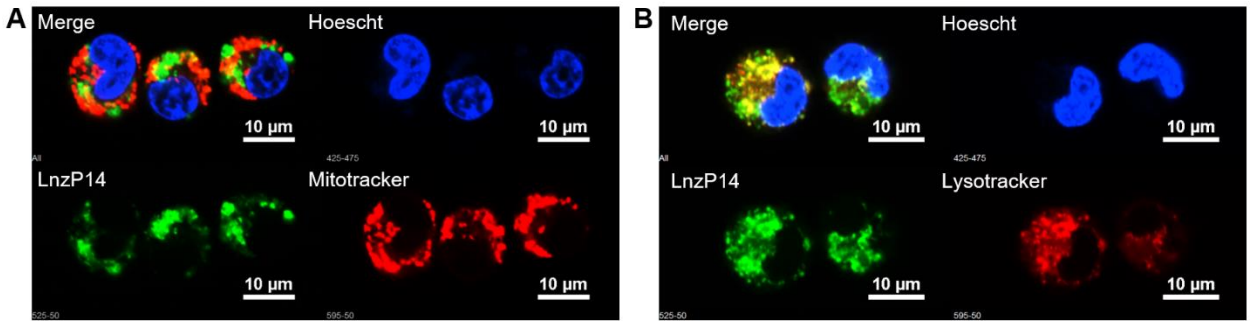

Figure 3.6. Confocal microscopy images of J774A.1 macrophage cells incubated with 2.5 µM **FlLnzP14** for 1 hr. (A) Merge (top left) and separate laser channels with Hoescht 33342 stain (blue), conjugate (green), and mitotracker mitochondrial stain (red). (B) Merge (top left) and separate laser channels with Hoescht 33342 nuclear stain (blue), conjugate (green), and lysotracker lysosomal (red). A yellow-orange color indicates colocalization of conjugate and selected red stain.

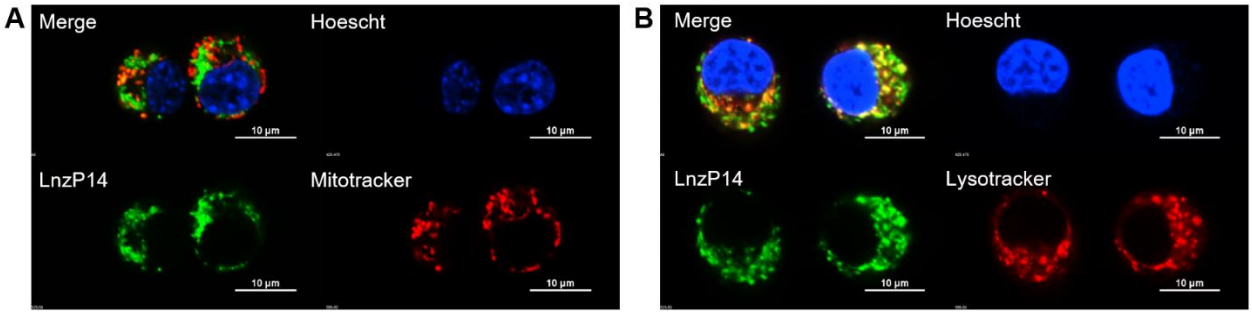

Figure 3.7. Confocal microscopy images of J774A.1 macrophage cells incubated with 2.5 µM **FlLnzP14** for 3 hr. (A) Merge (top left) and separate laser channels with Hoescht 33342 stain (blue), conjugate (green), and mitotracker mitochondrial stain (red). (B) Merge (top left) and separate laser channels with Hoescht 33342 nuclear stain (blue), conjugate (green), and lysotracker lysosomal (red). A yellow-orange color indicates colocalization of conjugate and selected red stain.

3.3 Conclusions

From these preliminary results, we have demonstrated that linezolid-CAPH conjugates have moderate activity against Gram-negative *E. coli* bacteria. This is a promising piece of data that indicate this conjugate may possess broad-spectrum activity, a characteristic linezolid does not show. The mode of action for this activity was determined to be non-lytic to bacterial membranes;

in addition, the **LnzP14** conjugate did not lyse human red blood cells. The conjugates demonstrate observable cytotoxicity to mammalian cells at concentrations 4 μM and above, indicating that toxicity may be problematic. Remarkably, the linezolid-CAPH conjugate showed superior cellular uptake compared to **P14LRR** with increases in uptake over 3 times higher than CAPH. Overall, the increase in cellular accumulation and subcellular localization within endosomes makes **LnzP14** a promising potential therapy to reach and target endosomally-trapped bacteria such as *S. aureus* and *Mycobacteria*.

3.4 Future Directions

In order to sufficiently determine the usefulness of **LnzP14** as a potential antibiotic therapy, more experiments are needed. Additional experiments to determine antibacterial activity against a range of pathogens, including drug-susceptible, drug-resistant, Gram-positive, and Gram-negative are currently planned. Once a selection of bacteria has been narrowed to those that the conjugate has good activity against, intracellular clearance experiments show be conducted to determine if **LnzP14** can clear these pathogens *in cyto*. More insight into the mode of action that this conjugate utilized will also be performed.

3.5 Materials and Methods

3.5.1 Materials

Starting material for unnatural amino acids, Fmoc-protected natural amino acids, and coupling reagents were purchased from Chem Impex (Wood Dale, IL) or Ana Spec, Inc. (Fremont, CA). H-Rink Amide ChemMatrix resin for peptide synthesis was purchased from PCAS Biomatrix Inc. (Quebec, Canada). Vancomycin hydrochloride was purchased from Millipore Sigma (Burlington, MA). Sterile DMEM supplemented with L-glutamine and Penicillin-Streptomycin were purchased from VWR (Batavia, IL). Buffers (1X PBS) and 10% fetal bovine serum (FBS) used in cell culture were purchased from Corning Inc. (Corning, NY) and Atlanta Biologicals, Inc. (Research and Diagnostic Systems, Inc., Minneapolis, MN), respectively. All bacteria and cell lines for culture were purchased form ATCC (Manassas, VA). All other chemicals and reagents were purchased commercially and were used without further purification unless mentioned from Sigma Aldrich (St. Louis, MO), Alfa Aesar (Haverhill, MA) or Thermo Fischer (Waltham, MA).

Peptides and conjugates were purified using a Waters Delta Prep 4000 HPLC equipped with a Phenomenex C18 semi-preparative column. CAPHs characterization was performed using matrix associated laser desorption ionization-time of flight (MALDI-TOF) mass spectrometry using an Applied Biosystem Voyager-DE TM BioSpectrometry workstation and analytical RP-HPLC using Waters Delta Prep 4000 HPLC equipped with a C18 reverse phase analytical column (5 μm, 4.6 mm x 250 mm; Phenomenex Luna). Cell uptake was measured using BD sciences Acurri and analyzed using BD software. Absorbance readings were obtained using microplate reader TECAN Infinite F PLEX. Confocal images were obtained using Nikon A1R-MP inverted confocal fluorescence microscope equipped with 60X oil objective. NIS Elements software was used to process images.

3.5.2 Synthesis of linezolid thioamide (T-Lnz)[212]

The synthesis followed protocol previously described,[205] with minor modifications. In a sealed reaction vial with stirrer under N_2 atmosphere, linezolid (680 mg, 2.0 mmol) and Lawesson's reagent (490 mg, 1.2 mmol) were refluxed in 10 mL dry THF for 18 h. The solvent was removed *in vacuo* and the reaction was purified by flash chromatography on silica with hexanes/ethyl acetate 1:3. The product **T-Lnz** was obtained as an amorphous solid weighing 640.3 mg (91% yield).

^{1}H NMR (400 MHz, $CDCl_3$): δ 8.55 (br d, J = 48 Hz, 1H), 7.38 (d, J = 12 Hz, 1H), 7.03 (d, J = 8 Hz, 1H), 6.90 (t, J = 8 Hz, 1H), 5.01-4.95 (m, 1H), 4.22-4.18 (m, 1H), 4.09 (dt, J = 8 Hz, J=24 Hz, 2H), 3.85-3.80 (m, 5H), 3.04 (br s, 4H), 2.58 (s, 3H)

^{13}C NMR (100 MHz, $CDCl_3$): δ 203.75, 156.53, 154.55, 154.08, 136.67, 132.36, 118.76, 114.06, 107.75, 107.49, 71.15, 66.83, 50.82, 47.84, 47.67, 33.81

3.5.3 Synthesis of imide-linked Linezolid-tether (Lnz-DTBA)[212]

The synthesis was adapted from previously reported procedure.[205] In a sealed reaction tube with stirrer under N_2 atmosphere, T-Lnz (600 mg, 1.7 mmol) and 4,4´-bis-dithiodibutyric acid (DTBA, 2.43 g, 10.2 mmol) were dissolved in 30 mL dry THF. Silver (I) carbonate (936 mg, 3.4 mmol) was carefully added, then the reaction was kept at room temperature and vigorous stirring for 18 h. The solvent was removed under reduced pressure and the reaction was purified by FCC on silica

gel. Eluent DCM/EtOAc/AcOH was applied at gradient steps of 98:0:2 (400 mL), 73:25:2 (400 mL) and 48:50:2 (800 mL). The combined pure fractions were evaporated three times with toluene to remove excess acetic acid. The product **Lnz-DTBA** was obtained as an amorphous solid weighing 650 mg (69% yield).

ESI (MS) Expected mass: 558 Da. Observed mass: 558.2 Da

^{1}H NMR (400 MHz, $CDCl_3$): δ 9.04 (br s, 1H), 7.39 (dd, J = 4 Hz, J = 12 Hz, 1H), 7.07 (dd, J = 4 Hz, J = 8 Hz, 1H), 6.91 (t, J = 8 Hz, 1H), 4.80 (br d, J = 8 Hz, 1 H), 4.16 (dd, J = 4 Hz, J = 16 Hz, 1H), 4.08 (t, J = 8, 1H), 3.92-3.84 (m, 5H), 3.70 (t, J = 8 Hz, 1H), 3.03 (t, J = 4 Hz, 4H), 2.89 (dt, J = 8 Hz, J = 4Hz, 2H), 2.71 (q, J = 8 Hz, 4H), 2.46 (s, 5H), 2.02 (dq, J = 24 Hz, J = 8 Hz, 4H)

^{13}C NMR (100 MHz, $CDCl_3$): δ 175.54, 173.53, 156.57, 154.12, 153.81, 136.57, 132.60, 118.80, 113.89, 107.58, 107.32, 71.62, 66.80, 50.83, 48.32, 47.86, 37.57, 36.00, 32.30, 29.58, 26.49, 23.86

3.5.4 Synthesis of resin bound conjugates[212]

Peptide-drug conjugates **LnzP14** and **FlLnzP14** were synthesized using Fmoc-based solid phase peptide synthesis (SPPS). Briefly, Rink amide ChemMatrix resin (0.045 mmol/g) was employed as solid support. Successive coupling and Fmoc-deprotection reactions were carried alternately until the desired sequence was achieved. A washing routine with 5 mL of DMF (2X), DCM (2X), MeOH (2X), DCM (2X), DMF (2X) was carried in between each reaction step. For the coupling protocol, the amino acids (2.0 equiv.) were dissolved in 5 mL DMF along with HATU (2.0 equiv.) and DIEA (4.0 equiv.) for carboxyl activation. Piperidine/DMF 1:3 was used for Fmoc deprotection. The drug-tether moiety **Lnz-DTBA** (2.0 equiv.) was coupled after the last amino acid of the sequence through its free carboxylic acid to the peptide´s N-terminus under the above coupling conditions. For the conjugate **FlLnzP14**, Fmoc-Lys(Mtt)-OH and Fmoc-Gly-OH were coupled at the end of the peptide sequence. 30% hexafluoroisopropanol (HFIP) in DCM (4 × 7 mL for 30 min. each) was used for removing the Mtt side chain protecting group. The free amino side chain of lysine was then reacted with 5(6)-carboxyfluorescein succinimidyl ester (Fl-NHS, 1.2 equiv.) in presence of DIEA (2.4 equiv.) in 5 mL DMF for 18 h. Then, the drug-tether moiety **Lnz-DTBA** (2.0 equiv.) was coupled to the N-terminus through its free carboxylic acid under the above coupling conditions.

3.5.5 Cleavage from resin and purification of LnzP14 and FlLnzP14[212]

For **LnzP14** and **FlLnzP14**, a cleavage cocktail of HFIP : triisopropylsilane (TIPS) : $HCl_{(conc)}$ 96 : 3 : 1 (0.12 N HCl) (8 mL) was added to the resin containing the conjugates and agitated for 3 h, as previously reported,[213] to prevent TFA induced hydrolysis of imide group. In each case, the solution was filtered through fritted glass into a 50 mL conical tube. The resin was rinsed with DCM (3 × 5 mL) and the filtrate collected into the same tube. The excess solvent was removed i*n vacuo* and the products were precipitated in cold diethyl ether. The supernatant from the precipitation was decanted, and the precipitate dissolved in acetonitrile (ACN): water 1:3 prior to semipreparative RP-HPLC purification. For this step, a Phenomenex C_{18} column was eluted with water with 0.1% TFA (solvent A) and ACN with 0.1% TFA (solvent B) at 12 mL/min under linear gradient of 25–65% B through 60 min and monitored by dual UV detection at 214 nm and 254 nm. The fractions containing the desired products were collected and lyophilized to yield **LnzP14** and **FlLnzP14**.

The purity of peptide-drug conjugates was assessed by analytical RP-HPLC using a Phenomenex C_{18} column was used with a binary solvent system composed by water with 0.1% TFA (solvent A) and ACN with 0.1% TFA (solvent B) at 1.2 mL/min under linear gradient of 20–65% B through 0–30 min, 65–95% B through 30–40 min, 95% B through 40–45 min and monitored by dual UV detection at 214 nm and 254 nm. Further characterization included the matrix assisted laser desorption ionization – time of flight mass spectrometry (MALDI-TOF-MS) using a Voyager DE Mass Spectrometer (Applied Biosystems) and α-cyano-4-hydroxycinnamic acid as support matrix. Analytical HPLC trace shown in **Figure A 13** for **LnzP14**. Analytical HPLC trace shown in **Figure A 14** for **FlLnzP14**.

MALDI-TOF-MS for **LnzP14**: expected m/z 3155.8, observed m/z 3154.6

MALDI-TOF-MS for **FlLnzP14**: expected mass 3700.9, observed mass 3698.2

3.5.6 Antibacterial activity against *Escherichia coli*[212]

Escherichia coli (ATCC 25922) was streaked on an agar plate and incubated at 37ºC for 18 h. Colonies of bacteria were recovered from agar and cultivated to mid-exponential phase in Tryptic Soy Broth (TSB) at 37 °C with shaking (5 colonies in 50 mL media). A 5 mL aliquot of the bacterial suspension was centrifuged for 5 min at 3000 rpm, and washed twice with Mueller

Hinton Broth (MHB). The pellet was re-suspended in MHB to a final optical density of 0.001 as measured by absorbance at 600 nm (OD_{600}). To a sterile transparent 96-well plate, 90 µL of the bacteria suspension was added along with 10 µL two-fold serially diluted drugs in water. Water was used as negative control and melittin as positive control. The plates were incubated for 20 h at 37 °C with shaking. The bacterial growth was measured at OD_{590} using a microplate reader (TECAN SpectraFluor Plus). The minimum inhibitory concentration (MIC) was determined as the lowest concentration of drug at which no growth was observed. Data was obtained in duplicates from at least two independent experiments.

3.5.7 An *E. coli* Beta-galactosidase release assay

Peptide solutions were prepared in deionized water to make concentrations at 2X and 4X the determined MIC values for peptides and conjugate against *E. coli* ATCC 25922. Five stationary colonies of *E. coli* ATCC 25922 were inoculated in 50 mL Mueller Hinton Broth (MHB) and grown at 37 ^{o}C for about 2 hours until the OD_{595} reached 0.1. Following, 5 mL of isopropyl-β-D thiogalactopyranoside (IPTG) (24 mg/10 mL PBS) was added to bacteria culture for a final concentration of 1 mM IPTG. The bacteria were induced until an OD_{595} between 0.3 and 0.5 was reached. A 10 mL aliquot of the bacteria in the IPTG/MHB media was removed and centrifuged at 3500 rpm for 5 min and spent media was decanted. The pelleted bacteria were then washed twice with 10 mL of fresh MHB and resuspended in 10 mL of MHB. The bacteria were plated in a 96-well plate at 90 µL per well, followed by the addition of 10 µL of the peptide solution. The bacteria were incubated with the peptide treatment for 1 hour. The 96-well plate was centrifuged for 5 min at 3500 rpm, and 80 µL of the supernatant was transferred to a new 96-well plate. Then, 20 µL of a freshly prepared 2-nitrophenyl-β-D-galactopyranoside (ONPG) (40 mg/10 mL of PBS) solution was added to each well for a final concentration of 0.8 mg/mL. The absorbances at 405 nm were read every 5 min over the course of 1 hour using a microplate reader to monitor the levels of o-nitrophenol formed.. The leakage of β-galactosidase was calculated based on the absorbance value obtained for treated samples, with a time zero absorbance value subtracted from each time point. For all experiments melittin was used as a positive control, PBS pH 7.4 was used as a negative control, and **FlP14LRR** was included as a reference. Data was obtained in duplicate from at least two independent experiments.

3.5.8 Hemotoxicity of conjugates on human red blood cells

Fresh human red blood cells (hRBCs) (Innovative Research, cat # IWB3CPDA1) were collected by centrifugation at 2000 rpm for 5 min followed by washing three times with 5 mL PBS 1X, pH 7.4. The supernatant of the final wash was aspirated and 200 µL of the concentrated cell suspension was added to 4.8 mL of PBS to make a 4% suspension (v/v). To a 96-well plate, was added 50 µL of the hRBC solution, followed by 50 µL of the peptide treatment prepared in PBS pH 7.4. The plate was incubated at 37 °C under 5% CO_2 for 1 h. The plate was subsequently centrifuged at 1200 rpm for 5 min at 4 °C. Next 75 µL aliquots of the supernatants in each well were carefully transferred to a new 96-well plate. The absorbances at 405 nm were read on a TECAN Infinite F PLEX microplate reader. As controls, hRBCs were treated with PBS 1X as a negative control, 0.1% Triton X-100 as a positive control, and melittin (Sigma M2272) as a positive control. The percent of hemolysis was calculated based on the 100% release with 0.1% Triton X-100. Data were obtained in duplicate from two independent experiments.

3.5.9 Cell culture

J774A.1 macrophage cell line was cultured in DMEM supplemented with 10% Fetal Bovine Serum (FBS), 1% L-glutamine, 1% penicillin-streptomycin. The cells were grown at 37 ^{o}C under a controlled humidified atmosphere with 5% carbon dioxide. Cells were sub-cultured biweekly.

3.5.10 *In vitro* cytotoxic activity against J744A.1 macrophages[212]

Analysis of the cytotoxicity of the conjugates against mouse macrophages (J774A.1) were carried out using methylthiazolyldiphenyl-tetrazolium bromide (MTT, Sigma M2128).[147] Cells were seeded in 96-well plates in 100 µL complete Dulbecco's Modified Eagle Medium (DMEM) supplemented with 10% fetal bovine serum (FBS) at density of 20,000 cells/well and incubated at 37 °C in a 5% CO_2 atmosphere for 24 h. The adherent cells were washed with PBS and 100 µL of fresh medium containing the conjugates two-fold serially diluted (0.5 – 32 µM) was added. The cells were incubated for 24 h and the spent media was aspirated and replaced with 100 µL fresh media, followed by the addition of 10 µL of a 5 mg/mL solution of MTT in PBS pH 7.4. After a 90-minute incubation period, the media was removed and the MTT formazan crystals were dissolved in 100 µL DMSO. The absorbance was then recorded at 590 nm using a microplate

reader. The percent cell viability was determined in comparison to the non-treated control. Data was obtained in duplicate from at least two independent experiments.

3.5.11 Analysis of reduction with dithiothreitol[212]

To a previously degassed phosphate buffered saline (PBS) solution pH = 7.4, was added **LnzP14** (40 µM) and internal standard quinine (10 µM). The reaction was preheated at 37 ºC and reducing agent dithiotreitol (DTT, 10 mM) was added to a final volume of 3 mL. The reaction was incubated at 37ºC for 90 minutes and 200 µL aliquots were collected at 0, 10, 20, 30, 40, 60 and 90 minutes and immediately frozen at -78 ºC in a acetone/dry ice bath to halt the reduction reaction. The reagent concentrations for this experiment are expressed as the final concentration for the reaction. The samples were injected in a Waters UPLC-MS system, with a positive mode electrospray detector. The analysis was conducted using a C18 column and a binary solvent system composed by water with 0.1% formic acid (solvent A) and ACN with 0.1% formic acid (solvent B) at 0.5 mL/min under linear gradient of 5–50% B through 0–10 min. This experiment was performed in duplicate and for each analysis a calibration curve for linezolid ranging from 1.23 to 120 µM in presence of 10 µM quinine as internal standard was constructed at the same conditions. The area under the curve corresponding to linezolid was corrected with the internal standard and the concentration calculated based on the linear regression equation obtained from the calibration curve. The concentration and standard deviation values for each timepoint were analyzed in GraphPad Prism software and the data was analyzed using a non-linear one phase decay regression curve regression curve to generate a half-life.

3.5.12 Analysis of reduction with glutathione

LnzP14 (25 µM) was incubated at 37 °C with 10 mM glutathione (GSH) in degassed phosphate buffered saline (PBS 1X, pH 7.4) containing 50 µM 6-quinolinecarboxylic acid as the internal standard in 1.5 mL total volume. When monitoring linezolid release, an 100 µL aliquot of the reaction mixture was taken at 0, 0.25, 0.5, 1, 2, 4, 6, and 18 hour time points and directly analyzed by a Waters UPLC-MS system, with a positive mode electrospray detector. The time points were analyzed using a C18 column consisting of 2-50% acetonitrile in water with 0.1% formic acid (0.5 ml/min, column temperature of 40 ºC). The peaks corresponding to the m/z for

quinolinecarboxylic acid (+1: 174), linezolid (+1: 338), and P14LRR-SH (+5: 545) were detected and extracted using MassLynx software. This experiment was performed in duplicate and for each analysis a calibration curve for linezolid ranging from 1 to 32 μM in presence of 50 μM 6-quinolinecarboxylic acid as internal standard was constructed at the same conditions. The area under the curve corresponding to linezolid was corrected with the internal standard and the concentration calculated based on the linear regression equation obtained from the calibration curve. The percentage of release vs. time was fitted using GraphPad Prism software to generate a half-life using a non-linear one phase decay regression curve.

3.5.13 Flow cytometry

Macrophage J774A.1 cells were plated in 500 μL of complete DMEM media at 150,000 cells/well in round bottom tubes (BD Biosciences) and incubated overnight at 37°C under 5% CO_2 atmosphere. The cells were centrifuged at 1200 rpm for 7 minutes at 4 ^{o}C, and the spent media was aspirated using a Pasteur pipet and vacuum filter. The cells were then treated with 300 μL of conjugates and peptide at concentrations ranging from 2.5- 10 μM prepared in complete DMEM media and were incubated for the desired incubation time at 37°C. Upon completion of the incubation period, the cells were centrifuged at 1200 rpm for 7 minutes at 4 ^{o}C, and the spent media was aspirated. The cells were then resuspended in 300 μL of cold PBS pH 7.4 and the fluorescence of the cells was measured using an Accuri flow cytometer (BD Biosciences). All samples were run in duplicate, and each experiment was repeated at least twice. The mean arbitrary fluorescence values of cells were measured and recorded upon excitation of the fluorophore, fluorescein, using a 488 nm laser. For each experiment, a negative control of cells that were incubated with DMEM was also analyzed.

Flow cytometry with Trypan Blue

After incubation with compounds, cells were centrifuged, and media aspirated as described in protocol above. The cells were then resuspended in 300 μL of 1 mg/mL trypan blue in PBS 1X without additional washing. Fluorescence was measured and analyzed as described.

3.5.14 Confocal microscopy in live mammalian cells

High resolution imaging of mammalian cells and subcellular localization of the peptides was performed in J774A.1 macrophage cell line using a Nikon A1R Multiphoton inverted confocal microscope with a 60X oil objective and 405 nm (blue), 488 nm (green), and 572 nm (red) 488 nm lasers employed. J774A.1 cells were seeded into 4-well μ-slide culture chamber (Ibidi, Cat. No. 80426) at a density of 125,000 cells/well with 500 μL of complete DMEM media. The cells were grown 20 hours (60% confluency) in a humidified 5% CO_2 atmosphere at 37°C. Cells were washed with 500 μL PBS, then, 400 μL of conjugate concentration prepared in DMEM was added to the wells at desired concentrations. The cells were incubated for 1 hour or 3 hours in the presence of the conjugate. Following incubation, the adherent cells were washed with 500 μL of PBS and aspirated. Then, 400 μL of either 100 nM Mitotracker mitochondrial strain, 1 μM Hoescht nuclear stain solution prepared in DMEM or 300 nM Lysotracker lysosome stain, 1 μM Hoescht nuclear stain prepared in DMEM were added to the wells and the cells were incubated for 30 minutes. After incubation, the adherent cells were washed with 500 μL of PBS and aspirated. Next, 500 μL of complete DMEM media was added to each well prior to imaging. Live cells were then imaged using Nikon A1R-MP inverted confocal fluorescence microscope equipped with 60X oil objective. NIS Elements software was used to process images.

REFERENCES

1. Aslam, B.; Wang, W.; Arshad, M. I.; Khurshid, M.; Muzammil, S.; Rasool, M. H.; Nisar, M. A.; Alvi, R. F.; Aslam, M. A.; Qamar, M. U.; Salamat, M. K. F.; Baloch, Z., Antibiotic resistance: a rundown of a global crisis. *Infection and drug resistance* **2018,** *11*, 1645-1658.

2. Zaman, S. B.; Hussain, M. A.; Nye, R.; Mehta, V.; Mamun, K. T.; Hossain, N., A Review on Antibiotic Resistance: Alarm Bells are Ringing. *Cureus* **2017,** *9* (6), e1403-e1403.

3. CDC *Antibiotic Resistance Threats in the United States, 2019*; Atlanta, GA, 2019.

4. Jackson, N.; Czaplewski, L.; Piddock, L. J. V., Discovery and development of new antibacterial drugs: learning from experience? *Journal of Antimicrobial Chemotherapy* **2018,** *73* (6), 1452-1459.

5. WHO *Antibacterial Agents in Clinical Development : An Analysis of the Antibacterial Clinical Development Pipeline*; Geneva, Switzerland, 2019.

6. PEW Tracking the Global Pipeline of Antibiotics in Development. https://www.pewtrusts.org/en/research-and-analysis/issue-briefs/2019/09/tracking-the-global-pipeline-of-antibiotics-in-development.

7. Fjell, C. D.; Hiss, J. A.; Hancock, R. E. W.; Schneider, G., Designing antimicrobial peptides: form follows function. *Nature Reviews Drug Discovery* **2012,** *11* (1), 37-51.

8. Koo, H. B.; Seo, J., Antimicrobial peptides under clinical investigation. *Peptide Science* **2019,** *111* (5), e24122.

9. Browne, K.; Chakraborty, S.; Chen, R.; Willcox, M. D.; Black, D. S.; Walsh, W. R.; Kumar, N., A New Era of Antibiotics: The Clinical Potential of Antimicrobial Peptides. *International Journal of Molecular Sciences* **2020,** *21* (19), 1-23.

10. Merrifield, R. B.; Merrifield, E. L.; Juvvadi, P.; Andreu, D.; Boman, H. G., Design and synthesis of antimicrobial peptides. *Ciba Foundation Symposium* **1994,** *186*, 5-20; discussion 20-6.

11. Li, F. F.; Brimble, M. A., Using chemical synthesis to optimise antimicrobial peptides in the fight against antimicrobial resistance. *Pure and Applied Chemistry* **2019,** *91* (2), 181-198.

12. al-Nawas, B.; Shah, P. M., Intracellular activity of vancomycin and Ly333328, a new semisynthetic glycopeptide, against methicillin-resistant Staphylococcus aureus. *Infection* **1998,** *26* (3), 165-167.

13. Darouiche, R. O.; Hamill, R. J., Antibiotic penetration of and bactericidal activity within endothelial cells. *Antimicrobial Agents and Chemotherapy* **1994,** *38* (5), 1059-1064.

14. Seral, C.; Van Bambeke, F.; Tulkens, P. M., Quantitative analysis of gentamicin, azithromycin, telithromycin, ciprofloxacin, moxifloxacin, and oritavancin (LY333328) activities against intracellular Staphylococcus aureus in mouse J774 macrophages. *Antimicrobial Agents and Chemotherapy* **2003,** *47* (7), 2283-2292.

15. Baltch, A. L.; Ritz, W. J.; Bopp, L. H.; Michelsen, P. B.; Smith, R. P., Antimicrobial Activities of Daptomycin, Vancomycin, and Oxacillin in Human Monocytes and of Daptomycin in Combination with Gentamicin and/or Rifampin in Human Monocytes and in Broth against Staphylococcus aureus. *Antimicrobial Agents and Chemotherapy* **2007,** *51* (4), 1559-1562.

16. Maurin, M.; Raoult, D., Use of aminoglycosides in treatment of infections due to intracellular bacteria. *Antimicrobial Agents and Chemotherapy* **2001,** *45* (11), 2977-2986.

17. Cohen, D. T.; Zhang, C.; Fadzen, C. M.; Mijalis, A. J.; Hie, L.; Johnson, K. D.; Shriver, Z.; Plante, O.; Miller, S. J.; Buchwald, S. L.; Pentelute, B. L., A chemoselective strategy for late-stage functionalization of complex small molecules with polypeptides and proteins. *Nature Chemistry* **2019,** *11* (1), 78-85.

18. Temsamani, J.; Vidal, P., The use of cell-penetrating peptides for drug delivery. *Drug Discovery Today* **2004,** *9* (23), 1012-1019.

19. Koren, E.; Torchilin, V. P., Cell-penetrating peptides: breaking through to the other side. *Trends in Molecular Medicine* **2012,** *18* (7), 385-393.

20. Chen, L.; Harrison, S. D., Cell-penetrating peptides in drug development: enabling intracellular targets. *Biochemical Society Transactions* **2007,** *35* (Pt 4), 821-825.

21. Gautam, A.; Singh, H.; Tyagi, A.; Chaudhary, K.; Kumar, R.; Kapoor, P.; Raghava, G. P. S., CPPsite: a curated database of cell penetrating peptides. *Database* **2012,** *2012*, bas015.

22. Zorko, M.; Langel, U., Cell-penetrating peptides: mechanism and kinetics of cargo delivery. *Advanced Drug Delivery Reviews* **2005,** *57* (4), 529 - 545.

23. Rodriguez Plaza, J. G.; Morales-Nava, R.; Diener, C.; Schreiber, G.; Gonzalez, Z. D.; Lara Ortiz, M. T.; Ortega Blake, I.; Pantoja, O.; Volkmer, R.; Klipp, E.; Herrmann, A.; Del Rio, G., Cell Penetrating Peptides and Cationic Antibacterial Peptides: Two Sides of the Same Coin. *Journal of Biological Chemistry* **2014,** *289* (21), 14448-14457.

24. Henriques, S. T.; Melo, M. N.; Castanho, M. A. R. B., Cell-penetrating peptides and antimicrobial peptides: how different are they? *The Biochemical Journal* **2006,** *399* (1), 1-7.

25. Bahnsen, J. S.; Franzyk, H.; Sandberg-Schaal, A.; Nielsen, H. M., Antimicrobial and cell-penetrating properties of penetratin analogs: Effect of sequence and secondary structure. *Biochimica et Biophysica Acta (BBA) - Biomembranes* **2013,** *1828* (2), 223-232.

26. Zhu, W. L.; Shin, S. Y., Effects of dimerization of the cell-penetrating peptide Tat analog on antimicrobial activity and mechanism of bactericidal action. *Journal of Peptide Science* **2009,** *15* (5), 345-52.

27. Zhu, W. L.; Shin, S. Y., Antimicrobial and Cytolytic Activities and Plausible Mode of Bactericidal Action of the Cell Penetrating Peptide Penetratin and Its Lys-linked Two-Stranded Peptide. *Chemical Biology & Drug Design* **2009,** *73* (2), 209-215.

28. Kahlenberg, J. M.; Kaplan, M. J., Little peptide, big effects: the role of LL-37 in inflammation and autoimmune disease. *Journal of Immunology* **2013,** *191* (10), 4895-4901.

29. Sandgren, S.; Wittrup, A.; Cheng, F.; Jönsson, M.; Eklund, E.; Busch, S.; Belting, M., The human antimicrobial peptide LL-37 transfers extracellular DNA plasmid to the nuclear compartment of mammalian cells via lipid rafts and proteoglycan-dependent endocytosis. *Journal of Biological Chemistry* **2004,** *279* (17), 17951-6.

30. Zhang, X.; Oglęcka, K.; Sandgren, S.; Belting, M.; Esbjörner, E. K.; Nordén, B.; Gräslund, A., Dual functions of the human antimicrobial peptide LL-37-target membrane perturbation and host cell cargo delivery. *Biochimica et Biophysica Acta* **2010,** *1798* (12), 2201-8.

31. Dougherty, P. G.; Sahni, A.; Pei, D., Understanding Cell Penetration of Cyclic Peptides. *Chemical Reviews* **2019,** *119* (17), 10241-10287.

32. Park, S. E.; Sajid, M. I.; Parang, K.; Tiwari, R. K., Cyclic Cell-Penetrating Peptides as Efficient Intracellular Drug Delivery Tools. *Molecular Pharmaceutics* **2019,** *16* (9), 3727-3743.

33. Oh, D.; Sun, J.; Nasrolahi Shirazi, A.; LaPlante, K. L.; Rowley, D. C.; Parang, K., Antibacterial Activities of Amphiphilic Cyclic Cell-Penetrating Peptides against Multidrug-Resistant Pathogens. *Molecular Pharmaceutics* **2014,** *11* (10), 3528-3536.

34. Mahlapuu, M.; Håkansson, J.; Ringstad, L.; Björn, C., Antimicrobial Peptides: An Emerging Category of Therapeutic Agents. *Frontiers in Cellular and Infection Microbiology* **2016,** *6*, 194.

35. Thangamani, S.; Nepal, M.; Chmielewski, J.; Seleem, M. N., Antibacterial activity and therapeutic efficacy of Fl-P(R)P(R)P(L)-5, a cationic amphiphilic polyproline helix, in a mouse model of staphylococcal skin infection. *Drug design, development and therapy* **2015,** *9*, 5749-5754.

36. Geisler, I.; Chmielewski, J., Cationic Amphiphilic Polyproline Helices: Side-Chain Variations and Cell-Specific Internalization. *Chemical Biology & Drug Design* **2009,** *73* (1), 39-45.

37. Fillon, Y. A.; Anderson, J. P.; Chmielewski, J., Cell Penetrating Agents Based on a Polyproline Helix Scaffold. *Journal of the American Chemical Society* **2005,** *127* (33), 11798-11803.

38. Rowe, J. L.; Chmielewski, J. Designing chemical strategies to promote therapeutic access to restricted sites in cyto. Dissertation, Purdue University, 2019.

39. Hernandez-Gordillo, V.; Geisler, I.; Chmielewski, J., Dimeric unnatural polyproline-rich peptides with enhanced antibacterial activity. *Bioorganic & Medicinal Chemistry Letters* **2014,** *24* (2), 556-559.

40. Nepal, M.; Mohamed, M. F.; Blade, R.; Eldesouky, H. E.; N. Anderson, T.; Seleem, M. N.; Chmielewski, J., A Library Approach to Cationic Amphiphilic Polyproline Helices that Target Intracellular Pathogenic Bacteria. *ACS Infectious Diseases* **2018,** *4* (9), 1300-1305.

41. Kalafut, D.; Anderson, T. N.; Chmielewski, J., Mitochondrial targeting of a cationic amphiphilic polyproline helix. *Bioorganic & Medicinal Chemistry Letters* **2012,** *22* (1), 561-563.

42. Blade, R.; Chmielewski, J. Strategic modifications to optimize a cell penetrating antimicrobial peptide. A dissertation Purdue University, 2019.

43. Nepal, M.; Thangamani, S.; Seleem, M. N.; Chmielewski, J., Targeting intracellular bacteria with an extended cationic amphiphilic polyproline helix. *Organic and Biomolecular Chemistry* **2015,** *13* (21), 5930-6.

44. Dietsche, T. A.; Eldesouky, H. E.; Zeiders, S. M.; Seleem, M. N.; Chmielewski, J., Targeting Intracellular Pathogenic Bacteria Through N-Terminal Modification of Cationic Amphiphilic Polyproline Helices. *The Journal of Organic Chemistry* **2020,** *85* (11), 7468-7475.

45. Kuriakose, J.; Hernandez-Gordillo, V.; Nepal, M.; Brezden, A.; Pozzi, V.; Seleem, M. N.; Chmielewski, J., Targeting Intracellular Pathogenic Bacteria with Unnatural Proline-Rich Peptides: Coupling Antibacterial Activity with Macrophage Penetration. *Angewandte Chemie International Edition* **2013,** *52* (37), 9664-9667.

46. Brown, E. D.; Wright, G. D., Antibacterial drug discovery in the resistance era. *Nature* **2016,** *529* (7586), 336-343.

47. CDC Treatment for TB Disease. https://www.cdc.gov/tb/topic/treatment/tbdisease.htm.

48. Kerantzas, C. A.; Jacobs, W. R., Origins of Combination Therapy for Tuberculosis: Lessons for Future Antimicrobial Development and Application. *mBio* **2017,** *8* (2), e01586-16.

49. Randhawa, H. K.; Gautam, A.; Sharma, M.; Bhatia, R.; Varshney, G. C.; Raghava, G. P. S.; Nandanwar, H., Cell-penetrating peptide and antibiotic combination therapy: a potential alternative to combat drug resistance in methicillin-resistant Staphylococcus aureus. *Applied Microbiology and Biotechnology* **2016,** *100* (9), 4073-4083.

50. Ratrey, P.; Dalvi, S. V.; Mishra, A., Enhancing Aqueous Solubility and Antibacterial Activity of Curcumin by Complexing with Cell-Penetrating Octaarginine. *ACS omega* **2020,** *5* (30), 19004-19013.

51. Sheard, D. E.; O'Brien-Simpson, N. M.; Wade, J. D.; Separovic, F., Combating bacterial resistance by combination of antibiotics with antimicrobial peptides. *Pure and Applied Chemistry* **2019,** *91* (2), 199-209.

52. Yarlagadda, V.; Manjunath, G. B.; Sarkar, P.; Akkapeddi, P.; Paramanandham, K.; Shome, B. R.; Ravikumar, R.; Haldar, J., Glycopeptide Antibiotic To Overcome the Intrinsic Resistance of Gram-Negative Bacteria. *ACS Infectious Diseases* **2016,** *2* (2), 132-139.

53. Yarlagadda, V.; Konai, M. M.; Manjunath, G. B.; Prakash, R. G.; Mani, B.; Paramanandham, K.; Ranjan, S. B.; Ravikumar, R.; Chakraborty, S. P.; Roy, S.; Haldar, J., In vivo antibacterial activity and pharmacological properties of the membrane-active glycopeptide antibiotic YV11455. *International Journal of Antimicrobial Agents* **2015,** *45* (6), 627-634.

54. Yarlagadda, V.; Samaddar, S.; Haldar, J., Intracellular activity of a membrane-active glycopeptide antibiotic against meticillin-resistant Staphylococcus aureus infection. *Journal of Global Antimicrobial Resistance* **2016,** *5*, 71-74.

55. Yarlagadda, V.; Akkapeddi, P.; Manjunath, G. B.; Haldar, J., Membrane Active Vancomycin Analogues: A Strategy to Combat Bacterial Resistance. *Journal of Medicinal Chemistry* **2014,** *57* (11), 4558-4568.

56. Sarkar, P.; Samaddar, S.; Ammanathan, V.; Yarlagadda, V.; Ghosh, C.; Shukla, M.; Kaul, G.; Manjithaya, R.; Chopra, S.; Haldar, J., Vancomycin Derivative Inactivates Carbapenem-Resistant Acinetobacter baumannii and Induces Autophagy. *ACS Chemical Biology* **2020,** *15* (4), 884-889.

57. Yarlagadda, V.; Sarkar, P.; Samaddar, S.; Manjunath, G. B.; Mitra, S. D.; Paramanandham, K.; Shome, B. R.; Haldar, J., Vancomycin Analogue Restores Meropenem Activity against NDM-1 Gram-Negative Pathogens. *ACS Infectious Diseases* **2018,** *4* (7), 1093-1101.

58. Yarlagadda, V.; Sarkar, P.; Samaddar, S.; Haldar, J., A Vancomycin Derivative with a Pyrophosphate-Binding Group: A Strategy to Combat Vancomycin-Resistant Bacteria. *Angewandte Chemie International Edition English* **2016,** *55* (27), 7836-40.

59. Guan, D.; Chen, F.; Qiu, Y.; Jiang, B.; Gong, L.; Lan, L.; Huang, W., Sulfonium, an Underestimated Moiety for Structural Modification, Alters the Antibacterial Profile of Vancomycin Against Multidrug-Resistant Bacteria. *Angewandte Chemie International Edition* **2019,** *58* (20), 6678-6682.

60. Okano, A.; Isley, N. A.; Boger, D. L., Peripheral modifications of [Ψ[CH2NH]Tpg4]vancomycin with added synergistic mechanisms of action provide durable and potent antibiotics. *Proceedings of the National Academy of Sciences* **2017,** *114* (26), E5052-E5061.

61. Wu, Z. C.; Isley, N. A.; Okano, A.; Weiss, W. J.; Boger, D. L., C1-CBP-vancomycin: Impact of a Vancomycin C-Terminus Trimethylammonium Cation on Pharmacological Properties and Insights into Its Newly Introduced Mechanism of Action. *Journal of Organic Chemistry* **2020,** *85* (3), 1365-1375.

62. McComas, C. C.; Crowley, B. M.; Hwang, I.; Boger, D. L., Synthesis and evaluation of methyl ether derivatives of the vancomycin, teicoplanin, and ristocetin aglycon methyl esters. *Bioorganic & Medicinal Chemistry Letters* **2003,** *13* (17), 2933-2936.

63. Crane, C. M.; Pierce, J. G.; Leung, S. S. F.; Tirado-Rives, J.; Jorgensen, W. L.; Boger, D. L., Synthesis and Evaluation of Selected Key Methyl Ether Derivatives of Vancomycin Aglycon. *Journal of Medicinal Chemistry* **2010,** *53* (19), 7229-7235.

64. Nakama, Y.; Yoshida, O.; Yoda, M.; Araki, K.; Sawada, Y.; Nakamura, J.; Xu, S.; Miura, K.; Maki, H.; Arimoto, H., Discovery of a Novel Series of Semisynthetic Vancomycin Derivatives Effective against Vancomycin-Resistant Bacteria. *Journal of Medicinal Chemistry* **2010,** *53* (6), 2528-2533.

65. Yoganathan, S.; Miller, S. J., Structure Diversification of Vancomycin through Peptide-Catalyzed, Site-Selective Lipidation: A Catalysis-Based Approach To Combat Glycopeptide-Resistant Pathogens. *Journal of Medicinal Chemistry* **2015,** *58* (5), 2367-2377.

66. Guan, D.; Chen, F.; Xiong, L.; Tang, F.; Faridoon; Qiu, Y.; Zhang, N.; Gong, L.; Li, J.; Lan, L.; Huang, W., Extra Sugar on Vancomycin: New Analogues for Combating Multidrug-Resistant Staphylococcus aureus and Vancomycin-Resistant Enterococci. *Journal of Medicinal Chemistry* **2018,** *61* (1), 286-304.

67. Printsevskaya, S. S.; Reznikova, M. I.; Korolev, A. M.; Lapa, G. B.; Olsufyeva, E. N.; Preobrazhenskaya, M. N.; Plattner, J. J.; Zhang, Y. K., Synthesis and study of antibacterial activities of antibacterial glycopeptide antibiotics conjugated with benzoxaboroles. *Future Medicinal Chemistry* **2013,** *5* (6), 641-52.

68. Antonoplis, A.; Zang, X.; Wegner, T.; Wender, P. A.; Cegelski, L., Vancomycin–Arginine Conjugate Inhibits Growth of Carbapenem-Resistant E. coli and Targets Cell-Wall Synthesis. *ACS Chemical Biology* **2019,** *14* (9), 2065-2070.

69. Antonoplis, A.; Zang, X.; Huttner, M. A.; Chong, K. K. L.; Lee, Y. B.; Co, J. Y.; Amieva, M. R.; Kline, K. A.; Wender, P. A.; Cegelski, L., A Dual-Function Antibiotic-Transporter Conjugate Exhibits Superior Activity in Sterilizing MRSA Biofilms and Killing Persister Cells. *Journal of the American Chemical Society* **2018,** *140* (47), 16140-16151.

70. Blaskovich, M. A. T.; Hansford, K. A.; Gong, Y.; Butler, M. S.; Muldoon, C.; Huang, J. X.; Ramu, S.; Silva, A. B.; Cheng, M.; Kavanagh, A. M.; Ziora, Z.; Premraj, R.; Lindahl, F.; Bradford, T. A.; Lee, J. C.; Karoli, T.; Pelingon, R.; Edwards, D. J.; Amado, M.; Elliott, A. G.; Phetsang, W.; Daud, N. H.; Deecke, J. E.; Sidjabat, H. E.; Ramaologa, S.; Zuegg, J.; Betley, J. R.; Beevers, A. P. G.; Smith, R. A. G.; Roberts, J. A.; Paterson, D. L.; Cooper, M. A., Protein-inspired antibiotics active against vancomycin- and daptomycin-resistant bacteria. *Nature Communications* **2018,** *9* (1), 1-17.

71. Jiang, Y.; Han, M.; Bo, Y.; Feng, Y.; Li, W.; Wu, J. R.; Song, Z.; Zhao, Z.; Tan, Z.; Chen, Y.; Xue, T.; Fu, Z.; Kuo, S. H.; Lau, G. W.; Luijten, E.; Cheng, J., "Metaphilic" Cell-Penetrating Polypeptide-Vancomycin Conjugate Efficiently Eradicates Intracellular Bacteria via a Dual Mechanism. *ACS Central Science* **2020**, 2267–2276.

72. Ruczyński, J.; Rusiecka, I.; Turecka, K.; Kozłowska, A.; Alenowicz, M.; Gągało, I.; Kawiak, A.; Rekowski, P.; Waleron, K.; Kocić, I., Transportan 10 improves the pharmacokinetics and pharmacodynamics of vancomycin. *Scientific Reports* **2019,** *9* (1), 1-15.

73. Umstätter, F.; Domhan, C.; Hertlein, T.; Ohlsen, K.; Mühlberg, E.; Kleist, C.; Zimmermann, S.; Beijer, B.; Klika, K. D.; Haberkorn, U.; Mier, W.; Uhl, P., Vancomycin Resistance Is Overcome by Conjugation of Polycationic Peptides. *Angewandte Chemie International Edition English* **2020,** *59* (23), 8823-8827.

74. Mühlberg, E.; Umstätter, F.; Domhan, C.; Hertlein, T.; Ohlsen, K.; Krause, A.; Kleist, C.; Beijer, B.; Zimmermann, S.; Haberkorn, U.; Mier, W.; Uhl, P., Vancomycin-Lipopeptide Conjugates with High Antimicrobial Activity on Vancomycin-Resistant Enterococci. *Pharmaceuticals* **2020,** *13* (6), 1-14.

75. Gomarasca, M.; F. C. Martins, T.; Greune, L.; Hardwidge, P. R.; Schmidt, M. A.; Rüter, C., Bacterium-Derived Cell-Penetrating Peptides Deliver Gentamicin To Kill Intracellular Pathogens. *Antimicrobial Agents and Chemotherapy* **2017,** *61* (4), 1-20.

76. Brezden, A.; Mohamed, M. F.; Nepal, M.; Harwood, J. S.; Kuriakose, J.; Seleem, M. N.; Chmielewski, J., Dual Targeting of Intracellular Pathogenic Bacteria with a Cleavable Conjugate of Kanamycin and an Antibacterial Cell-Penetrating Peptide. *Journal of the American Chemical Society* **2016,** *138* (34), 10945-10949.

77. Mohamed, M. F.; Brezden, A.; Mohammad, H.; Chmielewski, J.; Seleem, M. N., Targeting biofilms and persisters of ESKAPE pathogens with P14KanS, a kanamycin peptide conjugate. *Biochimica et Biophysica Acta (BBA) - General Subjects* **2017,** *1861* (4), 848-859.

78. Jones, L. R.; Goun, E. A.; Shinde, R.; Rothbard, J. B.; Contag, C. H.; Wender, P. A., Releasable Luciferin−Transporter Conjugates: Tools for the Real-Time Analysis of Cellular Uptake and Release. *Journal of the American Chemical Society* **2006,** *128* (20), 6526-6527.

79. Wender, P. A.; Goun, E. A.; Jones, L. R.; Pillow, T. H.; Rothbard, J. B.; Shinde, R.; Contag, C. H., Real-time analysis of uptake and bioactivatable cleavage of luciferin-transporter conjugates in transgenic reporter mice. *Proceedings of the National Academy of Sciences* **2007,** *104* (25), 10340-10345.

80. Deshayes, S.; Xian, W.; Schmidt, N. W.; Kordbacheh, S.; Lieng, J.; Wang, J.; Zarmer, S.; Germain, S. S.; Voyen, L.; Thulin, J.; Wong, G. C. L.; Kasko, A. M., Designing Hybrid Antibiotic Peptide Conjugates To Cross Bacterial Membranes. *Bioconjugate Chemistry* **2017,** *28* (3), 793-804.

81. Defaus, S.; Gallo, M.; Abengózar, M. A.; Rivas, L.; Andreu, D., A Synthetic Strategy for Conjugation of Paromomycin to Cell-Penetrating Tat(48-60) for Delivery and Visualization into Leishmania Parasites. *International Journal of Peptides* **2017,** *2017*, 4213037.

82. Riahifard, N.; Tavakoli, K.; Yamaki, J.; Parang, K.; Tiwari, R., Synthesis and Evaluation of Antimicrobial Activity of [R$_4$W$_4$K]-Levofloxacin and [R$_4$W$_4$K]-Levofloxacin-Q Conjugates. *Molecules* **2017,** *22* (6), 1-11.

83. Ghaffar, K. A.; Hussein, W. M.; Khalil, Z. G.; Capon, R. J.; Skwarczynski, M.; Toth, I., Levofloxacin and indolicidin for combination antimicrobial therapy. *Curr Drug Deliv* **2015,** *12* (1), 108-114.

84. Taheri-Ledari, R.; Maleki, A., Antimicrobial therapeutic enhancement of levofloxacin via conjugation to a cell-penetrating peptide: An efficient sonochemical catalytic process. *Journal of Peptide Science* **2020**, e3277.

85. Lei, E. K.; Pereira, M. P.; Kelley, S. O., Tuning the Intracellular Bacterial Targeting of Peptidic Vectors. *Angewandte Chemie International Edition* **2013,** *52* (37), 9660-9663.

86. Pereira, M. P.; Shi, J.; Kelley, S. O., Peptide Targeting of an Antibiotic Prodrug toward Phagosome-Entrapped Mycobacteria. *ACS Infectious Diseases* **2015,** *1* (12), 586-592.

87. Ahmed, M.; Kelley, S. O., Enhancing the Potency of Nalidixic Acid toward a Bacterial DNA Gyrase with Conjugated Peptides. *ACS Chemical Biology* **2017,** *12* (10), 2563-2569.

88. Sparr, C.; Purkayastha, N.; Kolesinska, B.; Gengenbacher, M.; Amulic, B.; Matuschewski, K.; Seebach, D.; Kamena, F., Improved Efficacy of Fosmidomycin against Plasmodium and Mycobacterium Species by Combination with the Cell-Penetrating Peptide Octaarginine. *Antimicrobial Agents and Chemotherapy* **2013,** *57*.

89. de la Torre, B. G.; Hornillos, V.; Luque-Ortega, J. R.; Abengózar, M. A.; Amat-Guerri, F.; Acuña, A. U.; Rivas, L.; Andreu, D., A BODIPY-embedding miltefosine analog linked to cell-penetrating Tat(48-60) peptide favors intracellular delivery and visualization of the antiparasitic drug. *Amino Acids* **2014,** *46* (4), 1047-58.

90. Luque-Ortega, J. R.; de la Torre, B. G.; Hornillos, V.; Bart, J. M.; Rueda, C.; Navarro, M.; Amat-Guerri, F.; Acuña, A. U.; Andreu, D.; Rivas, L., Defeating Leishmania resistance to miltefosine (hexadecylphosphocholine) by peptide-mediated drug smuggling: a proof of mechanism for trypanosomatid chemotherapy. *Journal of Control Release* **2012,** *161* (3), 835-42.

91. Bourré, L.; Giuntini, F.; Eggleston, I. M.; Mosse, C. A.; MacRobert, A. J.; Wilson, M., Effective photoinactivation of Gram-positive and Gram-negative bacterial strains using an HIV-1 Tat peptide–porphyrin conjugate. *Photochemical & Photobiological Sciences* **2010,** *9* (12), 1613-1620.

92. Li, Z.; Wang, X.; Teng, D.; Mao, R.; Hao, Y.; Yang, N.; Chen, H.; Wang, X.; Wang, J., Improved antibacterial activity of a marine peptide-N2 against intracellular Salmonella typhimurium by conjugating with cell-penetrating peptides-bLFcin6/Tat11. *European Journal of Medicinal Chemistry* **2018,** *145*, 263-272.

93. Li, Z.; Teng, D.; Mao, R.; Wang, X.; Hao, Y.; Wang, X.; Wang, J., Improved Antibacterial Activity of the Marine Peptide N6 against Intracellular Salmonella Typhimurium by Conjugating with the Cell-Penetrating Peptide Tat11 via a Cleavable Linker. *Journal of Medicinal Chemistry* **2018,** *61* (17), 7991-8000.

94. Lee, H.; Lim, S. I.; Shin, S.-H.; Lim, Y.; Koh, J. W.; Yang, S., Conjugation of Cell-Penetrating Peptides to Antimicrobial Peptides Enhances Antibacterial Activity. *ACS omega* **2019,** *4* (13), 15694-15701.

95. Li, J.; Shang, L.; Lan, J.; Chou, S.; Feng, X.; Shi, B.; Wang, J.; Lyu, Y.; Shan, A., Targeted and Intracellular Antibacterial Activity against S. agalactiae of the Chimeric Peptides Based on Pheromone and Cell-Penetrating Peptides. *ACS Applied Materials & Interfaces* **2020,** *12* (40), 44459-44474.

96. Wesolowski, D.; Alonso, D.; Altman, S., Combined effect of a peptide–morpholino oligonucleotide conjugate and a cell-penetrating peptide as an antibiotic. *Proceedings of the National Academy of Sciences* **2013,** *110* (21), 8686-8689.

97. Wesolowski, D.; Tae, H. S.; Gandotra, N.; Llopis, P.; Shen, N.; Altman, S., Basic peptide-morpholino oligomer conjugate that is very effective in killing bacteria by gene-specific and nonspecific modes. *Proceedings of the National Academy of Sciences of the United States of America* **2011,** *108* (40), 16582-16587.

98. Abushahba, M. F. N.; Mohammad, H.; Thangamani, S.; Hussein, A. A. A.; Seleem, M. N., Impact of different cell penetrating peptides on the efficacy of antisense therapeutics for targeting intracellular pathogens. *Scientific Reports* **2016,** *6* (1), 20832.

99. WHO, *Critically important antimicrobials for human medicine*. 6th rev. ed.; World Health Organization: Geneva, Switzerland, 2019.

100. Courvalin, P., Vancomycin resistance in gram-positive cocci. *Clinical Infectious Diseases* **2006,** *42 Suppl 1*, S25-34.

101. Faron, M. L.; Ledeboer, N. A.; Buchan, B. W., Resistance Mechanisms, Epidemiology, and Approaches to Screening for Vancomycin-Resistant Enterococcus in the Health Care Setting. *Journal of Clinical Microbiology* **2016,** *54* (10), 2436-2447.

102. Bugg, T. D. H.; Wright, G. D.; Dutka-Malen, S.; Arthur, M.; Courvalin, P.; Walsh, C. T., Molecular basis for vancomycin resistance in Enterococcus faecium BM4147: biosynthesis of a depsipeptide peptidoglycan precursor by vancomycin resistance proteins VanH and VanA. *Biochemistry* **1991,** *30* (43), 10408-10415.

103. McComas, C. C.; Crowley, B. M.; Boger, D. L., Partitioning the Loss in Vancomycin Binding Affinity for d-Ala-d-Lac into Lost H-Bond and Repulsive Lone Pair Contributions. *Journal of the American Chemical Society* **2003,** *125* (31), 9314-9315.

104. Healy, V. L.; Lessard, I. A. D.; Roper, D. I.; Knox, J. R.; Walsh, C. T., Vancomycin resistance in enterococci: reprogramming of the Ala ligases in bacterial peptidoglycan biosynthesis. *Chemistry & Biology* **2000,** *7* (5), R109-R119.

105. Billot-Klein, D.; Blanot, D.; Gutmann, L.; van Heijenoort, J., Association constants for the binding of vancomycin and teicoplanin to N-acetyl-D-alanyl-D-alanine and N-acetyl-D-alanyl-D-serine. *Biochemical Journal* **1994,** *304* (3), 1021-1022.

106. Lambert, P. A., Cellular impermeability and uptake of biocides and antibiotics in Gram-positive bacteria and mycobacteria. *Journal of Applied Microbiology* **2002,** *92 Suppl*, 46s-54s.

107. Thakur, A.; Mikkelsen, H.; Jungersen, G., Intracellular Pathogens: Host Immunity and Microbial Persistence Strategies. *Journal of Immunology Research* **2019,** *2019*, 1356540.

108. Theriot, J. A., The cell biology of infection by intracellular bacterial pathogens. *Annual Review of Cell and Developmental Biology* **1995,** *11*, 213-39.

109. Moldovan, A.; Fraunholz, M. J., In or out: Phagosomal escape of Staphylococcus aureus. *Cellular Microbiology* **2019,** *21* (3), e12997.

110. Fraunholz, M.; Sinha, B., Intracellular staphylococcus aureus: Live-in and let die. *Frontiers in Cellular and Infection Microbiology* **2012,** *2* (43).

111. Pumerantz, A.; Muppidi, K.; Agnihotri, S.; Guerra, C.; Venketaraman, V.; Wang, J.; Betageri, G., Preparation of liposomal vancomycin and intracellular killing of meticillin-resistant Staphylococcus aureus (MRSA). *Int J Antimicrob Agents* **2011,** *37* (2), 140-4.

112. Sande, L.; Sanchez, M.; Montes, J.; Wolf, A. J.; Morgan, M. A.; Omri, A.; Liu, G. Y., Liposomal encapsulation of vancomycin improves killing of methicillin-resistant Staphylococcus aureus in a murine infection model. *Journal of Antimicrobial Chemotherapy* **2012,** *67* (9), 2191-4.

113. Atashbeyk, D. G.; Khameneh, B.; Tafaghodi, M.; Fazly Bazzaz, B. S., Eradication of methicillin-resistant Staphylococcus aureus infection by nanoliposomes loaded with gentamicin and oleic acid. *Pharm Biol* **2014,** *52* (11), 1423-8.

114. Barcia-Macay, M.; Mouaden, F.; Mingeot-Leclercq, M. P.; Tulkens, P. M.; Van Bambeke, F., Cellular pharmacokinetics of telavancin, a novel lipoglycopeptide antibiotic, and analysis of lysosomal changes in cultured eukaryotic cells (J774 mouse macrophages and rat embryonic fibroblasts). *Journal of Antimicrobial Chemotherapy* **2008,** *61* (6), 1288-94.

115. Barcia-Macay, M.; Seral, C.; Mingeot-Leclercq, M. P.; Tulkens, P. M.; Van Bambeke, F., Pharmacodynamic evaluation of the intracellular activities of antibiotics against Staphylococcus aureus in a model of THP-1 macrophages. *Antimicrobial Agents and Chemotherapy* **2006,** *50* (3), 841-51.

116. Dhanda, G.; Sarkar, P.; Samaddar, S.; Haldar, J., Battle against Vancomycin-Resistant Bacteria: Recent Developments in Chemical Strategies. *Journal of Medicinal Chemistry* **2019,** *62* (7), 3184-3205.

117. Blaskovich, M. A. T.; Hansford, K. A.; Butler, M. S.; Jia, Z.; Mark, A. E.; Cooper, M. A., Developments in Glycopeptide Antibiotics. *ACS Infectious Diseases* **2018,** *4* (5), 715-735.

118. Zhanel, G. G.; Calic, D.; Schweizer, F.; Zelenitsky, S.; Adam, H.; Lagacé-Wiens, P. R. S.; Rubinstein, E.; Gin, A. S.; Hoban, D. J.; Karlowsky, J. A., New Lipoglycopeptides. *Drugs* **2010,** *70* (7), 859-886.

119. Ashford, P.-A.; Bew, S. P., Recent advances in the synthesis of new glycopeptide antibiotics. *Chemical Society Reviews* **2012,** *41* (3), 957-978.

120. Crowley, B. M.; Boger, D. L., Total Synthesis and Evaluation of [Ψ[CH2NH]Tpg4]Vancomycin Aglycon: Reengineering Vancomycin for Dual d-Ala-d-Ala and d-Ala-d-Lac Binding. *Journal of the American Chemical Society* **2006,** *128* (9), 2885-2892.

121. Okano, A.; Nakayama, A.; Schammel, A. W.; Boger, D. L., Total Synthesis of [Ψ[C(═NH)NH]Tpg4]Vancomycin and its (4-Chlorobiphenyl)methyl Derivative: Impact of Peripheral Modifications on Vancomycin Analogues Redesigned for Dual d-Ala-d-Ala and d-Ala-d-Lac Binding. *Journal of the American Chemical Society* **2014,** *136* (39), 13522-13525.

122. McAtee, J. J.; Castle, S. L.; Jin, Q.; Boger, D. L., Synthesis and evaluation of vancomycin and vancomycin aglycon analogues that bear modifications in the residue 3 asparagine. *Bioorganic & Medicinal Chemistry Letters* **2002,** *12* (9), 1319-22.

123. Nitanai, Y.; Kikuchi, T.; Kakoi, K.; Hanamaki, S.; Fujisawa, I.; Aoki, K., Crystal structures of the complexes between vancomycin and cell-wall precursor analogs. *Journal of Molecular Biology* **2009,** *385* (5), 1422-32.

124. Yarlagadda, V.; Konai, M. M.; Manjunath, G. B.; Ghosh, C.; Haldar, J., Tackling vancomycin-resistant bacteria with 'lipophilic–vancomycin–carbohydrate conjugates'. *The Journal of Antibiotics* **2015,** *68* (5), 302-312.

125. Bochicchio, B.; Tamburro, A. M., Polyproline II structure in proteins: Identification by chiroptical spectroscopies, stability, and functions. *Chirality* **2002,** *14* (10), 782-792.

126. Li, W.; Tailhades, J.; O'Brien-Simpson, N. M.; Separovic, F.; Otvos Jr., L.; Hossain, M. A.; Wade, J. D., Proline-rich antimicrobial peptides: potential therapeutics against antibiotic-resistant bacteria. *Amino Acids* **2014,** *46* (10), 2287-2294.

127. Mishra, A. K.; Choi, J.; Moon, E.; Baek, K.-H., Tryptophan-Rich and Proline-Rich Antimicrobial Peptides. *Molecules* **2018,** *23* (4), 815.

128. Rothbard, J. B.; Jessop, T. C.; Lewis, R. S.; Murray, B. A.; Wender, P. A., Role of Membrane Potential and Hydrogen Bonding in the Mechanism of Translocation of Guanidinium-Rich Peptides into Cells. *Journal of the American Chemical Society* **2004,** *126* (31), 9506-9507.

129. Kohn, E. M.; Shirley, D. J.; Arotsky, L.; Picciano, A. M.; Ridgway, Z.; Urban, M. W.; Carone, B. R.; Caputo, G. A., Role of Cationic Side Chains in the Antimicrobial Activity of C18G. *Molecules* **2018,** *23* (2), 329.

130. Beauregard, D. A.; Williams, D. H.; Gwynn, M. N.; Knowles, D. J., Dimerization and membrane anchors in extracellular targeting of vancomycin group antibiotics. *Antimicrobial Agents and Chemotherapy* **1995,** *39* (3), 781-785.

131. Sundram, U. N.; Griffin, J. H.; Nicas, T. I., Novel Vancomycin Dimers with Activity against Vancomycin-Resistant Enterococci. *Journal of the American Chemical Society* **1996,** *118* (51), 13107-13108.

132. Rao, J.; Lahiri, J.; Isaacs, L.; Weis, R. M.; Whitesides, G. M., A trivalent system from vancomycin.D-ala-D-Ala with higher affinity than avidin.biotin. *Science* **1998,** *280* (5364), 708-11.

133. Arimoto, H.; Nishimura, K.; Hayakawa, I.; Kinumi, T.; Uemura, D., Multi-valent polymer of vancomycin: enhanced antibacterial activity against VRE. *Chemical Communications* **1999,** (15), 1361-1362.

134. Nicolaou, K. C.; Hughes, R.; Cho, S. Y.; Winssinger, N.; Smethurst, C.; Labischinski, H.; Endermann, R., Target-Accelerated Combinatorial Synthesis and Discovery of Highly Potent Antibiotics Effective Against Vancomycin-Resistant Bacteria. *Angewandte Chemie International Edition English* **2000,** *39* (21), 3823-3828.

135. Xing, B.; Yu, C.-W.; Ho, P.-L.; Chow, K.-H.; Cheung, T.; Gu, H.; Cai, Z.; Xu, B., Multivalent Antibiotics via Metal Complexes: Potent Divalent Vancomycins against Vancomycin-Resistant Enterococci. *Journal of Medicinal Chemistry* **2003,** *46* (23), 4904-4909.

136. Yarlagadda, V.; Sarkar, P.; Manjunath, G. B.; Haldar, J., Lipophilic vancomycin aglycon dimer with high activity against vancomycin-resistant bacteria. *Bioorganic & Medicinal Chemistry Letters* **2015,** *25* (23), 5477-80.

137. Silverman, S. M.; Moses, J. E.; Sharpless, K. B., Reengineering Antibiotics to Combat Bacterial Resistance: Click Chemistry [1,2,3]-Triazole Vancomycin Dimers with Potent Activity against MRSA and VRE. *Chemistry* **2017,** *23* (1), 79-83.

138. Arnusch, C. J.; Bonvin, A. M. J. J.; Verel, A. M.; Jansen, W. T. M.; Liskamp, R. M. J.; de Kruijff, B.; Pieters, R. J.; Breukink, E., The Vancomycin−Nisin(1−12) Hybrid Restores Activity against Vancomycin Resistant Enterococci. *Biochemistry* **2008,** *47* (48), 12661-12663.

139. Long, D. D.; Aggen, J. B.; Chinn, J.; Choi, S. K.; Christensen, B. G.; Fatheree, P. R.; Green, D.; Hegde, S. S.; Judice, J. K.; Kaniga, K.; Krause, K. M.; Leadbetter, M.; Linsell, M. S.; Marquess, D. G.; Moran, E. J.; Nodwell, M. B.; Pace, J. L.; Trapp, S. G.; Turner, S. D., Exploring the positional attachment of glycopeptide/beta-lactam heterodimers. *The Journal of Antibiotics* **2008,** *61* (10), 603-14.

140. Hegde, S. S.; Okusanya, O. O.; Skinner, R.; Shaw, J. P.; Obedencio, G.; Ambrose, P. G.; Blais, J.; Bhavnani, S. M., Pharmacodynamics of TD-1792, a novel glycopeptide-cephalosporin heterodimer antibiotic used against Gram-positive bacteria, in a neutropenic murine thigh model. *Antimicrobial Agents and Chemotherapy* **2012,** *56* (3), 1578-83.

141. Blais, J.; Lewis, S. R.; Krause, K. M.; Benton, B. M., Antistaphylococcal activity of TD-1792, a multivalent glycopeptide-cephalosporin antibiotic. *Antimicrobial Agents and Chemotherapy* **2012,** *56* (3), 1584-7.

142. Mishra, N. M.; Briers, Y.; Lamberigts, C.; Steenackers, H.; Robijns, S.; Landuyt, B.; Vanderleyden, J.; Schoofs, L.; Lavigne, R.; Luyten, W.; Van der Eycken, E. V., Evaluation of the antibacterial and antibiofilm activities of novel CRAMP–vancomycin conjugates with diverse linkers. *Organic & Biomolecular Chemistry* **2015,** *13* (27), 7477-7486.

143. Santajit, S.; Indrawattana, N., Mechanisms of Antimicrobial Resistance in ESKAPE Pathogens. *BioMed research international* **2016,** *2016*, 1-8.

144. Pankey, G. A.; Sabath, L. D., Clinical Relevance of Bacteriostatic versus Bactericidal Mechanisms of Action in the Treatment of Gram-Positive Bacterial Infections. *Clinical Infectious Diseases* **2004,** *38* (6), 864-870.

145. Glukhov, E.; Stark, M.; Burrows, L. L.; Deber, C. M., Basis for selectivity of cationic antimicrobial peptides for bacterial versus mammalian membranes. *J Biol Chem* **2005,** *280* (40), 33960-7.

146. DeGrado, W. F.; Musso, G. F.; Lieber, M.; Kaiser, E. T.; Kézdy, F. J., Kinetics and mechanism of hemolysis induced by melittin and by a synthetic melittin analogue. *Biophysical Journal* **1982,** *37* (1), 329-38.

147. Mosmann, T., Rapid colorimetric assay for cellular growth and survival: application to proliferation and cytotoxicity assays. *Journal of Immunological Methods* **1983,** *65* (1-2), 55-63.

148. Rogers, D. E., Studies on bacteriemia. I. Mechanisms relating to the persistence of bacteriemia in rabbits following the intravenous injection of staphylococci. *Journal of Experimental Medicine* **1956,** *103* (6), 713-42.

149. Rogers , D. E.; Tompsett , R., The Survival of Staphylococci within Human Leukocytes. *Journal of Experimental Medicine* **1952,** *95* (2), 209-230.

150. Kapral, F. A.; Shayegani, M. G., Intracellular survival of staphylococci. *Journal of Experimental Medicine* **1959,** *110* (1), 123-38.

151. Melly , M. A.; Thomison , J. B.; Rogers , D. E., Fate of Staphylococci within Human Leukocytes. *Journal of Experimental Medicine* **1960,** *112* (6), 1121-1130.

152. Srivastava, G. K.; Reinoso, R.; Singh, A. K.; Fernandez-Bueno, I.; Hileeto, D.; Martino, M.; Garcia-Gutierrez, M. T.; Merino, J. M.; Alonso, N. F.; Corell, A.; Pastor, J. C., Trypan Blue staining method for quenching the autofluorescence of RPE cells for improving protein expression analysis. *Experimental Eye Research* **2011,** *93* (6), 956-62.

153. Nuutila, J.; Lilius, E. M., Flow cytometric quantitative determination of ingestion by phagocytes needs the distinguishing of overlapping populations of binding and ingesting cells. *Cytometry A* **2005,** *65* (2), 93-102.

154. Marschall, E.; Cryle, M. J.; Tailhades, J., Biological, chemical, and biochemical strategies for modifying glycopeptide antibiotics. *The Journal of biological chemistry* **2019,** *294* (49), 18769-18783.

155. Helander, I. M.; Mattila-Sandholm, T., Fluorometric assessment of Gram-negative bacterial permeabilization. *Journal of Applied Microbiology* **2000,** *88* (2), 213-219.

156. Wu, M.; Hancock, R. E. W., Interaction of the Cyclic Antimicrobial Cationic Peptide Bactenecin with the Outer and Cytoplasmic Membrane. *Journal of Biological Chemistry* **1999,** *274* (1), 29-35.

157. Sun, C.; Gu, L.; Hussain, M. A.; Chen, L.; Lin, L.; Wang, H.; Pang, S.; Jiang, C.; Jiang, Z.; Hou, J., Characterization of the Bioactivity and Mechanism of Bactenecin Derivatives Against Food-Pathogens. *Frontiers in Microbiology* **2019,** *10* (2593).

158. Vaara, M., Agents that increase the permeability of the outer membrane. *Microbiological reviews* **1992,** *56* (3), 395-411.

159. Muheim, C.; Götzke, H.; Eriksson, A. U.; Lindberg, S.; Lauritsen, I.; Nørholm, M. H. H.; Daley, D. O., Increasing the permeability of Escherichia coli using MAC13243. *Scientific Reports* **2017,** *7* (1), 17629.

160. Nygaard, R.; Romaniuk, Joseph A. H.; Rice, David M.; Cegelski, L., Spectral Snapshots of Bacterial Cell-Wall Composition and the Influence of Antibiotics by Whole-Cell NMR. *Biophysical Journal* **2015,** *108* (6), 1380-1389.

161. García-Alegría, A. M.; Anduro-Corona, I.; Pérez-Martínez, C. J.; Guadalupe Corella-Madueño, M. A.; Rascón-Durán, M. L.; Astiazaran-Garcia, H., Quantification of DNA through the NanoDrop Spectrophotometer: Methodological Validation Using Standard Reference Material and Sprague Dawley Rat and Human DNA. *International Journal of Analytical Chemistry* **2020,** *2020*, 8896738.

162. Te Winkel, J. D.; Gray, D. A.; Seistrup, K. H.; Hamoen, L. W.; Strahl, H., Analysis of Antimicrobial-Triggered Membrane Depolarization Using Voltage Sensitive Dyes. *Frontiers in cell and developmental biology* **2016,** *4*, 29-29.

163. Daniel, R. A.; Errington, J., Control of Cell Morphogenesis in Bacteria: Two Distinct Ways to Make a Rod-Shaped Cell. *Cell* **2003,** *113* (6), 767-776.

164. Benfield, A. H.; Henriques, S. T., Mode-of-Action of Antimicrobial Peptides: Membrane Disruption vs. Intracellular Mechanisms. *Frontiers in Medical Technology* **2020,** *2* (20).

165. Benincasa, M.; Pacor, S.; Gennaro, R.; Scocchi, M., Rapid and reliable detection of antimicrobial peptide penetration into gram-negative bacteria based on fluorescence quenching. *Antimicrobial Agents and Chemotherapy* **2009,** *53* (8), 3501-3504.

166. De Oliveira, D. M. P.; Forde, B. M.; Kidd, T. J.; Harris, P. N. A.; Schembri, M. A.; Beatson, S. A.; Paterson, D. L.; Walker, M. J., Antimicrobial Resistance in ESKAPE Pathogens. *Clinical Microbiology Reviews* **2020,** *33* (3), e00181-19.

167. Kaiser, E.; Colescott, R. L.; Bossinger, C. D.; Cook, P. I., Color test for detection of free terminal amino groups in the solid-phase synthesis of peptides. *Analytical Biochemistry* **1970,** *34* (2), 595-8.

168. Christensen, T.; Eriksson, A.; Thornell, L.-E., A Qualitative Test for Monitoring Coupling Completeness in Solid Phase Peptide Synthesis Using Chloranil. *Acta Chemica Scandinavica* **1979**, 763-766.

169. Institute, C. a. L. S., *Methods for dilution antimicrobial susceptibility tests for bacteria that grow aerobically*. 9th ed.; 2012; Vol. 32.

170. Mohammad, H.; AbdelKhalek, A.; Abutaleb, N. S.; Seleem, M. N., Repurposing niclosamide for intestinal decolonization of vancomycin-resistant enterococci. *International Journal of Antimicrobial Agents* **2018,** *51* (6), 897-904.

171. Hagras, M.; Abutaleb, N. S.; Ali, A. O.; Abdel-Aleem, J. A.; Elsebaei, M. M.; Seleem, M. N.; Mayhoub, A. S., Naphthylthiazoles: Targeting Multidrug-Resistant and Intracellular Staphylococcus aureus with Biofilm Disruption Activity. *ACS Infectious Diseases* **2018,** *4* (12), 1679-1691.

172. Zhu, X.; Zhang, L.; Wang, J.; Ma, Z.; Xu, W.; Li, J.; Shan, A., Characterization of antimicrobial activity and mechanisms of low amphipathic peptides with different α-helical propensity. *Acta Biomaterialia* **2015,** *18*, 155-67.

173. O'Neill, A. J.; Miller, K.; Oliva, B.; Chopra, I., Comparison of assays for detection of agents causing membrane damage in Staphylococcus aureus. *Journal of Antimicrobial Chemotherapy* **2004,** *54* (6), 1127-9.

174. Mohammad, H.; Reddy, P. V. N.; Monteleone, D.; Mayhoub, A. S.; Cushman, M.; Hammac, G. K.; Seleem, M. N., Antibacterial Characterization of Novel Synthetic Thiazole Compounds against Methicillin-Resistant Staphylococcus pseudintermedius. *PloS one* **2015,** *10* (6), e0130385-e0130385.

175. Zygmunt, W. A.; Browder, H. P.; Tavormina, P. A., Lytic action of lysostaphin on susceptible and resistant strains of Staphylococcus aureus. *Canadian Journal of Microbiology* **1967,** *13* (7), 845-53.

176. Bastos, M. D.; Coutinho, B. G.; Coelho, M. L., Lysostaphin: A Staphylococcal Bacteriolysin with Potential Clinical Applications. *Pharmaceuticals (Basel)* **2010,** *3* (4), 1139-1161.

177. Ament, P. W.; Jamshed, N.; Horne, J. P., Linezolid: its role in the treatment of gram-positive, drug-resistant bacterial infections. *American Family Physician* **2002,** *65* (4), 663-70.

178. Cupo-Abbott, J.; Louie, S. G.; Rho, J. P., A synthetic oxazolidinone antimicrobial for treatment of serious gram- positive infections. *Formulary* **2000,** *35*, 483-497.

179. Dryden, M. S., Linezolid pharmacokinetics and pharmacodynamics in clinical treatment. *Journal of Antimicrobial Chemotherapy* **2011,** *66* (suppl_4), iv7-iv15.

180. Livermore, D. M., Linezolid in vitro: mechanism and antibacterial spectrum. *Journal of Antimicrobial Chemotherapy* **2003,** *51* (2), ii9-ii16.

181. Metallidis, S.; Chatzidimitriou, M.; Nikolaidis, P.; Tsona, A.; Bisiklis, A.; Kollaras, P.; Tsiakiri, E.; Koumentaki, E.; Alexiou-Daniel, S., Comparative in vitro activity of linezolid and five other antimicrobials against nosocomial isolates of methicillin-resistant Staphylococcus aureus, methicillin-resistant Staphylococcus epidermidis and vancomycin-resistant Enterococcus faecium. *Journal of Chemotherapy* **2003,** *15* (5), 442-8.

182. Jevitt, L. A.; Smith, A. J.; Williams, P. P.; Raney, P. M.; McGowan, J. E., Jr.; Tenover, F. C., In vitro activities of Daptomycin, Linezolid, and Quinupristin-Dalfopristin against a challenge panel of Staphylococci and Enterococci, including vancomycin-intermediate staphylococcus aureus and vancomycin-resistant Enterococcus faecium. *Microbial Drug Resistance* **2003,** *9* (4), 389-93.

183. Sandberg, A.; Jensen, K. S.; Baudoux, P.; Van Bambeke, F.; Tulkens, P. M.; Frimodt-Møller, N., Intra- and extracellular activity of linezolid against Staphylococcus aureus in vivo and in vitro. *Journal of Antimicrobial Chemotherapy* **2010,** *65* (5), 962-73.

184. Pletz, M. W.; Burkhardt, O.; Welte, T., Nosocomial methicillin-resistant Staphylococcus aureus (MRSA) pneumonia: linezolid or vancomycin? - Comparison of pharmacology and clinical efficacy. *European journal of medical research* **2010,** *15* (12), 507-513.

185. Ehsan, M. M.; Fatima, G.; Ismail, M. O.; Memon, Z., Efficacy of vancomycin versus linezolid against coagulase-negative staphylococci in various clinical specimens. *Journal of Ayub Medical College Abbottabad* **2014,** *26* (2), 137-40.

186. WHO *Global Tuberculosis Report 2020*; World Health Organization: Geneva, 2020.

187. Jaspard, M.; Butel, N.; El Helali, N.; Marigot-Outtandy, D.; Guillot, H.; Peytavin, G.; Veziris, N.; Bodaghi, B.; Flandre, P.; Petitjean, G.; Caumes, E.; Pourcher, V., Linezolid-Associated Neurologic Adverse Events in Patients with Multidrug-Resistant Tuberculosis, France. *Emerging Infectious Disease journal* **2020,** *26* (8), 1792.

188. Schecter, G. F.; Scott, C.; True, L.; Raftery, A.; Flood, J.; Mase, S., Linezolid in the Treatment of Multidrug-Resistant Tuberculosis. *Clinical Infectious Diseases* **2010,** *50* (1), 49-55.

189. Singh, B.; Cocker, D.; Ryan, H.; Sloan, D. J., Linezolid for drug-resistant pulmonary tuberculosis. *The Cochrane database of systematic reviews* **2019,** *3* (3), 1-80.

190. Alghamdi, W. A.; Al-Shaer, M. H.; An, G.; Alsultan, A.; Kipiani, M.; Barbakadze, K.; Mikiashvili, L.; Ashkin, D.; Griffith, D. E.; Cegielski, J. P.; Kempker, R. R.; Peloquin, C. A., Population Pharmacokinetics of Linezolid in Tuberculosis Patients: Dosing Regimen Simulation and Target Attainment Analysis. *Antimicrobial Agents and Chemotherapy* **2020,** *64* (10), e01174-20.

191. Nguyen, H. M.; Graber, C. J., Limitations of antibiotic options for invasive infections caused by methicillin-resistant Staphylococcus aureus: is combination therapy the answer? *Journal of Antimicrobial Chemotherapy* **2009,** *65* (1), 24-36.

192. Jacqueline, C.; Caillon, J.; Le Mabecque, V.; Miègeville, A.-F.; Donnio, P.-Y.; Bugnon, D.; Potel, G., In vitro activity of linezolid alone and in combination with gentamicin, vancomycin or rifampicin against methicillin-resistant Staphylococcus aureus by time–kill curve methods. *Journal of Antimicrobial Chemotherapy* **2003,** *51* (4), 857-864.

193. Grohs, P.; Kitzis, M. D.; Gutmann, L., In vitro bactericidal activities of linezolid in combination with vancomycin, gentamicin, ciprofloxacin, fusidic acid, and rifampin against Staphylococcus aureus. *Antimicrob Agents Chemother* **2003,** *47* (1), 418-20.

194. Dailey, C. F.; Pagano, P. J.; Buchanan, L. V.; Paquette, J. A.; Haas, J. V.; Gibson, J. K., Efficacy of linezolid plus rifampin in an experimental model of methicillin-susceptible Staphylococcus aureus endocarditis. *Antimicrobial Agents and Chemotherapy* **2003,** *47* (8), 2655-8.

195. Tsaganos, T.; Skiadas, I.; Koutoukas, P.; Adamis, T.; Baxevanos, N.; Tzepi, I.; Pelekanou, A.; Giamarellos-Bourboulis, E. J.; Giamarellou, H.; Kanellakopoulou, K., Efficacy and pharmacodynamics of linezolid, alone and in combination with rifampicin, in an experimental model of methicillin-resistant Staphylococcus aureus endocarditis. *Journal of Antimicrobial Chemotherapy* **2008,** *62* (2), 381-3.

196. Ocampo, P. S.; Lázár, V.; Papp, B.; Arnoldini, M.; Abel zur Wiesch, P.; Busa-Fekete, R.; Fekete, G.; Pál, C.; Ackermann, M.; Bonhoeffer, S., Antagonism between Bacteriostatic and Bactericidal Antibiotics Is Prevalent. *Antimicrobial Agents and Chemotherapy* **2014,** *58* (8), 4573-4582.

197. Gonzales, R. D.; Schreckenberger, P. C.; Graham, M. B.; Kelkar, S.; DenBesten, K.; Quinn, J. P., Infections due to vancomycin-resistant Enterococcus faecium resistant to linezolid. *Lancet* **2001,** *357* (9263), 1179.

198. Rahim, S.; Pillai, S. K.; Gold, H. S.; Venkataraman, L.; Inglima, K.; Press, R. A., Linezolid-Resistant, Vancomycin-Resistant Enterococcus faecium Infection in Patients without Prior Exposure to Linezolid. *Clinical Infectious Diseases* **2003,** *36* (11), e146-e148.

199. Long, K. S.; Vester, B., Resistance to Linezolid Caused by Modifications at Its Binding Site on the Ribosome. *Antimicrobial Agents and Chemotherapy* **2012,** *56* (2), 603-612.

200. Yadav, G.; Thakuria, B.; Madan, M.; Agwan, V.; Pandey, A., Linezolid and Vancomycin Resistant Enterococci: A Therapeutic Problem. *Journal of clinical and diagnostic research : JCDR* **2017,** *11* (8), GC07-GC11.

201. Abbo, L.; Shukla, B. S.; Giles, A.; Aragon, L.; Jimenez, A.; Camargo, J. F.; Simkins, J.; Sposato, K.; Tran, T. T.; Diaz, L.; Reyes, J.; Rios, R.; Carvajal, L. P.; Cardozo, J.; Ruiz, M.; Rosello, G.; Cardona, A. P.; Martinez, O.; Guerra, G.; Beduschi, T.; Vianna, R.; Arias, C. A., Linezolid- and Vancomycin-resistant Enterococcus faecium in Solid Organ Transplant Recipients: Infection Control and Antimicrobial Stewardship Using Whole Genome Sequencing. *Clinical Infectious Diseases* **2019,** *69* (2), 259-265.

202. Kosecka-Strojek, M.; Sadowy, E.; Gawryszewska, I.; Klepacka, J.; Tomasik, T.; Michalik, M.; Hryniewicz, W.; Miedzobrodzki, J., Emergence of linezolid-resistant Staphylococcus epidermidis in the tertiary children's hospital in Cracow, Poland. *European Journal of Clinical Microbiology & Infectious Diseases* **2020,** *39* (9), 1717-1725.

203. Hamel, J. C.; Stapert, D.; Moerman, J. K.; Ford, C. W., Linezolid, critical characteristics. *Infection* **2000,** *28* (1), 60-4.

204. Zahedi Bialvaei, A.; Rahbar, M.; Yousefi, M.; Asgharzadeh, M.; Samadi Kafil, H., Linezolid: a promising option in the treatment of Gram-positives. *Journal of Antimicrobial Chemotherapy* **2016,** *72* (2), 354-364.

205. Shang, J.; Pourvali, A.; Cochrane, J. R.; Hutton, C. A., Steric and Electronic Effects in the Synthesis and Regioselective Hydrolysis of Unsymmetrical Imides. *Australian Journal of Chemistry* **2015,** *68* (12), 1854-1858.

206. Hou, J.; Liu, Z.; Cao, S.; Wang, H.; Jiang, C.; Hussain, M. A.; Pang, S., Broad-Spectrum Antimicrobial Activity and Low Cytotoxicity against Human Cells of a Peptide Derived from Bovine α(S1)-Casein. *Molecules (Basel, Switzerland)* **2018,** *23* (5), 1220.

207. LaPlante, K. L.; Sakoulas, G., Evaluating Aztreonam and Ceftazidime Pharmacodynamics with Escherichia coli in Combination with Daptomycin, Linezolid, or Vancomycin in an In Vitro Pharmacodynamic Model. *Antimicrobial Agents and Chemotherapy* **2009,** *53* (10), 4549-4555.

208. Schumacher, A.; Trittler, R.; Bohnert, J. A.; Kümmerer, K.; Pagès, J.-M.; Kern, W. V., Intracellular accumulation of linezolid in Escherichia coli, Citrobacter freundii and Enterobacter aerogenes: role of enhanced efflux pump activity and inactivation. *Journal of Antimicrobial Chemotherapy* **2006,** *59* (6), 1261-1264.

209. Li, J.; Koh, J.-J.; Liu, S.; Lakshminarayanan, R.; Verma, C. S.; Beuerman, R. W., Membrane Active Antimicrobial Peptides: Translating Mechanistic Insights to Design. *Frontiers in Neuroscience* **2017,** *11* (73).

210. Le, C. F.; Fang, C. M.; Sekaran, S. D., Intracellular Targeting Mechanisms by Antimicrobial Peptides. *Antimicrobial Agents and Chemotherapy* **2017,** *61* (4).

211. Forman, H. J.; Zhang, H.; Rinna, A., Glutathione: overview of its protective roles, measurement, and biosynthesis. *Molecular aspects of medicine* **2009,** *30* (1-2), 1-12.

212. Pitasse Santos, P.; Chmielewski, J., LnzP14: Unpublished Results. Purdue University: 2019.

213. Palladino, P.; Stetsenko, D. A., New TFA-Free Cleavage and Final Deprotection in Fmoc Solid-Phase Peptide Synthesis: Dilute HCl in Fluoro Alcohol. *Organic Letters* **2012,** *14* (24), 6346-6349.

APPENDIX A. ADDITIONAL DATA

Analytical HPLC Spectra

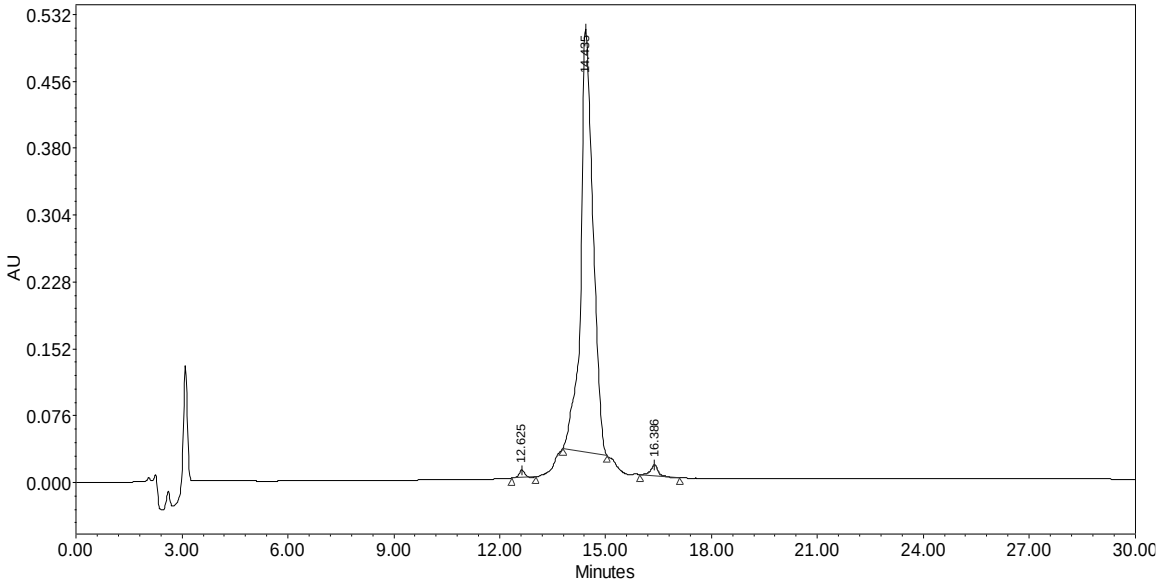

Figure A 1. Analytical purity HPLC spectrum of **P14LRR-SH**. C18 column, 214 nm, 1.2 mL/min. Gradient eluent, curve 6, 25-65% acetonitrile in water, 0.1% TFA. Product is 97% pure.

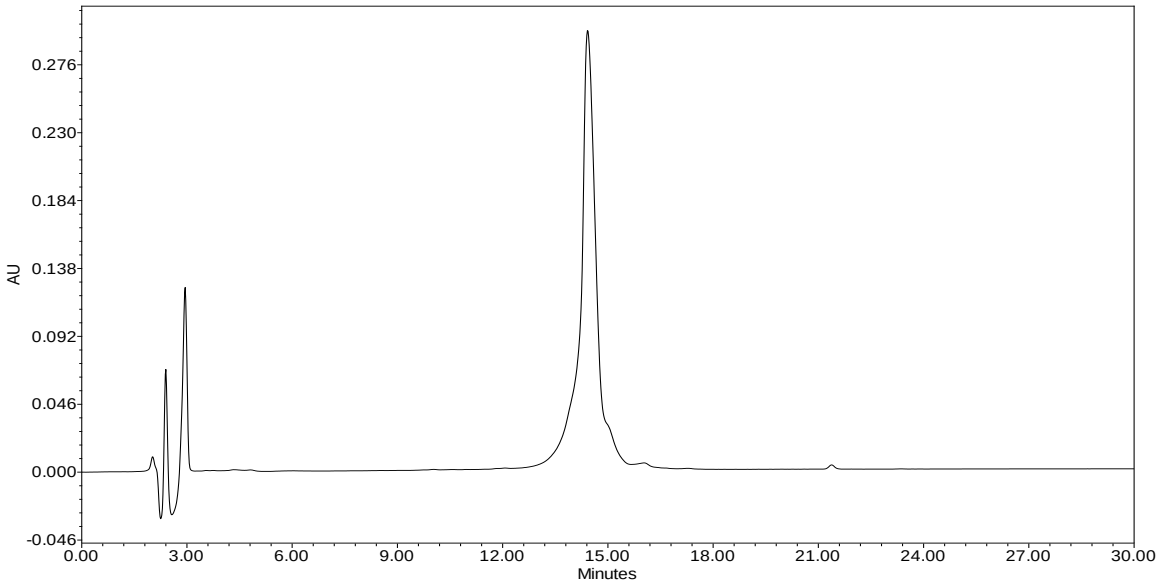

Figure A 2. Analytical purity HPLC spectrum of **FlP14LRR-SH**. C18 column, 214 nm, 1.2 mL/min. Gradient eluent, curve 6, 30-60% acetonitrile in water, 0.1% TFA. Product is 99% pure.

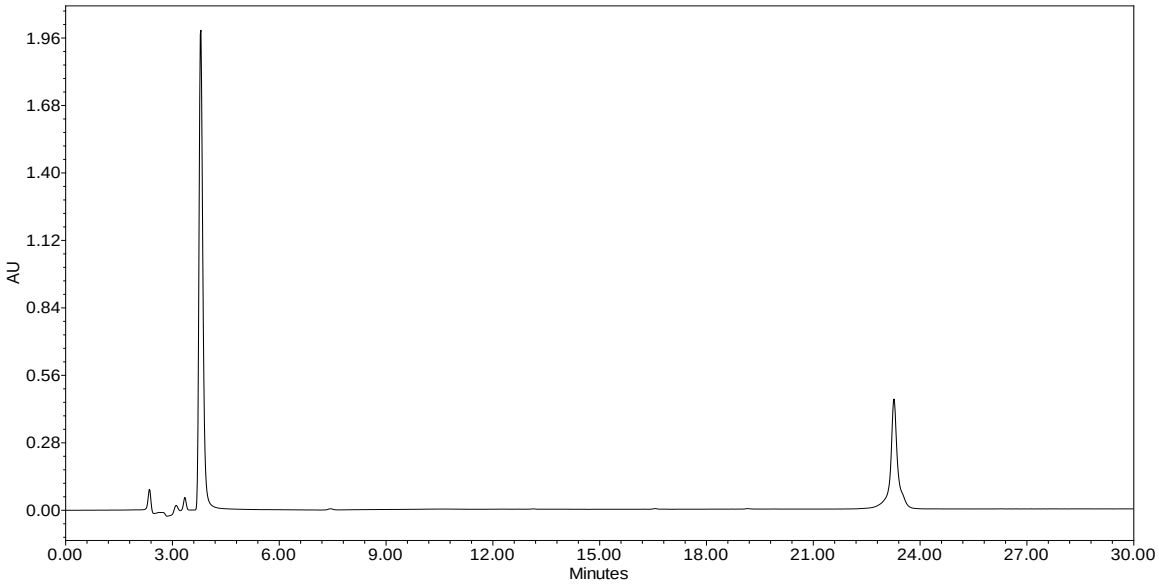

Figure A 3. Analytical purity HPLC spectrum of **VanP14S**. C18 column, 214 nm, 1.2 mL/min. Gradient eluent, curve 6, 5-60% acetonitrile in water, 0.1% TFA. Product is > 95% pure.

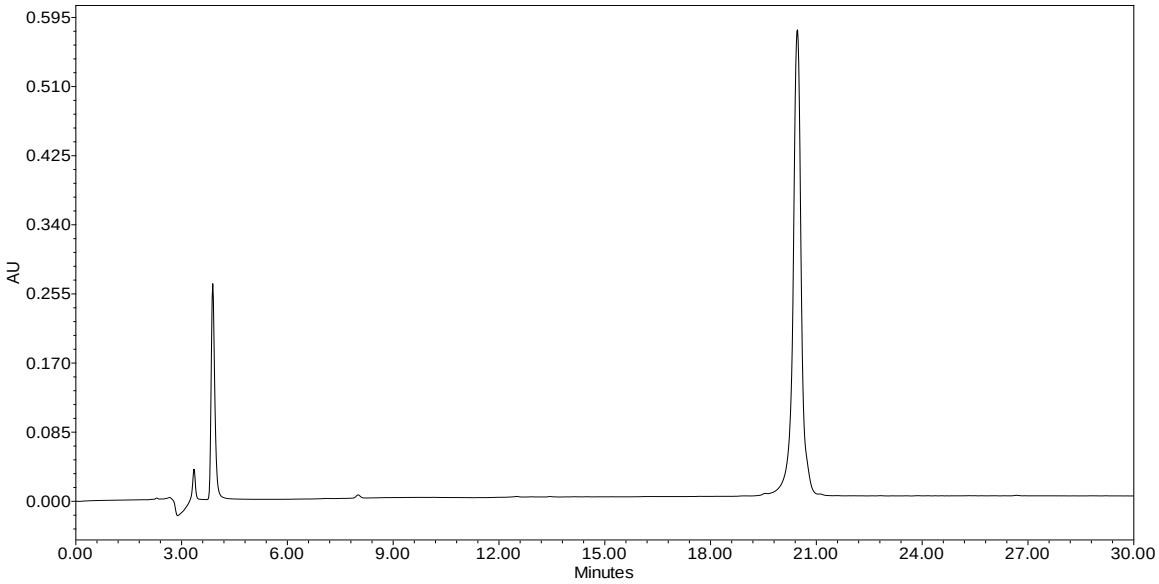

Figure A 4. Analytical purity HPLC spectrum of **VanMalP14**. C18 column, 214 nm, 1.2 mL/min. Gradient eluent, curve 6, 5-70% acetonitrile in water, 0.1% TFA. Product is > 95% pure.

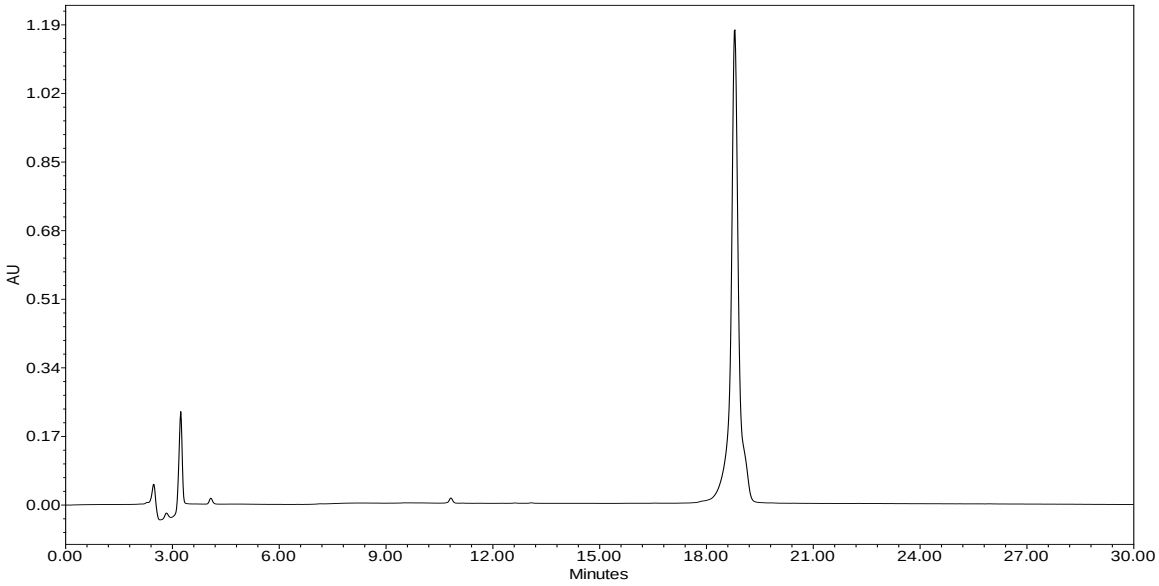

Figure A 5. Analytical purity HPLC spectrum of **FlVanP14S**. C18 column, 214 nm, 1.2 mL/min. Gradient eluent, curve 6, 10-80% acetonitrile in water, 0.1% TFA. Product is > 95% pure.

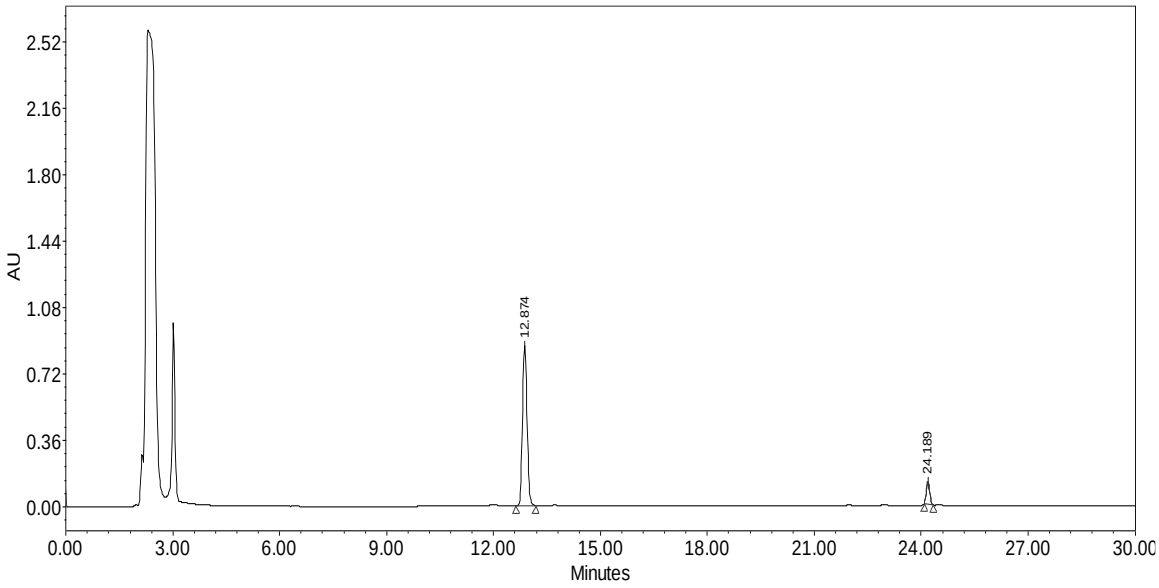

Figure A 6. Analytical purity HPLC spectrum of **FITC-Van**. C18 column, 214 nm, 1.2 mL/min. Gradient eluent, curve 6, 20-85% acetonitrile in water, 0.1% TFA. Product is 90% pure.

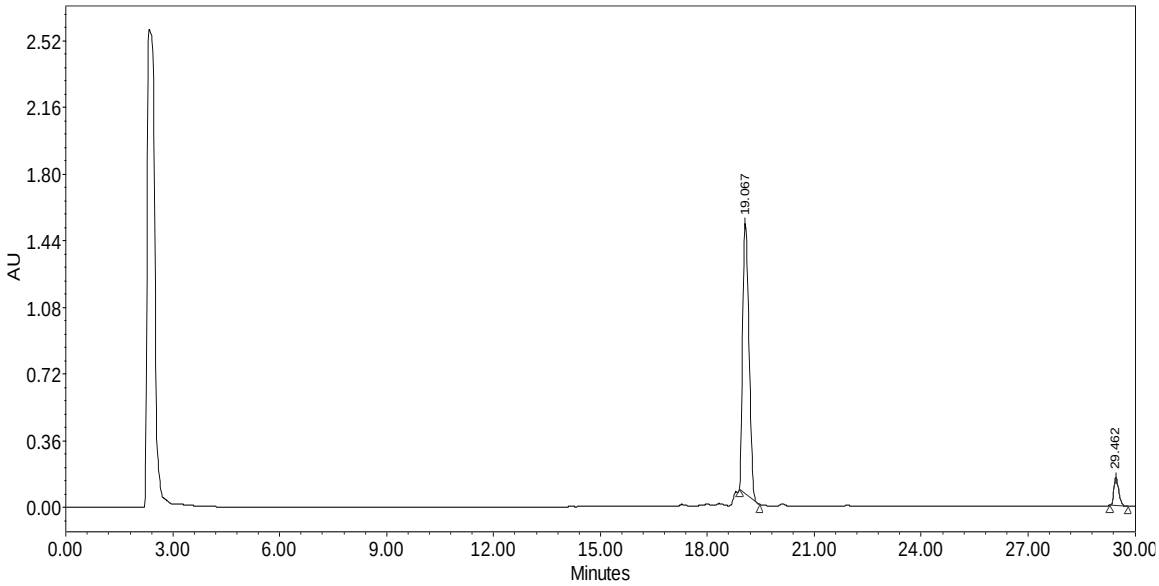

Figure A 7. Analytical purity HPLC spectrum of **RITC-Van**. C18 column, 214 nm, 1.2 mL/min. Gradient eluent, curve 6, 15-85% acetonitrile in water, 0.1% TFA. Product is 93% pure.

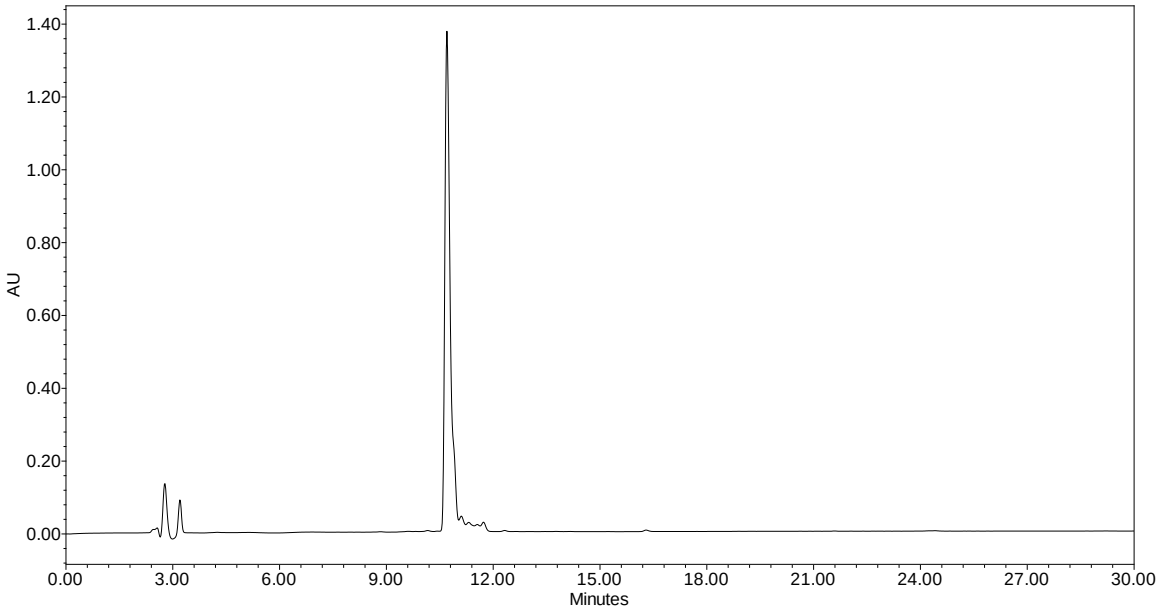

Figure A 8. Analytical purity HPLC spectrum of **Van-SH**. C18 column, 214 nm, 1.2 mL/min. Gradient eluent, curve 6, 10-70% acetonitrile in water, 0.1% TFA. Product is > 95% pure.

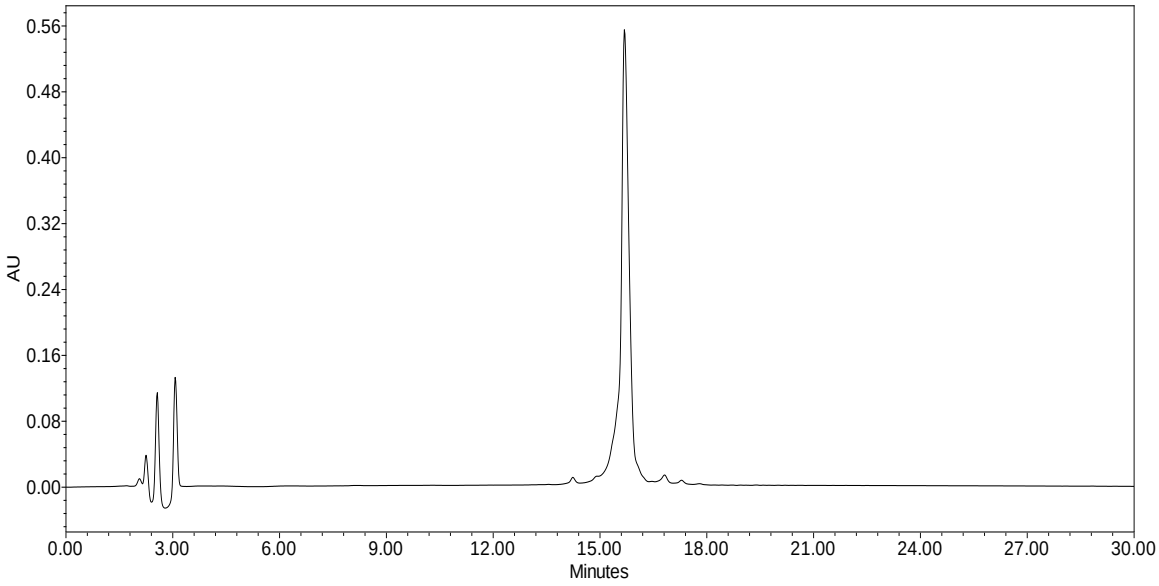

Figure A 9. Analytical purity HPLC spectrum of **P14GAP-SH**. C18 column, 214 nm, 1.2 mL/min. Gradient eluent, curve 6, 20-75% acetonitrile in water, 0.1% TFA. Product is > 95% pure.

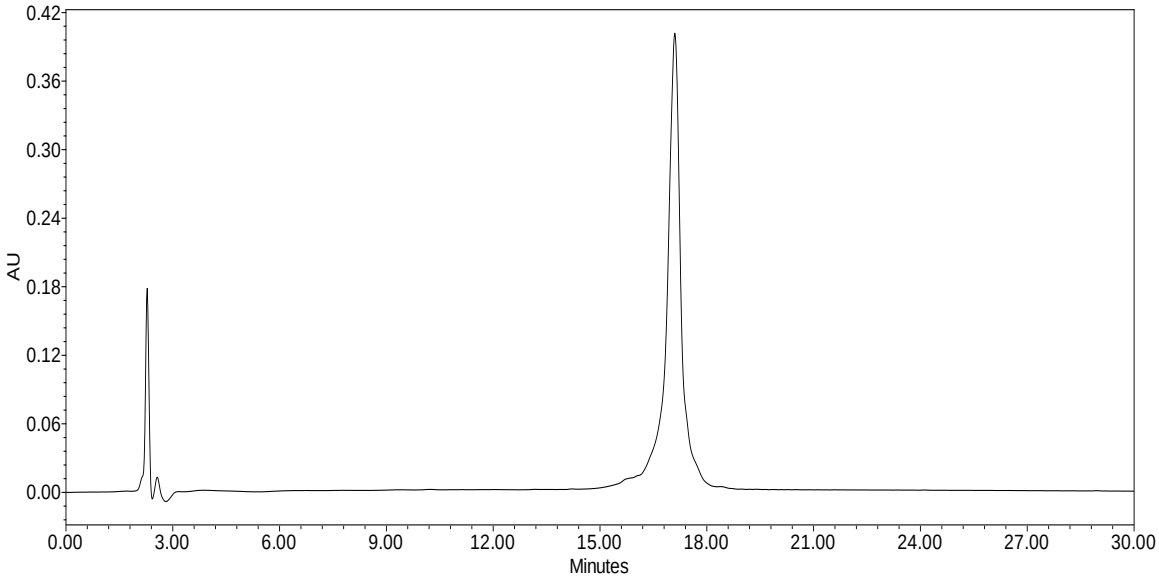

Figure A 10. Analytical purity HPLC spectrum of **FlP14GAP-SH**. C18 column, 214 nm, 1.2 mL/min. Gradient eluent, curve 6, 20-75% acetonitrile in water, 0.1% TFA. Product is > 95% pure.

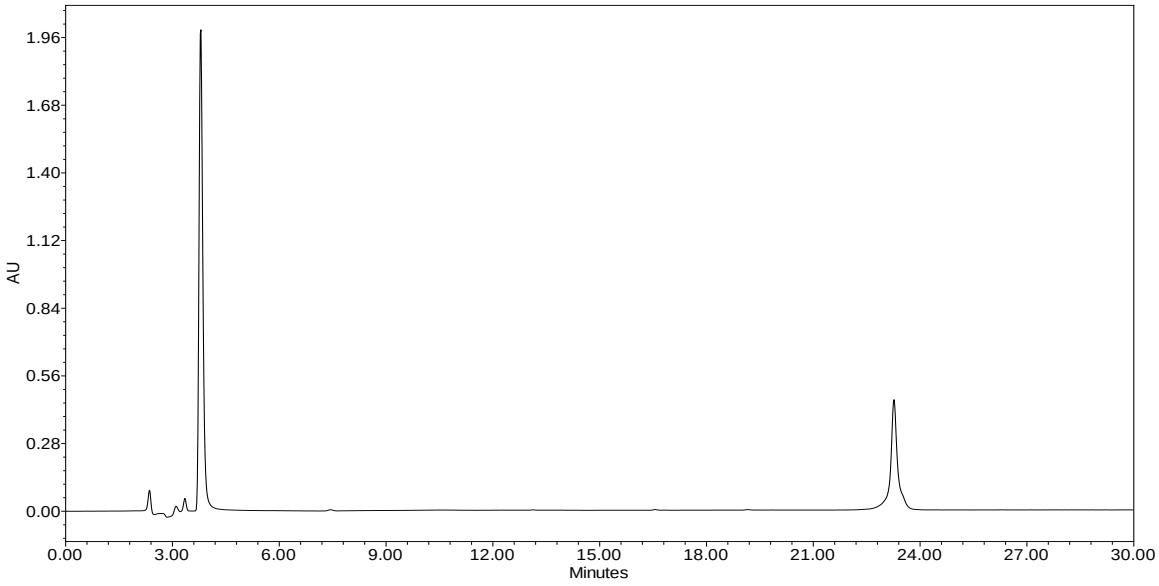

Figure A 11. Analytical purity HPLC spectrum of **VanP14GAPS**. C18 column, 214 nm, 1.2 mL/min. Gradient eluent, curve 6, 5-60% acetonitrile in water, 0.1% TFA. Product is > 95% pure.

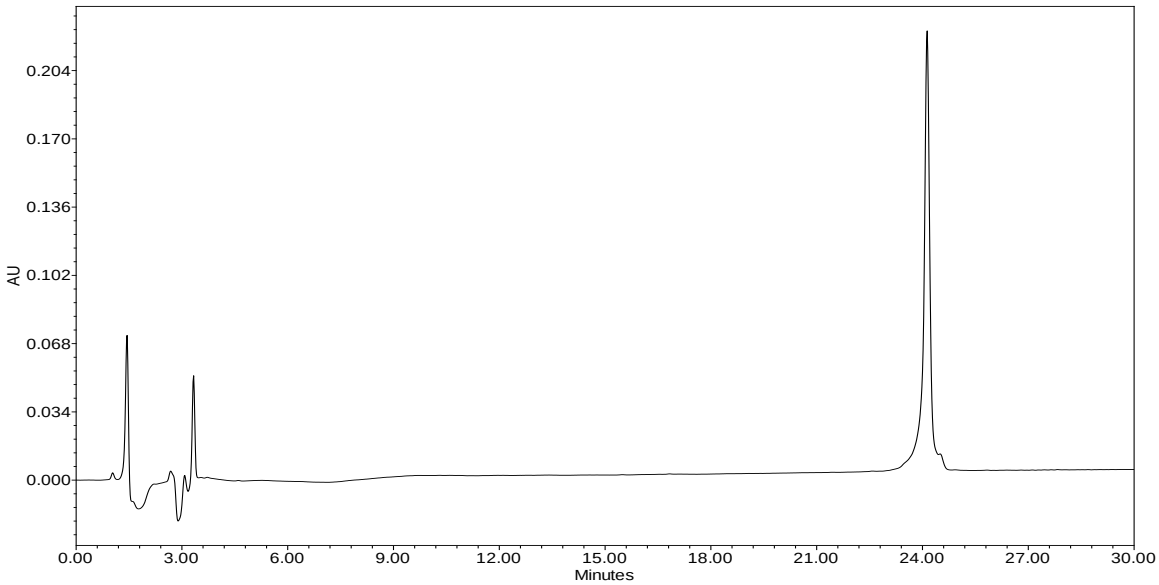

Figure A 12. Analytical purity HPLC spectrum of **FlVanP14GAPS**. C18 column, 214 nm, 1.2 mL/min. Gradient eluent, curve 6, 5-60% acetonitrile in water, 0.1% TFA. Product is > 95% pure.

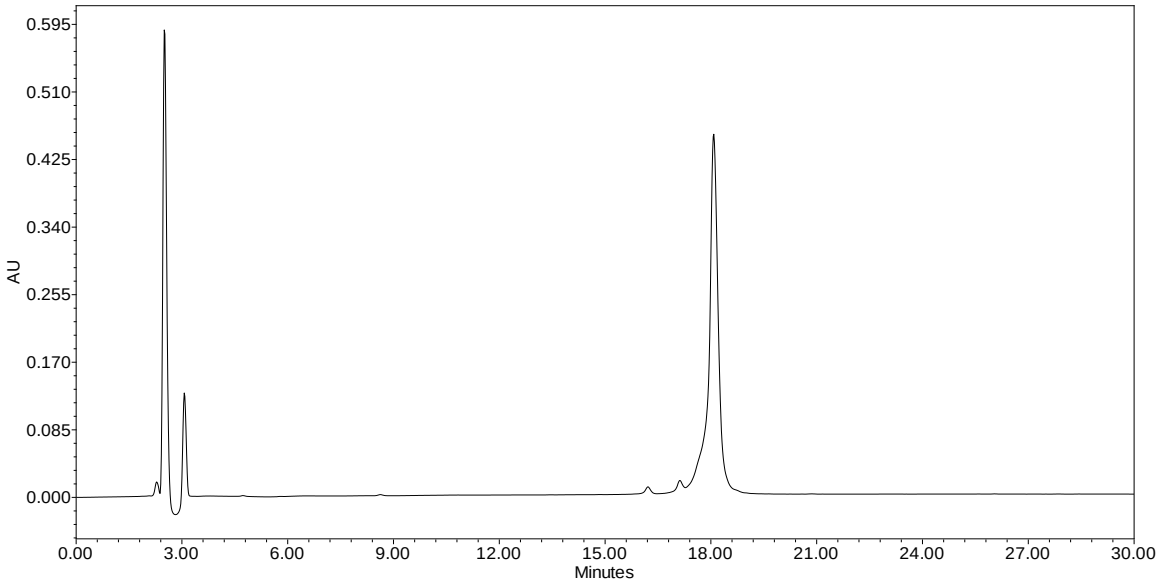

Figure A 13. Analytical purity HPLC spectrum of **LnzP14**. C18 column, 214 nm, 1.2 mL/min. Gradient eluent, curve 6, 20-80% acetonitrile in water, 0.1% TFA. Product is > 95% pure.

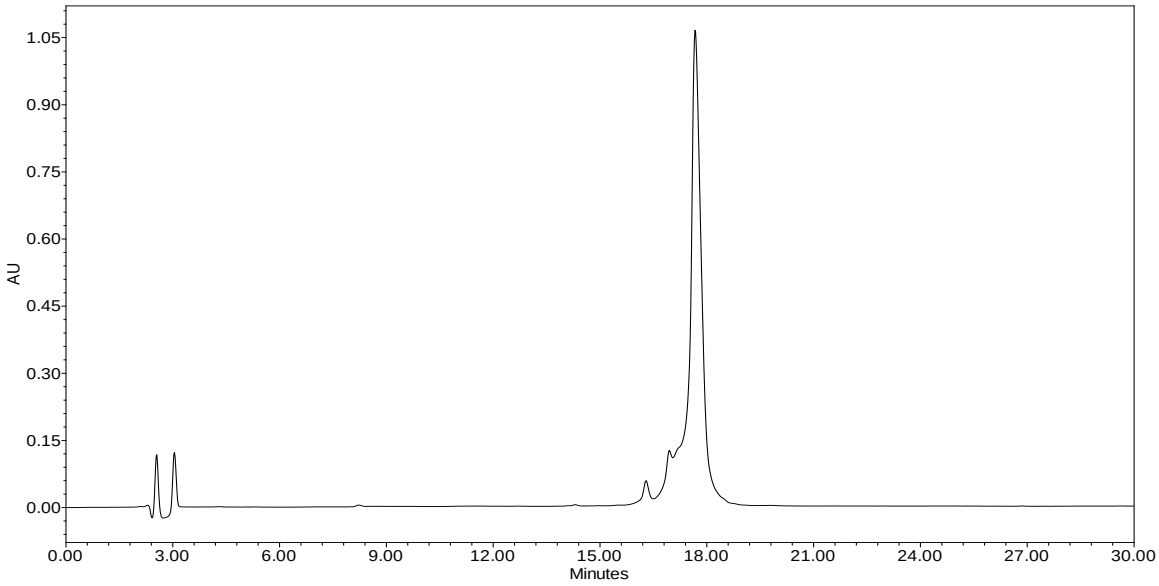

Figure A 14. Analytical purity HPLC spectrum of **FlLnzP14**. C18 column, 214 nm, 1.2 mL/min. Gradient eluent, curve 6, 20-80% acetonitrile in water, 0.1% TFA. Product is 95% pure.

NMR Spectra

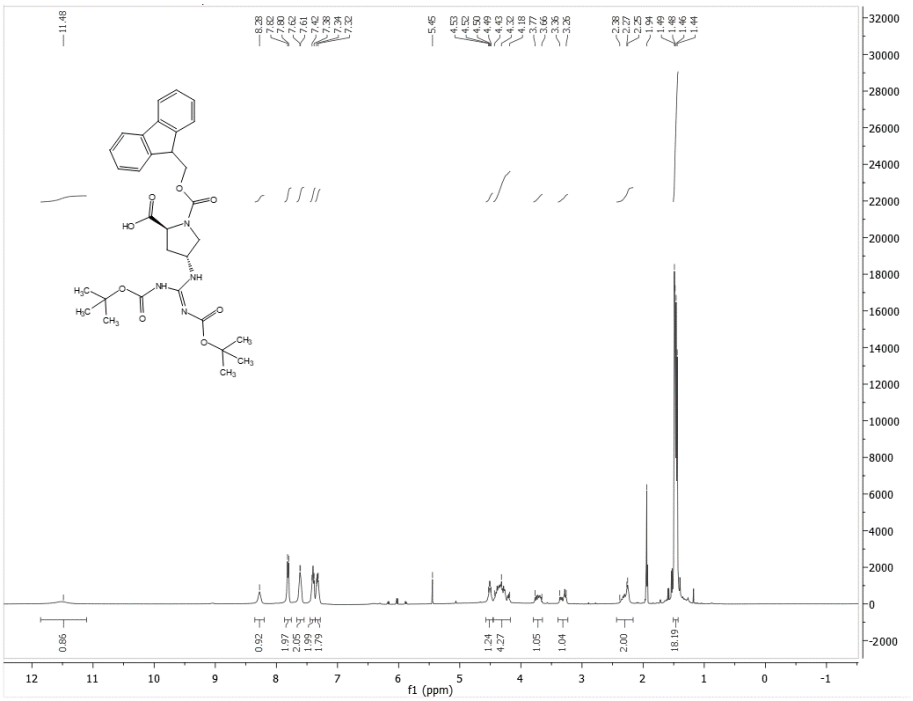

Figure A 15. ^{1}H NMR spectrum for **Fmoc-GAP**. Compound obtained from R. Blade.

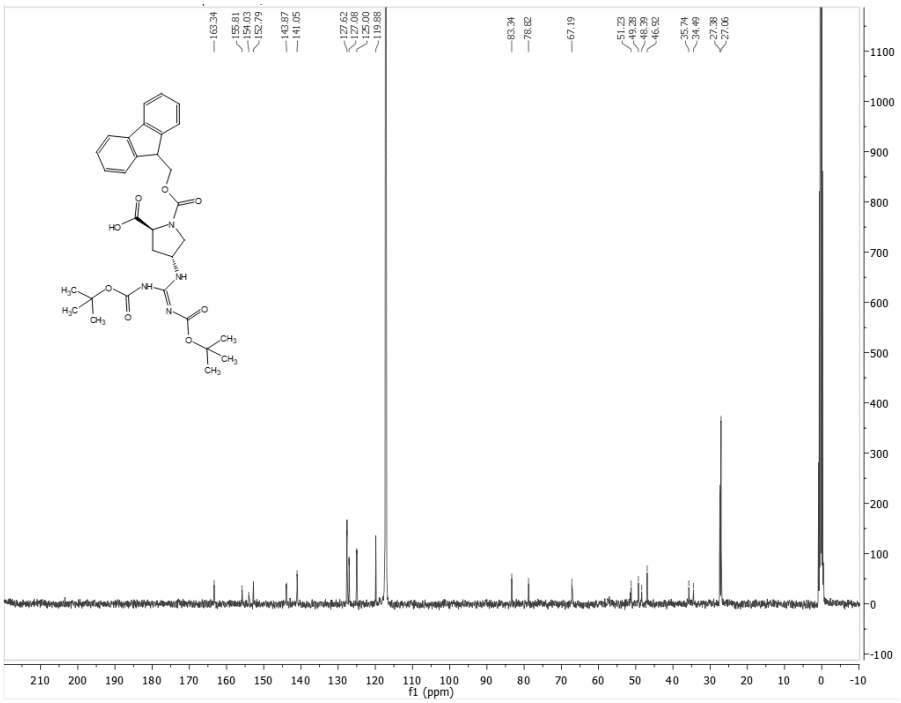

Figure A 16. ^{13}C NMR spectrum for **Fmoc-GAP**. Compound obtained from R. Blade.

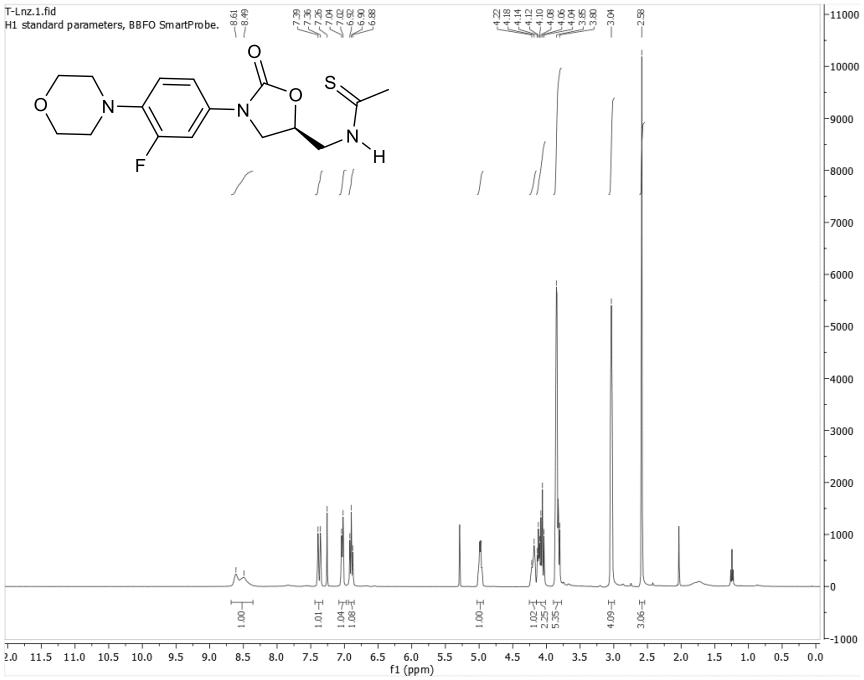

Figure A 17. ^{1}H NMR spectrum for **T-Lnz** as obtained by P. Pitasse Santos.

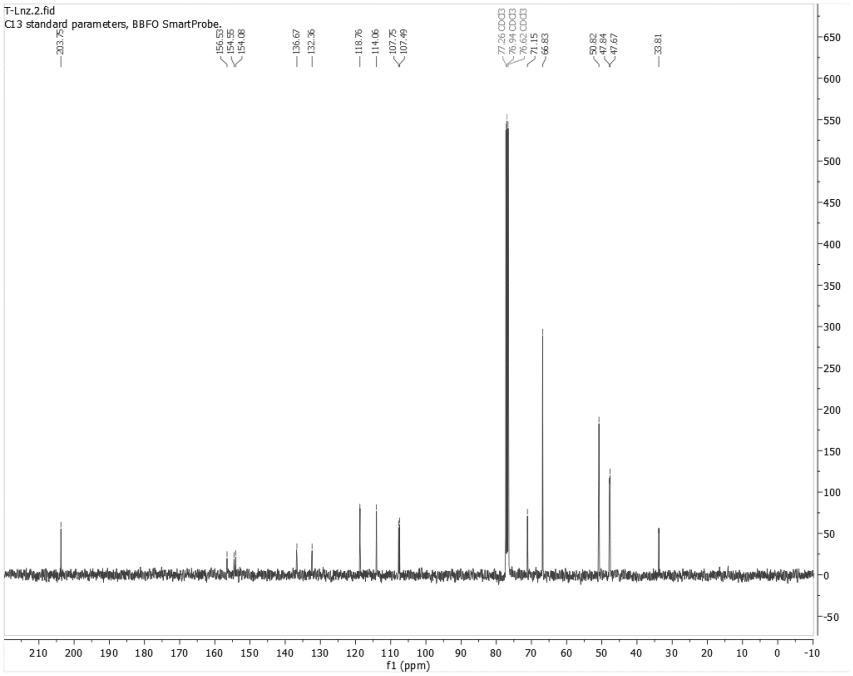

Figure A 18.^{13}C NMR spectrum for **T-Lnz** as obtained by P. Pitasse Santos. Note: in comparison to linezolid, the most significant signal shifts were observed at the amide and its neighboring positions, indicating the thionylation was selective to this group.

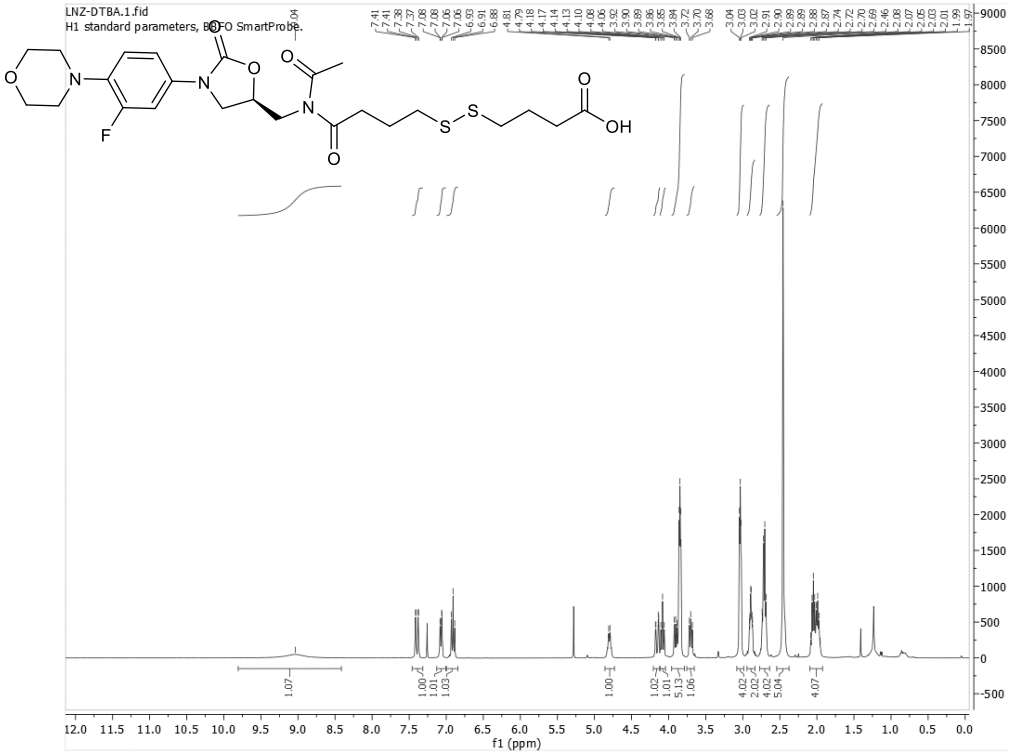

Figure A 19. ^{1}H NMR spectrum for **Lnz-DTBA** as obtained by P. Pitasse Santos.

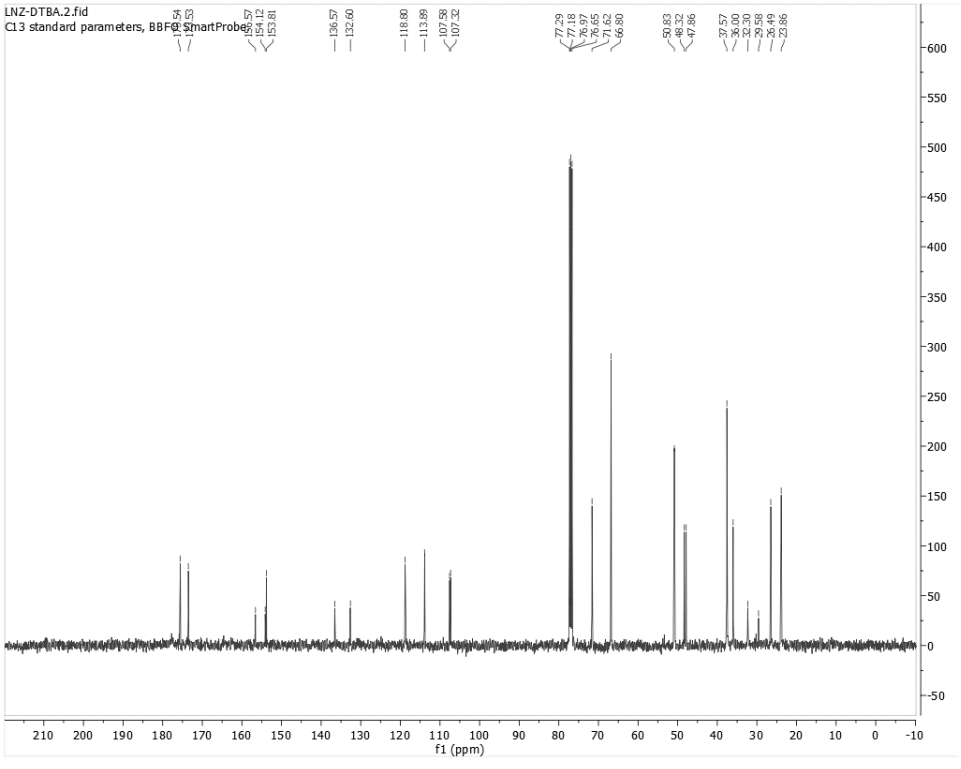

Figure A 20. ^{13}C NMR spectrum for **Lnz-DTBA** as obtained by P. Pitasse Santos.

MALDI-ToF Mass Spectra

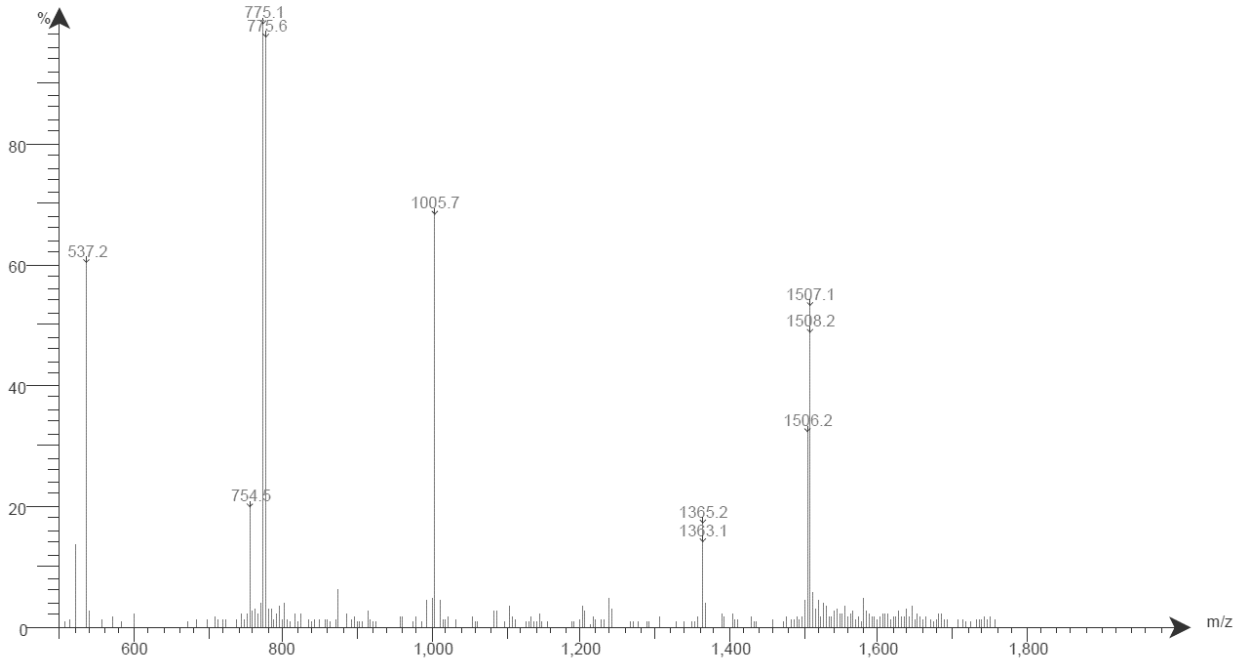

Figure A 21. **Van-SH**, Expected Mass: 1507, Observed Mass: 1507, 1508

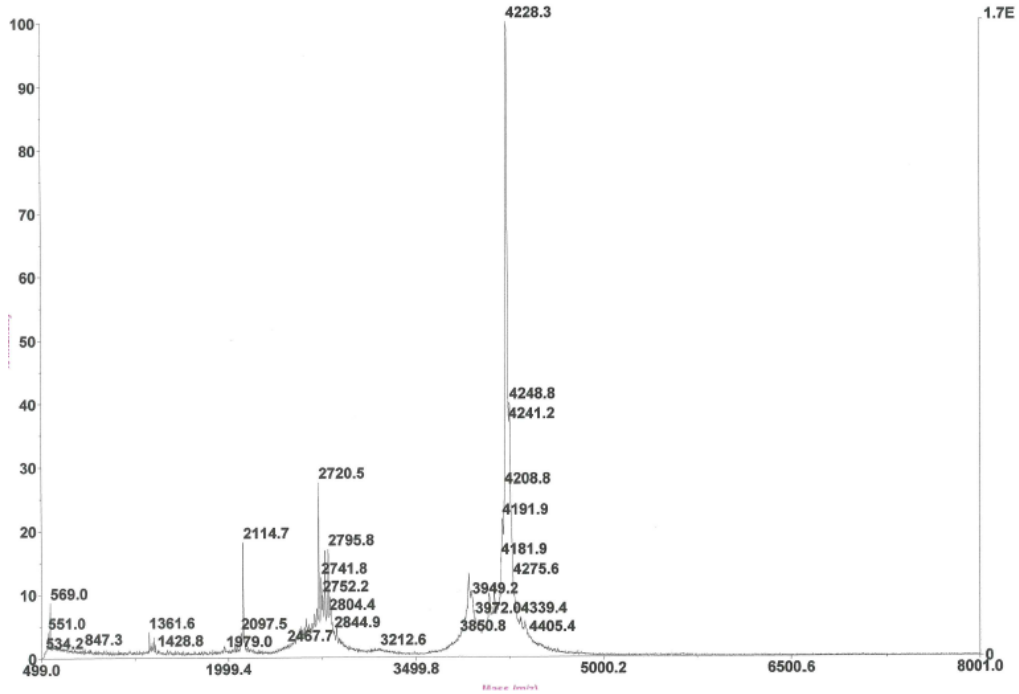

Figure A 22. **VanP14S**, Expected Mass: 4223, Observed Mass: 4228

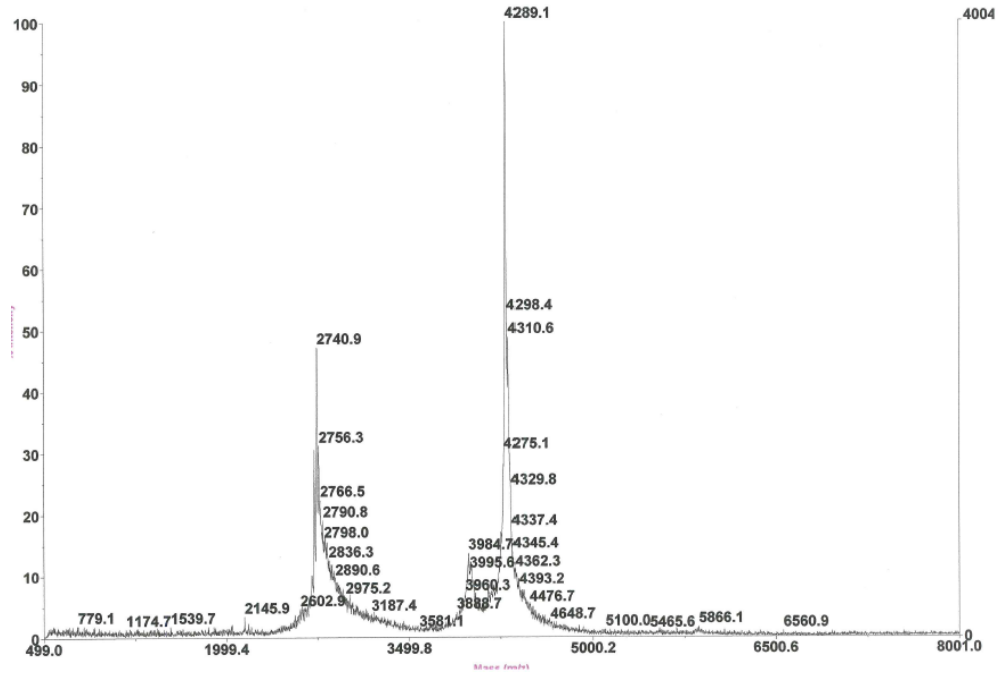

Figure A 23. VanMalP14, Expected Mass: 4286, Observed Mass: 4289

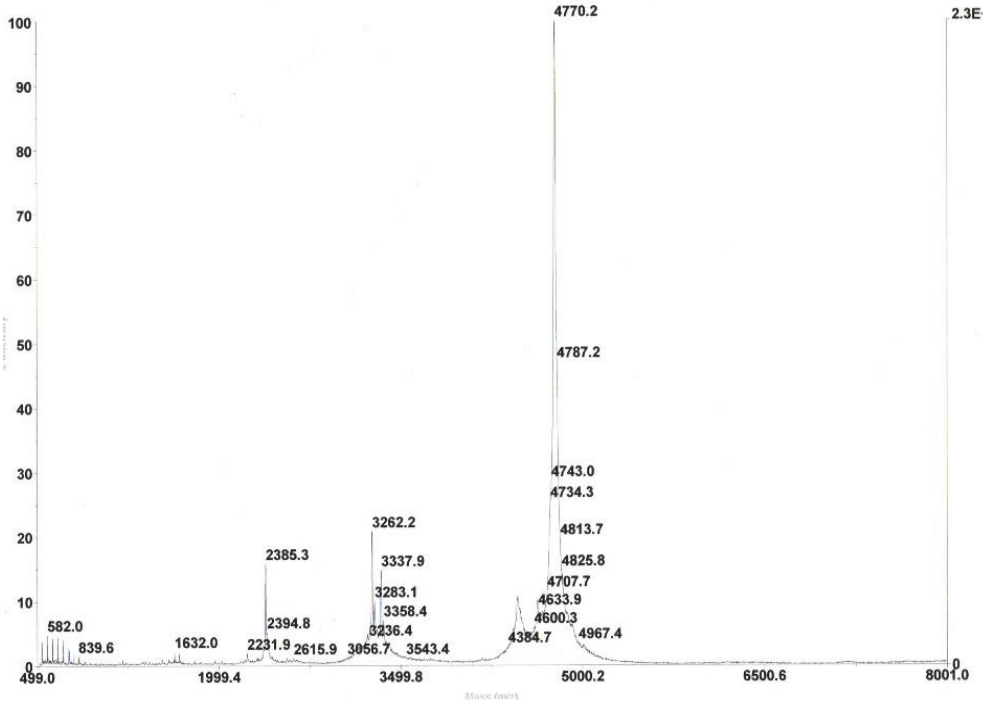

Figure A 24. FlVanP14S, Expected Mass: 4766, Observed Mass: 4770

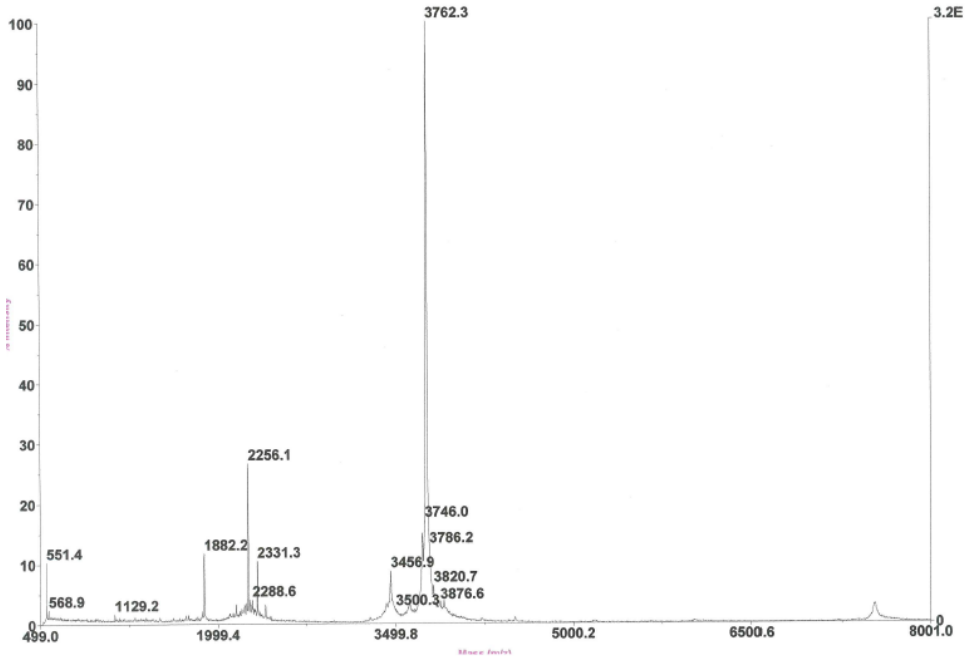

Figure A 25. VanP14GAPS, Expected Mass: 3758, Observed Mass: 3762

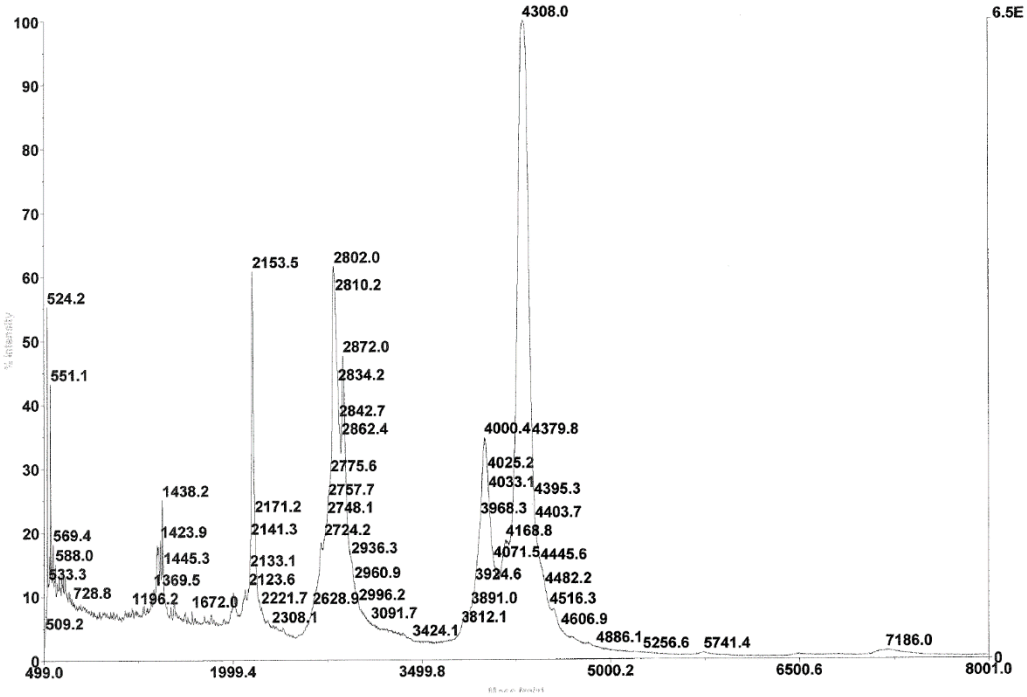

Figure A 26. FlVanP14GAPS, Expected mass: 4306, Observed mass: 4308

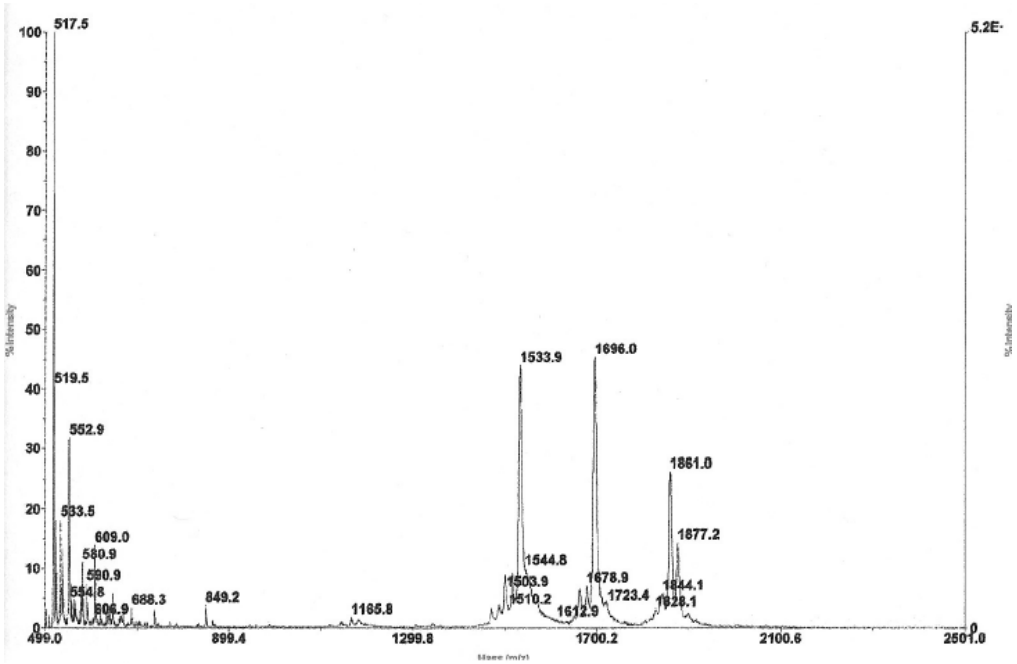

Figure A 27. FITC-Van; Expected masses: $[M+Na]^+$=**1861**, $[M+H]^+$=1839, $[M\text{-}Sugar+H]^+$= **1696**, $[M\text{-}2Sugar+H]^+$= **1533**; Observed masses: 1861, 1696, 1533

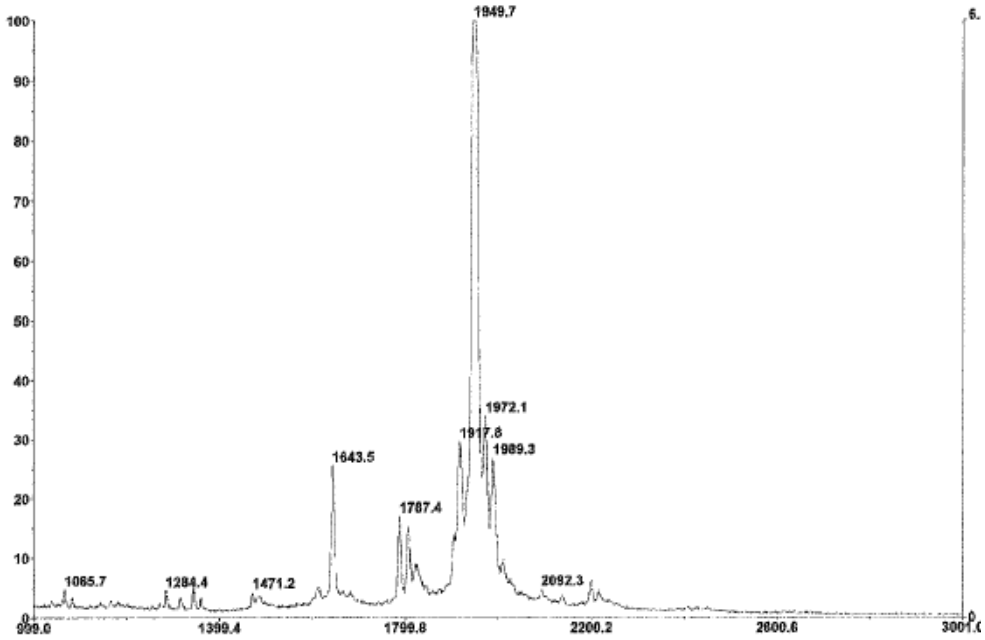

Figure A 28. RITC-Van; Expected masses: $[M+Na]^+$=1972, $[M+H]^+$=**1950**, $[M\text{-}Sugar+H]^+$=1807, $[M\text{-}Sugar\text{-}H2O+H]^+$=**1789**, $[M\text{-}2Sugar+H]^+$= **1645;** Observed masses: 1949, 1787, 1643

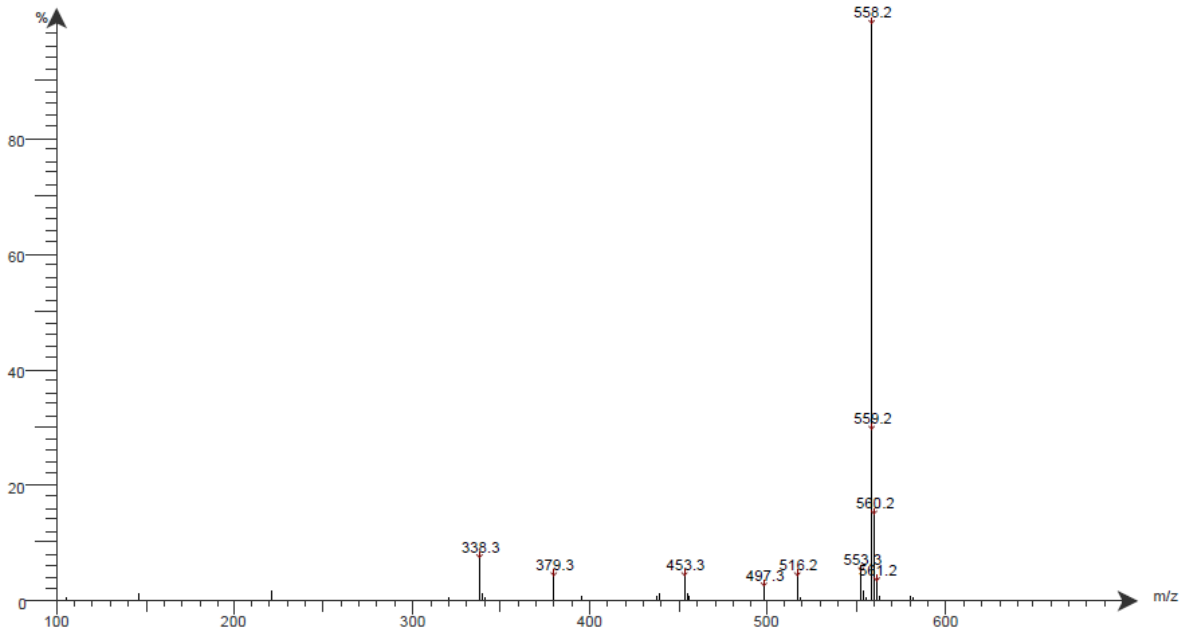

Figure A 29. Expected mass: 558, Observed mass: 558.2. Synthesized by P. Pitasse Santos.

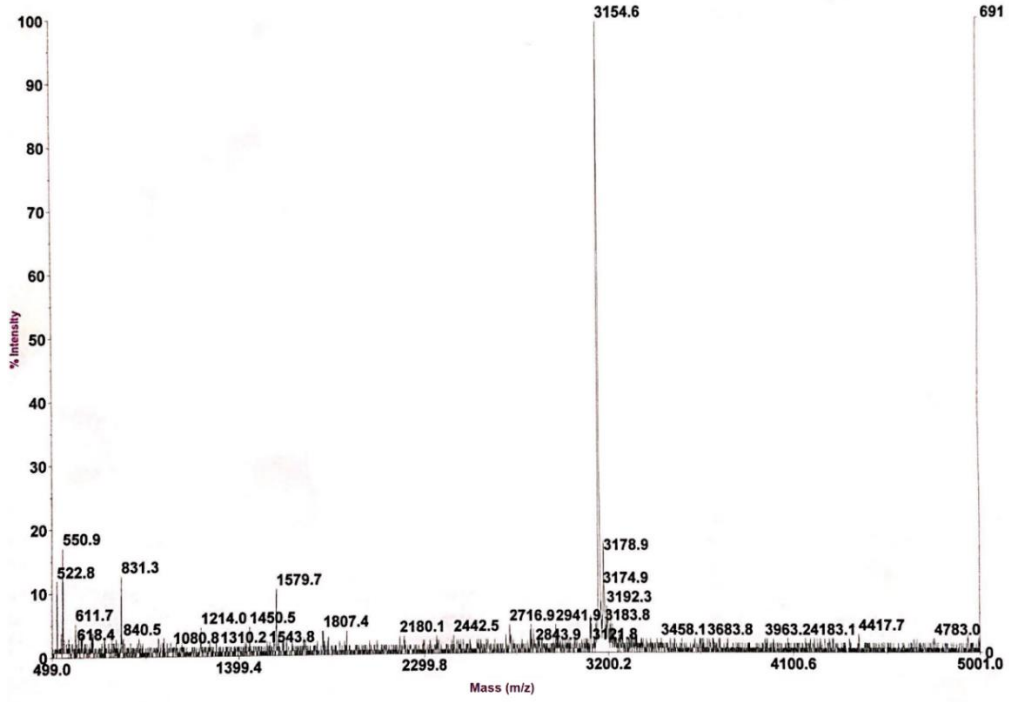

Figure A 30. LnzP14, Expected mass: 3156, Observed mass: 3155. Obtained by P. Pitasse Santos.

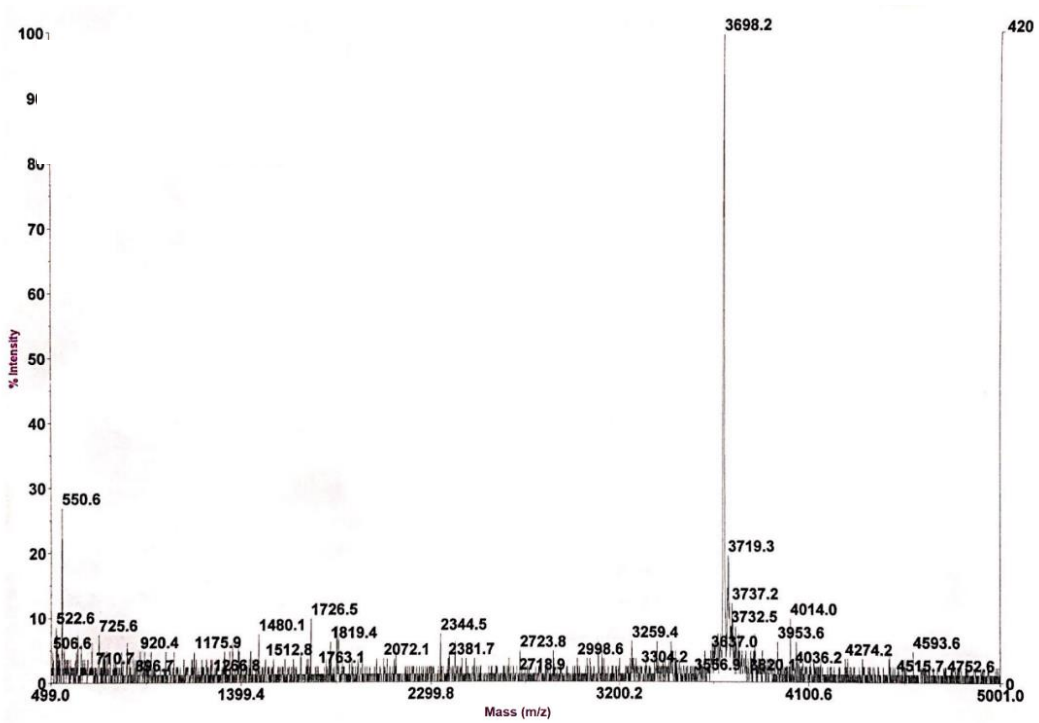

Figure A 31. FlLnzP14, Expected mass: 3700, Observed mass: 3698. Obtained by P. Pitasse Santos.

VITA

Samantha Zeiders was born and raised in Harrisburg, PA. Upon graduation from Susquehanna Township High School in 2011, she attended Lafayette College, a small liberal arts school in Easton, Pennsylvania. In 2015, she obtained her B.S. degree in biochemistry with a minor in mathematics after working on undergraduate research projects spanning the subjects of analytical chemistry, environmental chemistry, biochemistry, and organic chemistry. Her research first began in the lab of Dr. Steven Mylon, whom she worked with for two years including two summer research opportunities on various analytical and environmental chemistry projects. Her passion for organic chemistry was sparked the following summer with Dr. William Miles, with whom she coauthored her first paper. Her last year of undergraduate studies culminated in the laboratory of Dr. Charles Nutaitis with her senior research project to graduate with an honors degree in chemistry.

Following the completion of her degree, Samantha pursued a postbaccalaureate fellowship for one year at the National Institutes of Health in Bethesda, Maryland. She worked in the tuberculosis laboratory of the National Institute of Allergy and Infectious Disease under the supervision of Dr. Clifton Barry.

Ultimately, Samantha joined the chemistry department at Purdue University in August 2016. She will complete her studies in the area of chemical biology and organic chemistry under the direction of Jean Chmielewski and will receive her PhD in chemistry in May 2021. Her post-graduation plans are presently kept open in search of the best opportunity and fit.

PUBLICATION

JOC The Journal of Organic Chemistry

pubs.acs.org/joc Article

Targeting Intracellular Pathogenic Bacteria Through N-Terminal Modification of Cationic Amphiphilic Polyproline Helices

Thomas A. Dietsche, Hassan E. Eldesouky, Samantha M. Zeiders, Mohamed N. Seleem, and Jean Chmielewski*

Cite This: J. Org. Chem. 2020, 85, 7468−7475 Read Online

ACCESS | Metrics & More | Article Recommendations | Supporting Information

ABSTRACT: Intracellular pathogens can thrive within mammalian cells and are inaccessible to many antimicrobial agents. Herein, we present a facile method of enhancing the cell penetrating and antibacterial properties of cationic amphiphilic polyproline helices (CAPHs) with modifications to the hydrophobic moiety at the N-terminus. These altered CAPHs display superior cell penetration within macrophage cells, and in some cases, minimal cytotoxicity. Furthermore, one CAPH, **Pentyl-P14** exhibited excellent antibacterial activity against multiple strains of pathogenic bacteria and promoted the clearance of intracellular *Shigella* within macrophages.

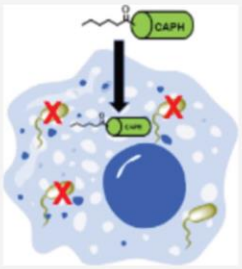

INTRODUCTION

The rise of antimicrobial resistance has created a global health crisis whereby many antibiotics have become ineffective. A number of antibiotic-resistant strains, including the multidrug-resistant *Acinetobacter baumannii* (*A. baumannii*), remain difficult to treat.[1,2] This problem is further compounded by the issue that many bacteria such as *Listeria monocytogenes* (*L. monocytogenes*), *Mycobacterium tuberculosis* (*M. tuberculosis*), and *Shigella flexneri* (*S. flexneri*) can invade mammalian cells.[3,4] Once inside the cell, these bacteria evade host immune responses and many therapeutics that do not accumulate sufficiently within cells.[5,6] To combat this challenge, new antibiotics are needed that can effectively penetrate mammalian cells and eliminate these pathogenic bacteria.

Delivery systems targeting intracellular pathogens have been developed, such as nanoparticles containing antibiotics.[7,8] An alternative approach has been to use cell-penetrating peptides in conjugation with antibiotics and peptide nucleic acids.[9−11] Cell-penetrating peptides with inherent antibacterial properties have also been developed.[12,13] These synthetic peptides were composed of a cationic amphiphilic polyproline helix (CAPH) scaffold and contained both hydrophobic and cationic groups to imbue the molecule with amphiphilicity (Figure 1A). One such CAPH, **P14LRR**, has displayed promising cell penetration, broad-spectrum antibacterial activity, and modest reduction of bacteria within macrophage cells.[14]

In efforts to facilitate greater cell penetration, peptides have previously been modified with various aliphatic fatty acid moieties at the N-terminus to generate lipopeptides. Although these lipopeptides demonstrated an improvement in cell uptake, they suffered from extensive cytotoxicity.[15] While long aliphatic fatty acids may be impractical for potential therapeutics, it is possible that other hydrophobic moieties at the N-terminus could improve the cell penetration of CAPHs, while remaining noncytotoxic. Herein, we present our efforts to develop potent CAPHs with N-terminal hydrophobic modifications that could easily be adapted to other peptides to improve cell penetration and antimicrobial activity, while remaining nontoxic to cells. Furthermore, we demonstrate that these modifications on CAPHs can be utilized to clear intracellular pathogens *in cyto*.

RESULTS AND DISCUSSION

Altering the CAPH hydrophobic face has resulted in enhanced targeting of intracellular bacteria.[16] Therefore, we wished to evaluate the role of N-terminal hydrophobic moieties on cell penetration and antimicrobial activity (Figure 1B). To this end, five different functionalities at the N-terminus of CAPHs were designed: acetyl and pentyl aliphatic groups, and phenyl, naphthyl, and quinolyl aromatic groups (Figure 1B). These functionalities could easily be introduced on the N-terminus of resin-bound peptides. A 4-methyltrityl (Mtt)-protected lysine

Received: April 8, 2020
Published: May 19, 2020

https://dx.doi.org/10.1021/acs.joc.0c00871
J. Org. Chem. 2020, 85, 7468−7475

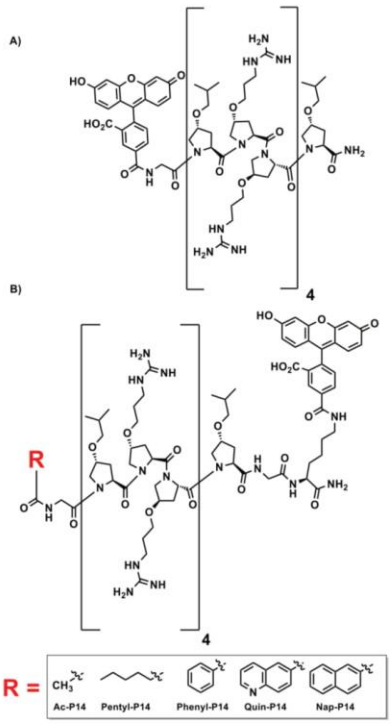

Figure 1. CAPHs. (A) Structure of **P14LRR** and (B) structure of CAPHs modified at the amino terminus with hydrophobic groups.

introduced at the carboxyl terminus of the peptide could be selectively deprotected and labeled with fluorescein for intracellular tracking. A glycine spacer between the (Mtt)-lysine residue was introduced to prevent unfavorable steric interactions with fluorescein.

The proline-modified unnatural amino acid containing the hydrophobic ($\mathbf{P_L}$) functionality was synthesized as previously described.[17] The guanidine-containing cationic $\mathbf{P_R}$ amino acid was synthesized following an improved three-step procedure (Scheme 1, top) as compared to the previously reported synthesis.[17] Briefly, amino acid analogue **2** was prepared by treating Cbz-hydroxyproline **1** with sodium hydride, followed by acrylonitrile. The Cbz protecting group of **2** was removed through hydrogenation and replaced with an Fmoc protecting group to provide analogue **3**. Finally, reduction of the nitrile group of **3**, followed by addition of *N*,*N*′-bis-Boc-1-guanylpyrazole yielded $\mathbf{P_R}$. This new synthetic strategy doubles the overall yield of the final product from 25 to 50% compared to the previously reported synthesis.[17]

The CAPH peptides were synthesized on a Rink amide resin using the standard Fmoc-based solid-phase peptide synthesis (SPPS) (Scheme 1, bottom). Following successful coupling at the N-terminus with the hydrophobic modifications, the (Mtt)-lysine was deprotected with hexafluoro-2-propanol (HFIP), and the resulting free amine was reacted with *N*-hydroxysuccinimide fluorescein. The peptides were cleaved from resin with concomitant side chain deprotection using a trifluoroacetic acid (TFA) cocktail. All peptides were purified to homogeneity by reverse-phase high-performance liquid chromatography (RP-HPLC) and characterized by matrix-assisted laser desorption ionization (MALDI) mass spectrometry.

Circular dichroism (CD) was used to evaluate the conformation of the newly synthesized CAPHs as it has previously been reported that modifications to polyproline type II (PPII) helices can affect conformational stability.[18] All CAPHs displayed a positive ellipticity at 225 nm that is

Scheme 1. Synthesis of $\mathbf{P_R}$ (Top) and On-Resin Coupling of Hydrophobic Functionalities on the N-Terminus of CAPH Peptides (Bottom)[a]

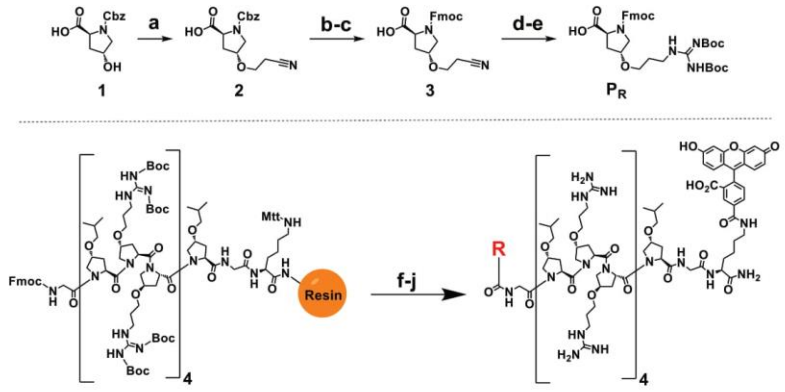

[a](a) Acrylonitrile, NaH, THF, 16 h, 80%. (b) H_2, Pd/C, MeOH. (c) Fmoc-OSu, $NaHCO_3$, acetone/H_2O, quant. (d) H_2, PtO_2, AcOH, MeOH, (e) *N*,*N*′-bis-Boc-1-guanylpyrazole, TEA, DCM, 62%, (f) piperidine (25% in DMF), 25 min. (g) R-CO_2H, DIEA, HATU, 3 h. (h) HFIP (30% in DCM), 2 × 30 min. (i) NHS-fluorescein, DIEA, DMF, 16 h. (j) 95% TFA, 2.5% TIPS, 2.5% H_2O, 2 h.

https://dx.doi.org/10.1021/acs.joc.0c00871
J. Org. Chem. 2020, 85, 7468−7475

characteristic of the PPII[19] (Figure S2), as was observed with the previous CAPHs.[17] These data support that the N-terminal modifications did not affect the secondary structure of the polyproline helix within CAPHs.

As many therapeutics suffer from the inability to effectively rescue mammalian cells from intracellular pathogens, it is imperative that antibacterial agents transverse the mammalian cell membrane. Thus, the N-terminal CAPHs were assessed for their ability to accumulate within J774A.1 macrophage cells using flow cytometry. Cells were incubated with each CAPH derivative, and the cellular fluorescence was measured in the presence of trypan blue (TB) to quench extracellular fluorescence that may be caused by a membrane-bound peptide.[20] Overall, the installation of various hydrophobic groups at the N-terminus drastically improved the ability of CAPHs to penetrate macrophage cells in comparison to **P14LRR** and the control peptide **Ac-P14** (Figure 2). Minor

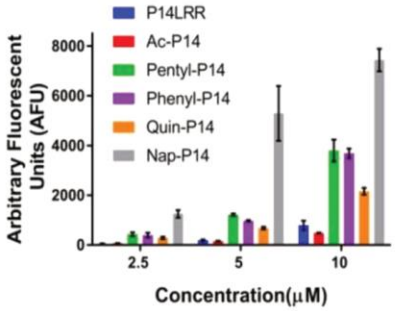

Figure 2. Cellular uptake of N-terminal CAPHs in J774A.1 macrophage cells. Cellular fluorescence was measured by flow cytometry after 1 h incubation with peptides. TB was used to quench fluorescence of membrane-bound peptides.

levels of membrane binding were observed for **Pentyl-P14**, **Phenyl-P14**, **Ac-P14**, and **Nap-P14**, as the decrease in cellular fluorescence with added TB was only 5−15% overall. In comparison, **Quin-P14** exhibited less-efficient cell penetration, as there was a decrease of up to 35% in cellular fluorescence when TB was added. At a concentration of 10 μM, **Phenyl-P14** and **Pentyl-P14** displayed about a fivefold increase in cell uptake compared to **P14LRR**, while **Quin-P14** displayed a more modest threefold increase. **Nap-P14** yielded the highest improvement compared to **P14LRR**, showing about an 11-fold higher cell uptake. Interestingly, **Nap-P14** displays almost four times the cell accumulation as **Quin-P14**, despite only differing by one nitrogen atom. Moreover, the CAPH derivative with the medium aliphatic chain, **Pentyl-P14**, was approximately eight times more efficient at cell penetration than **Ac-P14**, demonstrating that the length of the hydrophobic tail is crucial for cell penetration. These trends were consistent even at concentrations as low as 2.5 μM. Together, these results show that the N-terminal hydrophobic moiety can greatly impact the ability of CAPHs to penetrate mammalian cells.

Intracellular pathogens can take refuge in different subcellular locations such as vacuoles (*Mycobacterium*) and the cytosol (*L. monocytogenes* and *S. flexneri*), making treatment difficult. We had previously shown that altering the hydrophobic moieties on the backbone of CAPHs resulted in enhanced targeting of intracellular pathogens.[16] Similarly, we wished to investigate if the N-terminal modifications on CAPHs could affect their ability to localize to specific subcellular compartments. To this end, the subcellular localization of the N-terminal CAPHs was visualized via confocal microscopy. J774A.1 cells were incubated with CAPHs over a range of concentrations (2.5, 5, and 10 μM), and the cells were further treated with a Hoechst stain, Lysotracker, or Mitotracker to visualize the nucleus, endosomes, or mitochondria, respectively. At 5 μM, all CAPHs were found to localize primarily to the mitochondria with some cytosolic localization (Figure 3), whereas **Quin-P14** and **Nap-P14** also displayed nuclear localization in some cells (Figure S8). Interestingly, we observed concentration differences in the subcellular locations of these peptides. In all cases, with the exception of **Nap-14**, there was a threshold concentration at which the peptides switched from endosomal to mitochondrial localization; at 2.5 μM **Pentyl-P14**, **Phenyl-P14**, and **Quin-P14** were observed in both compartments, and for **Ac-P14**, this concentration was 5 μM (Figure S8). Below this concentration, the peptides were endosomal, and above this concentration, the peptides were localized to the mitochondria. This concentration dependence on subcellular location has been observed previously with **P14LRR**.[21] At all of the concentrations evaluated, Nap-P14 was found colocalized with Lysotracker and Mitotracker (Figure S8). These data demonstrate that the hydrophobic moieties at the N-terminus can direct CAPHs to the mitochondria and endosomes, with some cytosolic localization, and by fine-tuning the hydro-

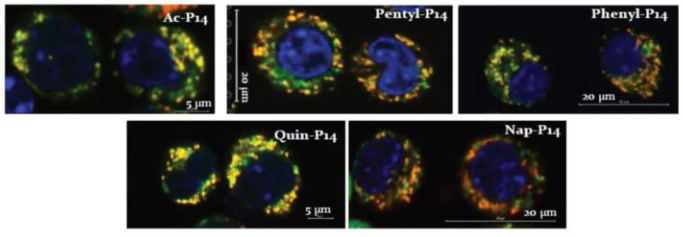

Figure 3. Subcellular localization of N-terminal CAPHs (green) in J774A.1 macrophage cells. Cells were treated with peptides (5 μM) (green) for 1 h. Following the incubation, cells were stained with Mitotracker (red) and Hoechst 3342 (blue) to visualize the mitochondria and nuclei, respectively. Cells were visualized by confocal microscopy, and the images show the overlay of the green, red, and blue channels for the treated cells.

https://dx.doi.org/10.1021/acs.joc.0c00871
J. Org. Chem. 2020, 85, 7468−7475

phobic group (bis-aromatic), CAPHs are found to localize in the nucleus as well.

To rescue macrophage cells from intracellular pathogens, mammalian cells must maintain their viability in the presence of antibiotic therapies. Thus, to ensure that the N-terminal modifications did not reduce cell viability below a reasonable level, CAPHs were screened against J774A.1 macrophage cells using the 3-(4,5-dimethylthiazol-2-yl)-2,5-diphenyltetrazolium bromide (MTT) assay at 10 μM for 9 h (Figure S3).[22] As mentioned earlier, long fatty acid N-terminal modifications have been shown to greatly improve cell penetration, but were toxic.[15] In contrast, four out of five of the N-terminally modified CAPHs displayed acceptable cell viability. **Ac-P14** and **P14LRR** displayed minimal toxicity in macrophage cells, whereas **Phenyl-P14**, **Pentyl-P14**, and **Quin-P14** showed acceptable cell viability (75−90%). **Nap-P14** displayed the lowest cell viability (60%), despite its improvement on cell penetration. From the cell uptake and cell viability data, it was determined that **Pentyl-P14** and **Phenyl-P14** satisfied two main requirements for application against intracellular pathogens: (1) efficient cell penetration and (2) limited toxicity in J774A.1 macrophage cells.

After determining that the N-terminal CAPHs boosted cell penetration, we investigated the antibacterial activity against a selection of Gram-positive and Gram-negative pathogens. An *in vitro* broth dilution assay was used to screen the potency of the CAPH derivatives against the intracellular bacteria *M. tuberculosis*, *L. monocytogenes*, and *S. flexneri*, *Escherichia Coli*, and the multidrug resistant *A. baumannii*.[11,23−25] **Quin-P14** was excluded because of the less-effective cell penetration, and **Nap-P14** was deemed to be too cytotoxic to continue forward. **Pentyl-P14** showed superior activity as compared to **Ac-P14** (Table 1), with two-fold increased potency against *M. tuberculosis*, *A. baumannii*, and *L. monocytogenes*, and four-fold enhanced potency against *E. coli* and *S. flexneri*. **Phenyl-P14** showed slightly lower activity against the before-mentioned pathogens as compared to **Pentyl-P14**. Although fluorophores were included within these peptides, we have previously shown that they play a minimal role in the antibiotic potency of CAPHs.[13]

Table 1. In Vitro Antibacterial Activity of CAPHs against Pathogenic Bacteria-MIC (μM)

	L. monocytogenes	*S. flexneri*	*M. tuberculosis*	*A. baumannii*	*E. coli*
P14LRR	8	8	16	16	4
Ac-P14	>16	16	16	16	8
Pentyl-P14	8	4	8	8	2
Phenyl-P14	16	8	16	8	4

A β-galactosidase release assay in *E. coli* was used to determine if the peptides acted through a cell lysis mechanism (Figure 4A). At 2× the minimum inhibitory concentration (MIC) values, **P14LRR** and **Pentyl-P14** showed minimal bacterial cell lysis, whereas the positive control mellitin displayed significant levels of lysis. **Ac-P14** and **Phenyl-P14** showed somewhat higher levels of lysis. At 4× the MIC values, the N-terminally modified CAPHs demonstrated lysis (Figure S4). This suggests that at higher peptide concentrations, membrane lysis could play a role in antibacterial activity.[26] However, there was no observed hemolysis with human red blood cells (hRBCs) up to 40 μM (Figure 4B), signifying that CAPHs may selectively lyse the bacterial membrane at higher concentrations, while leaving hRBCs intact.

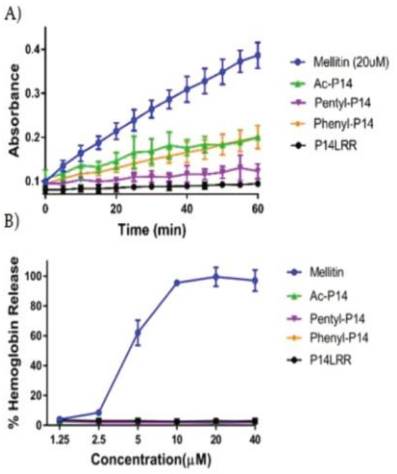

Figure 4. Investigating the mode of antimicrobial action of N-terminally modified CAPHs. (A) Leakage of β-galactosidase from *E. coli* after 1 h with CAPHs at 2× the MIC values. (B) Hemolysis of hRBCs when treated with CAPHs for 1 h.

With the confirmation that the N-terminally modified CAPHs possess both antibacterial activity and mammalian cell penetration, we probed clearance of the intracellular pathogen *S. flexneri* within J774A.1 macrophage cells.[27] **Pentyl-P14** was selected for this assay, as it exhibited the best combination of cell uptake, cell viability, and antimicrobial activity. **Ac-P14** was also evaluated, although it exhibited much lower cellular uptake and antibacterial activity. **Pentyl-P14** was found to clear ∼75% of *S. flexneri* within macrophage cells after 12 h, whereas **Ac-P14** exhibited a modest reduction (∼40%) of intracellular *S. flexneri* (Figure 5). These clearance results are likely due to a combination of several factors, including efficiency of cell penetration, antimicrobial activity, and

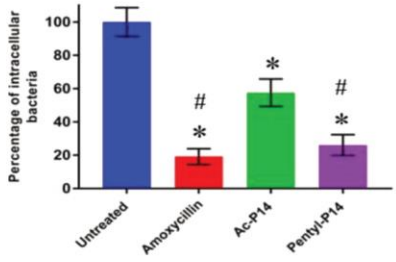

Figure 5. Intracellular bacterial clearance activity of **Pentyl-P14** and **Ac-P14** (10 μM) against *S. flexneri* in J774A.1 murine macrophage cells after 12 h. (*) denotes the statistical difference between the tested groups and the untreated control. (#) indicates a statistical significance with respect to **Ac-P14**. *#*P* values of <0.05 are considered significant.

https://dx.doi.org/10.1021/acs.joc.0c00871
J. Org. Chem. 2020, 85, 7468−7475

subcellular location. **Pentyl-P14** and **Ac-P14** were shown to localize mainly to the mitochondria with some cytosolic localization at 10 μM. Previous studies of CAPHs have shown a direct transport mechanism into the cytosol, followed by migration to the mitochondria.[28] While in the cytosol, **Pentyl-P14** is likely to interact with and eradicate *S. flexneri*, a cytoplasm-residing pathogen. Furthermore, **Pentyl-P14** possesses superior cell penetration and antibacterial activity against *S. flexneri* when compared to **Ac-P14**. Therefore, it stands to reason that **Pentyl-P14** would be more effective in clearing intracellular *S. flexneri*.

To further investigate if the pentyl moiety was an optimal N-terminal modification, four additional aliphatic modifications of CAPHs were synthesized containing C4−C7 tails: **Butyl-P14**, **Branched-P14**, **Hexyl-P14**, and **Heptyl-P14** (Figure 6).

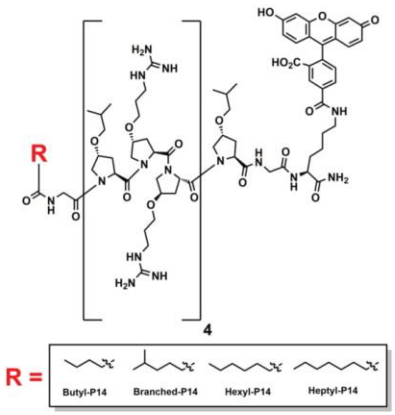

Figure 6. Structure of CAPHs modified at the amino terminus with additional aliphatic groups.

These CAPHs were assessed for their ability to penetrate mammalian cells via flow cytometry (Figure S6). At a concentration of 10 μM, **Butyl-P14** was about 10% less efficient at cell penetration as compared to **Pentyl-P14**. Conversely, **Branched-P14**, **Hexyl-P14**, and **Heptyl-P14** displayed increased cell accumulation at 10 μM as compared to **Pentyl-P14** (about four, two, and ninefold, respectively).

Unfortunately, the CAPHs that displayed superior cellular uptake as compared to **Pentyl-P14** also suffered from drastically reduced cell viability. **Branched-P14**, **Hexyl-P14**, and **Heptyl-P14** showed significant levels of toxicity, with cell viability ranging from 4 to 43% (Figure S7). The observation that longer N-terminal aliphatic chains result in severe cell toxicity is consistent with previous lipopeptide reports.[15] These data support the premise that the N-terminal pentyl modification represents the best compromise between cell accumulation and viability, as shorter aliphatic chains (**Ac-P14** and **Butyl-P14**) were not as efficacious in cell penetration. Conversely, longer aliphatic modifications (**Branched-P14**, **Hexyl-P14**, and **Heptyl-P14**) possessed greater cell penetration but were much more cytotoxic. Therefore, **Pentyl-P14** was deemed to be the most effective peptide, as it had excellent mammalian cell penetration while remaining noncytotoxic. We have previously observed an increase in cell toxicity with longer C6-aliphatic groups within the side chain functionalities of CAPHs.[16] Interestingly, this is also observed here with a single modification at the amino terminus.

■ CONCLUSIONS

In conclusion, combating intracellular bacteria remains a difficult challenge in the context of developing new therapeutics.[1−5] Functionalizing CAPHs with hydrophobic moieties at the N-terminus improved cell uptake and, in some cases, antibacterial activity. These N-terminal modifications are installed in a facile manner on a resin, making them easily adaptable to other peptides to improve their cell penetration or activity against intracellular pathogenic bacteria. By altering CAPHs to bear the five-carbon aliphatic chain, we found that **Pentyl-P14** was effective at clearing the intracellular pathogen *S. flexneri*. Therefore, **Pentyl-P14** is an excellent candidate to further the overarching goal of designing new therapeutics to target difficult-to-treat bacteria that reside within mammalian cells.

■ EXPERIMENTAL SECTION

Materials and Methods. Unless otherwise stated, common chemicals and solvents including Fmoc-protected amino acids, resins, carboxylic acids, and coupling reagents for SPPS were purchased from commercial sources and used without further purification. Compound **2** was purchased from Chem-Impex International. H-Rink Chem Matrix Rink amide resin (0.46 mmol/g) was purchased from Pcas Biomatrix Inc. Sterile media [Dulbecco's modified Eagle medium (DMEM) L-glutamine, fetal bovine serum (FBS), and penicillin−streptomycin], fluorescent dyes (NHS-fluorescein, Mitotracker, Lysotracker, and Hoechst), and buffers [phosphate buffered saline (PBS)] used in cell culture were purchased from commercial sources. Melittin and amoxycillin were purchased from Sigma-Aldrich.

Synthesis of Compound 2. The synthesis of **2** proceeded as previously reported,[17] with the following minor modifications. To a solution of NaH (1.58 g, 65.9 mmol) in tetrahydrofuran (THF, 150 mL) with 4 Å mol sieves at 0 °C and under N_2 atmosphere was added an ice-cooled solution of **1** (5.0 g, 18.8 mmol) in THF (50 mL). The mixture was stirred at 0 °C for 1 h. To this mixture was added acrylonitrile (5.0 mL, 93.4 mmol), and the reaction was allowed to warm to room temperature and stirred for 24 h. The reaction mixture was cooled to 0 °C, and water (100 mL) was added to quench the excess NaH. The THF was removed *in vacuo*, and HCl (10%) was added to bring the solution to a pH of 1. The resulting solution was extracted with EtOAc (3×), the organic layers were dried over anhydrous $MgSO_4$, and the solvent was removed *in vacuo*. The desired product was purified by silica gel column chromatography [95% dichloromethane (DCM), 4% MeOH, 1% AcOH] to provide **2** as a colorless oil in 80% yield. Characterization of **2** was previously reported.[17]

Synthesis of Compound 3. To a solution of **2** (600 mg, 1.9 mmol) in 20 mL of ethanol was added 10% Pd/C (60 mg). The solution was stirred under 1 atm of hydrogen for 3 h. The solution was gravity filtered through filter paper, the solvent was removed *in vacuo*, and the resulting material was used in the next step without further purification. The material from the previous step was dissolved in deionized water (10 mL), the solution was cooled to 0 °C, and sodium bicarbonate (475 mg, 5.7 mmol) was added. To this cooled mixture, a solution of Fmoc-OSu (699 mg, 2.1 mmol) in 10 mL of acetone was added dropwise, and the resulting slurry was allowed to warm to room temperature and stirred overnight. The reaction mixture was treated with 10% HCl to a pH of 1 and extracted with EtOAc (3×). The organic layers were dried over anhydrous Na_2SO_4, and the solvent was removed *in vacuo*. The desired product was purified by silica gel column chromatography (96% DCM, 3% MeOH, 1% AcOH) to provide **3** as a white solid in quantitative yield. ^{1}H NMR (400 MHz, $CDCl_3$): δ10.14 (br s, 1H), 7.73 (dd, J = 24 Hz, 8

https://dx.doi.org/10.1021/acs.joc.0c00871
J. Org. Chem. 2020, 85, 7468−7475

Hz, 2H), 7.55 (m, 2H), 7.34 (m, 4H), 4.40−4.51 (m, 3H), 4.24−4.36 (m, 1H), 4.13 (m, 1H), 3.51−3.75 (m, 4H), 2.55 (q, J = 8 Hz, 2H), 2.33−2.48 (m, 1H), 2.11−2.26 (m, 1H). ^{13}C NMR (100 MHz, $CDCl_3$): δ 177.2*, 175.6, 155.7, 154.5*, 143.6, 141.2, 129.0, 127.7, 127.0, 124.9, 119.9, 117.4, 67.9, 63.7, 57.9, 57.2*, 51.4, 47.0, 36.6*, 34.7, 19.0 (*indicates minor rotamer). HRMS (APCI): calcd for $C_{23}H_{22}N_2O_5$ [M + H$^+$], 407.1601 m/z; found, 407.1598.

Synthesis of P_R.[17] To a solution of **3** (700 mg, 1.7 mmol) in 20 mL of MeOH was added 1 mL of AcOH, followed by PtO_2 (70 mg). The solution was stirred under 1 atm of hydrogen overnight. The solution was filtered through celite, the solvent was removed *in vacuo*, and toluene was used to remove excess AcOH. The resulting material was used in the next step without further purification. The material from the previous step was dissolved in 15 mL DCM and cooled to 0 °C. To this cooled mixture, a solution of triethylamine (0.720 mL, 5.2 mmol) in 5 mL DCM was added dropwise, followed by *N*,*N*′-bis-Boc-1-guanylpyrazole (695 mg, 2.2 mmol). The resulting slurry was allowed to warm to room temperature and stirred overnight. The reaction was extracted with DCM (3×), the organic layers were dried over anhydrous Na_2SO_4, and the solvent was removed *in vacuo*. The desired product was purified by silica gel column chromatography (96% DCM, 3% MeOH, 1% AcOH) to provide $\mathbf{P_R}$ as a white solid in 62% yield. Characterization of $\mathbf{P_R}$ was previously reported.[17]

Peptide Synthesis. H-Rink Chem Matrix Rink amide resin (200 mg, 0.46 mmol/g, 100−200 mesh) was added to a 10 mL peptide synthesis flask and washed with DMF, CH_2Cl_2, MeOH, and CH_2Cl_2 (7 mL, 2× each). The resin was swelled by adding DMF (7 mL) to the flask, and the flask was agitating for 30 min. After 30 min, the DMF was drained, and the resin was washed with DMF, CH_2Cl_2, MeOH, and CH_2Cl_2 (7 mL, 2× each). Following this wash, Fmoc-protected amino acids [(Fmoc-P_R (2 equiv), Fmoc-P_L (2 equiv), Fmoc-Lys-Mtt (4 equiv), or Fmoc-gly (4 equiv)] were dissolved in 7 mL of DMF, and HATU (2 or 4 equiv) and DIEA (4 or 8 equiv) were added. This amino acid solution was added to the peptide flask and agitated for 3 h at room temperature. After 3 h, the solution was drained, and the resin was washed with DMF, CH_2Cl_2, MeOH, and CH_2Cl_2 (7 mL, 2× each). To deprotect the amino acid, a piperidine (7 mL, 25% in DMF) solution was added to the flask and agitated for 25 min. The piperidine solution was drained and washed with DMF, CH_2Cl_2, MeOH, and CH_2Cl_2 (7 mL, 2× each). This procedure was repeated for each sequential amino acid in the peptide sequence. The Fmoc-protecting group of the final amino acid was deprotected with piperidine (7 mL, 25% in DMF). The N-terminus of CAPHs was functionalized by adding a DMF (7 mL) solution of carboxylic acid [featuring one of the hydrophobic groups (4 equiv)], HATU (4 equiv), and DIEA (8 equiv) to the peptide flask and agitating for 3 h. Successful amino acid couplings/deprotections were monitored via Kaiser (1° amino acid) or Chloranil (2° amino acid) tests.[29,30]

Deprotection of MTT Side Chain, Coupling of Fluorescein. Following coupling of the hydrophobic group to the N-terminus, the above resin was washed with CH_2Cl_2, MeOH, and CH_2Cl_2 (7 mL, 2× each). For each N-terminus hydrophobic modification, an aliquot of resin (∼50 mg) was transferred to a separate 10 mL synthesis flask. The resin was treated with HFIP (7 mL, 30% in DCM) and agitated for 30 min. This procedure was repeated twice, and the resin was washed with CH_2Cl_2, MeOH, and CH_2Cl_2 (7 mL, 2× each) after each HFIP wash. Successful Mtt deprotection was monitored by the Kaiser test. The resin was washed with DMF, CH_2Cl_2, MeOH, and CH_2Cl_2 (7 mL, 2× each), and N-hydroxysuccinimide fluorescein (1.2 equiv) and DIEA (2.4 equiv) in DMF (7 mL) was allowed to react with the resin for 16 h in the dark. The resin was then washed with CH_2Cl_2, MeOH, and CH_2Cl_2 (7 mL, 2× each).

Cleavage and Purification of Peptides. A fresh TFA cocktail solution of 10 mL (95% TFA, 2.5% TIPS, 2.5% H_2O) was prepared and was added to the resin and agitated for 2 h. After 2 h, the solution was drained into a 50 mL centrifuge tube. The resin was subsequently washed with the TFA cocktail (10 mL, 2×) and CH_2Cl_2 (10 mL, 2×), and all the filtrate was collected. TFA was removed *in vacuo*, and the peptide was precipitated with ice-cold diethyl ether (15 mL) overnight at −79 °C. The filtrate was centrifuged (3500 RPM, 15 min) and dried. The peptide was purified to homogeneity (>95% pure, Figure S1) using RP-HPLC using a gradient of 25−80% of CH_3CN (0.1% TFA) in water (0.1% TFA). The gradient was run for 60 min using a Luna C18 semi-prep column, using a flow rate of 10.0 mL/min and monitored with a UV detector at 214 and 254 nm. The mass of the peptides was confirmed via MALDI-time of flight (MALDI-TOF) mass spectrometry, and the concentration of aqueous stock solutions of peptides were confirmed using UV−visible spectroscopy at a wavelength of 518 nm.

Circular Dichroism. Data were recorded on a Jasco CD spectropolarimeter (Model J-1500) at 25 °C using a 1 mm path length quartz cell. The spectra were averaged over three scans taken from 260 to 190 nm, with a data pitch and bandwidth of 1 nm, at a scan rate of 20 nm/min. All peptides were analyzed at 50 μM concentration in 20 mM phosphate buffer (pH 7.2). The spectra were background-subtracted and processed from degrees of rotation to mean residue ellipticity by dividing by the appropriate path length, peptide concentration, and number of residues in the peptide.

Cell Uptake. J774A.1 cells were cultured in DMEM supplemented with 10% FBS, and 1% penicillin/streptomycin at 37 °C under 5% CO_2 atmosphere. J774A.1 cells (125,000) were harvested and transferred to round-bottom tubes (BD Biosciences) and allowed to adhere overnight. The next day, these cells were treated with CAPHs (2.5−10 μM) in 10% FBS-supplemented DMEM (300 μL) and were incubated for 1 h at 37 °C. Cells with no CAPHs treatment (DMEM supplemented with 10% FBS only) served as a control for the experiment. Upon completion of the 1 h incubation period, the cells were centrifuged (1100 rpm, 7 min @ 4 °C), and the spent media was aspirated. The cells were resuspended in TB (400 μL, 1 mg/mL in PBS), and the fluorescence of the cells was measured using a FACSCalibur Flow Cytometer (BD Biosciences) equipped with a 488 nm argon laser. Emissions for fluorescein-labeled peptides were collected in the FL 1 channel. Data were obtained in duplicate from three independent experiments and processed using the BD software.

Cell Toxicity. The viability of J774A.1 cells with CAPHs peptides was determined via a colorimetric MTT assay. In Brief, J774A.1 cells (20,000) were cultured at 37 °C under 5% CO_2 atmosphere and were seeded into a sterile 96-well plate and allowed to adhere for 24 h. The spent media was aspirated, and the J774A.1 cells were treated with CAPHs (10 μM in DMEM supplemented with 10% FBS) for 9 h at 37 °C. After this incubation period, the treatment was aspirated, and the cells were washed with PBS. Next, 100 μL of fresh DMEM media was added to each well, followed by 10 μL of 12 mM MTT reagent. The plate was incubated for an additional 2 h at 37 °C under 5% CO_2 atmosphere. Finally, the MTT solution was aspirated, and 100 μL of DMSO was added to each well. The 96-well plate was allowed to shake for 5 min at room temperature, and the absorbance of each well was measured at 590 nm using a microplate reader. Results were expressed as the percentage of viable cells as compared to a control that contained no CAPHs treatment. Data were obtained in duplicate from three independent experiments.

Subcellular Localization. J774A.1 cells (200,000) were seeded in a 4-well Lab-Tek chambered slide and were allowed to adhere for 18 h at 37 °C under 5% CO_2 atmosphere. The media was then aspirated, and the cells were washed with PBS (400 μL). Next, CAPHs were added to each well in 400 μL of DMEM supplemented with 10% FBS. The cells were incubated for 1 h at 37 °C under 5% CO_2 atmosphere. After the incubation period, the treatment was aspirated and washed with PBS (400 μL). The cells were further treated with Hoechst 33342 (1000 nM) and either Mitotracker (100 nM) or Lysotracker (300 nM) for 30 min at 37 °C under 5% CO_2 atmosphere. The excess dye was aspirated, the cells were washed with 400 μL of PBS, and fresh serum-supplemented DMEM was added to each well. Imaging was performed using a Nikon A1R multiphoton inverted confocal microscope under a 60× oil objective. Fluorescein, Hoechst 33342, and Mitotracker/Lysotracker were excited using 488, 350, and 561 nm lasers, respectively.

***β*-Galactosidase Assay.** *E. coli* (ATCC 25922) was grown to the mid-exponential phase (OD_{590} = ∼0.6) in Mueller−Hinton Broth (MHB) at 37 °C with shaking. *β*-Galactosidase expression was

https://dx.doi.org/10.1021/acs.joc.0c00871
J. Org. Chem. 2020, 85, 7468−7475

induced for 1 h using a freshly prepared solution of isopropyl-β-D-thiogalactopyranoside in PBS (1 mM final concentration). Following the induction, an aliquot (10 mL) of the bacterial suspension was centrifuged, washed twice with fresh MHB, and plated into a sterile 96-well plate. Next, 10 μL aliquots of CAPHs were added to give final concentrations corresponding to 1×, 2×, or 4× the MIC value (against *E. coli*). Bacteria were also treated with sterile water and melittin (20 μM final concentration), which served as controls. The 96-well plate was incubated for 1 h at 37 °C. At the end of the incubation period, the plate was centrifuged at 4000 rpm for 10 min. A volume of 80 μL of the supernatant from each well as added to a new sterile 96-well plate. Next, 20 μL of freshly prepared 2-nitrophenyl-β-D-galactopyranoside in PBS was added to each well (0.8 mg/mL final concentration). The β-galactosidase activity was monitored at OD_{405nm} every 5 min over the course of 1 h using a microplate reader. Data were obtained in duplicate from at least two independent experiments.

Hemolysis. hRBCs were centrifuged at 1200 rpm at 4 °C for 5 min. The hRBCs were washed with PBS (pH 7.4) two times, and a 4% suspension (v/v) of hRBCs was prepared in PBS. A volume of 50 μL of the hRBCs solution was transferred to a sterile 96-well plate, and 50 μL of CAPHs in PBS was added to each well to give a final suspension of 2% (v/v) of hRBCs. The plate was then incubated for 1 h at 37 °C. At the end of the incubation, the plate was centrifuged at 1200 rpm for 5 min at 4 °C. From each well, 80 μL of the supernatant was then transferred to a new sterile 96-well plate. Finally, the release of hemoglobin caused by hemolysis was quantified by measuring the absorbance of the wells at 405 nm with a microplate reader. For controls, wells were treated with PBS, melittin, or 0.1% (final concentration) Triton X-100 in PBS. The percentage of hemolysis was calculated on the basis of the 100% hemolysis release with 0.1% Triton X-100. Data were obtained in duplicate from at least two independent experiments.

Antimicrobial Susceptibility Testing. The antimicrobial activity of the CAPHs and control antibiotics against the tested isolates, except for *M. tuberculosis*, was performed following the Clinical and Laboratory Standards Institute guidelines.[31] Briefly, bacterial cells were cultured overnight on trypticase soya agar plates (Becton Dickinson). Colonies were picked and suspended in NaCl 0.9% to a density of 0.5 McFarland. The bacterial suspensions were further diluted 1:60 in CA-MHB (cation adjusted Mueller−Hinton Broth Becton Dickinson), and 100 μl portions of the bacterial suspension were added to 96-well plates containing the CAPHs and control antibiotics at a concentration range of 0.125−16 μM. The 96-well plates were incubated for 16−20 h at 37 °C before recording the MIC values. The MICs reported represent the lowest concentration of each peptide or standard antibiotic necessary to inhibit the bacterial growth. For testing the antimicrobial activity of the CAPHs and control antibiotic against *M. tuberculosis*, a resazurin microtiter assay was performed following a previously reported protocol.[32] Briefly, mycobacterial colonies grown on the Lowenstein−Jensen (Becton Dickinson) medium were suspended in the 7H9-S broth, adjusted spectrophotometrically to a no. 1 McFarland tube standard, and further diluted 1:10 in 7H9-S broth. Then, 100 μl of the 7H9-S broth was dispensed in each well of a sterile flat-bottom 96-well plate, and serial twofold dilutions of each of the peptides and control antibiotics were prepared directly in the plate. One-hundred microliters of the prepared inoculum was added to each well. Plates were covered, sealed in a plastic bag, and incubated at 37 °C under a normal atmosphere. After 7 days of incubation, 30 μL of resazurin solution, 0.02% (w/v) in distilled water, was added to each well, and the plate was re-incubated overnight. A change in color from blue to pink indicated the growth of bacteria, and the MIC was defined as the lowest concentration of the compound that prevented this change in color.

Activity against Intracellular Bacteria. Following previously described protocols, the ability of the peptides to reduce the burden of intracellular *S. flexneri* was evaluated.[16,33] Murine macrophage cells (J774A.1) were cultured in DMEM supplemented with 10% FBS at 37 °C under a CO_2 (5%) atmosphere. J774.1 cells were infected with *S. flexneri* 1a ATCC 9199 cells at a multiplicity of infection of approximately 1:100. After 1 h of infection, J774A.1 cells were washed with DMEM and further incubated with gentamicin (100 μg/mL) for 1 h to kill extracellular bacteria. The peptides at the respective concentrations were added to each well (four replicates per test agent). After 12 h incubation at 37 °C with 5% CO_2, the compounds were removed, J774A.1 cells were washed and lysed using 0.1% Triton-X. The cell lysates were serially diluted in PBS and transferred to trypticase soy agar plates to determine viable bacterial cfu, inside the J774A.1 cells. The plates were incubated at 37 °C for 20 h before counting viable cfu/mL. Data are presented as the percentage of intracellular cfu/mL in treated murine macrophage cells relative to the untreated control.

■ ASSOCIATED CONTENT

Supporting Information

The Supporting Information is available free of charge at https://pubs.acs.org/doi/10.1021/acs.joc.0c00871.

Mass spectrometry data, RP-HPLC retention times and traces, and CD spectra of N-terminal CAPHs; cell viability test data; β-galactosidase assay data; Cellular uptake of aliphatic N-terminal CAPHs in J774A.1 macrophage cells; and cell localization data (PDF)

■ AUTHOR INFORMATION

Corresponding Author

Jean Chmielewski − *Department of Chemistry, Purdue University, West Lafayette, Indiana 47907-2027, United States;* orcid.org/0000-0003-4958-7175; Email: chml@purdue.edu

Authors

Thomas A. Dietsche − *Department of Chemistry, Purdue University, West Lafayette, Indiana 47907-2027, United States*

Hassan E. Eldesouky − *Department of Comparative Pathobiology, Purdue University, West Lafayette, Indiana 47907-2027, United States;* orcid.org/0000-0003-4718-6087

Samantha M. Zeiders − *Department of Chemistry, Purdue University, West Lafayette, Indiana 47907-2027, United States*

Mohamed N. Seleem − *Department of Comparative Pathobiology, Purdue University, West Lafayette, Indiana 47907-2027, United States;* orcid.org/0000-0003-0939-0458

Complete contact information is available at: https://pubs.acs.org/10.1021/acs.joc.0c00871

Author Contributions

The manuscript was written through contributions of all authors.

Notes

The authors declare no competing financial interest.

■ ACKNOWLEDGMENTS

The authors acknowledge support from the National Science Foundation (1609406-CHE).

■ REFERENCES

(1) Kumarasamy, K. K.; Toleman, M. A.; Walsh, T. R.; Bagaria, J.; Butt, F.; Balakrishnan, R.; Chaudhary, U.; Doumith, M.; Giske, C. G.; Irfan, S.; Krishnan, P.; Kumar, A. V.; Maharjan, S.; Mushtaq, S.; Noorie, T.; Paterson, D. L.; Pearson, A.; Perry, C.; Pike, R.; Rao, B.; Ray, U.; Sarma, J. B.; Sharma, M.; Sheridan, E.; Thirunarayan, M. A.; Turton, J.; Upadhyay, S.; Warner, M.; Welfare, W.; Livermore, D. M.;

Woodford, N. Emergence of a New Antibiotic Resistance Mechanism in India, Pakistan, and the UK: A Molecular, Biological, and Epidemiological Study. *Lancet Infect. Dis.* **2010**, *10*, 597−602.
(2) Navon-Venezia, S.; Ben-Ami, R.; Carmeli, Y. Update on Pseudomonas aeruginosa and Acinetobacter baumannii infections in the healthcare setting. *Curr. Opin. Infect. Dis.* **2005**, *18*, 306−313.
(3) Smith, I. Mycobacterium tuberculosis Pathogenesis and Molecular Determinants of Virulence. *Clin. Microbiol. Rev.* **2003**, *16*, 463−496.
(4) Flannagan, R. S.; Cosío, G.; Grinstein, S. Antimicrobial Mechanisms of Phagocytes and Bacterial Evasion Strategies. *Nat. Rev. Microbiol.* **2009**, *7*, 355−366.
(5) Diacovich, L.; Gorvel, J.-P. Bacterial Manipulation of Innate Immunity to Promote Infection. *Nat. Rev. Microbiol.* **2010**, *8*, 117−128.
(6) Carryn, S.; Chanteux, H.; Seral, C.; Mingeot-Leclercq, M.-P.; Van Bambeke, F.; Tulkens, P. M. Intracellular Pharmacodynamics of Antibiotics. *Infect. Dis. Clin.* **2003**, *17*, 615−634.
(7) Seleem, M. N.; Munusamy, P.; Ranjan, A.; Alqublan, H.; Pickrell, G.; Sriranganathan, N. Silica-Antibiotic Hybrid Nanoparticles for Targeting Intracellular Pathogens. *Antimicrob. Agents Chemother.* **2009**, *53*, 4270−4274.
(8) Kalluru, R.; Fenaroli, F.; Westmoreland, D.; Ulanova, L.; Maleki, A.; Roos, N.; Paulsen Madsen, M.; Koster, G.; Egge-Jacobsen, W.; Wilson, S.; Roberg-Larsen, H.; Khuller, G. K.; Singh, A.; Nystrom, B.; Griffiths, G. Poly(Lactide-Co-Glycolide)-Rifampicin Nanoparticles Efficiently Clear Mycobacterium Bovis BCG Infection in Macrophages and Remain Membrane-Bound in Phago-Lysosomes. *J. Cell Sci.* **2013**, *126*, 3043−3054.
(9) Lei, E. K.; Pereira, M. P.; Kelley, S. O. Tuning the Intracellular Bacterial Targeting of Peptidic Vectors. *Angew. Chem., Int. Ed.* **2013**, *52*, 9660−9663.
(10) Ahmed, M.; Kelley, S. O. Enhancing the Potency of Nalidixic Acid toward a Bacterial DNA Gyrase with Conjugated Peptides. *ACS Chem. Biol.* **2017**, *12*, 2563−2569.
(11) Alajlouni, R. A.; Seleem, M. N. Targeting Listeria Monocytogenes RpoA and RpoD Genes Using Peptide Nucleic Acids. *Nucleic Acid Ther.* **2013**, *23*, 363−367.
(12) Brezden, A.; Mohamed, M. F.; Nepal, M.; Harwood, J. S.; Kuriakose, J.; Seleem, M. N.; Chmielewski, J. Dual Targeting of Intracellular Pathogenic Bacteria with a Cleavable Conjugate of Kanamycin and an Antibacterial Cell-Penetrating Peptide. *J. Am. Chem. Soc.* **2016**, *138*, 10945−10949.
(13) Kuriakose, J.; Hernandez-Gordillo, V.; Nepal, M.; Brezden, A.; Pozzi, V.; Seleem, M. N.; Chmielewski, J. Targeting Intracellular Pathogenic Bacteria with Unnatural Proline-Rich Peptides: Coupling Antibacterial Activity with Macrophage Penetration. *Angew. Chem., Int. Ed.* **2013**, *52*, 9664−9667.
(14) Nepal, M.; Thangamani, S.; Seleem, M. N.; Chmielewski, J. Targeting Intracellular Bacteria with an Extended Cationic Amphiphilic Polyproline Helix. *Org. Biomol. Chem.* **2015**, *13*, 5930−5936.
(15) Lee, J. S.; Tung, C.-H. Lipo-Oligoarginines as Effective Delivery Vectors to Promote Cellular Uptake. *Mol. BioSyst.* **2010**, *6*, 2049.
(16) Nepal, M.; Mohamed, M. F.; Blade, R.; Eldesouky, H. E.; N Anderson, T.; Seleem, M. N.; Chmielewski, J. A Library Approach to Cationic Amphiphilic Polyproline Helices That Target Intracellular Pathogenic Bacteria. *ACS Infect. Dis.* **2018**, *4*, 1300−1305.
(17) Fillon, Y. A.; Anderson, J. P.; Chmielewski, J. Cell Penetrating Agents Based on a Polyproline Helix Scaffold. *J. Am. Chem. Soc.* **2005**, *127*, 11798−11803.
(18) Tseng, W.-H.; Li, M.-C.; Horng, J.-C.; Wang, S.-K. Strategy and Effects of Polyproline Peptide Stapling by Copper(I)-Catalyzed Alkyne−Azide Cycloaddition Reaction. *ChemBioChem* **2019**, *20*, 153−158.
(19) Helbecque, N.; Loucheux-Lefebvre, M. H. Critical Chain Length for Polyproline-II Structure Formation in H-Gly-(Pro)n-OH. *Int. J. Pept. Protein Res.* **1982**, *19*, 94−101.
(20) Bjerknes, R.; Bassøe, C.-F. Phagocyte C3-Mediated Attachment and Internalization: Flow Cytometric Studies Using a Fluorescence Quenching Technique. *Blut* **1984**, *49*, 315−323.
(21) Kalafut, D.; Anderson, T. N.; Chmielewski, J. Mitochondrial Targeting of a Cationic Amphiphilic Polyproline Helix. *Bioorganic Med. Chem. Lett.* **2012**, *22*, 561−563.
(22) Riss, T. L.; Moravec, R. A.; Niles, A. L.; Benink, H. A.; Worzella, T. J. Cell Viability Assays. *Assay Guidance Manual*; Eli Lilly & Company and the National Center for Advancing Translational Sciences, 2016; pp 1−31.
(23) Pereira, M. P.; Shi, J.; Kelley, S. O. Peptide Targeting of an Antibiotic Prodrug toward Phagosome-Entrapped Mycobacteria. *ACS Infect. Dis.* **2015**, *1*, 586−592.
(24) Bai, H.; You, Y.; Yan, H.; Meng, J.; Xue, X.; Hou, Z.; Zhou, Y.; Ma, X.; Sang, G.; Luo, X. Antisense Inhibition of Gene Expression and Growth in Gram-Negative Bacteria by Cell-Penetrating Peptide Conjugates of Peptide Nucleic Acids Targeted to RpoD Gene. *Biomaterials* **2012**, *33*, 659−667.
(25) Howard, A.; Donoghue, M. O.; Feeney, A.; Sleator, R. D. Acinetobacter Baumannii an Emerging Opportunistic Pathogen. *Virulence* **2012**, *3*, 243−250.
(26) Porter, E. A.; Weisblum, B.; Gellman, S. H. Mimicry of Host-Defense Peptides by Unnatural Oligomers: Antimicrobial β-Peptides. *J. Am. Chem. Soc.* **2002**, *124*, 7324−7330.
(27) Seleem, M. N.; Jain, N.; Pothayee, N.; Ranjan, A.; Riffle, J. S.; Sriranganathan, N. Targeting Brucella Melitensis with Polymeric Nanoparticles Containing Streptomycin and Doxycycline. *FEMS Microbiol. Lett.* **2009**, *294*, 24−31.
(28) Li, L.; Geisler, I.; Chmielewski, J.; Cheng, J.-X. Cationic Amphiphilic Polyproline Helix P11LRR Targets Intracellular Mitochondria. *J. Control. Release* **2010**, *142*, 259−266.
(29) Christensen, T.; Eriksson, A.; Thornell, L.-E. Qualitative Test for Monitoring Coupling Completeness in Solid-Phase Peptide-Synthesis Using Chloranil. *Acta Chem. Scand., Ser. B* **1979**, *33*, 763−766.
(30) Kaiser, E.; Colescott, R. L.; Bossinger, C. D.; Cook, P. I. Color Test for Detection of Free Terminal Amino Groups in the Solid-Phase Synthesis of Peptides. *Anal. Biochem.* **1970**, *34*, 595.
(31) Clinical and Laboratory Standards Institute (CLSI); Weinstein, M. P.; Zimmer, B. L.; Cockerill, F. R.; Wiker, M. A.; Alder, J.; Dudley, M. N.; Eliopoulos, G. M.; Ferraro, M. J.; Hardy, D. J.; Hecht, D. W.; Hindler, J. A.; Patel, J. B.; Powell, M.; Swenson, J. M.; Thomson, R. B.; Traczewski, M. M.; Turnidge, J. D. *Methods for Dilution Antimicrobial Susceptibility Tests for Bacteria that Grow Aerobically*; Approved Standard, 9th ed., 2012; Vol. 32.
(32) Martin, A.; Camacho, M.; Portaels, F.; Palomino, J. C. Resazurin microtiter assay plate testing of Mycobacterium tuberculosis susceptibilities to second-line drugs: rapid, simple, and inexpensive method. *Antimicrob. Agents Chemother.* **2003**, *47*, 3616−3619.
(33) Chiu, H.-C.; Kulp, S. K.; Soni, S.; Wang, D.; Gunn, J. S.; Schlesinger, L. S.; Chen, C.-S. Eradication of Intracellular Salmonella Enterica Serovar Typhimurium with a Small-Molecule, Host Cell-Directed Agent. *Antimicrob. Agents Chemother.* **2009**, *53*, 5236−5244.

https://dx.doi.org/10.1021/acs.joc.0c00871
J. Org. Chem. 2020, 85, 7468−7475